https://researchonline.lshtm.ac.uk

Combining reverse genetics and live microscopy to dissect *Plasmodium knowlesi* invasion of red blood cells

Melissa Natalie Hart

Thesis submitted in accordance with the requirements

for the degree of Doctor of Philosophy

University of London

October 2020

Department of Infection Biology

Faculty of Infectious and Tropical Diseases

London School of Hygiene and Tropical Medicine

Declaration

I, Melissa Natalie Hart, confirm that the work presented in this thesis is my own. Where information has been derived from other sources, I confirm that this has been indicated in the thesis.

Abstract

Plasmodium knowlesi is one of six *Plasmodium* species responsible for causing malaria in humans. Symptoms of the disease arise from the blood stage of the parasite's life cycle, when a form of the parasite, known as a merozoite, invades a red blood cell (RBC), develops and multiplies within it, and then bursts (egresses) from the host cell, releasing more invasive merozoites. Invasion progresses through several key steps, which can be visualised using live microscopy: weak parasite-host cell interactions, stronger interactions causing cell deformation and parasite re-orientation, and finally parasite entry and resealing of the host cell. Throughout invasion, the parasite secretes numerous proteins from specialised secretory organelles, called micronemes and rhoptries, which facilitate each step. Two protein families that have been shown to be essential for merozoite invasion are the Duffy binding protein (DBP) and reticulocyte binding like (RBL) proteins. In *P. falciparum*, these families consist of multiple members, with significant redundancy, which has led to difficulty assigning specific functions to each member, or even family. *P. knowlesi,* on the other hand, has a smaller repertoire of proteins within each family consisting of three DBPs (PkDBPα, PkDBPβ, and PkDBPγ) and two RBLs, the Normocyte binding proteins Xa and Xb (PkNBPXa and PkNBPXb). Of these proteins, only two are required for human red cell invasion: PkDBPα and PkNBPXa.

The first part of this study investigates how wild type parasites invade human erythrocytes, taking advantage of the large size and distinctly polarised shape of *P. knowlesi* merozoites to dissect the morphological steps of invasion in much greater detail than previously achieved for *P. falciparum*. Live microscopy has clarified the order of early events leading up to internalisation and revealed a new pre-internalisation step, gliding motility, which is required for deformation and enhances parasite-host cell interactions. The second part of this study uses this new understanding of invasion as a framework to investigate the roles of PkDBPα and PkNBPXa by performing live microscopic analysis of tagged and conditional knockout (cKO) parasite lines. Multi- tagged lines show both proteins share a similar localisation pre egress, but exhibit distinct localisations once released from apical organelles. Finally, live imaging has revealed distinct roles for both families, showing that PkNBPXa is essential for host cell deformation, while PkDBPα performs a function downstream of this process.

Acknowledgements

I would like to extend my sincere gratitude to my primary supervisor, Dr Rob Moon, for accepting me into his lab and supporting me throughout this project. Rob, thank you really doesn't seem enough. If one day I become half the scientist and mentor you are, I will consider that an honour. I promise to delete every second "though" and maybe every 4th comma in all future manuscripts – well, for now. I'd also like to thank my secondary supervisor, Professor Helen Saibil for her wise advice and helpful discussions over the course of this study.

Thank you also to the wonderful members of the Moon and Saibil labs. I'd especially like to thank Franzi for always having my back and encouraging me whenever the *knowlesi* decided to rebel and do, well, whatever they had in mind on any particular occasion. Thank you also to James T and James C - the Jamesi – for making the lab fun! "It's always wise to synchronise" still makes me laugh. Thank you also to Trishant and Claudine for patiently helping me out with the early stages of my project.

To all the current and past members of lab 380, it has been a joy to work with you all – thank you for being my village. Thank you especially to Stephanie, Gisela, Julian, and Aline for coffees, laughs, and more than a little bit of mischief. Thank you, Don, for being the cheeriest culture buddy I could have asked for and not laughing too hard at my attempts at singing along to the radio. To the rest of the Sutherland, Baker, and van Ooij lab members, your support has been so appreciated.

I would also like to say a massive thank you to both of my unofficial supervisors, Ellen Knuepfer and Christian Flueck. Your patient responses to every "why didn't this work?" "please can I borrow..." and "what do you think?" were so, so appreciated. Also…for coffee. Because, let's be honest, caffeinating a PhD student is sometimes equally beneficial to great advice. I think you both knew this.

Tremendous thanks also goes to my dear family. If I had received a pound every time I was asked if I had finished my thesis, I probably could have funded another year. Thank you all for keeping me motivated to put a pen to paper and for your continuous love, support, and prayers. Mum, you were my very first teacher, and I will always be grateful that you instilled a love of learning in me.

Finally, as always, *Soli Deo Gloria.*

Table of Contents

List of figures

List of tables

List of appendices

List of supplementary videos

Video 3.1: *P. knowlesi* merozoites deforming host cells in groups

Video 3.2: Example of host cell lysis

Video 3.3: Merozoites exhibiting directional movement after egress

Video 3.4: DMSO-treated merozoites gliding across PLL coated coverslips

Video 3.5: Cytochalasin D-treated merozoites do not exhibit gliding motility

Video 3.6: Gliding enables merozoite groups to break apart

Video 3.7: Merozoites gliding on glass coverslips

Video 3.8: Gliding PkNBPXa-mNeonGreen tagged parasite

Video 3.9: Merozoite undergoing corkscrew-like rotation

Video 3.10: Merozoite exhibit twirling behaviour

Video 3.11: Deformation beginning from the side of the erythrocyte

Video 3.12: Example *P. knowlesi* invasion 1

Video 3.13: Example *P. knowlesi* invasion 2

Video 3.14: Example *P. knowlesi* invasion 3

Video 3.15: A merozoite-RBC fusion/Ca^{2+} signalling event

Video 3.16: Example *P. knowlesi* invasion from the side of erythrocyte

Video 3.17: Example of half-cell echinocytosis

Video 3.18: Host cell lysis example 2

Video 3.19: *P. falciparum* invasion taken from Gilson and Crabb (2009)

Video 4.1: Secretion of PkAMA1-mNG

Video 4.2: Secretion of PkNBPXa-mNG

Video 4.3: Secretion of PkDBPα-mNG

Video 4.4: PkNBPXa-mNG invasion 1

Video 4.5: Gliding PkDBPα-mNG merozoite

Video 4.6: PkAMA1-mNG invasion

Video 4.7: PkDBPα-mNG invasion 1

Video 4.8: PkDBPα-mNG invasion 2

Video 4.9: PkNBPXa-mNG invasion 2

Video 4.10: Rapamycin treated PkNBPXa cKO parasites

Video 4.11: DMSO treated PkNBPXa cKO parasites

Video 4.12: α-human IgG treated merozoites

Video 4.13: α-DARC treated merozoites

Abbreviations

AMA-1	Apical membrane antigen 1
BSA	Bovine Serum Albumin
Cas9	CRISPR associated protein 9
cKO	Conditional knockout
CRISPR	Clustered regularly interspaced short palindromic repeats
CSP	Circumsporozoite protein
CyRPA	Cysteine-rich protective antigen
DAPI	4',6-. diamidino-. 2-. phenylindole
DARC	Duffy antigen receptor for chemokines
DBL	Duffy binding like
DBP	Duffy binding protein
DiCre	Dimerisable Cre recombinase
DNA	Deoxyribonucleic acid
DMSO	Dimethyl sulfoxide
EBA	Erythrocyte binding antigen
EBL-1	Erythrocyte binding ligand 1
EM	Electron microscopy
FACS	Fluorescent activated cell sorting
GAC	Glideosome associated connector
GAP	Glideosome associated protein
gDNA	genomic deoxyribonucleic acid
GIA	Growth inhibitory assay
GPA	Glycophorin A
HA	Haemagglutinin

hDHFR	Human dihydrofolate reductase
IFA	Indirect immunofluorescence assay
IgG	Immunoglobulin G
IMC	Inner membrane complex
kb	Kilo base-pair
kDa	Kilo Daltons
KO	knockout
mCh	mCherry
mg	Milligram
MIC	Microneme protein
MJ	Moving junction
ml	Millilitre
mM	Millimolar
mNG	mNeonGreen
MSP	Merozoite surface protein
MTRAP	Merozoite thrombospondin-related anonymous protein
MyoA	Myosin A
nM	Nanomolar
NBPXa/b	Normocyte binding protein a/b
ORF	Open reading frame
PAM	Protospacer adjacent motif
Pb	*P. berghei*
PBS	Phosphate-buffered saline
PCR	Polymerase chain reaction
Pf	*P. falciparum*
PFA	Paraformaldehyde

Pk	*P. knowlesi*
PM	Plasma membrane
PMSF	Phenylmethylsulfonyl fluoride
PTRAMP	*Plasmodium* thrombospondin-related apical merozoite protein
Pv	*P. vivax*
PV	Parasitophorous vacuole
PVM	Parasitophorous vacuole membrane
Py	*P. yoelii*
Rap	Rapamycin
RBC	Red blood cell
RBL	Reticulocyte binding like protein
RBP	Reticulocyte binding protein
Rh	Reticulocyte binding like homolog
RIPR	Rh5 interacting protein
RNA	Ribonucleic acid
ROM	Rhomboid
RON	Rhoptry neck protein
SDS	Sodium dodecyl sulphate
SPN	Subpellicular network
SUB	Subtilisin
μg	Microgram
μl	Microliter
μM	Micromolar
μm	Micrometer
UTR	Untranslated region
WHO	World Health Organisation

Chapter 1: General introduction

1.1 An introduction to malaria

Despite significant efforts towards its eradication, malaria remains a deadly threat to almost half the globe, spanning countries across Africa, South America, and Southeast Asia. Disease severity can range from mild, flu-like symptoms with fevers and chills to life-threatening developments, including severe anaemia, respiratory failure, and coma, leading to death (WHO, 2019). In 2018, WHO estimated 228 million cases worldwide, resulting in the deaths of approximately 405,000 people, with over two-thirds of these deaths attributable to infants and young children (WHO 2019).

Not only does malaria result in the tragic loss of life, but this disease also has a profound economic effect. The direct costs of malaria prevention and treatment are estimated to be over 12 billion USD per year (CDC, 2020). However, this figure does not take into account the overall loss of capital a nation experiences as a result of illness and death reducing the workforce and, more indirectly, interrupting access to education. The ensuing poverty, however, in turn directly impacts public health, as individuals and entire nations are less able to afford nutritious food, quality housing, and accessible healthcare (WHO Strategic Advisory Group on Malaria, 2020).

The etiological agent of malaria, *Plasmodium*, is an apicomplexan parasite transmitted to its vertebrate host by the female *Anopheles* mosquito (WHO, 2019). Six *Plasmodium* species are known to commonly infect humans (Rutledge et al., 2017). Of these, *P. falciparum* has the highest incidence and is the predominant cause of malaria in Africa, responsible for 99.7% of cases within this region. *P. vivax*, the second biggest contributor to disease burden, is the most prevalent species, giving rise to cases within 95 countries across the globe (Howes et al., 2016). However, the four remaining species, *P. ovale curtisi*, *P. ovale wallikeri*, *P. malariae*, and the zoonotic parasite, *P. knowlesi*, still contribute a considerable disease burden, and must not be ignored in the strive towards malaria eradication (WHO 2019; Rutledge et al., 2017).

Over the past 20 years, significant progress has been made towards reducing the number of cases of malaria globally. From 2000-2015, the number of deaths attributed to malaria decreased by roughly 50% (WHO, 2016). However, over 80 countries are still fighting to eradicate malaria, with 19 countries accounting for 85% of all global

cases. Additionally, despite persistent efforts to tackle malaria cases in each of these regions, the number of cases and deaths worldwide has plateaued in recent years, in stark contrast to the rapid decline seen over the previous decade (WHO, 2019). Numerous control strategies are currently employed by endemic nations to treat clinical cases and prevent malaria transmission. Some of these include antimalarial treatment regimens to cure active cases or treat vulnerable populations prophylactically during high transmission seasons. Further preventative measures include the use of insecticide sprays and insecticide-treated bed nets, both of which impede transmission via mosquito bite (WHO, 2019). However, the progression from control to elimination status is hindered for many endemic nations due to several parasitological challenges. Firstly, resistance to front line antimalarials, including artemisinin and partner drugs, continues to rise (Noedl et al., 2008; Ashley et al., 2014; Mairet-Khedim et al., 2020). Secondly, asymptomatic carriers and zoonotic sources create permanent reservoirs of infective parasites (Galatas et al., 2016; Grigg et al., 2017). Finally, hypnozoites, dormant forms of the parasite, cause relapsing *P. vivax* and *P. ovale* cases (Richter et al., 2010; Adams and Mueller, 2017). All of these challenges point to the need for an effective malaria vaccine: a tool that is not yet in our grasp.

The clinical symptoms of malaria arise from *Plasmodium* parasites invading erythrocytes, replicating within them, and finally bursting free to invade new host cells (Cowman et al., 2017). This work focuses on two protein families critical to erythrocyte invasion: the reticulocyte binding like (RBL) and the Duffy binding like (DBP) proteins. Both families are key determinants of host cell tropism and contribute to parasite virulence, for instance by restricting some species to grow in very young erythrocytes, while permitting others to invade a much wider range of host cells (Tham et al., 2012; Cowman et al., 2017). Critically, as exposure to the RBLs and DBPs has been associated with natural immunity from malaria, both families are prime vaccine candidates (Tham et al., 2012). However, precisely how the RBL and DBP ligands facilitate erythrocyte invasion is still uncertain. Previous attempts to investigate these complicated and sometimes large protein families have been hindered in part by a lack of appropriate genetic tools (Chan et al., 2019; Tham et al., 2012). However, in recent years the development of CRISPR Cas9 and Dimerisable Cre recombinase (DiCre) genome editing tools has revolutionised the way we can use experimental genetics in malaria and overcome many of the barriers to studying complex gene families like

these (Andenmatten et al., 2013; Collins et al., 2013; Lee et al., 2019). Furthermore, the recent adaptation of *P. knowlesi*, the species utilised in this study, to *in vitro* culture has provided another model of the asexual stages and invasion (Moon et al., 2013). Now with new tools in hand, thoroughly dissecting the roles of the RBL and DBP ligands will enable us to gain a greater understanding of invasion biology and help us to assess their suitability as vaccine candidates.

1.2 *P. knowlesi*: an emerging problem

Unlike the other species pathogenic to humans, the primary hosts of *P. knowlesi* are the long-tailed and pig-tailed macaques (Singh and Daneshvar, 2013). Early studies of this pathogen in the 1960s concluded that human infections, while possible, were uncommon (reviewed in Singh & Daneshvar, 2013). However, more recent studies investigating unusually severe cases of *P. malariae* in Malaysian Borneo, lead to the discovery that many of these cases had been misdiagnosed and were actually *P. knowlesi* infections (Millar and Cox-Singh, 2015). Since this study, many more have followed and established that *P. knowlesi* infections are widespread and are an emerging cause of potentially deadly infections throughout South-east Asia, despite a marked decrease in the incidence of the other *Plasmodium* species (Cox Singh et al., 2008; William et al., 2014, 2013; Yusof et al., 2014; Herdiana et al., 2016; Lubis et al., 2017; Yusof et al., 2014; Cooper et al., 2020).

The majority, if not all, human *P. knowlesi* infections are thought to arise from an *Anopheles* mosquito first biting an infected macaque and then transmitting parasites to the human host. This phenomenon means *P. knowlesi* infections are geographically restricted by the requirement for overlapping human, macaque, and vector populations, resulting in transmission being limited to S E Asia (Manin et al., 2016). Practically speaking, this also means that risk factors for contracting *P. knowlesi* include working in and around forested areas, farmlands, and plantations, where both macaques and mosquito vectors are present (Barber et al., 2012; Grigg et al., 2017). Importantly, since transmission between macaques cannot be curtailed with normal control measures, such as treatment with drugs, or using bed-nets, macaques remain a constant source of infection to humans within a given region (Grigg et al., 2017). Therefore, the development of a vaccine may be the only way to prevent *P. knowlesi* infections without also impacting macaque populations.

A potential reason for the rise in *P. knowlesi* infections is continuous deforestation, which ultimately brings human and macaque/vector populations into closer contact (Barber et al., 2012; Fornace et al., 2016; Brock et al., 2019; Stark et al., 2019). So in addition to the cases that can be traced directly back to workers returning from forested regions, there are also increasing numbers of 'peri-domestic' infections occurring: infections acquired within villages, as a result of macaques also living in and moving through the surrounding areas (Barber et al., 2012; Manin et al., 2016; Grigg et al., 2017). One study has even shown that the abundance of *Anopheles balabacensis*, the primary vector for *P. knowlesi* transmission in Sabah, Malaysia, increases when forest areas are disturbed. This can occur, for instance, by wheel ruts left in the mud by workers that fill with water, providing the perfect mosquito breeding conditions (Brant et al., 2016). So overall, the habitat changes of both primary host and vector have likely contributed significantly to the increase of zoonotic infections.

The recent increases in cases and their severity may also be indicative of changes in host-pathogen interactions and the emergence of some human-human transmission (Cooper et al., 2020). There is also evidence that the current increasing risk from *P. knowlesi* may be partly due to an indirect consequence of successfully controlling other human malaria parasites (William et al., 2013; William et al., 2014; Cooper et al., 2020). Recently, *P. vivax* antibodies targeting several erythrocyte invasion antigens demonstrated cross-inhibitory action against *P. knowlesi* parasites in culture. Thus the spread and intensity of *P. knowlesi* infections may be curbed by cross-immunity to *P. vivax* (Muh et al., 2020; Ndegwa et al., 2020), which is closely related and shares key erythrocyte invasion pathways mediated by DBP ligands (Haynes et al., 1988; Pain et al., 2008; Wertheimer and Barnwell, 1989). Encouragingly, this means that it may be possible to target both *P. vivax* and *P. knowlesi* with a single vaccine. So, as endemic regions strive towards elimination of all malaria species, renewed efforts towards a better understanding of shared erythrocyte invasion pathways and mechanisms of cross-resistance will be vital to the development of an efficacious vaccine.

1.3 The *Plasmodium* Life cycle

The life cycle of *Plasmodium* parasites is incredibly complex, consisting of two main phases: one taking place in the *Anopheles* mosquito vector, and the other taking place within a vertebrate host (Cowman et al., 2012; Figure 1.1). During each phase of the

life cycle, the parasite extensively remodels itself, taking on unique morphologies perfectly suited to survive and proliferate in each given environment. On the one hand, this complexity presents a challenge to understanding the fundamental biology driving the transition of one step to the next. However, on the other hand, a multi-step life cycle also presents many opportunities to exploit a variety of potential drug and vaccine targets (Phillips et al., 2017).
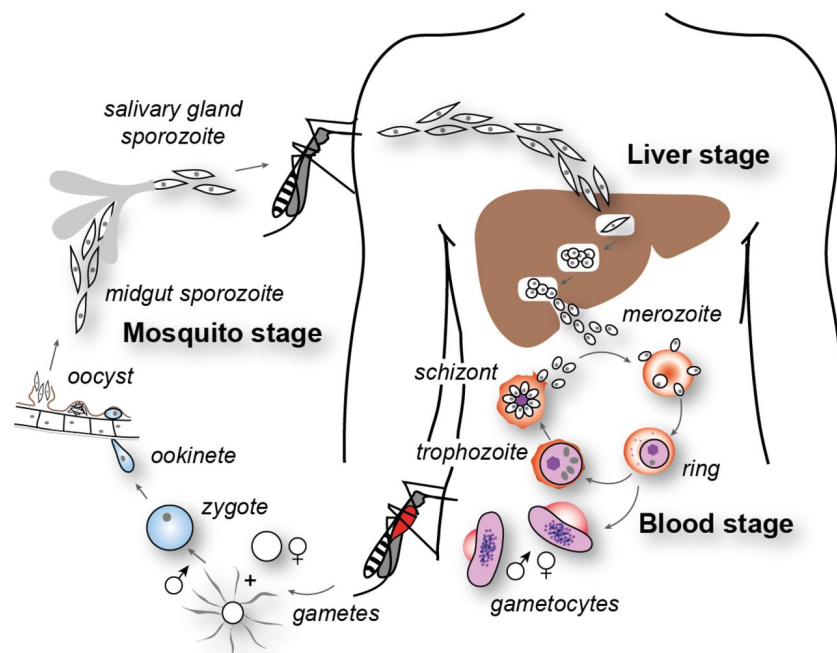
Figure 1.1 *Plasmodium* Life cycle (taken from Cowman et al., 2012). The *Plasmodium* life cycle can be divided into two phases, the first taking place in the mosquito vector and the second in the vertebrate host. Infection of the vertebrate host begins upon injection of sporozoites into the host's bloodstream. Sporozoites travel to the liver, where they invade hepatocytes and grow and divide intracellularly to form hepatic schizonts, containing hundreds of merozoites. Release of merozoites into the bloodstream begins the erythrocytic cycle (the blood stage), during which merozoites invade erythrocytes, develop from ring-stage parasites into mature schizonts, and egress, to release a fresh round of merozoites. These merozoites go on to invade more erythrocytes, thus continuing this cycle of invasion and egress. Additionally, some blood-stage parasites will develop into gametocytes, which are taken up during a mosquito's blood meal. This event triggers their development into gametes, which subsequently fuse to form zygotes. Zygotes then develop into motile ookinetes, which traverse through the midgut wall, where they form oocysts. Oocysts mature to produce thousands of sporozoites, which upon release travel to the mosquito's salivary glands, ready for injection into the next host.

1.3.1 The vertebrate phase

1.3.1.1 The liver stage

Infection of the mammalian host, in the case of *P. knowlesi* either a macaque or a human, begins when a mosquito injects sporozoites into the host's dermis during a blood meal. Sporozoites are motile, extracellular forms of the parasite, which use a unique form of locomotion known as gliding motility to move through the dermis until they reach blood vessels (Amino et al., 2006). Once in the bloodstream, they are carried along until they encounter the liver, where they traverse through a layer of endothelial cells and macrophages, known as the sinusoidal wall (Pradel and Frevert, 2001; Ishino et al., 2004; Tavares et al., 2013). After sporozoites have breached this barrier, they traverse through several hepatocytes, before finally invading a hepatocyte and taking up residence within a parasitophorous vacuole (PV), a membrane-enclosed home (Mota et al., 2001).

Subsequently, the parasite then proceeds to undergo multiple rounds of asexual replication to produce large, hepatic schizonts, containing potentially thousands of merozoites: specialist blood-stage invasive forms. Once maturation is complete (6-7 days for *P. falciparum*) (Vaughan et al., 2012) the parasite's parasitophorous vacuole membrane (PVM) ruptures and the host cell membrane pinches off around groups of merozoites, forming what are known as merosomes. These packages of merozoites are released into the bloodstream, which ensures their safe passage past macrophages lining the liver sinusoids. Finally, once clear of the liver, merosomes rupture to release free merozoites into the bloodstream, which go on to invade erythrocytes, beginning the blood stage of the parasite's lifecycle (Sturm et al., 2006; Baer et al., 2007).

Importantly, for both *P. vivax* and *P. ovale*, a proportion of sporozoites instead develop into dormant, uni-nucleate forms called hypnozoites (Dembélé et al., 2014; Krotoski et al., 1982; Richter et al., 2010; Robinson et al., 2015). Hypnozoites are resistant to most antimalarial drugs and can remain quiescent within the liver for weeks, even months, depending on the specific strain involved. However, upon activation, hypnozoites develop into hepatic schizonts, which release a fresh round of merozoites into the bloodstream, causing relapsing infections, which can also be transmitted to others via mosquito bite (Dembélé et al., 2014; Adams and Mueller, 2017). As a result, relapsing

infections create a significant hurdle to elimination efforts, again highlighting the need for an effective vaccine.

1.3.1.2 The blood-stage

Disease symptoms emerge as the blood stage of the parasite's life cycle begins. Merozoites invade erythrocytes in a highly efficient manner, usually within minutes of rupturing, or egressing, from their host cells (Boyle et al., 2010b). For *P. falciparum*, egress is an explosion-like event, which may propel merozoites into fresh erythrocytes (Glushakova et al., 2005; Gilson and Crabb, 2009). Once the free merozoite encounters a new erythrocyte, invasion is governed by a series of molecular steps, which rely upon key interactions between merozoite-derived ligands and corresponding receptors on the host cell surface (Cowman et al., 2017). Importantly, this means that this step has a major role in determining host cell tropism, both in terms of host species and erythrocyte age; as if the correct host cell receptors are not available, erythrocytes can be refractory to invasion.

Once a merozoite has invaded its host cell, like the invasive sporozoite, it resides within a (PV) (Bannister et al., 1975; Aikawa et al., 1978). Over the following 24-72 hours (depending on the species) the merozoite proceeds to develop from a ring-stage parasite into a trophozoite. Finally, during a process referred to as schizogony, several rounds of asynchronous nuclear division and organelle biogenesis ensue. This is followed by the formation of individual, membrane-bound merozoites (Bannister et al., 2000). The number of merozoites produced per schizonts is also species-dependent. For instance, each *P. knowlesi* schizont can contain up to 16 daughter merozoites, while *P. falciparum* schizonts sometimes produce double this number (Cowman and Crabb, 2006; Lee et al., 2009). Finally, once a schizont has fully matured, individual merozoites escape from the erythrocyte, when first the PVM and then the host cell membrane ruptures, releasing free merozoites into the bloodstream during egress (Wickham et al., 2003; Hale et al., 2017). Notably, the window of time between egress and re-invasion is the only point within the erythrocytic cycle that the parasite is extracellular, and thus directly exposed to the host immune system. For this reason, merozoite invasion ligands are critical targets for vaccine development (Wright and Rayner, 2014; Weiss et al., 2015).

1.3.1.3 Gametocytogenesis: preparing to change host

After invasion, a small proportion of merozoites will develop into male and female gametocytes, instead of schizonts, in a process called gametocytogenesis. These are in turn taken up by another female *Anopheles* mosquito, marking the beginning of the sexual phase of the parasite's life cycle. Interestingly, the morphology and maturation time of gametocytes varies between species. *P. falciparum* gametocytes mature through five different morphological stages over 9-12 days, with the final stage taking on a crescent-shaped appearance (Hawking et al., 1971; Sinden, 1982). These mature forms are infective for several days (Smalley and Sinden, 1977). For other *Plasmodium* species, gametocytes appear to mature at a much faster rate, take on a rounder morphology, and are infective for a shorter duration. For instance, *P. knowlesi* gametocytes mature over a 30-hour period, giving rise to infectious gametocytes surviving for only a few hours (Hawking et al., 1968).

1.3.2 The mosquito phase

Once taken up in the mosquito blood meal, gametocytes are "activated" within the mosquito midgut by the lower temperature and the presence of the mosquito factor xanthurenic acid. This event triggers gametogenesis: the transformation of gametocytes into gametes (Bennink et al., 2016; Billker et al., 1997; Garcia et al., 1998). For male gametocytes, this process involves three rounds of mitotic division and the synthesis of eight flagella, to produce eight motile microgametes, which exit the host erythrocyte during exflagellation (Janse et al., 1988, 1986). Female gametocytes must also exit the host cell and begin translation of previously repressed transcripts, which are now required for fertilization steps and beyond (Mair et al., 2006).

Subsequently, male and female gametes then fuse to form a zygote, which is quickly followed by meiotic division and the differentiation of the zygote into another invasive zoite stage: the ookinete (Janse 1986; Janse 1988; Sinden, 1982). The ookinete can then escape the harsh conditions of the mosquito midgut by gliding through the blood meal to the midgut wall, after which it traverses through the midgut epithelial cells to reach the midgut basal lamina (Vlachou et al., 2004). The parasite then transforms again, this time into the stationary oocyst. Several rounds of mitotic division and organelle replication ensue, to form thousands of sporozoites in a process called

sporogony (Canning and Sinden, 1973). Finally, once released from the oocyst, individual sporozoites travel to the mosquito's salivary glands, again using gliding motility, where they remain until they are injected into a new host during another blood meal (Pimenta et al., 1994).

1.4 Combating malaria with blood-stage vaccines?

An efficacious, long-lasting vaccine has the potential to prevent severe disease and parasite transmission. Three basic categories of *Plasmodium* vaccines are being proposed. These include vaccines to target pre-erythrocytic stages (sporozoites and infected hepatocytes), blood stages (merozoites and infected erythrocytes), and finally, parasite transmission (sexual stages) (Draper et al., 2018; Beeson et al., 2019). Although a transmission-blocking vaccine would be a highly advantageous tool to curb malaria incidence, targeting the sexual stages alone would not prevent an already infected person from experiencing disease symptoms. Thus efforts over the previous decades have focused primarily on developing vaccines aimed at preventing liver and blood-stage infections: both options that in theory could also block transmission (Beeson et al., 2019).

For *P. falciparum*, the most successful pre-erythrocytic vaccine is RTS,S/AS01, the first (and only) malaria vaccine to reach stage IV clinical trials so far. This vaccine induces antibodies targeting the C-terminus of the *P. falciparum* circumsporozoite protein (PfCSP), which coats the outer surface of sporozoites (Draper et al., 2018). However, vaccination with RTS,S provides only moderate protection from clinical malaria cases, with phase III trials recording an efficacy of up to 56% in young children within the first year post-vaccination (RTS, S Clinical Trials Partnership, 2011). Additionally, immunity wanes quickly, with efficacy dropping below 30% without a booster, and below 40% even with a booster, over a 48-month follow-up period from the first vaccination (RTS, S Clinical Trials Partnership, 2015). Work to develop a more efficacious pre-erythrocytic *P. falciparum* vaccine, as well as a *P. vivax* equivalent, is currently underway (Kisalu et al., 2018; Tan et al., 2018). However, the 'leakiness' of the RTS,S vaccine highlights the need to continue to strive for a blood-stage vaccine. Even if no blood-stage antigen can induce complete protection from disease, the best candidates could still potentially be used along with sporozoite and sexual stage antigens to produce a combination vaccine: one which

targets all stages of the parasite life cycle, providing the maximum protection possible (Draper et al., 2018; Beeson et al., 2019).

1.5.1 Challenges associated with blood-stage vaccine design

Encouragingly, natural immunity to severe *Plasmodium* infections is associated with antibodies targeting blood-stage antigens (Cohen et al., 1961; Healer et al., 2018). However, the challenge going forward is to develop a vaccine that does not merely mimic this natural immunity but improves upon it. Several difficulties have hindered vaccine development efforts. Firstly, many blood-stage antigens, such as the highly expressed and immunogenic merozoite surface protein 1 (MSP1) and apical membrane antigen 1 (AMA-1), are highly polymorphic. Therefore, attempts to generate a vaccine that induces strain-transcending protection based on either of these candidates, have not been successful thus far (Ogutu et al., 2009; Sheehy et al., 2012; Thera et al., 2011). Secondly, merozoites often use highly redundant sets of ligands to achieve the same molecular goal; so targeting one particular ligand frequently results in the use of alternative ligand-receptor interactions This phenomenon is especially true for *P. falciparum* strains, which express multiple RBL and DBP members (reviewed in Tham et al., 2012). Therefore a clear understanding of invasion biology is required to determine which parasite ligands are absolutely essential for invasion. However, even if a critical ligand with highly conserved epitopes is identified, a third problem still exists: the fact that merozoites are exposed to the host immune system for a very short (1-2 min) duration (Gilson and Crabb, 2009; Boyle et al., 2010). Therefore, the ideal vaccine immunogen also needs to be able to induce high titres of protective antibodies, which can rapidly access and bind to their target antigen in an extremely efficient manner (Draper et al., 2018).

The use of structural techniques to guide vaccine design and to overcome these challenges is becoming increasingly important (Kwong, 2017). These methods involve isolating antibody-producing immune cells from human volunteers vaccinated with either attenuated whole parasites or recombinant parasite antigens and then using immunoglobulin mRNA sequences from these immune cells to express recombinant antibodies. A series of recombinant protein screens and growth inhibitory activity (GIA) assays subsequently identifies which antibodies demonstrate the best binding affinity and kinetics to target recombinant antigens as well as how successfully they

inhibit parasite growth *in vitro*. Finally, antibody-antigen complexes are examined by X-ray crystallography to identify specific epitopes bound by the best performing antibodies. Thus critical antigen residues can be considered for inclusion within a subunit vaccine, whilst residues which may be immuno-dominant but do not invoke a protective response can potentially be excluded. Such methods have been used to identify important PfCSP epitopes not featured in RTS,S, but which may be included in subsequent versions (Kisalu et al. 2018; Tan et al., 2018). Excitingly, structural based techniques are also being applied to blood-stage antigen design, including the leading *P. falciparum* vaccine candidate, PfRh5 (Alanine et al., 2019).

1.5.2 Targeting the *P. falciparum* Rh5 complex

The current leading blood-stage *P. falciparum* vaccine candidate, the reticulocyte binding protein homolog 5 (PfRh5) is an essential merozoite invasion ligand (discussed in more detail in section 1.6.2.3), which is secreted by the parasite, immediately before erythrocyte entry and just in time to interact with its host cell receptor, Basigin (Rodriguez et al., 2008; Baum et al., 2009; Crosnier et al., 2011). Once secreted to the merozoite surface, it exists as part of a complex with the *P. falciparum* Rh5-interacting protein (PfRipr) and the *P. falciparum* cysteine-rich protective antigen (PfCyRPA). Both partner proteins are also critical to invasion, although their precise functions are still being determined (Chen et al., 2011; Reddy et al., 2015).

Surprisingly, although PfRh5 is essential, it appears to be extremely well conserved among *P. falciparum* isolates and does not appear to succumb to the strong immune selection associated with many blood-stage antigens (Douglas et al., 2011; Pearson et al., 2019). In line with this, anti-PfRh5 antibodies can be detected in serum samples from patients who have experienced clinical malaria episodes, although at significantly lower levels compared to other merozoite antigens, including PfMSP1 and PfAMA-1 (Douglas et al., 2011; Tran et al., 2014). The reasons for this may be that Rh5 expression levels are significantly lower and that this ligand is exposed to the host immune system for an even shorter duration than MSP1 and AMA-1, both of which are present on the merozoite surface at an earlier point (Baum et al., 2009; Ragotte et al., 2020; Riglar et al., 2011a). Excitingly, though, phase Ia trials have shown that vaccination with full-length PfRh5 induces a much stronger Rh5-specific immune

response than is seen in the context of a natural infection. Furthermore, IgG antibodies isolated from vaccinated individuals showed promising inhibitory action against *P. falciparum* growth *in vitro*, for multiple different strains, giving hope that at last generating a blood-stage vaccine, which induces an immune response superior to natural immunity may be possible (Payne et al., 2017b). Recombinant human monoclonal antibodies, generated in a follow on study, also supported these results and demonstrated that the most potent inhibitory antibodies prevent PfRh5 from binding to its erythrocyte receptor, Basigin (Crosnier et al., 2011; Alanine et al., 2019).

Like PfRh5, PfRipr and PfCyRPA are also highly conserved and do not appear to invoke a strong immune response over the course of a natural infection (Richards et al., 2013; Partey et al., 2018; Pearson et al., 2019). To date, no human vaccination trials have been performed for either candidate. However, mouse monoclonal antibodies raised against both proteins show promising inhibitory potential, although their precise mechanisms of neutralization remain mostly unclear (Ragotte et al., 2020). Going forward, a better understanding of which epitopes are targeted by inhibitory antibodies in the context of human vaccination will provide critical information needed to develop PfRipr and PfCyRPA based vaccines. Importantly, since different combinations of antibodies targeting all three members of the Rh5 complex can have a synergistic effect, it may be that the best course of action is to include components of all three members into a single vaccine (Reddy et al., 2015; Healer et al., 2019).

1.5.3 Towards non-*falciparum* vaccines

Despite the exciting progress made over the last few years towards generating a blood-stage vaccine for *P. falciparum*, efforts to develop a *P. vivax* vaccine have lagged far behind, and the other four species infecting humans have been entirely ignored. One of the main reasons for this is because up until 2013, only *P. falciparum* asexual stages could be maintained in continuous culture. An *in vitro* culture system now also exists for *P. knowlesi*; however, the remaining four species, including *P. vivax*, still cannot be maintained long-term *in vitro* (Moon et al., 2013). Therefore, for these species, attempts to perform GIA assays, such as are routinely performed for *P. falciparum*, are difficult at best, and have traditionally been reliant upon the availability of clinical isolates (Russell et al., 2011).

Importantly, protection from *P. vivax* is associated with antibodies, which target PvDBP, the only DBP ligand expressed by this species (Miller and Carter, 1976; King et al., 2008; Cole-Tobian et al., 2009; Nicolete et al., 2016). Likewise, anti-PvDBP antibodies, purified from vaccinated animals as well as human volunteers, have been shown to inhibit the binding of recombinant PvDBP to its host cell receptor, the Duffy antigen receptor for chemokines (DARC), in protein binding assays (Moreno et al., 2008; Payne et al., 2017a; Singh et al., 2018). For these reasons, PvDBP is the lead blood-stage candidate for *P. vivax*. However, it is important to note that we still do not understand the precise role of PvDBP during invasion, or how this ligand might act in conjunction with other invasion ligands. Understanding these critical details could enable the development of multi-component vaccines, targeting sequential steps of invasion. Therefore, there is an urgent need to understand the functions of current vaccine candidates and to identify new vaccine candidates, especially for the remaining neglected species.

1.5 Erythrocyte Invasion

1.5.1 The merozoite: an invasion machine

A detailed understanding of how merozoites invade erythrocytes is critical to the development of clinical interventions, such as monoclonal therapies (Kisalu et al., 2018; Maskus et al., 2016), new drugs (Burns et al., 2019), and vaccines (Draper et al., 2018). As such, invasion has been the subject of intense research for over 60 years. At least 50 parasite-derived proteins are predicted to play a direct role during invasion (Wright and Rayner 2014). Many of these ligands (Fig 1.2) are present on the surface of the merozoite prior to egress, such as the merozoite surface proteins (MSPs). Others, however, are secreted from the merozoite's apical organelles throughout each step of invasion, so that they can interact with their corresponding erythrocyte receptors as required (Cowman et al., 2017). Others still, lying under the merozoite's plasma membrane, form the basis of the parasite's molecular motor, which drives host cell entry (Frénal et al., 2017). Unravelling the individual roles of these proteins and determining their relative importance has been challenging and is far from being entirely understood.

The merozoite is a highly polarized cell (Figure 1.2), marked by three polar rings and a collection of secretory organelles, known as the apical complex, at one end and a nucleus and endomembrane system towards the other. (Hepler et al., 1966; Aikawa, 1967, 1966; Aikawa et al., 1978; Bannister et al., 1975, 2000). These secretory organelles include the exonemes, whose contents play important roles during egress, and are therefore secreted into the PV before host cell rupture (Janse and Waters, 2007; Yeoh et al., 2007). Another class of apical organelles, the dense granules, secrete their contents after invasion is completed, in line with their proposed roles of host cell remodelling, PV development, and nutrient uptake (Torii et al., 1989; Hanssen et al., 2013; Morita et al., 2018) Finally, the rhoptries and micronemes secrete ligands the merozoite requires to attach to and invade a new host cell (Cowman et al., 2017).

Three interconnected structures are collectively responsible for the morphology and motility of all apicomplexan zoites, including merozoites. Firstly, all zoites possess a double membrane structure, the inner membrane complex (IMC), which lies directly underneath the plasma membrane (PM). (Hepler et al.,1966; Aikawa, 1966 &1967; Bannister et al., 1975). Secondly, 2-3 subpellicular microtubules are attached to the largest of the apical polar rings and run beneath the pellicle, down the longitudinal axis of the merozoite. Finally, both the pellicle and subpellicular microtubules are connected via an intermediate network of filamentous proteins making up the merozoite cytoskeleton, known as the subpellicular network (SPN) (Bannister and Mitchell, 1995; Mann and Beckers, 2001; Tremp et al., 2014). Notably, the space between the PM and IMC houses the parasite's acto-myosin motor, which the merozoite uses to actively drive itself into the host cell by a mechanism referred to as gliding motility (reviewed in Frenal et al., 2017, and discussed in more detail in section 1.5.3).
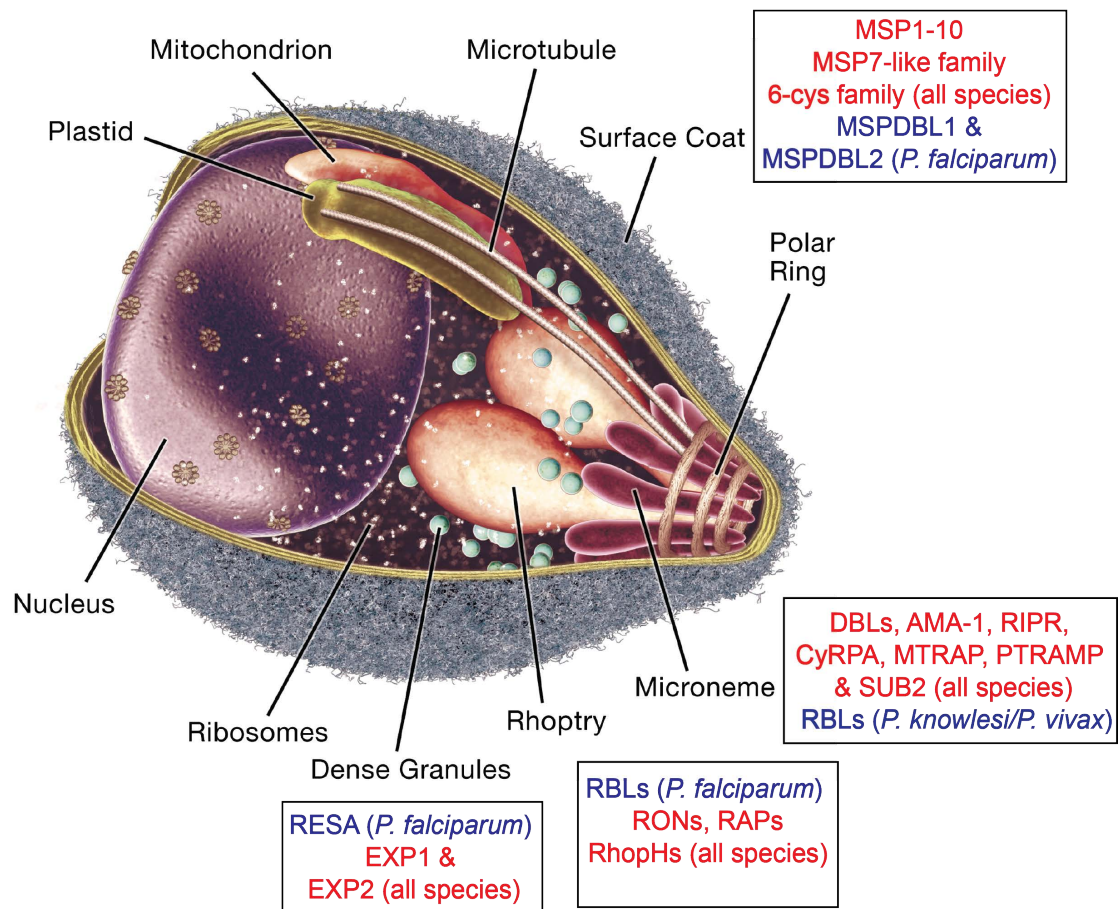
Figure 1.2. The *Plasmodium* merozoite (Adapted from Cowman and Crabb, 2006). The invasive form of the blood stages, the merozoite, is a polarized cell, containing an apical complex and specialized secretory organelles (rhoptries, micronemes, and dense granules) at one end, and a nucleus and endo-membrane system towards the other. While proteins making up the merozoite's "fuzzy" surface coat may mediate the initial, weak host cell interactions, ligands released from the secretory organelles govern subsequent steps required for host cell selection, moving junction formation, and internalisation. Secretory organelles are hypothesized to release their contents in an orderly manner, exposing ligand subsets only as required for specific roles, and thus protecting them from the host immune system (Harvey et al., 2012).

1.5.1.1 The rhoptries

Each merozoite possesses two club-shaped rhoptries (Figure 1.3), which have a narrow 'neck' region facing towards the merozoite apex, and a wider 'bulb' region at the opposite end (Hepler et al., 1966; Aikawa, 1966 & 1967; Bannister 1975). These large, electron-dense organelles were first implicated in invasion when it was discovered that their contents appeared to be secreted during red cell entry, a process marked by a reduction in electron density and total organelle volume as invasion

progresses (Bannister et al., 1975; Hanssen et al., 2013). Furthermore, when invasion is stalled by the addition of cytochalasin D, a potent inhibitor of actin polymerisation, membranous whorls, which might ordinarily contribute to the expansion of the PVM, are extruded from the merozoite into the erythrocyte as small vacuoles (Bannister et al., 1986; Hanssen et al., 2013; Miller et al., 1979). A rhoptry bulb protein, RAP1, has since been localized to these whorls, supporting the hypothesis that they are at least in part, rhoptry derived (Riglar et al., 2011).

Many molecular studies aimed at characterizing rhoptry contents have followed these early investigations. For *P. falciparum*, proteins predicted to be involved in host cell selection, such as the RBL ligands (also called the reticulocyte binding like homologs/Rh ligands) are localized to the extremities of the rhoptry necks. Next, the rhoptry neck (RON) proteins, several of which play a role in moving junction formation, lie posterior to the RBLs, but still within the rhoptry necks (Duraisingh et al., 2003a; Zuccala et al., 2012). Finally, rhoptry proteins responsible for the later steps of invasion, the formation of the PV as entry progresses, and even during subsequent parasite development, are localized to the rhoptry bulb (Richard et al., 2010; Riglar et al., 2011b; Zuccala et al., 2012; Sherling et al., 2017; Ghosh et al., 2017). So overall, it appears that rhoptry proteins are organized spatially so that they can be secreted just in time to perform their respective roles (Zuccala et al., 2012). However, exceptions to this rule exist, such as PfRON12, which is localized to the rhoptry neck, but secreted post invasion. Thus it does not play a role during the early steps of invasion, as might have been predicted by its localization (Knuepfer et al., 2014). Although membranous 'whorls' have also been observed within the rhoptries (Bannister et al., 1986), no clear membrane divisions between different regions of the rhoptries have been established. Thus, it is not clear how rhoptry organization is achieved, or how a specific ligand could be withheld, while others are simultaneously secreted. At the commencement of invasion, it has been proposed that both rhoptries are fused together, to form one organelle (Hanssen et al., 2013). From this point, the now single rhoptry tip appears to be continuous with the merozoite's plasma membrane, exposing internal rhoptry contents to the merozoite surface (Hanssen et al., 2013). However, it is not clear what the significance of merging both rhoptries is, or whether any protein secretion commences from individual rhoptries before this fusion event.
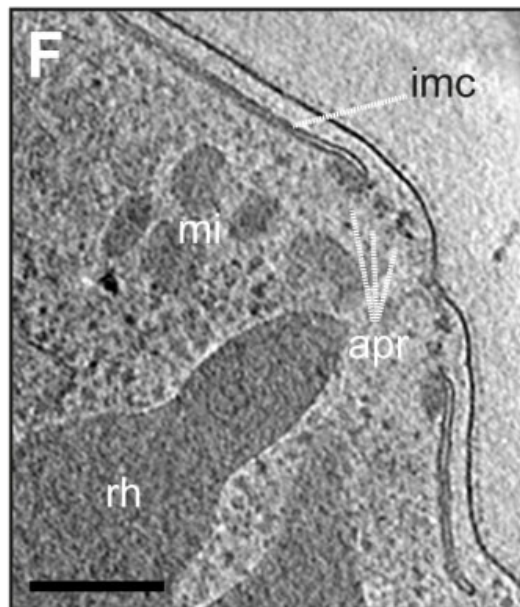
Figure 1.3. The apical organelles of Plasmodium merozoites (Adapted from Hanssen *et al.*, 2013). A computational section through the merozoite's apical tip taken with cryo-electron tomography. Large rhoptries (rh) are surrounded by smaller micronemes (mi). Also depicted are the merozoite's inner membrane complex (imc) and apical rings (apr). Scale bar is 200nm.

1.5.1.2 The micronemes

Surrounding the rhoptries are up to 40, smaller, tear-drop shaped micronemes (Figure 1.3) (Bannister et al., 2003). Micronemal ligands perform a variety of roles (reviewed in Cowman et al., 2017), some of which overlap functionally or act in conjunction with rhoptry neck proteins. Significant examples include the DBP ligands, also proposed to be involved in host cell selection, as well as apical membrane antigen 1 (AMA-1), a critical component of the moving junction (Lee Sim et al., 1992; Adams et al., 1990; Healer et al., 2002).

Like the rhoptries, the mechanism of micronemal secretion is not entirely clear. The tips of micronemes and rhoptries are often seen to be in close contact at the merozoite apex. So one hypothesis is that secretion may occur via the rhoptries, by micronemes fusing with and secreting their contents into the rhoptry tips (Bannister et al., 2003). However, no data, even from a more recent study of invasion utilizing 3D electron tomography, has been able to confirm this theory (Hanssen et al., 2013). Additionally, another study exploring apical secretion by the related apicomplexan parasite, *Toxoplasma gondii*, showed that micronemal secretion could occur independently of rhoptry secretion, in genetic mutants with mis-localised rhoptries (Mueller et al., 2013). So an alternative theory is that *Plasmodium* micronemes simply release their contents by directly fusing with the plasma membrane. However, if this is the case, is there an order to microneme and rhoptry secretion, or can both organelle classes be secreted concurrently?

Whether micronemal secretion might lead to rhoptry secretion or vice versa is a hotly debated topic. For instance, one study showed that secretion of a key *P. falciparum* DBP ligand, PfEBA-175 from the micronemes is triggered at egress by a complex Ca^{2+} signalling cascade and that the subsequent interaction of EBA-175 with its RBC receptor, glycophorin A, triggers the release of PfRh2b, an RBL ligand from the rhoptry neck (Singh et al., 2010). However, conflicting studies demonstrated at least partial secretion of the micronemal ligand, PfAMA-1, pre-egress (Treeck et al., 2009; Riglar et al., 2011) and that PfEBA-175 release was not triggered by egress, but rather by the binding of another rhoptry RBL ligand, PfRh1, to its RBC receptor (Gao et al., 2013).

An additional interesting note is that, unlike their *P. falciparum* counterparts, the *P. knowlesi* and *P. vivax* RBL homologs are not localized to the rhoptries, but are instead localized to the micronemes (Meyer et al., 2009; Han et al., 2016). Thus for both of these species, the RBL and DBL ligands may be released at the same time, from the same set of organelles, in line with their predicted roles as mediators of host cell selection and the steps leading up to moving junction formation. However, if like their *P. falciparum* homologs these two families are released in a specific order relative to each other, an alternative explanation could be that merozoites may contain sub-populations of micronemes, which are released sequentially.

T. gondii tachyzoites appear to produce micronemal subsets, as do *Plasmodium* sporozoites (Arredondo et al., 2018; Kremer et al., 2013). Indeed, evidence for micronemal sub-populations in *P. falciparum* is growing (Hans et al., 2013) and could explain the early release of PfAMA-1, relative to PfEBA-175 (Riglar et al., 2011). Dual immuno-EM labelling of AMA-1 and EBA-175 in *P. falciparum* schizonts also lends support to this theory. Healer et al. (2002) showed that the majority of micronemes within a given schizont contained either EBA-175 or AMA-1, but rarely both antigens together. So, regardless of whether EBA-175 secretion occurs before or after rhoptry neck proteins, physical separation of both micronemal proteins could at least explain their different secretion profiles. Furthermore, EM tomograms depicting merozoites caught at various stages of invasion show the presence of individual micronemes throughout invasion, which could indicate that micronemes are secreted in several waves (Hanssen et al., 2013).

So overall, despite the extensive research into the composition of microneme and rhoptry contents, as well as the timing and order of their release, many questions remain unanswered. However, a carefully orchestrated sequence of secretion events is thought not only to underpin each mechanical step of invasion but also to prevent critical invasion ligands from being exposed to the host immune system any longer than necessary (Harvey et al., 2012; Cowman et al., 2017). Therefore, a greater understanding of secretion will aid our understanding of the individual roles of invasion ligands.

1.5.2 An overview of the molecular steps of invasion

Both live microscopy and electron microscopy have been fundamental in revealing the overall mechanics of invasion (Aikawa et al., 1978; Miller et al., 1979; Dvorak et al., 1975; Gilson and Crabb, 2009; Yahata et al., 2012; Weiss et al., 2015). The very first video microscopy study detailing these events featured *P. knowlesi* merozoites and showed that invasion begins with weak, reversible contact between parasite and host cell along any point of the merozoite. Subsequently, stronger interactions are formed, causing "waves of deformation" along the surface of the RBC, that in many instances result in the RBC completely wrapping around the merozoite (Dvorak et al., 1975; Gilson and Crabb, 2009). Either during this phase or potentially just after, the parasite re-orientates itself, so that its apical end is in contact with the RBC (Aikawa et al., 1978; Dvorak et al. 1975; Gilson and Crabb, 2009). Electron micrographs by Aikawa et al. (1978) showed that next, an electron-dense interface, subsequently called the moving junction, forms between parasite and host cell (Figure 1.4). After these preparatory steps, the merozoite proceeds to enter the host cell, through an invagination of the erythrocyte membrane. As it does so, the moving junction travels back across the merozoite until entry is complete, the host cell is re-sealed, and the merozoite is engulfed within a PV (Aikawa et al., 1978). Finally, the erythrocyte membrane shrivels and shrinks, forming spicules, in a step called echinocytosis. However, this phase is temporary and within minutes the erythrocyte returns to its original morphology, marking the end of invasion (Dvorak et al., 1975; Gilson and Crabb, 2009). Since these early studies, great effort has focused on understanding the molecular events underlying each morphological step of invasion, described in more detail below.
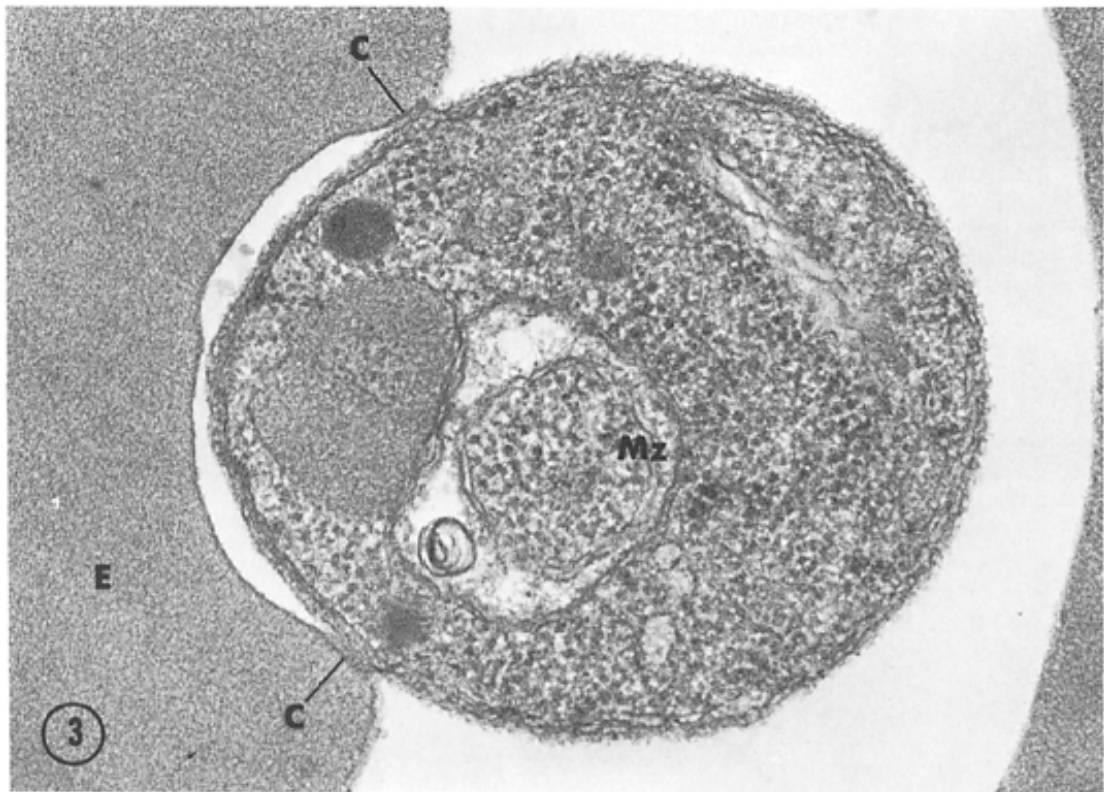
Figure 1.4 Electron micrograph showing moving junction progression (taken from Aikawa et al. 1978) Merozoite invasion of RBCs proceeds after the formation of a circular interface between parasite (marked 'Mz') and host cell, called the moving junction (marked 'C'). This electron dense structure travels across the parasite throughout invasion and seals the parasite into a parasitophorous vacuole upon closure, when invasion is complete.

The early, reversible contacts between parasite and host cell may be mediated by the Merozoite Surface Proteins (MSPs), which are associated with the merozoite surface membrane (Aikawa et al., 1978; Holder and Freeman, 1984; Lin et al., 2014; Weiss et al., 2015). MSP1 is the most abundant protein found on the merozoite surface, appearing by EM as a 'fuzzy coat' that decorates the parasite's plasma membrane (Holder and Freeman, 1982). PfMSP1 may bind to either Band 3 or glycophorin A on the erythrocyte surface (Baldwin et al., 2015; Goel et al., 2003). Additionally, PfMSP1 has been shown to interact with heparin-like molecules, a hypothesis that is supported by live microscopy showing that *P. falciparum* merozoites cannot invade host cells in the presence of heparin (Boyle et al., 2010a). However, a more recent study produced a functional KO of PfMSP1 for the first time and demonstrated that these parasites can still invade host erythrocytes without surface-bound PfMSP1 (Das et al., 2015). Surprisingly, PfMSP1 instead plays a critical role during egress, potentially by interacting with spectrin to destabilize the host cell cytoskeleton. So while MSP1 may

still play a helpful, but non-essential role during invasion, in an unexpected turn of events, the surface localization of PfMSP1 is instead vital for egress.

Following weak binding, the merozoite must then form a series of stronger interactions with the host cell, committing itself to invasion. The interactions between the Duffy binding like (DBP) and Reticulocyte binding like (RBL) proteins with their respective host cell receptors (discussed extensively in section 1.5.4) are predicted to perform this role and align the merozoite for host cell entry (Weiss et al., 2015). However, for *P. falciparum* one atypical RBL ligand lacking a transmembrane domain, PfRH5, is predicted to act downstream of the other RBL/DBP ligands. Once secreted from the rhoptry neck, this essential protein forms a complex with The *P. falciparum* Cysteine-Rich Protective Antigen (PfCyRPA) and the *P. falciparum* Rh5-interacting protein (PfRipr), before binding to its host cell receptor, Basigin (Hayton et al., 2008; Baum et al., 2009; Chen et al., 2011; Reddy et al., 2015). Recent work has shown that this complex is likely required for a merozoite-host cell fusion event indicative of rhoptry secretion (Weiss et al., 2015; Volz et al., 2016). This phenomenon can be visualized by pre-loading erythrocytes with a fluorescent calcium-sensitive dye, Fluo-4-AM (Weiss et al., 2015). Several seconds before internalization ensues, a punctate calcium signal can be observed at the merozoite's apex, indicating that merozoite derived calcium, likely stemming from secretion of the calcium rich rhoptries, is coming into contact with the dye from the erythrocyte cytosol. Thus, the PfRh5 complex likely acts just before the formation of the moving junction.

Junction formation begins when the merozoite secretes rhoptry neck proteins, RON2, RON4, and RON5 into the erythrocyte, where they assemble as a complex, associated with the erythrocyte membrane (Alexander et al., 2006; Cao et al., 2009; Lamarque et al., 2011; Richard et al., 2010b; Riglar et al., 2011a; Srinivasan et al., 2011). Studies using *T. gondii* tachyzoites as a model for host cell invasion have shown that TgRON2 is inserted into the erythrocyte membrane, while TgRON4 and TgRON5 localise to the cytosolic face of the erythrocyte membrane, where they potentially interact with RON2, anchoring it to the underlying host cell cytoskeleton (Lamarque et al., 2011; Straub et al., 2011; Takemae et al., 2013). Once associated with the erythrocyte membrane, both membrane-embedded PfRON2 and TgRON2 act as receptors for their respective AMA-1 homologs. PfAMA-1 binding to PfRON2 forms the nascent

junction, effectively beginning the next phase of invasion: internalisation (Lamarque et al. 2011; Srinivasan et al., 2011).

During internalisation, the merozoite actively drives itself into an invagination of the RBC membrane, which becomes the PV, using a molecular motor (Aikawa et al., 1978; Baum et al., 2006b). As invasion progresses, several rhomboid-like and subtilisin-like proteases mediate shedding of merozoite surface proteins, as well as trans-membrane adhesive ligands secreted from the apical organelles to the merozoite surface (Baker et al., 2006; Harris et al., 2005; O'Donnell et al., 2006). Cleavage events likely release AMA-1, as well as other junction/motor associated ligands from their respective host cell receptors as the moving junction sweeps across the merozoite's body, thus enabling smooth passage into the host cell. Additionally, proteolytic cleavage may aid the re-sealing of the host cell membrane, and the release of the PVM enclosed parasite into the erythrocyte so that it can continue its development into a ring-stage parasite. Recently the subtilisin-like protease, SUB2, which cleaves the ectodomains of MSP1, AMA-1, and PTRAMP from the merozoite surface, has been implicated in this process (Harris et al., 2005; Green et al., 2006b). Conditional PfSUB2 knockout parasites exhibit a severe invasion phenotype, where although some parasites can enter erythrocytes, host cells soon lyse, sometimes ejecting merozoites in the process (Collins et al., 2020). Thus protease-mediated shedding also appears to be an important step for host cell re-sealing, and the presence of bulky, un-processed ligands at the 'end' of the junction may hinder this process.

1.5.3 Powering invasion and motility

Gliding motility is a unique form of movement by which apicomplexan zoites travel in a polarized fashion across cellular surfaces without any obvious morphological changes, such as the extension of pseudopodia, or use of cellular projections, such as cilia or flagella (Frenal et al., 2017). Gliding has perhaps been best described for *T. gondii* tachyzoites and *P. berghei* sporozoites, both of which exhibit helical motion in 3D environments (Bichet et al., 2014; Håkansson et al., 1999; Kudryashev et al., 2012; Vanderberg, 1974). Video microscopy of invading *T. gondii* tachyzoites shows that invasion also progresses by this corkscrew-like motion (Bichet et al., 2014; Pavlou et al., 2018). Importantly, treatment of both sporozoites and tachyzoites with either cytochalasin D, which inhibits actin polymerization, or butanedione monoxime, a

myosin inhibitor, stalls both extracellular motility and host cell invasion, suggesting that both events are driven by an acto-myosin based motor (Ryning and Remington, 1978Stewart et al., 1986; Dobrowolski et al., 1997; Håkansson et al., 1999; Matuschewski et al., 2001).

Later work discovered that the components of this motor, collectively called the "glideosome", are localized to the space between the parasite's IMC and plasma membrane (Figure 1.5) and are generally conserved between apicomplexan zoites, including merozoites (Opitz and Soldati, 2002; Baum et al., 2006b; Frenal et al., 2017). According to the linear motor model (Figure 1.5), gliding is a substrate-dependent process. Transmembrane micronemal ligands are secreted at the apical end of the zoite, where they bind to receptors on the surface of the host cell via their ectodomains while connecting to the acto-myosin motor through their cytoplasmic tails (Frenal et al., 2017). Subsequently, MyoA engagement with actin pulls both actin and the receptor bound-ligand rearwards and in the process, drives the zoite forwards. Finally, the external domains of surface-bound ligands are cleaved by parasite-derived proteases, thus disengaging them from their host cell receptors (Harris et al., 2005; O'Donnell et al., 2006; Baker et al. 2006; Frenal et al., 2017). Importantly, deletion of key motor components, including PfMyoA (Robert-Paganin et al., 2019), PfGAP45 (Perrin et al., 2018), and PfACT1 (Das et al., 2017), completely inhibits *P. falciparum* merozoites from invading host erythrocytes, demonstrating the essentiality of the acto-myosin motor for erythrocyte invasion, even though merozoites are not thought to glide across extra-cellular surfaces (Baum et al., 2006b). However, very interestingly, studies examining mutant *T. gondii* parasites show that although deletion of multiple motor components, including the non-redundant TgACT1, severely impairs parasite motility, KO parasites still exhibit a residual capacity for extracellular gliding and invasion (Andenmatten et al., 2013; Egarter et al., 2014; Bichet et al., 2016; Whitelaw et al., 2017). These results suggest that while on the whole, the acto-myosin motor is incredibly important; it may not be the only contributor to parasite motility.

One such alternative mechanism, predicted to act synergistically with the acto-myosin motor, is the fountain model, which involves a retrograde flow of membrane and micronemal proteins from the apical to the basal end of the zoite, independently of motor function, followed by recycling of membrane and adhesins by endocytosis (Gras et al., 2019). This hypothesis is supported by studies showing that nano-beads bound

to parasite surfaces are trans-located to the basal end of the zoite (also known as "capping") regardless of treatment with cytochalasin D, or the deletion of motor complex members, demonstrating that a continuous, retrograde membrane flow occurs without the aid of a molecular motor (Quadt et al., 2016; Whitelaw et al., 2017). However, without a functioning motor, zoites struggle to attach to surfaces, and therefore fail to generate the force required for efficient movement. Thus it appears that both the apicomplexan zoite's motor and a secretory-endocytosis cycle may together drive motility (Gras et al., 2019).

Currently, it is not clear which adhesive ligands mediate merozoite motility. *Plasmodium* sporozoites and ookinetes and *Toxoplasma* tachyzoites all rely on members of the TRAP family, binding to as of yet, unknown receptors (Frenal et al., 2017). *Plasmodium* merozoites also express a TRAP homolog, merozoite TRAP (MTRAP), in addition to a TRAP-like ligand, the *Plasmodium* thrombospondin related apical merozoite protein (PTRAMP) (Thompson et al., 2004; Baum et al., 2006b). However, MTRAP appears to be dispensable for the asexual stages, and no clear link between PTRAMP and the merozoite motor has been demonstrated yet (Bargieri et al., 2016; Diaz et al., 2016). Another prominent theory is that the cytoplasmic tail of AMA-1 interacts with actin, either directly or indirectly, and thus links the moving junction with the molecular motor, providing traction for entry (Cowman et al., 2017). As invasion progresses, the RON2/AMA-1 interface between merozoite and host cell appears to progress rearwards over the zoite body (Riglar et al., 2011). A ring of actin also travels over the parasite, closely following this junction, and supporting the theory that the two may be connected (Riglar et al., 2011; Angrisano et al., 2012). Additional studies around the same time pointed to both TgAMA-1 and PfAMA-1, as well as several Tg/PfTRAP proteins connecting to actin via an intermediate, actin binding protein, aldolase (Jewett and Sibley, 2003; Sheiner et al., 2010; Srinivasan et al., 2011;
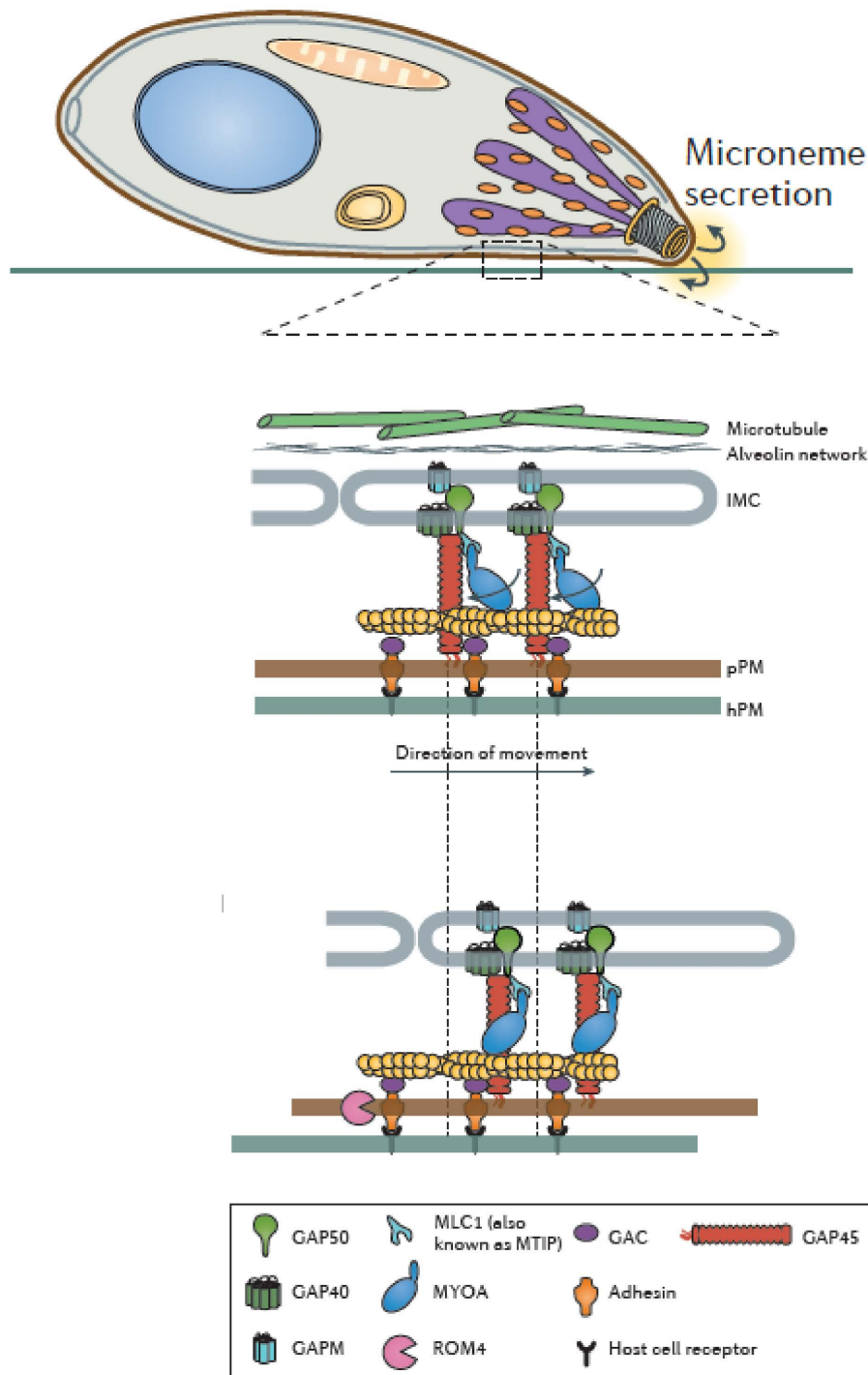
Figure 1.5 Gliding motility of apicomplexan zoites (Adapted from Frenal et al., 2017) Zoite motility (including *T. gondii* tachyzoites, pictured above) involves the coordinated interaction between transmembrane adhesins, secreted from the micronemes to the merozoite surface, and the zoite's molecular motor, localized beneath the parasite's plasma membrane. Micronemal adhesins, such as members of the TRAP family of ligands, bind to host cell receptors via their ecto-domains, while at the same time connecting to the motor through their cytoplasmic tails. While the exact topology and arrangement of motor components is still debated, a leading theory is that MyoA is anchored to the IMC through several glideosome-associated ligands. Engagement of the MyoA head with filamentous actin drags the adhesin-bound actin backwards, and the zoite forwards. Adhesins are subsequently disengaged from their respective receptors by the action of rhomboid-like proteases, releasing their ecto-domains into the culture supernatant.

Diaz et al., 2016). However, since these findings, it has been shown that aldolase is not required for *T. gondii* invasion of host cells (Shen and Sibley, 2014). TgMIC2, a *T. gondii* TRAP homolog, may instead connect to the motor via the glideosome-associated connector (GAC), another actin binding protein. However, so far, no data has been published regarding whether Tg/PfAMA-1 follows suit (Jacot et al., 2016). Therefore, the questions of which ligands drive internalization, and how the acto-myosin motor may be connected to the moving junction remain open for debate.

1.5.4 The RBL and DBP ligands

The molecular steps of invasion preceding PfRh5-Basigin interactions and junction formation are considerably less well defined. For *P. falciparum,* members of the RBL and DBP families are hypothesized to facilitate erythrocyte deformation and merozoite re-orientation (Weiss et al., 2015). However, although these families are conserved across all malaria parasite species, significant redundancy within and possibly between the two families has hampered dissection of their roles.

The *P. knowlesi* Duffy binding protein alpha (PkDBPα) was the first DBP member to be identified, followed by its closely related *P. vivax* ortholog, PvDBP (Haynes et al., 1988; Wertheimer and Barnwell et al., 1989). Importantly, both PkDBPα and PvDBP bind to the Duffy antigen receptor for chemokines (DARC receptor) on the surface of RBCs, a step that is required for invasion and that limits the proliferation of these two species to growth in Duffy positive erythrocytes (Miller et al., 1975; Haynes et al., 1988; Wertheimer and Barnwell, 1989). Binding to DARC occurs via a shared 5' cysteine-rich region, later termed the 'Duffy binding like' or DBL domain when homologous sequences were identified in *P. falciparum* and *P. yoelii* invasion ligands, all of which bind to a variety of additional host cell receptors (Fang et al., 1991; Adams et al., 1992; Prasad et al., 2003). So as the nomenclature implies, DBP family members contain at least one DBL domain, with some *P. falciparum* members possessing two domains. Additionally, DBP ligands also generally share a signal peptide, a C-terminal cysteine-rich domain of unknown function as of yet, a single transmembrane domain, and a short cytoplasmic tail (Adams et al., 1992; Tolia et al., 2005). Interestingly, each human *Plasmodium* species expresses a differing number of DBP ligands. So, for instance, while *P. vivax* expresses a single DBP ligand (PvDBP), *P. knowlesi* expresses three DBPs (PkDBPα, PkDBPβ, and PkDBPγ), and *P.*

falciparum parasites can express up to four members (EBA-175, EBA-140, EBA-181, and EBL-1) (Cowman et al., 2017; See Table 1.1 for abbreviations and individual references).

Table 1.1. The Duffy binding like protein (DBP) homologs of *P. falciparum*, *P.vivax*, and *P. knowlesi*

Ligand	Erythrocyte Receptor	References
P. falciparum (Erythrocyte binding antigen/ligand, PfEBA/EBL)		
EBA-175	Glycophorin A (GPA)	Camus and Hadley, 1985; Lee Sim et al., 1992
EBA-140	Glycophorin C (GPC)	Adams et al., 2001; Lobo et al., 2003
EBA-181	Unknown	Adams et al., 2001
EBL-1	Glycophorin B (GPB)	Peterson and Wellems, 2000; Mayer et al., 2009
P. vivax (Duffy binding protein, PvDBP)		
PvDBP	Duffy antigen for chemokines (DARC)	Wertheimer and Barnwell et al., 1989; Barnwell et al., 1989
P. knowlesi (Duffy Binding Protein, PkDBP)		
DBPa	Duffy antigen for chemokines (DARC)	Miller et al., 1975; Haynes et al., 1988
DBPb	Unknown	Adams et al., 1990
DBPy	Unknown	Adams et al., 1990

The importance of PvDBP-DARC (or PkDBPα-DARC) interactions cannot be understated. Within human populations, DARC expression on the surface of erythrocytes is determined primarily by two co-dominant alleles, FY*A, and FY*B, encoding the Fya and Fyb antigens, respectively. However, a single mutation within the promoter region of the FY*B allele (FY^{ES}) severely reduces the expression of this receptor, and individuals who possess two mutant copies (FY^{ES}/FY^{ES}) are described as "Duffy negative" (Tournamille et al., 1995). For many years, the prevailing view has been that Duffy negative individuals are completely protected from *P. vivax* and *P. knowlesi* infections. Indeed, from a clinical standpoint, this is very apparent, as *P. vivax* infections in Sub-Saharan Africa, where the prevailing genotype is reported to be FY*B^{ES}/FY*B^{ES}, are virtually non-existent (Miller et al., 1976; Howes et al., 2011). However, more recently, asymptomatic cases of *P. vivax*, as well as very rare instances of symptomatic cases, have been reported for Duffy negative individuals living within

mixed Duffy populations (Cavasini et al., 2007; Ménard et al., 2010; Woldearegai et al., 2013; Lo et al., 2019). Although these parasites may indeed rely on alternative molecular invasion pathways yet to be determined (Popovici et al., 2020), another explanation is that a subset of very young reticulocytes from Duffy negative individuals is capable of expressing lower, but significant levels of DARC as compared to their Duffy positive counterparts. So, this small subset of cells may support even more restricted parasite replication in Duffy negative individuals, leading to mostly asymptomatic infections, which are not detected outside of active screening measures (Dechavanne et al., 2018). It is still unclear, though, whether the very low parasitaemias resulting from these infections could support transmission. Thus the hypothesis that *P. vivax* and *P. knowlesi* transmission appears to be severely restricted in populations where the Duffy negative phenotype prevails, likely still holds true.

The first RBL proteins were identified in *P. vivax* and were found to bind specifically to reticulocytes, hence the family name that has come to include orthologs from additional species, some of which do not bind to reticulocyte specific receptors but instead mediate invasion of normocytes (Galinski et al., 1992; Tham et al., 2012; Chan et al., 2020). The sequences of different RBL members vary considerably between species, both at a nucleotide level and amino acid level. However, most RBL genes share a similar structure including a short exon encoding a signal peptide, followed by a much longer exon, encoding an RBC binding domain towards the N-terminus of the protein, and a single C-terminal transmembrane domain followed by a short cytoplasmic tail (Chan et al., 2020). Like the DBPs, the number of RBLs human *Plasmodium* species express varies considerably (See table 1.2). *P. knowlesi* expresses two RBL ligands, the normocyte binding proteins (NBPXa and NBPXb), while *P. vivax* expresses five full-length reticulocyte binding proteins (PvRBP1a, PvRBP1b, PvRBP2a, PvRBP2b, and PvRBP2c), and *P. falciparum* can express up to five reticulocyte binding like homologs (PfRh1, PfRh2a, PfRh2b, PfRh4, and PfRh5) (Cowman et al., 2017; Chan et al., 2020; See Table 1.2 for abbreviations and individual references).

Importantly, for *P. vivax* the interactions of its RBL ligands with reticulocyte specific receptors, such PvRBP2b binding to TfR1 (Transferrin receptor 1), limit this species to growth in reticulocytes (Gruszczyk et al., 2018). Practically speaking, this means that *P. vivax* infections rarely achieve parasite densities in the peripheral blood that are

comparable to those reached by unchecked *P. falciparum* parasites, which can use their RBL ligands to proliferate in normocytes (Lim et al., 2016; Malleret et al., 2014). As a result*, P. vivax* disease symptoms are typically, although not always, milder than those seen for *P. falciparum*. Thus the RBL ligands are important determinants of host cell tropism and key moderators of parasite virulence. Most research addressing the molecular functions of the RBL/DBL families has been performed in the context of *P. falciparum*.

Table 1.2. The reticulocyte binding like (RBL) homologs of *P. falciparum*, *P.vivax*, and *P. knowlesi*

Ligand	Erythrocyte Receptor	References
P. falciparum (<u>R</u>eticulocyte binding like <u>h</u>omolog, PfRh)		
Rh1	Unknown	Rayner et al., 2001
Rh2a	Unknown	Rayner et al., 2000
Rh2b	Unknown	Rayner et al., 2000
Rh4	Complement receptor 1 (CR1)	Kaneko et al., 2002; Tham et al., 2010
Rh5	Basigin	Baum et al., 2009; Crosnier et al., 2011
P. vivax (<u>R</u>eticulocyte <u>b</u>inding <u>p</u>rotein, PvRBP)		
PvRBP1a	Unknown	Galinski et al., 1992
PvRBP1b	Unknown	Carlton et al., 2008
PvRBP2a	Unknown	Carlton et al., 2008
PvRBP2b	Transferrin receptor 1 (TfR1)	Carlton et al., 2008; Gruszczyk et al., 2018
PvRBP2c	Unknown	Galinski et al., 1992
P. knowlesi (<u>N</u>ormocyte <u>B</u>inding <u>p</u>rotein, PkNBP)		
NBPXa	Unknown	Meyer et al. 2009
NBPXb	Unknown	Meyer et al. 2009

Most research addressing the molecular functions of the RBL/DBL families has been performed in the context of P. falciparum. Simultaneously inhibiting the majority of PfRBL/DBP-receptor interactions prevents the formation of the moving junction between merozoite and host cell (Riglar et al., 2011). Additionally, video microscopy shows that under these conditions, parasites cannot deform host cells (Weiss et al., 2015; Tham et al., 2015). Therefore, the *P. falciparum* RBL and DBP families are hypothesized to be required for deformation, and potentially also re-orientation. However, determining the individual roles of each RBL and DBP protein has been challenging, as all of the *P. falciparum* members can be disrupted individually, except for the atypical RBL, PfRh5. Unlike the other RBL family members, this ligand is

soluble, lacks a transmembrane domain, and acts downstream of deformation (Duraisingh et al., 2003a; Duraisingh et al., 2003b; Gilberger et al., 2003; Maier et al., 2003; Stubbs et al., 2005; Weiss et al., 2015). Since none of the remaining RBL/DBL proteins are essential in their own right, a high level of redundancy is thought to exist within each family. This is further illustrated by the fact that not every *P. falciparum* strain expresses every member of each family (Thompson et al., 2001; Stubbs et al., 2005; Triglia et al., 2005; Duraisingh et al., 2003a; See table 1.3).

Table 1.3. Expression patterns of RBL and DBP members vary between *P. falciparum* strains

Ligands	*P. falciparum* strains					
	3D7	**W2mef**	**D10**	**T994**	**7G8**	**References**
Rh1	Yes (low)	Yes	Yes (low)	Yes	Yes	Rayner et al., 2000; Duraisingh et al., 2003a/b; Triglia et al., 2005
Rh2a	Yes	Yes	Yes	No	Yes	Rayner et al., 2000; Durasingh et al., 2003a/b; Triglia et al., 2005;
Rh2b	Yes	Yes	No	No	Yes	Rayner et al., 2000; Duraisingh et al., 2003a/b; Triglia et al., 2005;
Rh4	Yes	No	Yes	Yes	Yes	Stubbs et al., 2005; Baum et al., 2005; Tham et al., 2011
Rh5	Yes	Yes	Yes	Yes	Yes	Baum et al., 2009
EBA-175	Yes	Yes	Yes	Yes	Yes	Lee Sim et al., 1992; Durasingh et al., 2003; Tham et al., 2011;
EBA-140	Yes	Yes	No	?	Yes	Thompson et al., 2001; Maier et al., 2009;
EBA-181	Yes	Yes	Yes	?	Yes	Gilberger et al., 2003; Maier et al., 2009; Baum et al., 2005
EBL-1	No	Yes	Putative	?	Putative	Peterson and Wellems, 2000; Cowman et al., 2017

Furthermore, redundancy may also exist between the two families, potentially acting as a failsafe mechanism and allowing the parasite to achieve the same goals via alternative molecular pathways if one particular invasion pathway is unavailable (Weiss et al., 2015; Cowman et al., 2017). This is evident in studies of *P. falciparum* invasion into enzyme-treated erythrocytes that have been stripped of specific invasion receptors (Dolan et al., 1990). For instance, PfW2mef parasites ordinarily rely on the EBA proteins, particularly EBA-175 binding to its host cell receptor, Glycophorin A (GPA), to invade host erythrocytes (Duraisingh et al., 2003b; Stubbs et al., 2005). However, treatment of erythrocytes with neuraminidase strips them of the EBA (and PfRh1) receptors, while leaving the remaining PfRh receptors unscathed (Sim et al., 1994; Mayer et al., 2001; Rayner et al., 2001; Duraisingh et al., 2003a; Gilberger et al., 2003; Stubbs et al., 2005; DeSimone et al., 2009; Mayer et al., 2009). Initially, W2mef parasites exhibit very poor growth in neuraminidase treated cells. However, after a prolonged period of slow growth, PfW2mef parasites do eventually adapt to efficiently invade these cells (Dolan et al., 1990). Close examination of adapted parasites reveals that they significantly up-regulate their expression of PfRh4, which enables them to achieve replication rates in treated cells comparable to those seen in untreated cells. Similarly, deletion of EBA-175 in the W2mef background also results in up-regulation of PfRh4, even when parasites are grown in untreated RBCs. Therefore, it appears that PfRh4 can directly complement PfEBA-175 in this strain, demonstrating that at least these two proteins may perform overlapping functions (Dolan et al., 1990; Duraisingh et al., 2003b; Stubbs et al., 2005; Gaur et al., 2006).

However, it remains unclear whether all *P. falciparum* RBL/DBPs perform entirely complementary roles, functioning additively together to enhance overall invasion efficiency, or whether some members may perform unique functions, even on top of shared roles. For instance, deletion of either PfRh2a or PfRh2b in the adapted W2mef background results in a small, but significant reduction in invasion efficiency into neuraminidase treated erythrocytes compared to the parental line, indicating that each protein does likely play at least a minor role under these conditions (DeSimone et al., 2009). However, W2mef Rh4 KO parasites cannot adapt to growth in neuraminidase treated RBCs, which suggests that even the combined action of PfRh2a and PfRh2b cannot compensate for the loss of PfRh4, and by extension, EBA-175. Therefore PfRh2a/b may be performing different roles (Stubbs et al., 2005). Finally, processed

products of PfEBA-175 and PfRh1 have been localized to the moving junction of merozoites halted mid-invasion (O'Donnell et al., 2006; Triglia et al., 2009; Gunalan et al., 2020). Thus although the primary function of the PfRBL/DBPs is likely host cell selection, some may play a secondary role during moving junction formation and progression.

Interestingly, although studies investigating the RBL and DBP families of non-*P. falciparum* species have lagged behind their *P. falciparum* counterparts, the limited data available so far suggests that both families may perform distinct roles in some species, including one of the rodent malaria species, *P. yoelii*, as well as *P. knowlesi*. *P. yoelii* parasites possess a large multi-gene RBL family, referred to as the Py235 family, but only a single DBP ligand, PyEBL (Prasad et al., 2003; Gunalan et al., 2013). Studying the Py235 family has been a particularly complicated endeavour, as each merozoite within a given schizont is predicted to express only a small subset of the Py235 genes. Thus many different variant merozoites are present in any given culture (Preiser et al., 1999; Gunalan et al., 2013). Therefore, it has not been possible so far to assign a specific role to individual PyRBLs. However, analysis of PyEBL null parasites shows that these parasites cannot invade host erythrocytes, but they can strongly deform them. These results suggest that despite expressing a multitude of different Py235 ligands, none of these ligands can act as a substitute for PyEBL, unlike PfRh4 complementing PfEBA-175. Additionally, these results indicate that PyEBL appears to perform a role downstream of deformation, either during re-orientation, or beyond (Kegwara et al., 2018).

P. knowlesi parasites also require only one DBP protein (PkDBPα) and very likely only one RBL protein (PkNBPXa) to invade human erythrocytes. Importantly, deletion of either gene encoding PkNBPXa or PkDBPα restricts *P. knowlesi* parasites to growth in macaque RBCs, demonstrating that at least in the context of human erythrocyte invasion, that the PkDBP ligands cannot act as substitutes for the PkRBLs and vice versa (Singh et al., 2005; Moon et al., 2016). Importantly, the remaining DBP proteins, DBPβ and DBPγ, have been shown to bind to macaque RBCs. Furthermore, simultaneously deleting both genes does not impair the ability of *P. knowlesi* parasites to invade human erythrocytes, confirming that their primary role is probably to facilitate invasion of macaque erythrocytes (Dankwa et al., 2016; Mohring et al., 2019). Similarly, PkNBPXb also likely performs a role during macaque erythrocyte

invasion, as protein derived from parasite supernatants has been shown to bind to macaque erythrocytes (Meyer et al., 2009). However, whether PkNBPXb also contributes to human erythrocyte invasion in any vital way remains to be seen. Overall, the PkDBP and PkRBL families seem to exhibit far less functional redundancy, both within families, and certainly between families, compared to *P. falciparum*.

Little is known about the specific role of NBPXa in *P. knowlesi*, other than the fact that NBPXa null parasites cannot invade human erythrocytes, and by smear, merozoites are observed to stick to the outside surfaces of RBCs instead of internalizing and forming new rings (Moon et al., 2016). Whether NBPXa KO parasites can deform their host cells, apically re-orientate, and even form the beginnings of the moving junction, remains to be seen. To date, no video microscopy of DBPα null parasites has been performed either; however, wild type *P. knowlesi* parasites have been reported to be able to deform Duffy negative erythrocytes (Miller et al., 1975). Therefore, like PyEBL, PkDBPα might perform a role during re-orientation or even beyond, but PkDBPα-DARC interactions do not appear to be required for host cell deformation. Thus for at least two species, the DBP proteins appear to act downstream of deformation.

Importantly, the fact that *P. vivax* generally expresses only one essential DBP protein, PvDBP, which shares the same human erythrocyte receptor as PkDBPα (Miller et al., 1975; Haynes et al., 1988; Barnwell et al., 1989; Wertheimer and Barnwell et al., 1989), indicates that this species may also follow suit, and highlights the need to study the RBL and DBP families in non-*P. falciparum* species to better understand their functions – especially if *P. falciparum* may actually be a variation to the rules. For several years, the *P. falciparum* RBL/DBP ligands were considered top vaccine candidates, as antibodies against these ligands are associated with protective immunity (Tham et al, 2012). However, redundancy between family members has meant that targeting even a combination of PfRBL/DBP ligands is unlikely to be successful in protecting against multiple *P. falciparum* strains (Beeson et al., 2016; Duffy and Gorres, 2020). In contrast, if the remaining human malaria species do rely on specific RBL/DBP combinations, designing vaccines targeting strategic RBL and DBP combinations may provide efficacious, strain transcending protection. Thus, there is an urgent need to re-visit the functions of these families – both to answer basic questions

regarding how merozoites invade erythrocytes, and to determine whether targeting both families in tandem is a feasible vaccine strategy.

1.6 *P. knowlesi* as a model for erythrocyte invasion

Despite early work on *P. knowlesi* in the late 1970s providing foundational knowledge about the mechanics of invasion, the majority of work since has been directed towards *P. falciparum* (Dvorak et al., 1975; Bannister et al., 1975; Aikawa et al., 1978). This is likely in part because before the adaptation of *P. knowlesi* to growth in human erythrocytes, long-term maintenance could only be achieved by *in vivo* infections and later by culturing in rhesus erythrocytes (Butcher, 1979; Kocken et al., 2002; Grüring et al., 2014; Moon et al., 2013). So, with the adaptation of *P. falciparum* to *in vitro* culture and the need to develop antimalarial drugs and vaccine candidates targeting this devastating pathogen, the attention of the malaria community turned instead to *P. falciparum* (Haynes et al., 1976; Trager and Jensen, 1976). The recent adaptation of *P. knowlesi* to growth in human erythrocytes (Moon et al., 2013) has provided the means to study the *P. knowlesi* asexual stages, including erythrocyte invasion once again. Importantly, *P. knowlesi* is a much closer relative to *P. vivax* than the divergent *P. falciparum* (Pain et al. 2008) and therefore provides a better model for many aspects of *P. vivax* biology, including their shared DBP-DARC invasion pathways (Haynes et al., 1988; Wertheimer and Barnwell et al., 1989). Furthermore, *P. knowlesi* transfections are much more efficient than their *P. falciparum* counterparts (Kocken et al., 2002; Moon et al., 2013). This fact, in combination with *P. knowlesi's* genome being much more GC rich than *P. falciparum* (Pain et al., 2008) means that on a practical level, from transfection construct design to the use of genetic techniques such as CRISPR Cas9, which relies upon strategically located 'NGG' sites within target loci (Mojica et al. 2009; Jinek et al. 2012), *P. knowlesi* provides a much more efficient platform for genetic manipulation and reverse genetics studies (Mohring et al., 2019).

In addition to these benefits, the biology of *P. knowlesi* parasites also provides several other clear advantages over *P. falciparum* with regards to studying erythrocyte invasion and the molecular steps it entails. Firstly, *P. knowlesi* merozoites are double the size of their *P. falciparum* counterparts (2-3 μm vs 1-1.5 μm in length), a feature, which should dramatically enhance live imaging techniques that have been so critical towards discovering what is now known about invasion dynamics (Gilson and Crabb,

2009; Dasgupta et al., 2014; Weiss et al., 2015; Lyth et al., 2018). Secondly, while *P. falciparum* merozoites are characteristically round, *P. knowlesi* merozoites exhibit elongated teardrop-like morphologies (Dasgupta et al., 2014; Lyth et al., 2018). Attempting to discern which end of the merozoite is the apical end when imaging *P. falciparum* merozoites is often very difficult (Gilson and Crabb, 2009; Weiss et al., 2015). However, accurately phenotyping mutant parasite lines frequently depends on doing just this! For instance, while overall inhibition of the PfDBP/RBL families clearly prevents merozoites from deforming host cells, it is difficult to tell by video microscopy whether re-orientation can occur or not under these conditions. Therefore, examining both wild type and mutant *P. knowlesi* lines will enable clarification on these matters, as it should, in theory, be considerably easier to observe re-orientation or the lack of it for this species.

Finally, *P. knowlesi* is especially well suited for the study of the RBL/DBP families by virtue of its limited repertoire and limited redundancy of ligands required for invasion of human erythrocytes. In contrast, studying the role of the larger and redundant RBL/DBP repertoire of *P. falciparum* has relied upon combinations of single genetic modifications, enzymatic treatment of RBCs, and inhibitory antibodies (Mayer et al., 2001; Rayner et al., 2001; Duraisingh et al., 2003a; Gilberger et al., 2003; Stubbs et al., 2005; DeSimone et al., 2009; Weiss et al., 2015). In any case, determining the individual roles of every RBL/DBL ligand using these techniques has simply not been possible. Even with the genetic toolkit available today, thoroughly characterizing the *P. falciparum* RBL/DBPs using reverse genetics would likely be a complicated endeavour. In contrast, the relative simplicity of the *P. knowlesi* RBL/DBL families means that determining the roles of these ligands and dissecting the early steps of invasion will likely be a considerably more straightforward process.

1.7 Project Aims and Objectives

The aims of this project are two-fold. The first is to characterize how *P. knowlesi* merozoites invade human erythrocytes, particularly focusing on the mechanical steps leading to internalization. This aim will be achieved by using live microscopy to record wild type *P. knowlesi* merozoites invading human erythrocytes and undertaking a thorough analysis of parasite-host cell interactions. Although *P. knowlesi* merozoites have already been filmed while invading macaque erythrocytes, very few invasions were captured at the time (Dvorak et al., 1975). Analysis of a greater number of events will help to address some outstanding questions regarding the mechanics of invasion, likely applicable to all *Plasmodium* species, regardless of host cell preference. Additionally, though, PkA1-H.1 parasites have never been filmed while invading human erythrocytes. A thorough analysis of the kinetics of human erythrocyte invasion may provide insight into the ways this zoonotic parasite has adapted to growth in human erythrocytes. Overall, this aim will seek to address the following questions:

1) What is the order of the mechanical steps (deformation, re-orientation, and the calcium flux) leading up to internalisation?

2) Is re-orientation a distinct step to host cell deformation?

3) Which pre-internalisation step is the point of no return, or commitment to invasion? For instance, can merozoites detach from host cells and interact with other host cells after triggering a calcium flux, or re-orientating?

4) Do *P. knowlesi* merozoites require more contacts overall, or extended interactions with human erythrocytes for successful invasions, compared to what is seen for *P. falciparum*?

Aim number two is to understand the role(s) that the *P. knowlesi* Duffy binding protein alpha (PkDBPα) and normocyte binding protein Xa (PkNBPXa) proteins fulfil during merozoite invasion of human erythrocytes. This aim will be achieved firstly by attempting to generate conditional PkNBPXa and PkDBPα KO lines, using the inducible DiCre system (Andenmatten et al., 2013; Collins et al., 2013) and phenotyping these lines using a live microscopy approach. Secondly, attempts will be made to tag both PkDBPα and PkNBPXa, along with known moving junction markers PkAMA-1 and PkRON2, with epitope and fluorescent tags. Tagged lines will be used to localize PkNBPXa and PkDBPα before and after egress as well as during invasion,

using a combination of immunofluorescence and live imaging techniques. In doing so, aim number two will attempt to address the following questions:

1) Can PkDBPα null parasites deform host erythrocytes to the same degree as wild type parasites?
2) Can merozoites undergo apical re-orientation in the absence of DBPα-DARC interactions?
3) Which steps of invasion are impeded when PkNBPXa is absent?
4) Do PkNBPXa and PkDBPα co-localise to the same micronemes in schizonts, or do they appear to occupy discrete subsets of micronemes?
5) What is the localization of PkNBPXa and PkDBPα once secreted from micronemal stores and during each step of invasion?
6) Is there a definitive order to the secretion of the *P. knowlesi* RBL/DBP ligands?

The results from aim number one are addressed in chapter 3, and those from aim number two, in chapter 4. Overall, dissecting the individual events of invasion in greater detail, particularly those leading up to host cell entry, will provide valuable insight into the ways in which merozoites of all *Plasmodium* species navigate commitment to invasion. This, in turn, could aid drug and vaccine designs. In particular, the essential nature of PkDBPα and PkNBPXa means that both antigens have the potential to be excellent candidates for a *P. knowlesi* vaccine. Thus determining when these ligands act, what their individual roles are, and whether targeting both antigens at once could inhibit multiple, successive invasion steps could provide further critical information regarding their suitability as vaccine candidates.

Chapter 2: Materials and Methods

2.1 Bioinformatics

2.1.1 DNA and protein sequence analysis

P. knowlesi gene sequences were obtained from the PlasmoDB database (https://plasmodb.org/plasmo/app). DNA and protein sequence alignments were performed using Clustal Omega (http://www.ebi.ac.uk/Tools/msa/clustalo/). Putative protein transmembrane domains were identified using TMPred (https://embnet.vital-it.ch/software/TMPRED_form.html).

2.1.2 Generation of a recodonised mNeonGreen sequence

The mNeonGreen sequence (Shaner et al., 2013) was recodonised for *P. knowlesi* expression using the SMS reverse translate program (found at http://www.bioinformatics.org/sms2/rev_trans.html) followed by manual curation to increase GC content of primer binding sites. GeneArt synthesized the recodonised sequence.

2.1.3 Assessment of potential Cas9 target sites

Cas9 target sequences were assessed for their uniqueness using Protospacer Workbench software (version 0.0.1 alpha) (MacPherson and Scherf, 2015). Guides with off target sequences scoring less than 0.3 were accepted.

2.2 Molecular biology techniques

2.2.1 Polymerase chain reaction (PCR)

All PCR products used for molecular cloning were amplified by CloneAmp HiFi polymerase (Clonetech) from either parasite genomic DNA (gDNA) or plasmid DNA, according to the manufacturer's instructions. A typical reaction was run with 32 cycles of: 5 s at 98°C, 15 sec at 55°C, and 5-30 s at 72°C (extension time of 5 s/kb).

2.2.2 Generation of Cas9 repair templates

Donor DNA templates used to modify PkDBPα, PkNBPXa, PkRON2, and PkAMA-1 with either tags or LoxP sites (Table 2.1) were generated by overlapping PCR and then either transfected as PCR products or cloned into plasmid backbones for sequencing prior to transfection.

Table 2.1. List of Cas9 repair templates generated in this study

Construct name	Purpose	Transfected as?
NBPXa-mNG	Modifying PkNBPXa C-term with an mNeonGreen tag	PCR product
pL_PkDBPα-mNG	Modifying PkDBPα C-term with an mNeonGreen tag	Plasmid
AMA1-mNG	Modifying AMA1 C-term with an mNeonGreen tag	PCR product
RON2-mNG	Modifying RON2 C-term with an mNeonGreen tag	PCR product
AMA1-HA	Modifying AMA1 C-term with HA tag	PCR product
RON2-HA	Modifying RON2 C-term with HA tag	PCR product
NBPXa-mCh	Modifying PkNBPXa C-term with mCh tag	PCR product
pL_NBPXaCtermHA/LoxP	Modifying PkNBPXa C-term with a HA tag/stop codon/LoxP sequence	Plasmid
pL_NBPXaNtermLoxP1	Inserting a LoxP sequence into the PkNBPXa intron (position 1)	Plasmid
pL_NBPXaNtermLoxP2	Inserting a LoxP sequence into the PkNBPXa intron (position 2)	Plasmid
pL_floxedRecDBPα	Replacing the WT PkDBPα sequence with a floxed and C-terminally HA tagged recodonised version	Plasmid

2.2.2.1 Generation of constructs by overlapping PCR

Donor DNA templates to target PkDBPα, PkNBPXa, PkRON2, and PkAMA-1 with either tags or LoxP sequences (Table 2.1) were generated using a series of overlapping, nested PCR steps. Firstly, homology regions (HR1 and HR2) targeting each locus were amplified from parasite gDNA with at least 20-30 bp overhangs to the intervening tag or LoxP module, using primers listed in Table 2.2. All HRs were designed to be at least 400 bp long and all apart from those targeting PkDBPα were amplified from WT gDNA. HRs targeting PkDBPα were instead amplified from gDNA extracted (see section 2.3.5) from the recodonised PkDBPα line. The intervening mNeonGreen, mCherry, and LoxPint sequences were amplified from plasmids using primers listed in Table 2.2. Subsequently, all HR, tag, and LoxPint PCR products were purified by gel extraction (Qiagen) to remove all primers and any non-specific amplicons.

Next, if the overhangs attached to each HR covered the entire intervening tag or LoxP sequence, HR1 and HR2 products were fused together with a nested PCR step. Primers for this step were positioned 50-100 bp inside of each HR. This methodology was used to generate PkRON2-HA and PkAMA1-HA tagging constructs. On the other hand, if the overhangs between HR1 and HR2 did not quite cover the entire tag/LoxP insert, as was the case when both an 27bp HA tag and a 34 bp LoxP site were inserted between two homology arms, a second amplification step was carried out to extend the overhang of HR1. Once gel purified, the extended HR1 and accompanying HR2 were fused together as above, with a nested PCR step. Finally, for longer inserts (fluorescent tags or LoxPint modules), which could not be added to homology regions with primers alone, HR1 was fused to the insert in a nested PCR step. After gel purifying this product, each HR1/insert fusion was joined to its respective HR2, in a final nested PCR step, to create the finished product. All homology regions, inserts, intermediate products, and final constructs are listed in Table 2.2, along with the primer pairs used to generate them and the expected PCR product sizes. All primer sequences are listed in Appendix Table 1.

Table 2.2. Primers used to synthesize CRISPR Cas9 DNA repair templates for this study. Names of primers used to generate homology regions and PCR fusion products listed in the above table. Corresponding primer sequences can be found in Appendix, table 1.

Construct	Fwd primer	Rev primer	product size (bp)	Template
mNeonGreen tag				
mNG PCR product	MH297	MH295	836	mNeonGreen plasmid
mCherry tag				
mCh PCR product	MH1057	MH295	514	mCherry plasmid
PkNBPXa-mNG				
HR1	MH227	MH229	514	Wt gDNA
HR2	MH306	MH231	553	Wt gDNA
HR1/mNG	MH227	MH296	1222	HR1 + mNG PCR products
Full	MH298	MH299	1566	HR1/mNG + HR2 PCR products
PkDBPα-mNG				
HR1	MH221	MH223	524	RecDBPα gDNA
HR2	MH224	MH225	521	RecDBPα gDNA
HR1/mNG	MH221	MH296	1232	HR1 + mNG PCR products
Full	MH222	MH226	1637	HR1/mNG + HR2 PCR products
PkRON2-mNG				
HR1	MH847	MH337	1089	Wt gDNA
HR2	MH1062	MH851	1005	Wt gDNA
HR1/mNG	MH847	MH296	1797	HR1 + mNG PCR products
Full	MH848	MH852	2579	HR1/mNG + HR2 PCR products
PkAMA1-mNG				
HR1	MH841	MH331	868	Wt gDNA
HR2	MH1063	MH845	878	Wt gDNA
HR1/mNG	MH841	MH296	1576	HR1 + mNG PCR products
Full	MH842	MH846	2217	HR1/mNG + HR2 PCR products
PkRON2-HA				
HR1	MH847	MH849	1092	Wt gDNA
HR2	MH850	MH851	1007	Wt gDNA
Full	MH848	MH852	1874	HR1 + HR2 PCR products
PkAMA-1-HA				
HR1	MH841	MH843	872	Wt gDNA
HR2	MH844	MH845	880	Wt gDNA
Full	MH842	MH846	1512	HR1 + HR2 PCR products
PkNBPXa N-term LoxP1 insert				
HR1	MH953	MH963	1011	Wt gDNA
HR2	MH962	MH957	1000	Wt gDNA
Full	MH954	MH958	1651	HR1 + HR2 PCR products
PkNBPXa N-term LoxP2 insert				
HR1	MH953	MH967	1037	Wt gDNA
HR2	MH966	MH957	974	Wt gDNA

Full	MH954	MH958	1651	HR1 + HR2 PCR products
PkNBPXa C-termLoxP insert				
HR1	MH835	MH238	858	Wt gDNA
HR1e	MH835	MH837	895	HR1 PCR product
HR2	MH838	MH839	852	Wt gDNA
Full	MH975	MH1023	1507	HR1e + HR2 PCR products
PkDBPα N-term LoxPint Insert				
HR1	FM62	MH1347	628	RecDBPα gDNA
HR2	MH1350	MH1367	1824	RecDBPα gDNA
NBPXaLoxPint1 module	MH1348	CH204	721	Pl_NBPXaLoxPint1 plasmid
HR1/NBPXa_LoxPint1	FM62	MH1349	872	NBPXaLoxPint1 + HR1 PCR products
Full	FM62	MH1367	2669	HR1/NBPXaLoxPint1 + HR2 PCR products
PkDBPα C-term/HA/LoxP Insert				
Insert	MH1341	MH1343	1591	RecDBPα gDNA
Insert extended	MH1342	MH1344	1566	Insert PCR product
PkNBPXa mCherry				
HR1	MH227	MH229	514	Wt gDNA
HR2	MH1058	MH231	524	Wt gDNA
HR1/mCh	MH227	MH1059	1219	HR1 + mCh PCR products
Full	MH298	MH299	1566	HR1/mCh + HR2 PCR products

2.2.2.3 Cloning of pL_PkDBPα-mNG plasmid

The final PCR amplification step of the PkDBPα-mNG construct added a SacII
restriction site to the 5' end of the construct and an EcoR1 site to the 3' end. This
construct and vector pPkB1 (Appendix Figure 1A) were digested with SacII/ EcoR1
(NEB), purified by gel extraction (Qiagen), and ligated together using T4 DNA Ligase
(Promega), according to the manufacturer's instructions to create final vector
pL_PkDBPα-mNG (Appendix Figure 1B)

2.2.2.3 Cloning of pL_NBPXaCtermHA/LoxP, pL_NBPXaNtermLoxP1, and pL_NBPXaNtermLoxP2 plasmids

The final PCR amplification step of PkNBPXa-NtermLoxP1, PkNBPXa-NtermLoxP2,
and PkNBPXa-CtermLoxP/HA constructs added a SacII restriction site to the 5' ends
of constructs and a NotI restriction site to the 3' ends. These PCR products, along with
vector backbone pPkB1 (Appendix Figure 1A), were subsequently digested with
restriction enzymes SacII and Not1 (NEB). Gel purified inserts and vector (Qiagen)
were ligated together using T4 DNA Ligase (Promega) according to the

manufacturer's instructions, creating plasmids pL_NBPXaNtermLoxP1, pL_NBPXaNtermLoxP2, and pL_NBPXaCtermHA/LoxP (Appendix Figure 2).

2.2.2.4 Cloning of pL_floxedRecDBPα plasmid

PkDBPα_NtermLoxP and PkDBPαCtermHA/LoxP PCR products were cloned into vector pPkg5_DBPα (Mohring et al., 2019; Appendix Figure 3A), which contains a copy of a recodonised PkDBPα sequence. The PkDBPαCtermHA/LoxP PCR product and vector pPkg5_DBPα were first digested with NotI and BbvCI restriction enzymes (NEB) and gel purified (Qiagen). Digestion of pPkg5_DBPα removed a 1410 bp fragment that was replaced the digested PkDBPαCtermHA/LoxP PCR product by ligating vector and insert together with T4 DNA Ligase (Promega), to create vector pL_DBPα_CtermHA/LoxP. Next, the PkDBPα_NtermLoxP PCR product and pL_DBPα_CtermHA/LoxP vector were digested with BbvCI and SpeI restriction enzymes (NEB). An 1813 bp product was removed from pL_DBPα_CtermHA/LoxP and replaced with digested PkDBPα_NtermLoxP, creating the final vector, pL_floxedRecDBPα (Appendix Figure 3B).

2.2.3 Generation of Cas9 guide plasmids

All Cas9 guide sequences were inserted into pCas9/sg (Mohring et al., 2019; Appendix, Figure 4A), which contains the Cas9 and sgRNA cassettes as well as positive (*hdhfr*) and negative (*yfcu*) selection markers. The DBPα RNA targeting sequence was inserted into pCas9/sg using a protocol developed by Marcus Lee (unpublished). This insert was prepared using complementary primers (MH359 and MH360 from Appendix Table 2) containing the DBPα target sequence with 4bp overhangs to BtgZI cut sites, generated upon digestion of pCas9/sg. Primers were mixed and phosphorylated with T4 Polynucleotide Kinase (PNK) according to the supplier's instructions, for 30 mins at 37°C. Phosphorylated primers were subsequently annealed by incubation at 95°C for 5 mins and allowed to slowly cool down to room temperature. This annealed primer mix was then diluted 1:200 in distilled water, and 1µl was ligated into 50 ng digested and dephosphorylated (Antarctic phosphatase, NEB) vector using T4 DNA ligase (Promega). T4 DNA ligase was subsequently heat inactivated at 65°C, and each reaction digested with NruI (NEB) to remove uncut vector before transformation.

All other Cas9 guide sequences were inserted into pCas9/sg by annealing complementary primers (Table 2.3) carrying the 20 bp guide sequence and flanked by 15bp overhangs to BtgZI digested pCas9/sg, as outlined in Mohring et al. (2019 & 2020). Annealed oligos were inserted into digested pCas9/sg by Infusion cloning (TaKaRa). Primers carrying the guide sequences are listed in Appendix, Table 2.

Table 2.3. Primers used to generate pCas9/sg inserts. All primer sequences can be found in Appendix, table 2.

Target	Fwd primer	Rev primer
PkNBPXa-Cterm	MH235	MH236
PkNBPXa-Nterm1 (LoxPint1)	MH964	MH965
PkNBPXa-Nterm2 (LoxPint2)	MH968	MH969
PkRON2 C-term	FM512	FM513
PkAMA-1 C-term	FM510	FM511

Initially, because of difficulty cloning the PkNBPXa C-terminal guide sequence into pCas9/sg (using either of the above methods), this guide was instead inserted into a second Cas9 vector, pL_11HF (Avnish Patel, LSHTM; See Appendix Figure 4B). The pL_11HF plasmid contains all component of pCas9/sg, but has a different, smaller backbone and a high fidelity (HF) Cas9 sequence instead of the wild type version. Insertion of the PkNBPXa C-terminal guide into PL_11HF was achieved by amplifying the entire guide cassette using overlapping primers containing the PkNBPXa RNA targeting sequence (Table 2.4). This PCR product was digested with PspXI and BstEII (NEB) and ligated into the pL_11HF plasmid using T4 DNA ligase (Promega).

Table 2.4. Primers used to generate pL11HF PkNBPXa C-terminal guide insert. All primer sequences can be found in Appendix, table 2.

PCR product	Fwd primer	Rev primer	product size (bp)	Template
HR1	FM400	MH236	442	pL_11HF
HR2	MH235	MH295	704	pL_11HF
Full	FM401	FM285	662	HR1 + HR2 PCR products

2.2.4 Bacterial transformation

Donor DNA plasmids were transformed into DH5α bacterial cells (Invitrogen), and pCas9/sg plasmids were transformed into XL10 Gold competent cells (Agilent) according to the supplier's instructions.

2.2.5 Plasmid purification

Plasmid DNA was isolated for cloning purposes using a Qiaprep mini-prep kit (Qiagen), according to the manufacturer's instructions. Large-scale plasmid production was performed using a high-speed plasmid maxi-prep kit (Qiagen), also according to the manufacturer's instructions.

2.3 *P. knowlesi* cell culture

2.3.1 *In vitro* maintenance and synchronization of *P. knowlesi* parasites

Blood stage A1-H.1 *P. knowlesi* parasites were cultured in human erythrocytes (UK National Blood Transfusion Service) at a 2% haematocrit with custom made RPMI-1640 medium, supplemented with 10% Horse Serum (v/v) and 0.292 grams/litre (2 mM) L-glutamine according to previously established methods (Moon et al., 2013).

Parasites were tightly synchronized for experiments by one of two different methods. The first (Moon et al., 2013) involves two rounds of density gradient centrifugation steps using 55% Nycodenz (Axis-Shield). Mature schizonts collected from the first centrifugation step were allowed to egress and re-invade fresh red cells over a 2 h window. Newly formed 1-2 h ring stages were then collected after the second density gradient centrifugation step and cultured until maturation again. Alternatively, after the

re-invasion period, parasites were incubated with 140mM guanidine hydrochloride for 10 minutes, according to a protocol outlined by Ngernna et al., (2019), which killed all parasites older than 5 hours, leaving only young rings behind.

2.3.2 Transfection of *P. knowlesi* parasites

Transfections were performed with 10 μl mature schizonts, 10 μg of the Cas9 plasmid, and 20 μg of the donor DNA using the Amaxa 4-D Nucleofactor X machine (Pulse code FP158) and P3 Primary Cell Kit (Lonza), according to protocols described by Moon *et al.* (2013) and Mohring *et al.* (2019). Donor DNA was transfected in either plasmid form or as a PCR construct. To prepare PCR constructs for transfection, six to eight 50μl final PCR reactions (Table 2) were pooled. All PCR constructs and plasmids were concentrated by ethanol precipitation and re-suspended in sterile TE buffer prior to transfection, according to methods outlined in Mohring *et al.* (2019). Parasites were mixed with fresh erythrocytes (50 % haematocrit) immediately after transfection for 1 h to allow for re-invasion. Haematocrit was subsequently adjusted to 4% for continuous growth. Transfected parasites were cultured with 100 nM pyrimethamine for 5 days following transfection in order to select for parasites that had taken up the Cas9 plasmid. Parasites were then grown for a week without any drugs before being treated with 1 μM 5-Fluorocytosine for 7 days (Mohring et al., 2019). Finally, transgenic parasites were cloned by limiting dilution (Moon et al., 2013).

2.3.3 Rapamycin treatment of conditional knockout lines

Immediately after synchronization, ring stage *P. knowlesi* cultures were split into two and incubated in complete media containing rapamycin (Sigma-Aldrich) or the equivalent volume of its carrier, DMSO, as a control. For IFA excision assays, parasites were treated with 10-200 nM rapamycin in 0.005-0.1% (v/v) DMSO or the equivalent volume of DMSO only. Treated parasites were incubated with drug at 37°C for either the entire cycle or for 3 hours only, before drug or DMSO containing media was removed and parasites were re-suspended in fresh, drug-free complete media.

For the single cycle multiplication assay in human and macaque cells (section 2.3.4), parasites were treated with 100 nM rapamycin or 0.1% (v/v) DMSO for 3 hours, before drug or DMSO containing media was removed and parasites were re-suspended

in fresh, drug-free complete media. For the two-cycle growth assay and all video microscopy experiments, parasites were treated with 10 nM rapamycin or 0.005% (v/v) DMSO for 3 hours, before drug was removed and parasites were re-suspended in fresh media.

2.3.4 Parasite multiplication rate assays

To determine the multiplication rate of mutant parasites, ring stage DMSO and rapamycin-treated cultures were adjusted to a parasitaemia of 0.5% and a 2% haematocrit and were grown in 24 well plates in a gassed chamber at 37°C. After 24 hours, a starting reading was taken when parasites were roughly 24-27 hours old. A second reading was taken 26 hours later. For dual cycle assays, a third reading was taken roughly 26 hours later again.

For single cycle assays, cultures were set up in duplicate using both macaque (National Institute for Biological Standards and Control) and human erythrocytes, and 2 biological replicates were performed. For the multi-cycle assays, cultures were set up in triplicate in human erythrocytes. A total of three biological replicates were performed. Parasitaemia was measured using a flow cytometry (FACS) based assay. Samples were fixed in 2% paraformaldehyde (Sigma) and 0.2% glutaraldehyde (Sigma) in PBS for 1 h at 4°C, washed 3 times in PBS, permeabilised with 0.3% Triton X-100, and washed 3 times in PBS again. Finally, samples were treated for 1 h at 37°C with RNase (MP Biomedicals) before staining with SYBR Green I (Life Technologies) and performing FACS analysis. Assays were analysed either on a Becton Dickenson LSR-II or an Attune NxT flow cytometer using FACSDiva 6.1.3 software. Data were analysed using FlowJo_V10.

2.3.5 Isolation of parasite material for DNA extraction

Parasite culture was pelleted at 700 x g, washed 3 times in RPMI, and snap frozen. Genomic DNA was extracted from parasite pellets using a DNeasy blood and tissue kit (Qiagen) according to the manufacturer's instructions.

2.3.6 Isolation of parasite material for western blot

Parasite culture or purified schizonts were pelleted at 700 x g and saponin lysed with 1.5 x pellet volume of 0.15% saponin in PBS for 10 min on ice. Samples were

subsequently centrifuged at 12,000 x g for 5 min and then washed 3 times in cold PBS, before being snap frozen in dry ice. COmplete, EDTA-free protease inhibitors (Roche) were included for each step.

2.3.7 Diagnostic PCR for detection of integration and excision events

To assess integration of constructs containing LoxP sites and tags, diagnostic PCRs were carried out on extracted gDNA (Section 2.3.5) using GoTaq Green master mix (Promega) and the following conditions: 3 min at 96°C, then 30 cycles of 25 s at 96°C, 25 s at 52°C, and 1 min/kb at 64°C. Primers used to detect integrated and wild type parasites for each transfection along with the expected PCR product sizes are listed in Table 2.5. A positive control using primers RM75 and RM76, which amplified a 1043bp product from the *PkMTIP* locus, was also included in each set of reactions.

Likewise, to detect excision of *PkNBPXa* from rapamycin treated PkNBPXa cKO parasites, diagnostic PCRs were carried out on extracted gDNA from rapamycin and DMSO treated parasites, using GoTaq Green master mix (Promega). Primers CH203 and CH206, positioned outside of each LoxP site amplified a 606 bp product indicative of excision using the following conditions: 3 min at 96°C, then 30 cycles of 25 s at 96°C, 25 s at 52°C, and 1 min/kb at 64°C. Primers MH1543 and CH206 flanking the C-terminal LoxP site were used to detect un-excised parasites, with an expected product size of 404 bp for un-excised but floxed parasites, and 340 bp for the parental (non-tagged) control. WT products were amplified using the same conditions as above, except using 27 cycles, instead of 30

Table 2.5. Primers used to detect wild type (WT) and Integrated (Int) parasites after transfection. All corresponding primer sequences can be found in Appendix, Table 3.

Detecting	Fwd primer	Rev primer	Expected product size (bp)
RON2 tags			
WT	MH890	MH909	1209
Int mNG	MH890	MH291	1338
Int HA tag	MH890	MH563	1221
PkAMA-1 tags			
WT	MH892	MH904	984
Int mNG	MH892	MH291	1113
Int HA	MH892	MH563	996
PkNBPXa mNG			
WT	MH835	MH1128	1565 (If integrated) OR (863 if WT)
Int mNG	MH835	MH291	973

NBPXa LoxPint1			
WT	MH959	MH1353	1228
Int	MH959	MH1171	1250
NBPXa LoxPint2			
WT	MH959	MH1143	1261
Int	MH959	MH1172	1284
NBPXa C-term LoxP			
WT	MH1129	MH1128	1004
Int	MH1129	MH563	997
DBPa mNG			
WT	FM421	MH225	1778 (If integrated) OR 1046 (WT)
Int mNG	FM421	MH291	691
Floxed PkDBPa			
WT	CH193	MH1041	849
Int	MH562	MH1041	824
Control locus			
PkMTIP product	RM75	RM76	
NBPXa mCherry			
WT	1129	1128	863
Int	1129	1160	1053
DiCre p230p			
WT	FM49	FM50	969
Int	FM90	FM32	891

2.4 Protein and immunohistochemistry techniques

2.4.1 Immunoblot analysis

Saponin released schizonts (2.1.6) were lysed in four volumes of a CoIP buffer containing: 10 mM Tris/Cl pH 7.5, 150 mM NaCl, 0.5 mM EDTA, 0.5% NP-40, 1mM PMSF, and 2x cOmplete EDTA free protease inhibitors (Roche). Lysates were incubated on ice for 10 min and then centrifuged at 12,000 x g for 20 min to remove residual solid material. Subsequently, 1 volume of 2x LDS sample buffer (Invitrogen) was added to the soluble fraction. Samples were boiled for 5 minutes before being separated by SDS PAGE by running samples on precast 3-8% Tris-Acetate NuPAGE gels (Invitrogen).

SDS-PAGE fractionated proteins were transferred to a nitrocellulose membrane using a semidry Trans-Blot Turbo Transfer System (Bio-rad). Membranes were blocked in 10% (w/v) milk in 0.1 % PBS-Tween-20 (PBST) over night before incubation with

primary antibodies, diluted to the concentrations indicated in Table 2.5, in 1% (w/v) skimmed milk in PBST for at least 1 h Membranes were subsequently washed 3 times for 10 min/wash in PBST, and incubated for 1 h. with secondary antibodies conjugated to near infra-red dyes, at concentrations listed in Table 2.5. Membranes were washed 3 times for 10 min in PBST and then dried between Whatman 3MM blotting papers. Finally, immunoblots were imaged using a Chemidoc imaging system (Bio-Rad).

2.4.2 Indirect immunofluorescence assays (IFA)

Late stage schizonts were thinly smeared on glass slides, dried, and fixed in 4% paraformaldehyde (PFA) in PBS for 30 minutes, followed by 0.1% Triton X-100 in PBS for 10 min. Slides were subsequently blocked in 3% BSA in PBS overnight at 4°C, and then incubated with primary antibodies diluted to appropriate concentrations (listed in Table 2.6) in blocking solution for at least 1 h. Next, slides were washed 3x in PBS, for 10 min/wash and incubated with secondary antibodies (Table 2.6) for 1 h. After a final wash in PBS (3x 10 min), slides were mounted in ProLong Gold Antifade Mountant containing DAPI (Thermo Fisher Scientific).

For in solution IFAs, merozoites were captured mid-invasion by treating egressing cultures with 100 nM cytochalasin D (Sigma) for 30 min and then gently spinning cultures down at 1500 x g for 1 minute. Parasite pellets were re-suspended in a 4%PFA/0.0025% glutaraldehyde solution in PBS, and then loaded into a poly-L-lysine coated μ-Slide VI $^{0.4}$ (Ibidi). Parasites were incubated in fixative solution for 30 min before fixative was removed by pipetting the solution out of the channel slides. Channels were then washed 5x by gently pipetting PBS into the channel and then removing it in the same manner as the fixative. Subsequently, parasites were incubated with 0.1% Triton X-100 in PBS for 10 min, followed by 5 wash steps in PBS. Washed parasites were blocked with 3% BSA in PBS for at least 1 h and then incubated with primary antibodies, diluted in blocking solution at concentrations indicated in Table 2.6, for 1 h. This was followed with 5 x wash steps in PBS, and then incubation for 1 h with the appropriate secondary antibody (Table 2.6), also in 3% BSA. After the final wash steps, parasites were incubated in PBS containing Hoechst 33342 (Cell Signaling Technology) for half an hour prior to imaging. All samples were imaged with a Nikon Ti E inverted microscope using a 100x or 60 x oil immersion objective and an ORCA

Flash 4.0 CMOS camera (Hamamatsu). Images were acquired, processed and statistically analysed using the NIS Advanced Research software package.

Table 2.6. List of primary and secondary antibodies used to detect proteins by western blot and IFA for this study

Primary antibodies				
Target	**Species (clone)**	**IFA**	**Western**	**Provider/manufacturer**
α-HA	Rat (3F10)	1/500	1/5000	Sigma
α-mNeonGreen	Mouse (32F6)	1/500	NA	Chromotek
α-PkMSP1	Rabbit (polyclonal)	1/2000	NA	Ellen Knuepfer (Francis Crick Institute)
α-PkDBPα	Rabbit (polyclonal)	NA	1/1000	Han lab (Muh *et al.,* 2020)
Secondary antibodies				
Target	**Conjugate**	**IFA**	**Western**	**Provider/manufacturer**
α -rat IgG (H +L)	Alexa Fluor-594	1/1000	NA	Invitrogen
α -rat IgG (H +L)	IRDye 680 RD	1/1000	1/5000	LI-COR Odyssey
α -mouse IgG (H +L)	Alexa Fluor-488	1/1000	NA	Invitrogen
α -rabbit IgG (H +L)	Alexa Fluor-488	1/1000	NA	Invitrogen
α -rabbit IgG (H +L)	DyLight 800	NA	1/5000	Invitrogen

2.5 Time lapse imaging

2.5.1 Invasion assays

For all invasion assays (Table 2.6), purified schizonts were added to fresh erythrocytes to make a 10-15% parasitaemia and 2.5% haematocrit culture. The haematocrit was subsequently adjusted to 0.25%, and 150 μl culture was loaded into a PLL coated μ-Slide VI $^{0.4}$ (Ibidi). For the anti-DARC assay, either 5μg/mL human anti-DARC (2C3 clone, Absolute Antibody), or 5μg/mL anti-human IgG (Invitrogen) was first added to the 0.25% haematocrit culture, prior to loading samples into the channel slides. For the calcium flux assay, erythrocytes were first incubated with 5μM fluo-4-AM

(Invitrogen) in RPMI for 1h at 37°C. Cells were subsequently washed three times in RPMI, and then allowed to rest at 37°C for a further half an hour for de-esterification to occur, prior to mixing with parasites. Loaded slides were subsequently transferred to the Nikon Ti E inverted microscope chamber, pre-warmed to 37°C. Samples were imaged using a 100x or 60 x oil immersion objective and an ORCA Flash 4.0 CMOS camera (Hamamatsu), with conditions outlined in table 2.7. Videos were acquired and processed using the NIS Advanced Research software package.

Table 2.7. Imaging conditions used to capture P. knowlesi merozoites invading human erythrocytes

Assay	Line	Treatment	Channels/exposure time	Image acquisition rate (FPS)
PkNBPXa cKO	NBPXa cKO	DMSO	Brightfield/100msec	1
	NBPXa cKO	10 nM rapamycin	Brightfield/100msec	1
α-DARC block	NBPXa cKO	5μg/mL α-DARC	Brightfield/100msec	1
	NBPXa cKO	5μg/mL α-human IgG	Brightfield/100msec	1
WT invasions	NBPXa LoxPint1	None	Brightfield/100msec	Either 1 or 10
	NBPXa LoxPint1	Fluo-4-AM (erythrocytes)	Brightfield/100msec; 488nm/100msec	1
	NBPXa-mNG	None	Brightfield/100msec; 488nm/100msec	1
	DBPα-mNG	None	Brightfield/100msec; 488nm/100msec	0.25 or 1
	AMA1-mNG	None	Brightfield/100msec; 488nm/100msec	0.5

2.5.2 Gliding assays

Synchronized late stage schizonts (PkNBPXaNtermLoxP1 line) were loaded into poly-L-lysine-coated polymer, uncoated polymer, or glass μ-Slides $^{0.4/0.5}$ (Ibidi) and imaged using the same microscopy set-up as described above. Parasites loaded into PLL coated slides were treated with either 0.1μM cytochalasin D in 0.005 (v/v) DMSO (Sigma), or with the equivalent volume of DMSO. Time-lapse brightfield images (50-100msec exposure) were collected at a rate of 1-10 frames/second. Gliding speed was calculated manually, using the distance measurement tools in the NIS Advanced Research software package. The tangential speed of each merozoite was determined by calculating the number of rotations it performed/minute and multiplying this value by the circumference of the widest portion of the merozoite (merozoite diameter x π). The

angle of the merozoite motor was calculated using the formula $\text{Tan}(x) = R/L$, where x = the angle of the motor, R = the average distance each merozoite rotated/per body length travelled forward, and L = the body length of the merozoite, from its apical tip to the basal end.

2.5.3 Secretion assays

Synchronized late stage PkNBPXa-mNG, PkDBPa-mNG, and PkAMA1-mNG schizonts were loaded (either plus or minus fresh erythrocytes) into PLL-coated μ-Slides $^{0.4}$ (Ibidi) and transferred to a pre-warmed microscope, as described in the above sections. Time-lapse brightfield and fluorescent images were acquired at a rate of 1 frame/sec (100 msec exposure for each channel). The fluorescence intensity around the periphery or down the length of each merozoite was measured using the intensity profile feature of the NIS Advanced Research software package.

Chapter 3: Results I - Dissecting the morphological steps of invasion

3.1 Introduction

The very first video microscopy study describing invasion featured *P. knowlesi* merozoites (Dvorak et al., 1975). Not only did this pivotal investigation demonstrate how rapid invasion is, lasting less than a minute from start to finish, but it also visualized key mechanical steps for the first time. These included deformation of the host cell membrane, internalisation of the apically aligned merozoite into the erythrocyte, and echinocytosis of the host cell in response to invasion (Dvorak et al., 1975). Subsequent studies imaging *P. falciparum*, as well as the rodent malaria parasite, *P. yoelii*, have sought to examine invasion in greater detail. Analysing hundreds of invading merozoites enabled them to investigate the kinetics of invasion and to determine if the events described for *P. knowlesi* are conserved across different species and characteristic of all invasions (Gilson and Crabb, 2009; Weiss et al., 2015; Yahata et al., 2012)

The multi-step process of invasion begins when freshly egressed merozoites encounter erythrocytes and form reversible attachments (Dvorak et al., 1975; Gilson and Crabb, 2009). For *P. falciparum,* the majority of merozoites (~ 85%, for 3D7 parasites) will invade the first cell that they contact, and the majority of these contacts will occur within 1 minute of egress (Gilson and Crabb, 2009; Weiss et al., 2015). Unlike other typical zoites, including *Plasmodium* sporozoites and *T. gondii* tachyzoites, *Plasmodium* merozoites are not thought to use gliding motility to encounter new host cells (Vanderberg, 1974; Håkansson et al., 1999; Baum et al., 2006). Rather, host cell contacts are proposed to arise from random interactions, as a result of merozoites moving by Brownian motion and tumbling across erythrocyte surfaces in the context of a moving blood stream (Dvorak et al., 1975; Pinder et al., 2000; Weiss et al., 2015).

These engagements frequently, but not always, cause the merozoite to deform the host cell to a varying extent, ranging from a slight indentation of the erythrocyte membrane, to interactions so forceful that the erythrocyte appears to wrap around the merozoite (Dvorak et al., 1975; Gilson and Crabb, 2009; Weiss et al., 2015). Weiss et al. (2015) investigated merozoite-host cell interactions of both invading and non-invading

parasites in detail, by scoring them from 0-3 based on deformation intensity. Contacts that did not elicit any deformation were designated a score of 0, while contacts resulting in the most intense deformation were given a score of 3. Critically, a high scoring contact was far more likely to result in successful invasion compared to a lower scoring contact, highlighting the potential importance of this step (Weiss et al., 2015).

Prior to host cell entry, merozoites must also undergo apical re-orientation - the alignment of the merozoite's apical tip with the erythrocyte surface (Ladda et al., 1969; Aikawa et al., 1978). Interestingly, an early description of *P. knowlesi* merozoites deforming host cells postulated that deformation is the result of the merozoite attempting to embed its apical end into the erythrocyte, as deformation was observed only when the merozoite's apical end was in contact with the host cell (Dvorak et al., 1975). Thus re-orientation was not described as a separate invasion step per se, although correct alignment was of course required for entry. However, very few invasion events were captured for this study, and so the matter was not definitively resolved. Later, after observing many more *P. falciparum* invasion events, Gilson and Crabb (2009) came to a similar conclusion: that re-orientation likely happens during deformation itself, because when deformation subsided, *P. falciparum* merozoites were not observed to move again, prior to internalisation. Thus, the authors concluded that re-orientation occurs as the parasite is rolled around the erythrocyte surface during deformation. However, it is worth noting that the round morphology of *P. falciparum* merozoites likely hindered efforts to address this issue, as it is often difficult to determine the orientation of *P. falciparum* merozoites. Conversely, a more recent study, observing *P. yoelii* merozoites, which are slightly larger and less spherical than *P. falciparum*, showed examples of re-orientation occurring after deformation, and by a pivoting motion (Yahata et al., 2012). Furthermore, another study showed that treating *P. falciparum* merozoites with the actin polymerization inhibitor cytochalasin D inhibits deformation, but does not prevent the formation of the moving junction, a step that is theorized to take place only after apical alignment (Riglar et al., 2011; Weiss et al., 2015). Thus, in combination these later results seem to suggest that re-orientation could indeed be a discrete invasion step not strictly reliant on forces generated from deformation.

A further molecular milestone, which takes place just prior to internalisation, is a

fusion event between the merozoite's apex and the host erythrocyte (Weiss et al., 2015; Volz et al., 2016; Introini et al., 2018). This event can be observed when merozoites invade erythrocytes loaded with Fluo-4-AM, a calcium-sensitive fluorescent dye (Weiss et al., 2015; Introini et al., 2018). Approximately 3-4 seconds prior to host cell entry, a fluorescent spot appears at the apical end of the merozoite, which has been termed a calcium "flux", because it may correspond with the secretion of calcium-rich rhoptry contents into the host cell (Weiss et al., 2015; Volz et al., 2016; Introini et al., 2018). However, these experiments have only been performed using *P. falciparum* parasites, and it is still not entirely clear when this event occurs in relation to re-orientation.

Finally, after all of these events the merozoite initiates internalisation. For all species investigated so far, host cell entry appears to be rapid, usually occurring within a 30 second window (Dvorak et al., 1975; Gilson and Crabb, 2009; Yahata et al., 2012; Weiss et al., 2015). Within a minute of internalisation, the erythrocyte then becomes echinocytotic. The reasons for this phenomenon are not entirely clear; but it may be triggered by secretion of rhoptry components (Gilson and Crabb, 2009; Weiss et al., 2015). Intriguingly, echinocytosis does not occur in around 10-20% of cases for *P. falciparum*, and erythrocyte swelling, rather than echinocytosis, was reported for some *P. knowlesi* invasions (Dvorak et al., 1975; Weiss et al., 2015). When echinocytosis does occur, though, the erythrocyte returns to its biconcave shape within several minutes, marking the very end of a successful invasion (Dvorak et al., 1975; Gilson and Crabb, 2009).

Importantly, understanding the invasion kinetics of *P. falciparum* and *P. yoelii* parasites has been critical to interpreting the phenotypes of genetic mutants that cannot invade erythrocytes, or those which can invade, but less efficiently (Yap et al., 2014; Tham et al., 2015; Weiss et al., 2015; Kegawa et al., 2018). However, the molecular steps driving the early events of invasion, in particular those performed by the RBL and DBP ligands, remain largely enigmatic. One reason for this is that despite great efforts so far, basic questions regarding the mechanics of invasion, such as the order of deformation, re-orientation, and calcium flux steps, remain unanswered.

In theory, the larger size (2-3 μm long), and clearly polarized morphology of *P. knowlesi* merozoites, as compared to *P. falciparum* merozoites (Lyth et al., 2018),

should enable these basic questions to be addressed. However, since *P. knowlesi's* debut appearance in 1975, no further live imaging studies featuring this species have been published elaborating on questions which have arisen since this early work (Dvorak et al., 1975). Furthermore, the 1975 study described invasion of macaque RBCs and did not include any data regarding human RBC invasion (Dvorak et al., 1975). Although the basic morphological steps of invasion are likely to be the same for both species, *P. knowlesi* parasites exhibit a preference for macaque RBCs over human, and therefore the mechanisms underlying host cell selection and the timings involved may differ significantly (Moon et al., 2016). Additionally, *P. knowlesi* merozoites exhibit much longer half-lives compared to *P. falciparum* merozoites, which suggests that invasion dynamics might also differ between these species (Dennis et al., 1975; Boyle et al., 2010; Lyth et al., 2018).

Therefore, before characterizing transgenic *P. knowlesi* lines produced in this study (described in chapter 4), the first logical step was to thoroughly analyse the invasion mechanics and kinetics of the PkA1-H.1 line, to gain an understanding of how *P. knowlesi* merozoites interact with human erythrocytes, and how the early events of invasion unfold. Notably, a second goal was also to compare the dynamics of human vs. macaque invasions. However, unfortunately, due to the fact that macaque erythrocytes are difficult to obtain in the UK, these experiments could not be performed yet. Attempts will be made to explore the dynamics of macaque invasions in the future. It is also important to note that the results in this chapter are largely observational. However, in addition to providing the basis for understanding the phenotypes of transgenic parasites produced in Chapter 4, dissecting the early events of wild type *P. knowlesi* invasions may provide valuable insight into invasion mechanisms shared by all *Plasmodium* species. Thus, taking the time to carefully analyse wild type *P. knowlesi* invasions will likely ultimately advance current *P. falciparum* and *P. vivax* research.

3.2 From egress to first contact: going house hunting

3.2.1 *P. knowlesi* merozoites exhibit incomplete dispersal post egress

In order to examine A1-H.1 merozoites invading human erythrocytes, tightly synchronised late stage schizonts (~1h pre egress) were purified by nycodenz and mixed with fresh RBCs at a 0.2-0.3% haematocrit and 10-15% parasitaemia. This dilution was loaded into a poly-L-lysine (PLL) coated μ-Slide VI [0.4] (Ibidi) to create a loose monolayer of erythrocytes along the channel coverslip. Schizont egresses and subsequent invasions were imaged at a rate of 1 frame/second over a 10-minute window with a 60x lens in bright field.

Prior to visualizing any invasion events, an immediate difference was observed between the manner in which *P. falciparum* and *P. knowlesi* merozoites are dispersed post egress. Unlike *P. falciparum* merozoites, which are released in an "explosion" like manner, scattering individual parasites (Gilson and Crabb, 2009), *P. knowlesi* merozoites often emerged from host erythrocytes in pairs or small groups (Figure 3.1), and occasionally, with all merozoites still attached to the residual body or each other. Parasite groups frequently remained connected throughout the recordings and strongly deformed nearby RBCs in unison. If individual parasites within a group attached to adjacent RBCs, the ensuing deformations could pull RBCs together, creating clumps of RBCs and parasites (Video 3.1). These multi-parasite-RBC deformation events often allowed parasite groups to break apart, releasing individual merozoites, which could be more easily tracked from this point onwards. However, RBC clumping also obscured the view of other interactions and in some cases prevented determining the end fates of these merozoites (as invaders or non-invaders).

Dvorak et al. (1975) also noted that parasites taken from macaques could remain attached to the residual body post egress and that multiple *P. knowlesi* merozoites attempting to invade the same macaque erythrocyte could cause it to lyse. Therefore, the incomplete dispersal of PkA1-H.1 merozoites is unlikely to merely be an artefact of adaptation to growth in human cells. Interestingly, some successful double invasions into a single host cell were observed during this experiment. However, at least two examples of host cells lysing due to the invading merozoite remaining attached to either another (non-invading) merozoite or the residual body were observed (example in Video 3.2). Thus, incomplete dispersal could clearly be a hindrance to

parasite survival. It is worth noting, though, that these observations may only be representative of invasions happening in static cultures. It is possible that the shear forces parasites are exposed to under flow conditions in the bloodstream may also disperse parasite groups effectively *in vivo*.

On a practical note, *P. knowlesi's* tendency to pull RBCs together, forming clumps of erythrocytes, meant that often the fates of individual merozoites were unclear due to parasites being hidden within these clumps. So, out of all the merozoites imaged in the following invasion experiments (from 20 different schizonts), 47 invaded RBCs, 102 did not invade, and at least 38 were classed as 'unclear'. A proportion of 'unclear' merozoites likely did invade, though, as evidenced by echinocytosis events within RBC clumps. However, because RBC clumping obscured the view of these invasions, it was not clear how many merozoites invaded any one cell or whether every echinocytosis event was definitely caused by an invasion. Therefore, while the average number of invasions recorded here was around 2-3/schizont, this value is very likely higher and more reflective of the replication rate (3-5 invasions/schizont) measured under standard culturing conditions (Moon et al., 2016).
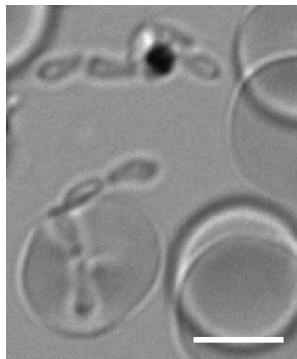
Figure 3.1. *P. knowlesi* schizont exhibiting incomplete dispersal. In static cultures, *P. knowlesi* merozoites frequently emerge from erythrocytes and contact new host cells while remaining attached to each other and/or the residual body. Scale bar = 5μm.

3.2.2 Gliding motility facilitates merozoite movement across RBC and solid surfaces

Another striking feature of dispersing *P. knowlesi* merozoites was that they appeared to exhibit directional movement across the coverslip and erythrocyte surfaces, travelling away from their site of egress (Video 3.3; Figure 3.2). This surprising feature was especially apparent when a merozoite appeared to travel across an erythrocyte, detach from its surface, and then travel across the surface of the coverslip before attaching to another erythrocyte several microns away from the first (Figure 3.2,

white arrows). Notably, this movement occurred in one orientation, with the wide end of the parasite leading forward movement along the surface of attachment. So it appeared that *P. knowlesi* merozoites might be capable of active motility and not merely relying on Brownian motion for dispersal and initiating contacts with potential host cells. Therefore, to investigate this surprising feature further, we sought to verify that this movement was not simply Brownian motion alone and to characterize this new and potentially important invasion step.
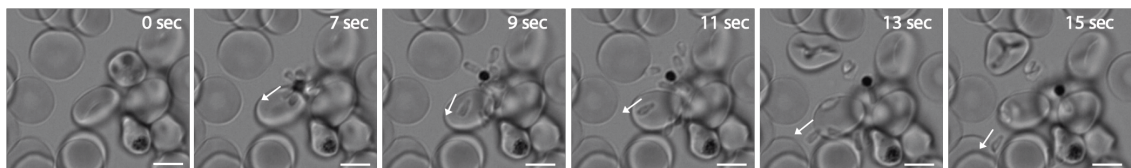
Figure 3.2. *P. knowlesi* merozoites travel away from their site of egress. White arrows depict a merozoite moving across the surface of an erythrocyte, before transitioning to the poly-L-lysine coated coverslip and attaching to a second erythrocyte. Stills taken from video 3.3.
Scale bars = 5µm

3.2.2.1 Merozoite motility is an actin dependent process

Inhibition of actin polymerisation with cytochalasins disrupts the acto-myosin motor and stalls host cell invasion as well as surface gliding of *Plasmodium* sporozoites, *T. gondii* tachyzoites, and *B. bovis* merozoites (Ryning and Remington, 1978; Miller et al., 1979; Stewart and Vanderberg, 1988; Håkansson et al., 1999; Asada et al., 2012). Therefore, the first logical step in characterising potential gliding activity of *P. knowlesi* merozoites was to compare the motility of parasites treated with cytochalasin D (cyto D) or its carrier, DMSO.

Treated purified schizonts (n = 20 schizonts for each group) were monitored in the absence of fresh RBCs for 10 minutes post rupture. Control merozoites appeared to stick to the poly-L-lysine coated coverslip surface, and as noted before, move in one orientation, with the wider end of the merozoite leading (Figure 3.3A; Video 3.4). Each glide ended when the merozoite in question stopped forward motion and detached from the coverslip, resuming random motion (Denoted with a black arrow in Figure 3.3A, panel 10). While half-attached parasites could occasionally appear to exhibit forward movement for a couple of seconds, random motion also caused them to wobble from side to side. As such, a 'glide' was defined as continuous forward motion

across the coverslip surface, for at least 5 seconds, as this time frame easily ruled out forward motion due to random movement alone. Using these parameters, 69% of DMSO-treated merozoites in a given schizont exhibited gliding motility (Figure 3.3B). In stark contrast, not one gliding merozoite was identified for the cyto D-treated parasites (video 3.5), indicating that like other *Plasmodium* zoites, merozoite motility is also actin-dependent.
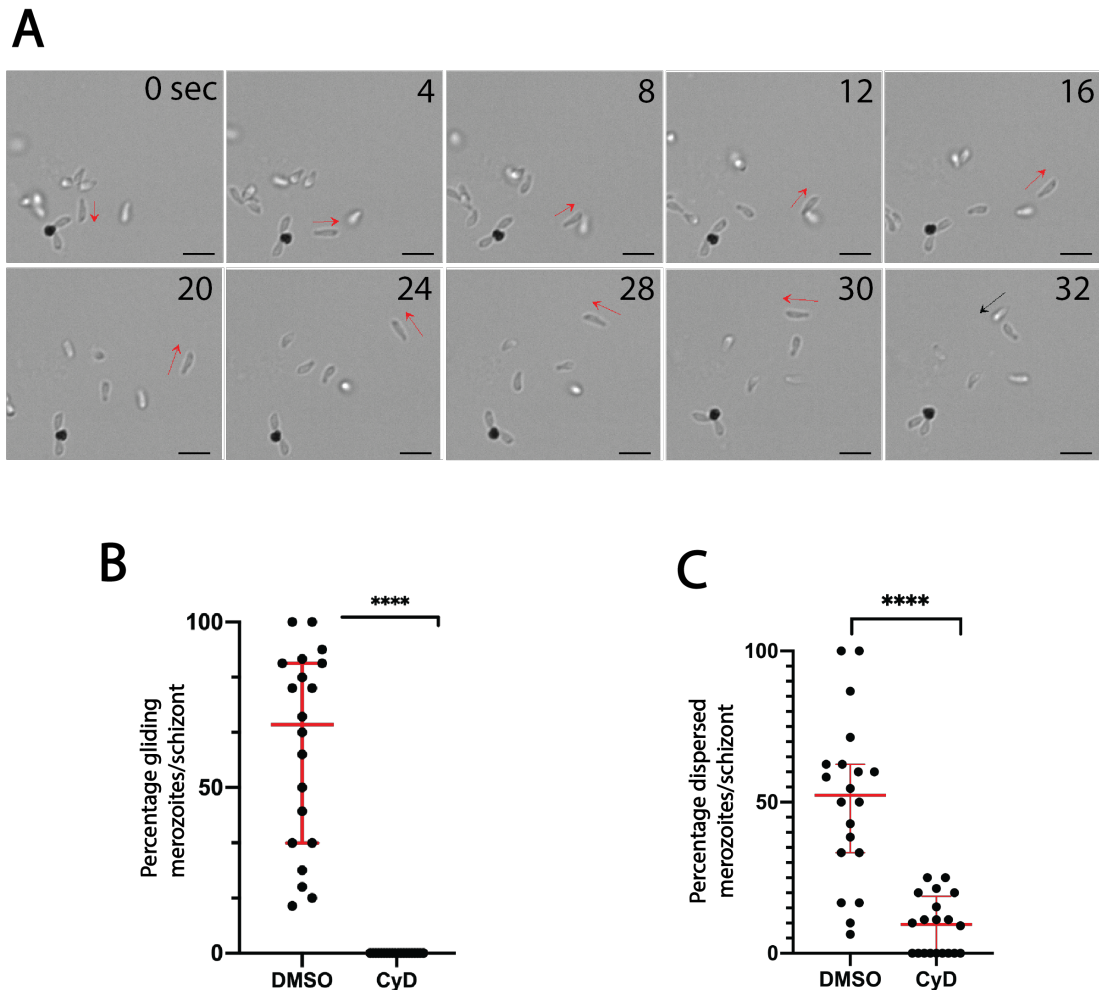
Figure 3.3. *P. knowlesi* merozoites exhibit gliding motility across poly-L-lysine-coated coverslips. (A) Panels from Video 4. DMSO treated *P. knowlesi* merozoites attach to PLL coated surfaces and move in one orientation across the slide, with their wide ends leading (direction shown with red arrows in panels 1-9). Forward movement ends when the wide end of the merozoite detaches from the coverslip surface (depicted with a black arrow, at 32 sec). Scale bars = 5μm. **(B)** Cytochalasin D (CyD) treated merozoites do not exhibit any forward motion across coverslip surfaces, while for DMSO treated parasites, a median 69% of merozoites in a given schizont demonstrate forward motility. ****Indicates p<0.0001 (Mann-Whitney U-test). **(C)** Significantly fewer cyD-treated merozoites in a given schizont are dispersed (median = 10%), compared to DMSO treated parasites (median = 51%). **** indicates p<0.0001 (Mann-Whitney U-test). For both graphs, thick red bars indicate medians, and error bars indicate interquartile ranges.

Interestingly, almost all cyto D-treated schizonts stayed attached to each other and the residual body, and only occasionally would a merozoite or two disperse from the group. However, it is important to note that the erythrocyte membrane of cyto D-treated samples can clearly be seen to burst, releasing the entire schizont (video 3.5), indicating that egress as such, was not stalled by cyto D. Also, the release of a whole schizont as opposed to individual, separated merozoites is also common in non-cyto D-treated parasites. However, once merozoites within DMSO-treated schizonts settled on the coverslip, they could pull away from the schizont and glide away from the group (Video 3.6). Overall, 51% of DMSO treated parasites either egressed as individual merozoites or became individual merozoites by pulling apart from pairs/groups. In contrast, only 10% of the cyto D-treated parasites emerged as individual merozoites (Figure 3.3C). Thus, motility, and therefore also dispersal are impacted when parasites are treated with actin-polymerisation inhibitors.

3.2.2.2 The efficiency of gliding motility is dependent on the surface substrate

Having established that *P. knowlesi* merozoite movement is not due to Brownian motion alone, an important question is, why have gliding merozoites not been observed before? Are gliding merozoites only characteristic of certain *Plasmodium* species, and even if this is the case - why did the original *P. knowlesi* study not reveal that these parasites are motile? Interestingly, Dvorak and Miller (1975) did observe *P. knowlesi* merozoites demonstrating 'pivotal motion' and bending, once they had settled to the bottom of glass coverslips. This motion was predicted at the time to be distinct from Brownian movement, but these results were never investigated further. Therefore, one hypothesis as to why merozoite motility has not been readily observed previously is that glass coverslips, frequently used for invasion imaging, may not support efficient gliding. This is certainly the case for *Plasmodium* sporozoites, which require a BSA coating to glide effectively across glass surfaces (Vanderberg, 1974). In contrast, the poly-L-lysine (PLL) coated polymer coverslips used in this study appear to facilitate *P. knowlesi* merozoite attachment and therefore have allowed productive gliding to be detected for the first time.

To test this theory, motility of parasites on uncoated polymer or glass surfaces was assessed using the same parameters as for the PLL conditions. While some motility

was observed on both uncoated surfaces, overall, fewer merozoites/schizont exhibited motility, with only 32% of parasites gliding on the uncoated polymer surface, and 24% of parasites on the glass coverslips (Video 3.7), as compared to the 69% of parasites on PLL surfaces (Figure 3.4A).   Furthermore, even in the absence of an inhibitor, parasites on uncoated surfaces also exhibited reduced dispersion. Only 14% and 32% of egressing merozoites were able to disperse as individuals on uncoated polymer and glass surfaces, respectively (Figure 3.4B). These values are greater than the 10% seen for cytochalasin D treatment, as would be expected, given that some Brownian motion is observed under these conditions. However, the reduction in dispersal, as compared to the dispersal rates on PLL surfaces (51%), supports the hypothesis that gliding does indeed contribute to this process. Therefore, while it is possible to observe motility on these alternative surfaces, glass surfaces, in particular, provide less than optimal conditions for gliding, and as such, could make motility appear far less apparent without scrutiny.
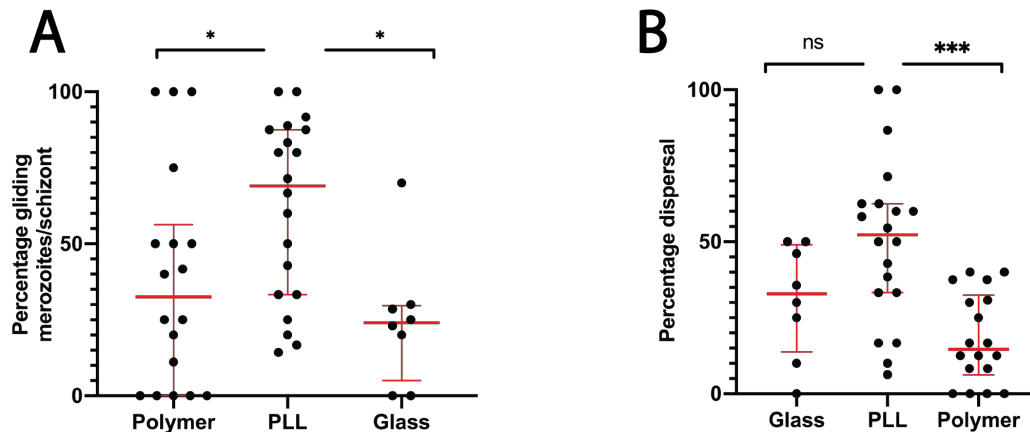
Figure 3.4. Efficiency of gliding motility is impacted by the surface substrate (A) poly-L-lysine (PLL) coated polymer coverslips facilitate maximum motility (median of 69% merozoites in a given schizont demonstrating motility), while glass and uncoated polymer surfaces facilitate significantly lower levels of motility (medians of 32.5% and 24% respectively). Differences were assessed using one-way ANOVA, with Dunnett's multiple comparison test. *Indicates p<0.05. **B)** Fewer merozoites/schizont disperse from each other when schizonts egress on glass (median= 14.6%) and un-coated polymer surfaces (median = 32.9%) compared to PLL (median = 51%) coverslips. Differences were assessed using one-way ANOVA, with a Kruskal-Wallis test. *** indicates p=0.0002. For both graphs: n = 20 schizonts for PLL, 17 schizonts for uncoated polymer, and 8 schizonts for glass coverslip. For both graphs, thick red bars indicate medians and error bars indicate interquartile ranges.

3.2.2.3 The merozoite's apical end is wider than its basal end

The observation that *P. knowlesi* merozoites glide with their wide ends leading was also a surprising finding. *Plasmodium* merozoites are normally depicted as teardrop like forms with the wide end forming the basal side and the thinner tip housing the apical complex (Figure 3.5A) (Bannister et al., 2003; Cowman and Crabb, 2006). Thus, at first, it appeared that *P. knowlesi* merozoites might be travelling in the opposite direction to which they would during invasion.

Apical orientation was examined with a fluorescently labelled line (See chapter 4 for further details regarding the generation of tagged lines) to investigate whether the apical end of *P. knowlesi* merozoites might, in fact, be the wide end. A line expressing a PkNBPXa-mNeonGreen fusion protein clearly showed that this tagged micronemal ligand (Meyers et al., 2009) localizes to the wide end, and not the thin, pointy end of

free merozoites (Figure 3.5B). Tagged parasites could also clearly be seen to glide via their wide, fluorescently labelled ends (Figure 3.5B, Video 3.8). Thus *P. knowlesi* merozoites were not moving "backwards", and the apical end of the zoite did indeed appear to be the wide end. It is also worth noting that as a merozoite glides, it appears to stretch, and a small, pointed tip becomes apparent towards one side of the wide end of the zoite (Figure 3.5C, inset). This tip likely corresponds to the apical complex, which is depicted in transmission electron microscopy (TEM) images of apically aligned merozoites just before host cell entry (Figure 3.5C). Thus, the observation of this small, pointy tip by TEM could explain why early studies concluded that merozoites were entering host cells via their thinner ends.

Overall, although surprising, the finding that the apical end of the *P. knowlesi* merozoite is its wide end does make sense in light of previous studies. These studies showed that within mature *P. knowlesi* schizonts, the thin, pointed ends of merozoites attach to the residual body, while the rounded ends face outwards, fanning around the residual body in a flower-like configuration (Figure 3.5D) (Moon et al., 2013; Mohring et al., 2019). Thus the arrangement of merozoites within the *P. knowlesi* schizont means they are perfectly positioned, upon egress, to glide away from the site of egress (and each other) after the host erythrocyte ruptures, as seen in Video 3.3.

A
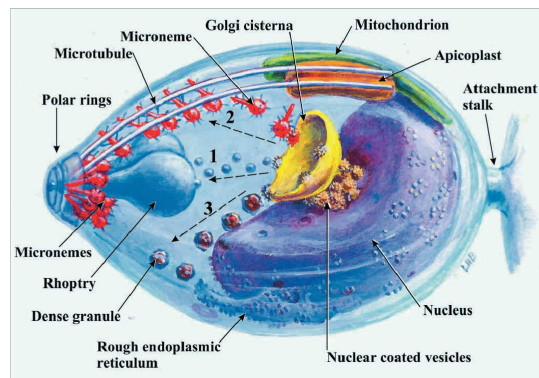
Taken from Bannister *et al.,* 2003

B
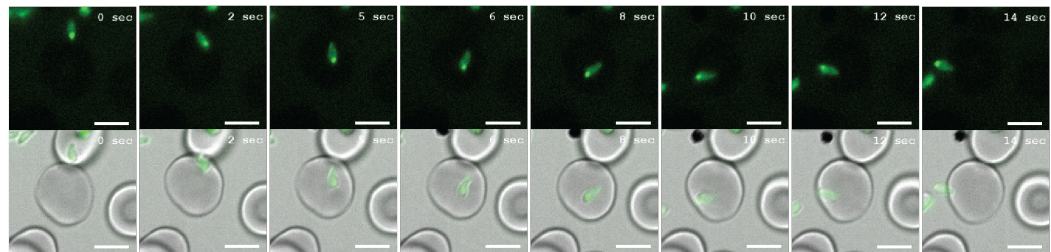
C
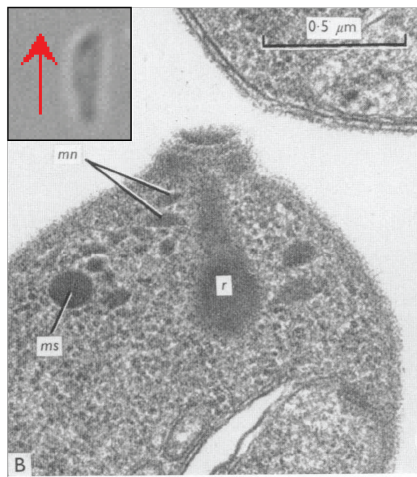
Adapted from Bannister *et al.,* 1975

D
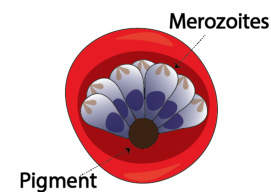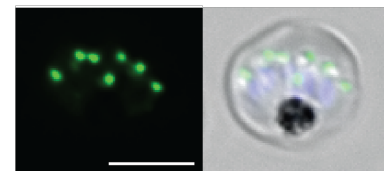
Figure 3.5. The apical end of a *P. knowlesi* merozoite is the wider than its basal end (A) Cartoon taken from Bannister *et al.,* (2003) depicting a typical representation of a *Plasmodium* merozoite, with the apical complex displayed at the merozoite's thin tip. **(B)** Stills from Video 8, showing gliding NBPXa-mNeonGreen tagged merozoites, with their wide, fluorescently labeled ends leading forward motion. **(C)** Electron micrograph taken from Bannister *et al.,* (1975) depicting the apical complex of a *P. knowlesi* merozoite. Mn = micronemes. Ms = microspheres. Inset: brightfield image of a stretched, gliding *P. knowlesi* merozoite, exhibiting a pointed tip at its wide, apical end, which may correspond to the apical complex. **(D)** NBPXa-mNeonGreen tagged merozoites in a mature schizont. The apical ends of merozoites, marked by green dots, face outwards, while the thin basal ends are attached to the residual body, as depicted in the cartoon below. Scale bars = 5μm

3.2.2.4 Corkscrew-like rotation drives efficient forward motion

When examining gliding *P. knowlesi* merozoites closely, it became clear that they, like the other apicomplexan zoites, undergo the classically described 'corkscrew' motion (Video 3.9) to drive forward movement (Håkansson et al., 1999; Asada et al., 2012). Attempts were made to visualize this rotation by observing parasites stained with mitotracker, but it produced a symmetrical staining pattern, so that rotation could not be followed by fluorescence. However, a dark spot to one side of the merozoite's apical end could be seen by brightfield, which rotated along with the parasite (Figure 3.6A). Tracking this dark spot revealed that parasites completed one full rotation approximately every 3.7 seconds, showing a clear positive correlation between the number of turns completed per glide and distance travelled forward (Figure 3.6B). Like *Plasmodium* sporozoites, *P. knowlesi* merozoites were found to rotate in a clockwise (right-handed) manner 90% of the time. Taking into account the merozoite's circumference (on average 3.58 μm), merozoites were found to rotate at a tangential speed of 61 μm/min. Practically speaking, this means that a 3.1 μm-long merozoite (the average length) completes 0.78 turns/body length travelled forward, consistent with a linear motor running at a 42° angle along the longitudinal axis of the merozoite (n = 10 merozoites; Figure 3.6C).

Gliding speed varied, depending on whether merozoites travelled in pairs/groups or alone. Not surprisingly, single merozoites travelled at a faster speed (1.06 μm/s) than merozoites in pairs/groups (0.87 μm/s) (Figure 3.6D). This faster speed is comparable to that recorded for *B. bovis* merozoites (1.2 μm/s), which are a similar size to *P. knowlesi* merozoites, but slower than speeds recorded for larger zoites, such as *Plasmodium* sporozoites and *T. gondii* tachyzoites (~1-2 μm/s). However, when considering the smaller size of *P. knowlesi* merozoites compared to larger zoites (2-3 μm in length, as opposed to *Plasmodium* sporozoites, which are 8-14 μm in length), *P. knowlesi* merozoites demonstrate remarkable efficiency despite possessing presumably, a shorter motor (Håkansson et al., 1999; Siden-Kiamos et al., 2006; Asada et al., 2012). Interestingly, speed decreased over subsequent glides. Figure 3.6E compares the first and final glide speeds of individual merozoites (on PLL coverslip) and shows that on average, initial glide speeds were faster (1.09 μm/s) than the final glides recorded for the same merozoites (0.90 μm/s). This difference could possibly be due to a slower rate of adhesin secretion as micronemal stores diminish over time, or potentially cleavage of surface adhesins already in place.
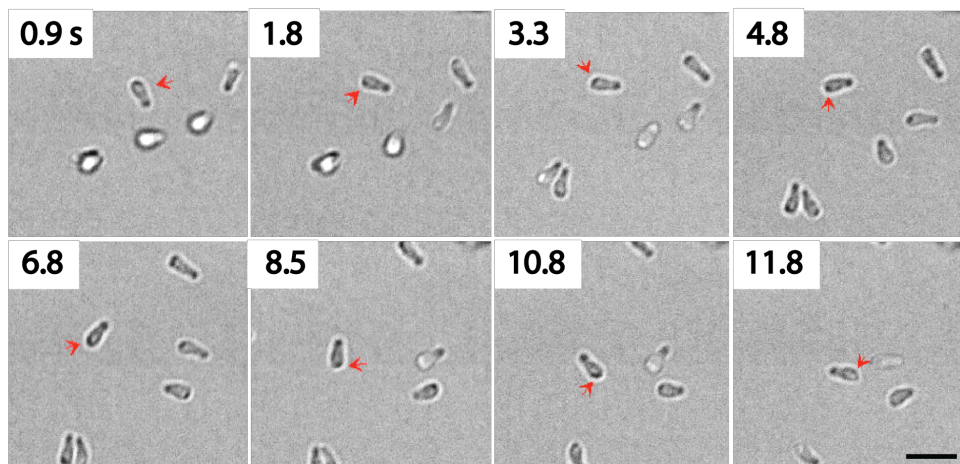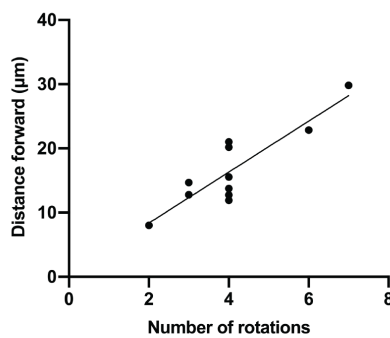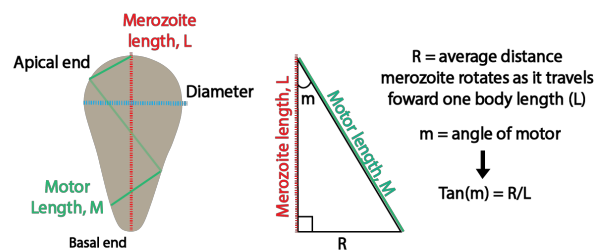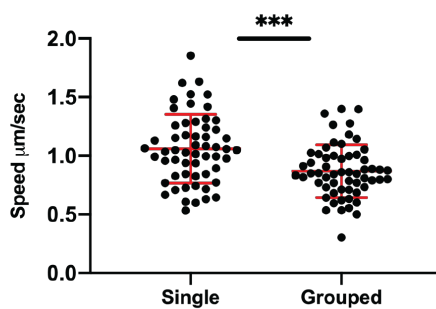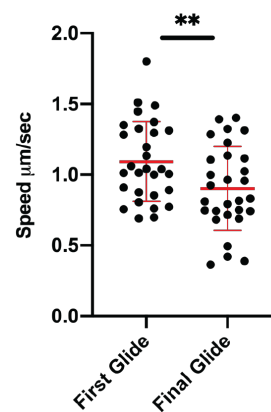
Figure 3.6. Corkscrew like rotation drives efficient motility (A) Gliding merozoites exhibit corkscrew-like rotation as they travel forwards. Rotation is evident when tracking a dark patch at the merozoite's apical end (indicated by a red arrow in each frame), which turns around the merozoite's circumference as the zoite travels forwards. Scale bar = 5μm. **(B)** By determining the length of the merozoite (L) and calculating the average distance it rotates for every body length it moves forward (R, or the number of turns/body length travelled forward x merozoite circumference), it is possible to calculate the length of the motor (M), and the angle at which it runs (m) using the formula Tan(m) = R/L. **(C)** The number of rotations a merozoite completes is positively correlated with the distance it travels forward **(D)** Gliding merozoites travel at an average speed of 1.1μm/s, and up to a maximum of 1.9 μm/s (n= 57 merozoites) when they are detached from other merozoites or the residual body ('single merozoites'). Gliding speed is significantly slower (0.9μm/s; n = 59 merozoites) when merozoites travel in pairs or groups. *** Indicates P = 0.0001 (determined by a two-tailed, un-paired T-test).

84

(E) A small, but significant difference was observed between the average speeds of a merozoite's first glide (1.1µm/sec) vs its last glide (0.9 µm/sec). ****** Indicates P= 0.0032, as determined by a two-tailed, paired T-test (n= 29 merozoites). For all graphs, red error bars indicate means and standard deviations.

3.2.2.5 Gliding duration corresponds with invasive capacity

After egress, merozoites required a settling period of around 30-60 seconds to allow them to sink to the coverslip and make contact necessary to glide on a solid surface. Following this, merozoites spent a median 15 seconds and up to a maximum of 315.5 seconds gliding before any further movement continued as random motion (Figure 3.7A). Gliding was often discontinuous, with merozoites gliding for short periods before detaching from the coverslip, and then re-starting after a brief interval. As such, the longest continuous glide time was 207.5 seconds, with a median length of 14.2 seconds (Figure 3.7B).
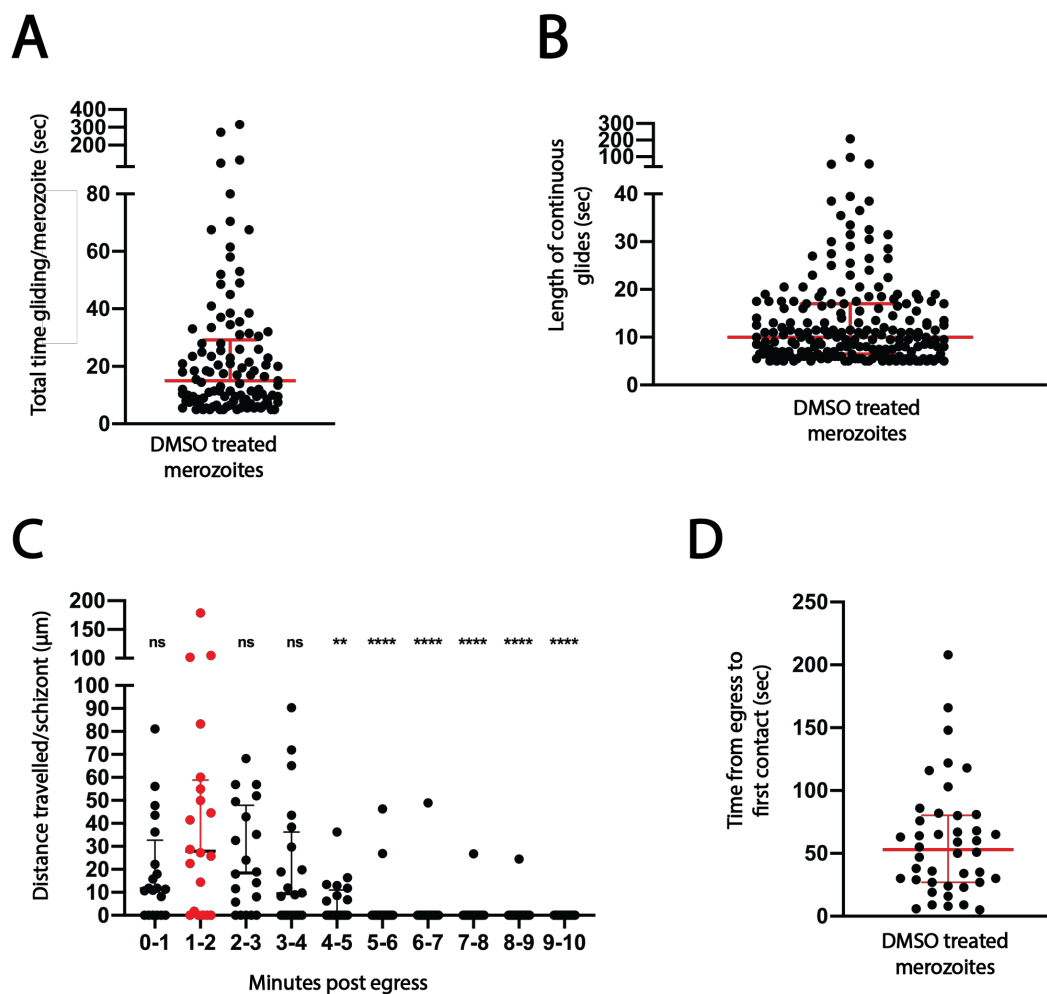
Figure 3.7. legend next page

Figure 3.7. Period of peak gliding corresponds with the invasive window of *P. knowlesi* merozoites (A) Each merozoite spent a median length of 15 seconds and up to 315.5 seconds gliding in total post egress (n= 109 merozoites). **(B)** The median length of each individual glide was 10 seconds (and up to a maximum of 207 seconds; n= 204 glides). **(C)** The majority of gliding occurred within 4 min of egress. Peak gliding occurred 1-2 min after egress (window highlighted in red) with all the merozoites in a given schizont travelling a median, cumulative distance of 28μm during this window. A comparison of the median values across each window of time with the peak median value was performed using one-way ANOVA, with Dunnett's multiple comparison test (**, **** indicates p< 0.05; ns indicates p > 0.05). No merozoites demonstrated motility beyond 9 minutes post egress. **(D)** Merozoites took a median length of 53 seconds and up to 208 seconds after egress, to contact the cell they would invade. For all graphs, thicker red/black bars indicate medians and error bars indicate interquartile ranges.

The majority of gliding occurred within the first 5 minutes post egress (Figure 3.7C), with less than 5% of parasites continuing to glide beyond this point. Interestingly, this time frame appeared to correlate with the invasive capacity of *P. knowlesi* merozoites observed under these same conditions. The majority of merozoite-RBC contacts that lead to an invasion were also initiated within the first 3-4 minutes post egress (Figure 3.7D). Thus, when merozoites lose the capacity to glide on extra-cellular surfaces, they may also lose their ability to invade erythrocytes.

3.2.2.6 Gliding facilitates multiple RBC contacts

Each merozoite travelled a median total distance of 14μm, and up to a maximum of 198.6μm (Figure 3.8A). This distance, in theory, could allow parasites to glide over and contact multiple adjacent cells before committing to invasion. By examining gliding in the presence of RBCs, this hypothesis was found to hold true. On average, gliding merozoites contacted three RBCs, while non-gliding merozoites contacted only two cells (Figure 3.8B).

This feature becomes especially relevant when considering the percentage of merozoite-RBC contacts that lead to successful invasions. Out of 284 merozoite-RBC interactions considered (from 20 schizont ruptures), all lasting at least 2 seconds and occurring during the window of time ranging from egress to the final invasion recorded (208 seconds), only 15% lead to invasion. Many of these interactions were made by merozoites that ultimately never invaded. Interestingly, though, when considering only those merozoites that did invade, only 40% invaded the first cell they contacted.

Conversely, the remaining invasive merozoites made a median of 3 RBC contacts (including the cell they invaded), with some merozoites forming up to 7 intermediate contacts prior to the cell they invaded (Figure 3.8C). Furthermore, 87% of these intermediate contacts were also unique events, meaning that each invading merozoite rarely contacted the same RBC more than once.

While these results contrast with what is seen for *P. falciparum*, with ~85% of Pf3D7 invasive merozoites entering the first RBC they contact (Weiss et al., 2015), they are not altogether too surprising, given that human RBCs are not the natural host cells for *P. knowlesi*, as they are for *P. falciparum*. Thus, *P. knowlesi* merozoites may require a much more extensive human RBC selection process than *P. falciparum* merozoites do - a hypothesis that could be investigated by comparing the number of contacts *P. knowlesi* merozoites make when interacting with macaque vs. human erythrocytes.

Finally, an additional observation worth noting is that as merozoites stop and then re-start productive gliding motility, they were frequently observed to rise up on their basal ends, with their wide apical ends waving above the coverslip surface. Without erythrocytes present, the merozoite's basal end would also quickly detach from the coverslip surface, resulting in the merozoite floating or bobbling above the coverslip surface temporarily, before it re-attached and began rotational movement along the coverslip again (See Video 3.4 for examples). However, in the presence of erythrocytes, the merozoite's basal end could remain attached to an erythrocyte surface, and the merozoite could briefly "twirl" on its basal end (Video 3.10), akin to what has been described for *T. gondii* tachyzoites (Håkansson et al., 1999). While this feature did not seem particularly helpful in the context of static monolayer cultures, as used for video microscopy, it is possible that merozoites may use twirling motions *in vivo* to access cells flowing above the cell they are attached to. Thus, twirling may be another mechanism *P. knowlesi* merozoites use to contact multiple erythrocytes and a potential mechanism to "actively" leave a cell.
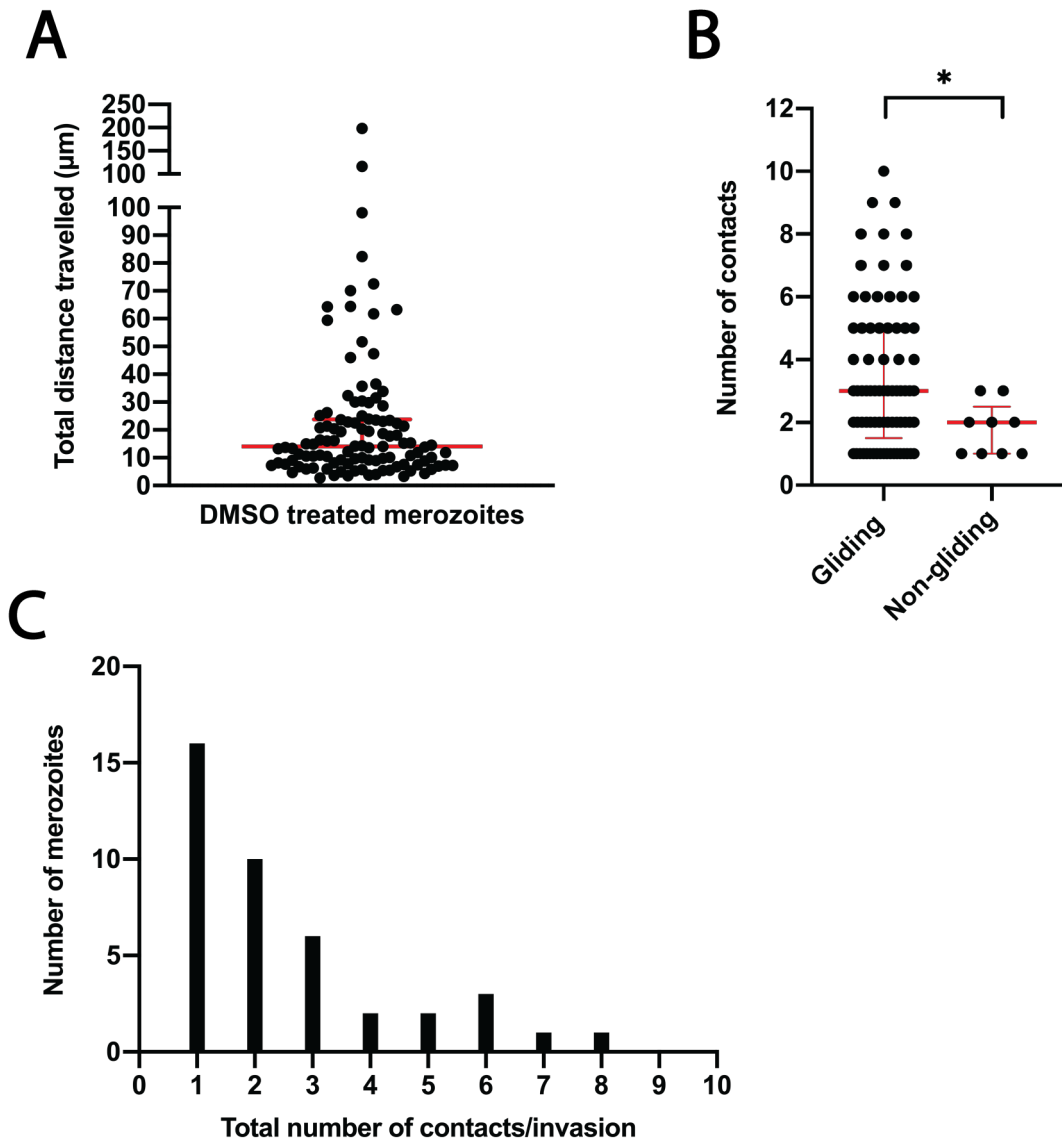
Figure 3.8. Gliding facilitates multiple RBC contacts (A) Individual merozoites travelled a median cumulative distance of 14μm and up to a maximum of 198.6μm. **(B)** Gliding merozoites contacted a median of 3 and up to 10 erythrocytes throughout filming, while non-gliding merozoites contacted significantly fewer erythrocytes overall (median of 2 and a maximum of 3 erythrocytes). * Indicates P=0.0361 as determined using a Mann-Whitney U-test. **(C)** 16/42 merozoites invaded the first cell they contacted, while the remaining merozoites made at least 1 additional, and up to 7 additional contacts prior to their last host cell contact, culminating with an invasion. For all graphs, red thick red bars indicate medians and error bars indicate interquartile ranges.

3.3 Deformation and apical re-orientation: selecting the perfect new home

3.3.1 Gliding leads into erythrocyte deformation

A close examination of *P. knowlesi* merozoite-RBC interactions showed that 35% (98/277 clear interactions; see Figure 3.9A) eventually resulted in deformation of the host cell within 2-36 seconds (Figure 3.9B) of the merozoite contacting the host cell. While Dvorak and Miller (1975) originally described this event as the apically aligned merozoite attempting to drive its apical end into the erythrocyte, Gilson and Crabb (2009) proposed that deformation occurs when any part of the merozoite comes into contact with the erythrocyte. In partial agreement with Dvorak et al. (1975), observations of *P. knowlesi* merozoite-RBC interactions showed that deformation did frequently begin when a merozoite glided into the side of an erythrocyte, bending it around itself (Figure 3.10A, bottom panels; also see Video 3.11, frames 1-2). However, deformation was also often observed when merozoites were running parallel to the erythrocyte surface. In this instance, the erythrocyte membrane appeared to pinch or wrap around the length of the merozoite (Fig 3.10A, top panels; also see Video 3.11, frames 3-7). Interestingly, though, imaging parasite-RBC interactions with a faster frame-rate (10 frames/sec vs. 1 frame/sec for other videos) revealed that as merozoites glide forwards on erythrocyte surfaces, 'ripples' of deformation, starting towards their apical ends, would travel down the lengths of their bodies (Video 3.12). Thus, although deformation did not appear to result from an apically aligned merozoite trying to drive itself into the host cell, deformation might still originate from the merozoite's apex, rather than any random point on the zoite.

Importantly, in almost all cases, deformation coincided with gliding. At least 92% of deformation events (82/89 clear interactions) began simultaneously with, or within 1 (minimum) – 24 (maximum) seconds of merozoites beginning to glide on erythrocyte surfaces (Figure 3.9C). As per the definition of a "glide" used in section 3.2.2.1, only events where the merozoite exhibited continuous forward motion across the RBC surface (or a combination of the RBC surface + coverslip) for at least 5 seconds were included as gliding events. However, it is worth noting that this strict cut-off excluded 7/89 events from the gliding + deformation group. Of these interactions, 6 did display short (<5 sec) glides, below the cut-off, and only 1 deformation interaction was
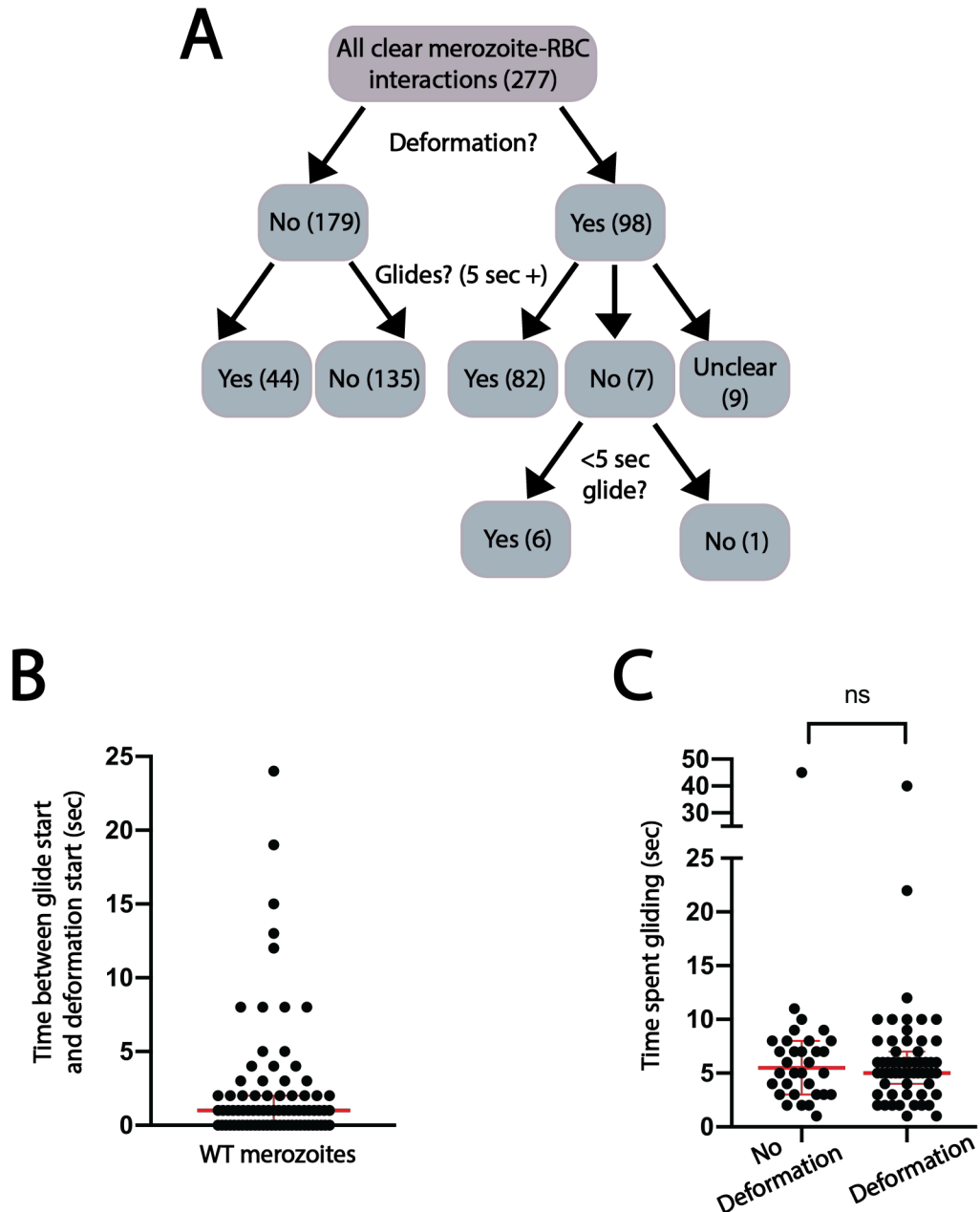
Figure 3.9. Host cell deformation correlates with gliding. (A) Flowchart depicting classification of merozoite-RBC interactions, starting with 277 (out of a total of 284) interactions, which could confidently be divided into interactions resulting in deformation, or no deformation. **(B)** Merozoites typically began deforming host erythrocytes a median of 1 second, and up to 24 seconds after gliding commenced (n= 79 interactions). **(C)** There was no significant difference (ns) between the length of time merozoites spent gliding on erythrocytes when they deformed them (median = 5.5 sec) vs. when they did not cause deformation (median = 5 sec). P=0.8236 (Mann-Whitney U-test). For both graphs, thick red bars indicate medians and error bars, interquartile ranges.

observed without any apparent sign of gliding. Thus, the percentage of deformation interactions coupled to gliding calculated with the 5-second cut-off (92%), is likely an under-estimate. So, overall there is a strong link between gliding and deformation, and it may even be that gliding is required for this process to occur.

Conversely, not every gliding interaction progressed into deformation. For 35% of gliding interactions (44/126 gliding events), merozoites would travel over erythrocytes without ever indenting them, or causing any wrapping motions (See examples in Video 3.3). Interestingly, there was no significant difference between the lengths of time merozoites spent gliding on erythrocytes they did not deform, vs. those they did (Fig 3.9C). Therefore, merozoites did not appear to "try harder" to initiate deformation by gliding on a given cell for longer durations, when deformation did not occur.

3.3.2 Strong host cell deformation is associated with *P. knowlesi* invasion of human RBCs

Previous analysis of *P. falciparum* invasions determined that almost all invasions, across three different strains (3D7, D10, and W2mef), were preceded by deformation. Furthermore, there was a strong association between the extent of that deformation and the likelihood of invasion (Weiss et al., 2015). To determine the importance of deformation for *P. knowlesi* invasion and to investigate whether the level of deformation could be used to predict the likelihood of invasion, parasite-host cell interactions were scored similarly to those described in Weiss et al. (2015), from 0-3. Figure 3.10A shows example top and side views for each deformation score. A score of 0 indicated no deformation, and a score of 1 indicated a slight indentation to the RBC. Score 2 deformations were seen as deeper indentations from the side, with the merozoite appearing to be partially embedded into the RBC. From the top view, this score produced a slight 'pinching' of the RBC membrane down the length of the merozoite. The strongest interactions score 3 deformations, resulted in the entire RBC 'folding' down the length of the merozoite, almost entirely enveloping it so that only a small portion of the merozoite could be seen.

A breakdown of the maximum deformation scores for each interaction is summarised in Figure 3.10B. When considering interactions of parasites that did not invade at any point, score 0 interactions contributed to the majority (76.9%) of these, with the next biggest contributors being score 1 and 2 interactions (10.4% and 11.5% respectively).

The strongest score 3 interactions accounted for just 1.2% of non-invader interactions. In stark contrast, all invasions were preceded by deformation. A breakdown of these scores shows that over 95% of these interactions were composed of score 2 (43.9%) and score 3 (51.2%) interactions, with the remaining scores being weak, score 1 interactions. Therefore, as is the case for *P. falciparum*, strong deformation correlates with successful *P. knowlesi* invasion events.
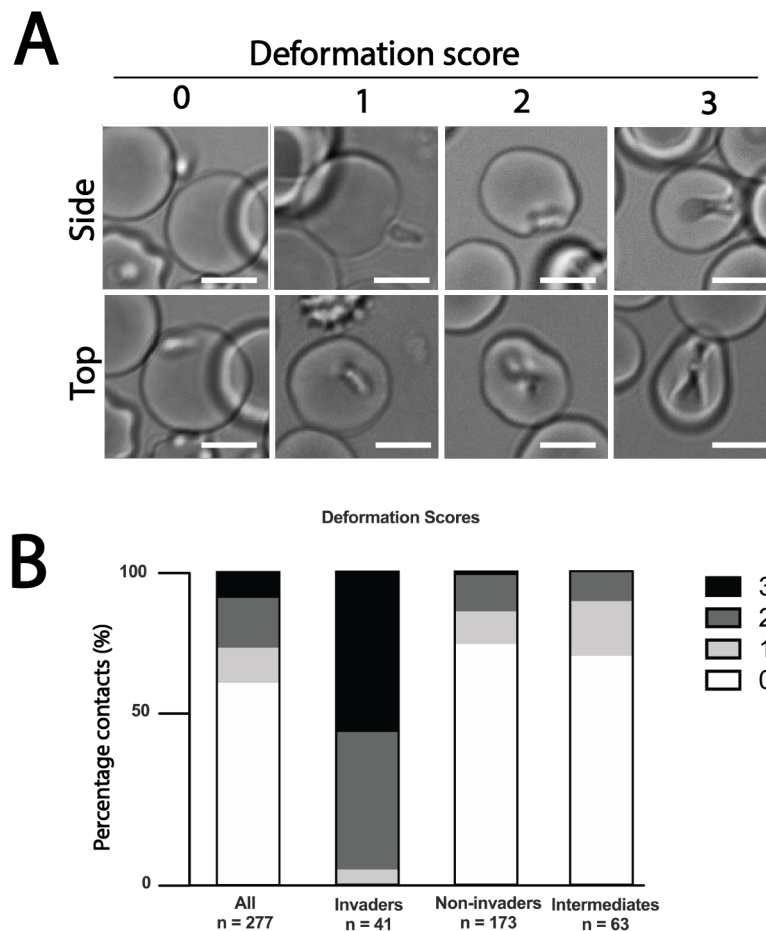
Figure 3.10. **Strong deformation correlates with invasion**. **(A)** Host cell deformation scoring based on indentation level and the extent of merozoite wrapping. Score 0 = no deformation; score 1 = shallow indentations/shallow membrane pinching; score 2 = deeper indentations to the side of the erythrocyte/host cell membrane pinching around the middle of the zoite; score 3 = full host cell bending/wrapping around the merozoite. Scale bars = 5μm. **(B)** A breakdown of deformation scores for 1) every merozoite-RBC interaction (all interactions), 2) interactions leading directly to invasion (invaders), 3) interactions from merozoites which never invade (non-invaders), and finally, 4) interactions happening prior to the final interaction resulting in invasion (intermediates).

To investigate why this could be the case, each scored subgroup was analysed to determine the relative likelihood of invasion success. Overall, 91.3% of all score 3 interactions culminated in invasion, while only 40.9% of score 2, and a mere 6.5% of score 1 interactions led to invasion. Thus, while merozoites performed double the number of score 2 vs. score 3 events (44 events vs. 23), score 3 events had more than double the chances of leading to invasion than score 2 events did. Therefore, as for *P. falciparum*, it is likely that it is the extent of the wrapping motions themselves that contributes to this success, perhaps by increasing the surface area of the RBC that the merozoite is exposed to, or vice versa, so that the molecular interactions required for subsequent steps can be formed.

3.3.3 Weak deformation scores characterize intermediate contacts

As already explored in previous sections, additional RBC contacts precede around 60% of invasion events. This subset of contacts, the 'intermediate' interactions, was of great interest, as they are initiated by parasites that are proven to be viable, but yet require several attempts to invade. Furthermore, the majority of these intermediate contacts (86%) were unique, suggesting that cell sampling, especially enabled by gliding motility, contributed to the ultimate ability of the parasite to invade eventually. Yet, why are intermediate cells deemed inadequate for invasion?

In order to begin to address this complex question, the deformation scores of intermediate contacts were assessed to see whether they were more reflective of interactions from parasites that never invaded, or could perhaps be predictors of their eventual ability to invade. Interestingly, the scoring for this group (Figure 3.10B) was almost identical to the scoring of the non-invaders, with over half of interactions given a score of 0 (73%), and the rest composed of score 1 and 2 interactions. No score 3 interactions were observed for this group.

However, 58% (n= 37/64 interactions) of intermediate interactions were also gliding interactions. Thus, the reason for this overall lack of deformation did not appear to be linked to parasite motility, per se. Perhaps instead it is due to another parasite related factor, such as delayed secretion of a particular ligand necessary for deformation, or due to a host cell factor, such as variations in RBC deformability or surface receptor densities (Koch et al., 2017; Sisquella et al., 2017). Again, an ideal way to assess these theories would be to compare *P. knowlesi* invasion of human RBCs with invasion of

macaque RBCs. In theory, if intermediate contacts are rejected primarily due to host cell factors, *P. knowlesi's* preference for macaque erythrocytes (Moon et al., 2016) may mean that fewer intermediate macaque RBC contacts would be observed overall.

3.3.4 Merozoites cease forward motion and deformation prior to re-orientation

Confusingly, apical re-orientation is frequently described in the literature as the merozoite "[orientating] its apical end onto the erythrocyte surface" (Weiss et al., 2015). On one level, this is true; the merozoite's apical end does need to come into contact with the erythrocyte membrane prior to internalization. However, the merozoite apex contacts the erythrocyte multiple times throughout the pre-internalization steps. Gliding merozoites almost always contact erythrocytes apical end first, because they glide with the apical end leading. Yet, is the act of simply landing in the right position synonymous with achieving "re-orientation"?

A careful analysis of the steps leading up to internalization showed that for *P. knowlesi*, re-orientation occurred in two phases. Firstly, towards the end of deformation, which lasted from 3-45 seconds (a median of 9 seconds, Figure 3.11A), the merozoite appeared to attach itself to the erythrocyte surface firmly, and forward gliding motion ceased (Seen at around 13 sec in Video 3.12, and at 53 s in Video 3.13). It was difficult to determine the exact timing of this event for all invasions, as strong deformation frequently obscured the view of the merozoite. However, by looking at invasions preceded only by score 1 and 2 deformation events (such as video 3.13), on average merozoites paused forward gliding movement 4 seconds before deformation had subsided and the erythrocyte had returned to its original shape (Figure 3.11B). Notably, as the erythrocyte recovered from deformation, the stationary merozoite could be seen to lie lengthwise across the surface of the erythrocyte (Figure 3.11C panels 1 and 2; videos 3.12-3.14). Intriguingly, sometimes if the merozoite was attached to the side of the erythrocyte, the apical end appeared to cling to the erythrocyte membrane as it returned from a deformed to a relaxed state (Figure 3.11C, panel 2, and video 3.14, at 9 sec). This indicated that the apical end, in particular, is firmly attached to the erythrocyte at this point in time. Subsequently, phase two of re-orientation ensued. This involved the release of the basal end of the merozoite from the erythrocyte surface, while the apical end simultaneously pivoted on the spot, as

previously described by Yahata et al. (2012) until it was perpendicular to the erythrocyte membrane (Videos 3.12-3.14, Figure 3.11B panels 3-7). The median length of time a merozoite took to pivot from a flat to perpendicular orientation was 3 seconds, although this process ranged from 2-8 seconds (Figure 3.11D). Strikingly, for all invasions (n = 26 clear examples), merozoite pivoting
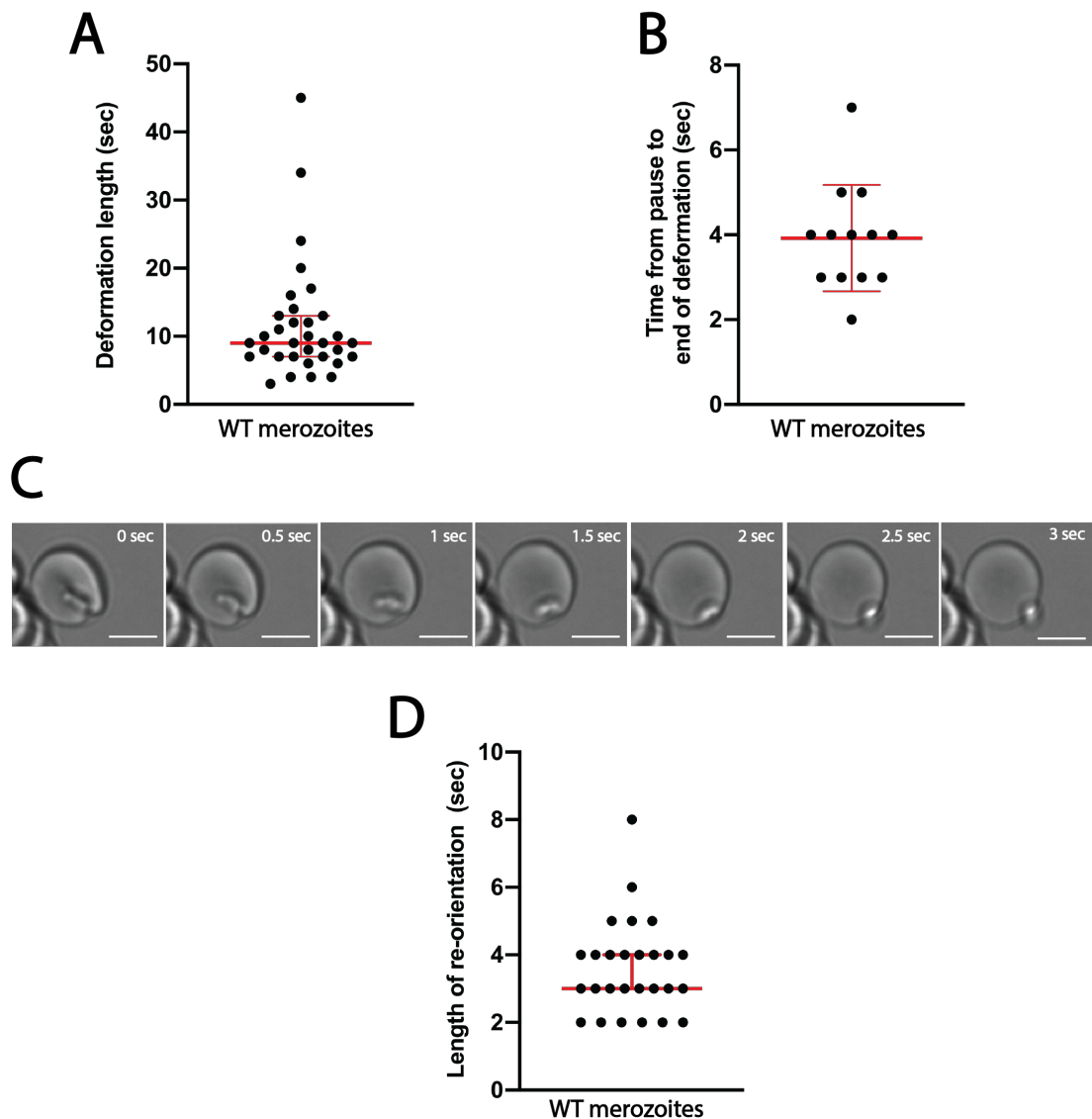
Figure 3.11. Re-orientation occurs after deformation. **(A)** Merozoites deform host cells for a median of 9 seconds and up to 45 seconds, prior to beginning to pivot on their apical ends. **(B)** Merozoites pause forward movement a median 4 seconds (and up to 7 seconds) before deformation ends and the host cell recovers to a relaxed, biconcave shape. **(C)** Stills from video 3.14. Panel 1 shows the erythrocyte recovering from deformation. Panels 1 and 2 show the merozoite's apical end firmly attached to, and holding the erythrocyte membrane inwards. Panels 3-7 show the merozoite pivoting on its apical end, until re-orientation is complete. Scale bars = 5µm. **(D)** Apical pivoting was completed within a median of 3 seconds (and up to 8 seconds). For all graphs, red error bars indicate medians and interquartile ranges.

consistently began immediately after the last wave of deformation had ceased, and the RBC had returned or had very nearly returned to its original morphology (Videos 3.12-3.14). Therefore, these findings confirmed that the mechanical act of deformation itself does not merely tilt the merozoite into the correct angle for entry. Clearly, re-orientation is a carefully orchestrated process, governed potentially by several molecular steps, which are yet to be fully understood. Importantly, in line with this, no parasites were observed to re-orientate and then detach from the erythrocyte. Thus, commitment to invasion likely occurs in the steps leading up to re-orientation.

3.3.5 A calcium flux between merozoite and host cell occurs prior to re-orientation

Having established that *P. knowlesi* merozoites exhibit a very clear "paused" phase just before re-orientation, where the apical end of the zoite is pinned to the erythrocyte surface, the next question to address was whether or not a calcium flux also occurs within this window. To address this question, *P. knowlesi* merozoites were observed while invading Fluo-4-AM loaded erythrocytes. For 11/14 invasions observed, a bright fluorescent dot appeared at the apical end of merozoites after they had paused on the erythrocyte surface, but on average 2.5 seconds prior to the beginning of re-orientation (Figure 3.12A and 3.12B, Video 3.15). Thus, for the majority of invasions, the order of events could be seen to be: 1) deformation and gliding begin, 2) the merozoite ceases forward gliding motility, 3) a calcium signal appears at the merozoite's apex, 4) deformation ceases, and finally, 5) re-orientation begins. Notably, for 3/14 invasions, the calcium flux was observed at a later point, either during re-orientation, or as entry progressed. While the findings for these three invasions could be significant, it is important to note that in these instances, the merozoite's apical end may simply have been out of focus; thus, if the calcium flux did begin prior to re-orientation, it may not have been apparent. Still, a much greater sample size will be needed to validate this theory. Finally, and in contrast to what has been observed for *P. falciparum*, no examples of the dot-like signal spreading to the rest of the host cell, causing it to turn green, were observed (Weiss et al., 2015; Introini et al., 2018). Instead, 8/15 apical signals ceased during or within several seconds of internalization, and 7/15 signals continued for a time beyond this point (Figure 12A, Panel 7 and Video 15), even up to 156 seconds post internalization (Figure 3.12C).
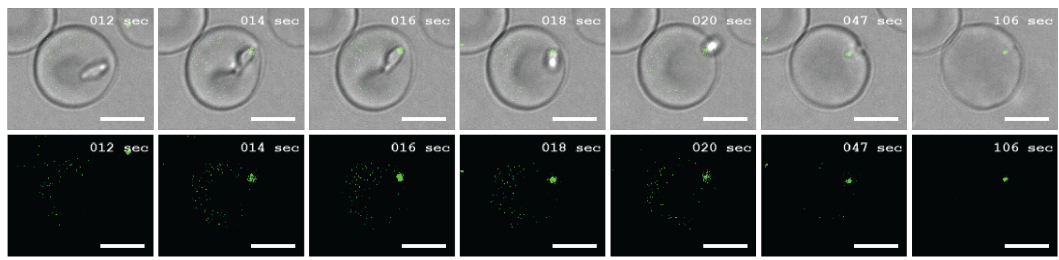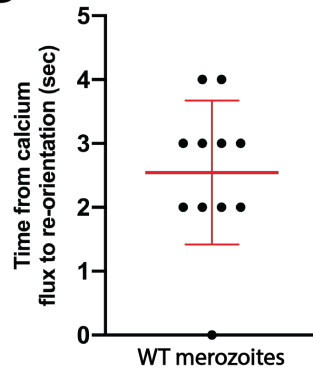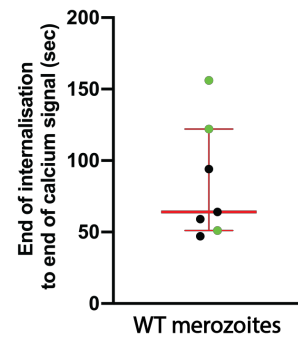
Figure 3.12. A calcium flux between merozoite and host cell begins prior to re-orientation. **(A)** *P. knowlesi* merozoites display a calcium flux between their apical ends and host cell cytosol of Fluo-4-AM loaded erythrocytes. Panels taken from Video 3.15. The fluorescence signal appears to originate at the merozoite's apex (Panel 2) and remain localised to a single dot from start to finish. It begins when the merozoite has ceased forward gliding movement and **(B)** a median of 2.5 sec (and up to 4 sec) prior to the beginning of re-orientation. **(C)** The calcium signal remained at the apical end of the merozoite for a median of 64 seconds post internalisation for 7/15 invasions. Green dots represent where no end point was observed (e.g. the end of filming prevented determining the true end point). For both graphs, thick red bars indicate medians and thinner error bars, interquartile ranges. Scale bars = 5µm.

3.4 Internalisation: moving on in

3.4.1 Re-orientation seamlessly leads to internalization

A previous study reported that after re-orientation, *P. falciparum* merozoites appeared to pause briefly on the surface of the erythrocyte, a step which was hypothesized to allow merozoites time to secrete rhoptry contents needed for moving junction formation (Gilson and Crabb, 2009). In contrast to these findings, our data indicates that the calcium flux begins prior to re-orientation, and that subsequently, re-orientation seamlessly leads into internalization, without a noticeable break between the two events. This was especially apparent when observing merozoites invading from the side of the erythrocyte, rather than top down (Video 3.16).
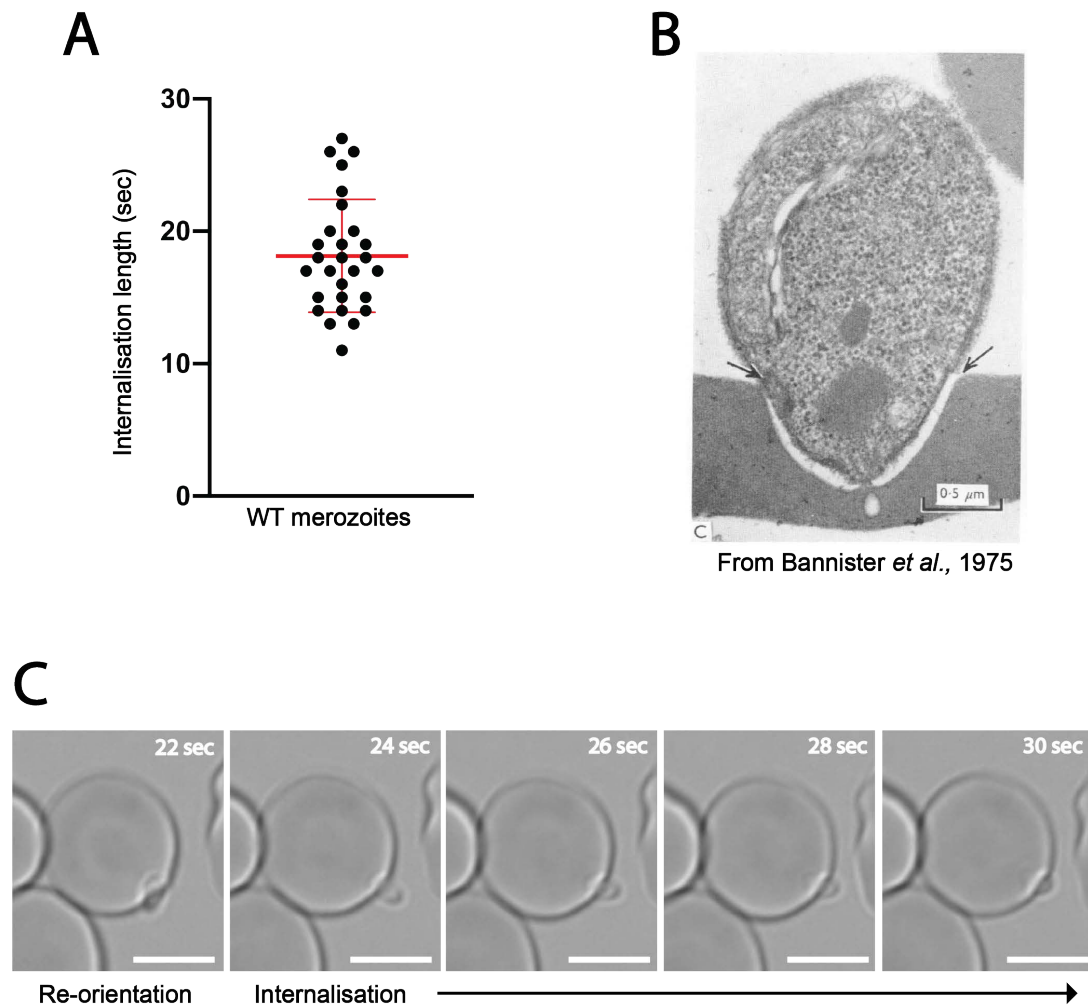
Figure 3.13. Merozoites rapidly re-orientate and drive themselves into host cells. (A) *P. knowlesi* merozoites are internalized within 18 sec (mean) and up to 27 sec post re-orientation. Thick red bar indicates mean, and error bars indicate standard deviation. **(B)** Electron micrograph of an invading *P. knowlesi* merozoite (taken from Bannister et al., 1975), which depicts the apical end of the zoite being compressed as it travels through the junction. **(C)** Panels from Video 3.16 showing that the basal end of the merozoite expands during entry. Scale bar = 5μm.

However, similarly to what has been observed for both *P. falciparum* and *P. yoelii* (Gilson and Crabb, 2009; Yahata et al., 2012) once internalisation began, *P. knowlesi* merozoites rapidly entered host cells, completing this step within 11-27 seconds (Fig 3.13A).

3.4.2 Merozoite morphology changes during internalisation

As discussed in previous sections, *P. knowlesi* merozoites invade wide end first. To begin with, this seemed particularly baffling, as many electron micrographs, depicting invading *P. knowlesi* merozoites show what looks to be entry from the thin end of the

zoite (Figure 3.13B) (Bannister et al., 1975). However, it became apparent during this study that as merozoite entry into the host cell progresses, the basal end of the merozoite appears to expand, rounding out (Figure 3.13C and Video 3.16, at 25-30 sec) presumably as a result of the physical pressure placed around the merozoite-RBC junction, as the merozoite attempts to squeeze through. Therefore, static electron microscopy images likely depict this phenomenon, hence why it frequently appears that merozoites are invading via their thin ends. Additionally, it is worth noting that most examples of early EM images were taken from very thin sections of merozoites. Thus, only a single plane was ever visualized at once, making it even more challenging to determine the full morphology of the cell.

3.5 Post invasion: getting settled

3.5.1 Host cell recovery: when moving house is successful

The final phase of invasion, reported to occur within 30-60 seconds after internalisation is completed, is echinocytosis, the formation of spicules over the entire erythrocyte surface. These spicules remain for several minutes, but eventually, the erythrocyte returns to its biconcave shape (Dvorak et al., 1975; Gilson and Crabb, 2009; Weiss et al., 2015). Interestingly, whilst 70-90% (depending on the specific strain) of *P. falciparum* invasions reportedly culminate in echinocytosis (Weiss et al., 2015), a small proportion does not, for reasons that are not entirely clear.

In good agreement with these studies, whilst the majority of successful *P. knowlesi* invasions lead to echinocytosis (35/38 clear events), 3 invasions did not culminate in echinocytosis. Interestingly, echinocytosis progressed in a variety of ways. In most instances (79% of events), the RBC membrane appeared to twist around the site of merozoite entry, causing the cell to buckle, and fold at that site (Figure 3.14A; Video 3.13 at 75-86 sec, and Video 3.17, at 161-167 sec). This then led to the formation of spicules over the RBC membrane, as the RBC shrivelled into an echinocyte. In 74% of these cases, membrane shrivelling and spiking appeared to spread from the site of buckling across the entire RBC (Video 3.13). However, for the remaining events, membrane spiking remained localized to the half of the RBC inhabited by the newly invaded merozoite (As in Figure 3.14A and Video 3.17). Some echinocytosis events, however, were not preceded by membrane twisting or buckling. For these events, membrane spiking began evenly across the surface of the RBC, and no half-cell

echinocytes were observed (e.g. Video 3.16 at 59 sec onwards). This last group may represent invasions where host cell re-sealing and the pinching away of the parasitophorous vacuole occurred more efficiently.

Overall, the median time at which maximal echinocytosis occurred was 46 seconds post internalisation (Figure 3.14B; n = 29 clear events), which is similar to what has previously been observed for *P. falciparum*. Full recovery, marked not only by the absence of membrane spicules, but also a return of the RBC to its original biconcave shape occurred slowly over the next 3-12 minutes for 26/35 echinocytosis events (Figure 3.14C). However, for the remaining echinocytosis events (9/35 events) the recovery phase was not observed at any point over the duration of the video, either due to erythrocyte clumping, or the end of filming occurring first. Therefore, to investigate the recovery phase more fully, further imaging for a longer duration is needed. However, what has been observed here is consistent with past work for *P. knowlesi* (echinocytosis lasting 10-15 min, from Dvorak et al., 1975), which is a little longer than has been observed for *P. falciparum* (5-10 min; from Gilson and Crabb, 2009).
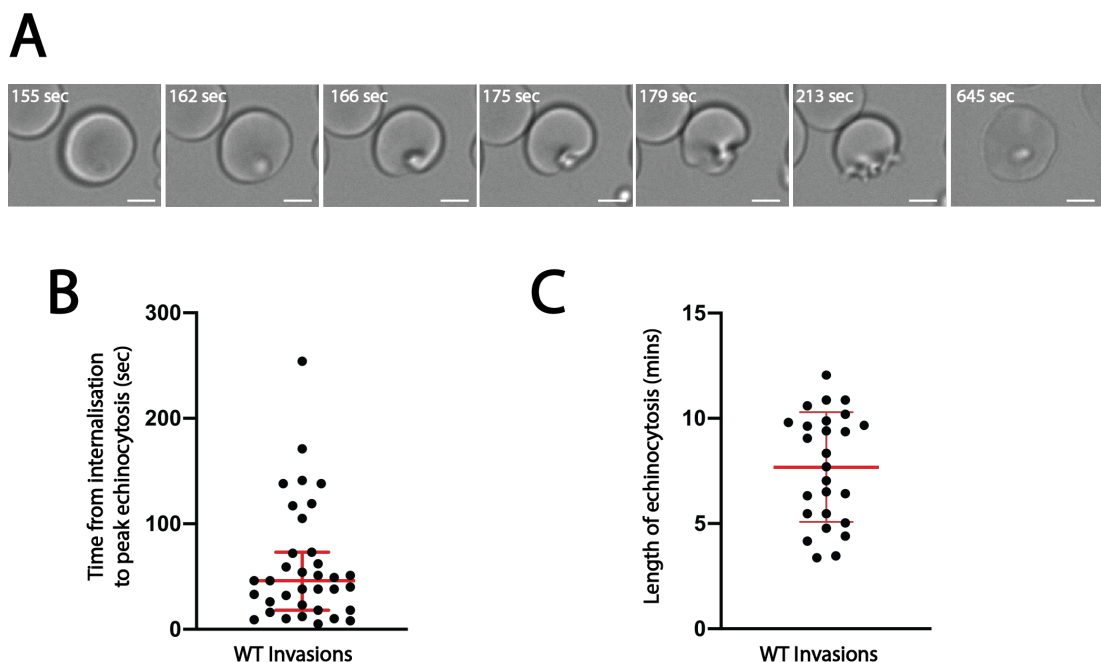
Figure 3.14. Most *P. knowlesi* invasions culminate with echinocytosis. (A) Stills taken from Video 17. Immediately after entry is completed (panel 1), the erythrocyte membrane begins to twist and fold (Panels 2-5). Membrane spikes, indicative of echinocytosis, then form, sometimes remaining localized to one side of the erythrocyte (Panel 6). Finally, the erythrocyte recovers, and the invaded parasite can be seen as a lump under the erythrocyte membrane (Panel 7). Scale bars = 5μm. **(B)** Peak membrane spiking occurs around 46 sec (median) post entry, but can be observed as late as 254 s post entry. Thick red bar indicates median and errors bars show interquartile range. **(C)** Erythrocyte recovery occurs 3-12 min (mean = 7.7 min) after onset of echinocytosis. Thick red bar indicates mean, while error bars indicate standard deviation.

3.5.2 Host cell lysis: when merozoites are evicted from the property

Three failed invasion events were also observed during this study, marked by erythrocyte lysis rather than recovery from echinocytosis. Two of these events appeared to be because a second merozoite or the residual body remained attached to the invading merozoite and prevented it from fully invading and the host cell from re-sealing (Video 3.2). However, a third event was noted, where after a normal invasion and the onset of echinocytosis, a group of additional merozoites bound to, and strongly deformed the echinocyte, which then immediately lysed (Video 3.18). Therefore, it appears that cells undergoing echinocytosis are also particularly sensitive to additional deformation from outside sources. Given that overall 3/47 (total) invasion events ended in lysis, this presents an impairment that likely does affect the replication rate of *P. knowlesi* parasites, unless having more RBCs available at a higher haematocrit and the shear forces merozoites are exposed to *in vivo,* prevents these problems from arising. However, since lysis events were also observed by Dvorak et al. (1975) for similar reasons when merozoites were invading macaque erythrocytes, these failures do not appear to be host-cell specific. Thus, so far, there is no indication that post-invasion lysis events prevent *P. knowlesi* parasites from expanding in human cells any more than they would in macaque cells.

3.6 Summary and discussion of the mechanics of invasion

Overall, our results have demonstrated a very clear order to the morphological steps of invasion, clarifying several pertinent questions. Figure 3.15 summarizes these results, outlining the steps that *P. knowlesi* merozoites take to invade human erythrocytes. These steps include initial contact, which may occur by the merozoite gliding to the host cell upon egress or by Brownian motion causing a random merozoite-RBC contact. Regardless, next, the merozoite initiates gliding motility to progress into erythrocyte deformation. Towards the end of deformation, the merozoite stops forward movement, pausing on the erythrocyte surface with its apical end in contact with the erythrocyte surface. This leads to a calcium flux between merozoite and host cell and finally to the merozoite pivoting on its apical end so that it is correctly orientated to drive itself into the erythrocyte.
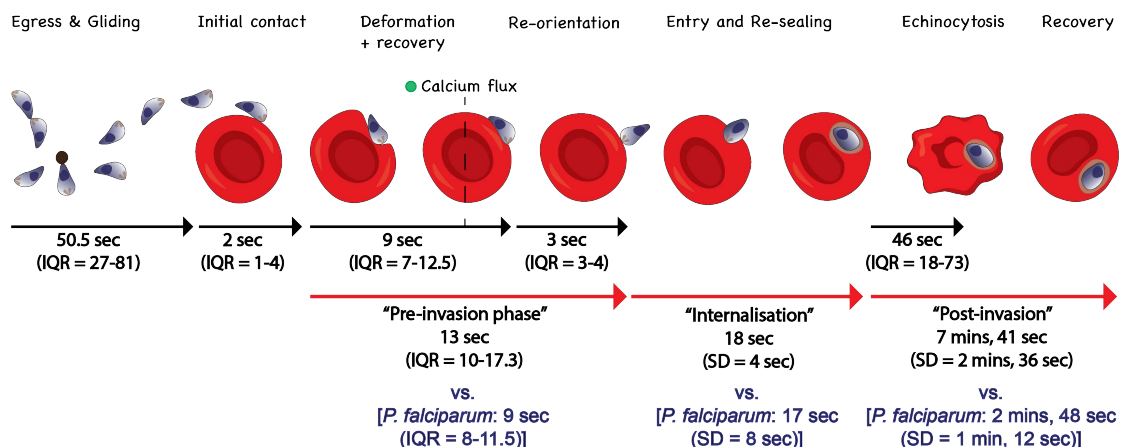
Figure 3.15. An overview of the morphological steps leading to invasion. Black arrows indicate individual steps of invasion. From left to right: Egress → first contact; first contact → beginning of deformation; beginning of deformation → recovery of deformation; beginning of apical pivoting → completion of re-orientation; and finally completion of host cell entry → peak echinocytosis. Red arrows indicate lengths of phases outlined by Gilson and Crabb (2009): "Pre-invasion phase" (the window of time covering the beginning of deformation → immediately prior to internalisation) "Internalisation", and "Post-invasion (window of time covering echinocytosis and recovery to the erythrocyte's original shape). Black text indicates timings for *P. knowlesi* invasion steps. Blue text outlines *P. falciparum* timings reported by Gilson and Crabb, (2009).

Roughly 31 seconds pass from the onset of host cell deformation to the completion of internalisation, although this can range significantly, from 22-73 seconds. Overall, this value is longer than what has been recorded for *P. falciparum* parasites (26 seconds; data from Gilson and Crabb, 2009). Interestingly, both species were internalised in a

similar time (mean time of 18 seconds for *P. knowlesi*, and 17 seconds for *P. falciparum*), despite *P. knowlesi* merozoites being almost double the length of *P. falciparum*. The most significant differences in timings, then, lay between pre-internalisation steps (or "pre-invasion steps", as referred to by Gilson and Crabb, 2009; also see figure 3.15). In particular, while *P. knowlesi* merozoites spent a median length of 9 seconds and up to a maximum of 45 seconds deforming host cells, *P. falciparum* merozoites spent considerably less time doing so (median of 6 seconds and up to a maximum of 8 seconds; data from Gilson and Crabb, 2009). This perhaps indicates that *P. knowlesi* merozoites are generally less efficient at forming the interactions with human RBCs required for subsequent steps. *P. knowlesi* merozoites do exhibit a preference to invade macaque erythrocytes over human (Dankwa et al., 2016; Moon et al., 2016). One reason for this preference could be that specific pre-invasion steps are carried out more efficiently during macaque vs. human invasions, leading to higher invasion success rates overall. One practical reason for the difference in the duration of host cell deformation between *P. falciparum* and *P. knowlesi* could be the difference in densities between species-specific receptors. For instance, while each human erythrocyte contains roughly 1 million copies of the PfEBA-175 receptor, Glycophorin A, on its surface, far fewer copies (only 6000-13,000) of the PkDBPα receptor, DARC, are present (Salinas and Tolia, 2016). Thus *P. falciparum* invasions facilitated by EBA-175 binding to GPA may be more efficient than *P. knowlesi* invasions mediated by PkDBPα-DARC binding if a critical threshold of these respective DBP interactions is required for invasion to progress beyond deformation. Therefore, an interesting experiment in the future will be to compare the invasion dynamics of *P. knowlesi* merozoites invading human vs. macaque erythrocytes to see, for instance, whether or not *P. knowlesi* merozoites deform macaque erythrocytes for a shorter duration before internalisation. Given a chance to invade erythrocytes from its natural host, *P. knowlesi* may exhibit the same propensity observed for *P. falciparum*, to commit to invasion rapidly.

Excitingly, our work has identified gliding motility as a new pre-internalisation step. Despite the long-held theory that merozoites only exhibit gliding motility during host cell entry (Baum et al., 2006; Tardieux and Baum, 2016), imaging *P. knowlesi* merozoites has clearly shown that they are also capable of gliding along host cell surfaces prior to internalization. This feature may allow *P. knowlesi* merozoites to

sample several different host cells before committing to host cell entry. Another reason for *P. knowlesi*'s preference for macaque erythrocytes (Dankwa et al., 2016; Moon et al., 2016) could be that a much smaller subset of human erythrocytes, compared to macaque erythrocytes, are deemed suitable for invasion. *P. knowlesi* parasites exhibit higher growth rates in reticulocyte enriched human blood vs. human normocytes (Moon et al., 2016). Furthermore, PkA1-H.1 parasites can ultimately achieve much higher parasitaemias in macaque erythrocytes than they can in human cells (Moon et al., 2013). Therefore, these results suggest that older macaque erythrocytes might be more amenable to invasion than human normocytes are. Thus the ability to glide and contact multiple erythrocytes may be a huge benefit for this species, enabling it to proliferate in not just macaques, but also humans (Singh and Daneshvar, 2013). Again, future work examining *P. knowlesi* merozoites invading macaque erythrocytes will be required to address this question. However, in theory, if a greater proportion of macaque vs. human erythrocytes is suitable for invasion, merozoites should contact fewer macaque erythrocytes overall, before committing to invasion.

Yet, an important question, which remains outstanding, is how might cell sampling work *in vivo*? Can merozoites transfer from cell to cell, even under flow conditions? In this study, merozoites frequently contacted erythrocytes by travelling across the coverslip, attaching to erythrocytes, and then gliding on to them. If multiple erythrocytes were positioned adjacent to each other, the merozoite could glide across several of them, with intermediate erythrocytes essentially forming a bridge to the merozoite's final destination. While these conditions are indeed artificial, in the 3D environment of the vasculature, erythrocytes may still form bridges, as such. For instance, live *in vivo* imaging of erythrocytes flowing through capillaries shows that they are frequently attached to each other for prolonged periods of time, travelling together at roughly the same rate (McKay et al., 2020). Thus, in theory, this could potentially facilitate the transfer of merozoites from cell to cell. Furthermore, *P. knowlesi* merozoites also possess the ability to rise up on their tails and twirl, akin to what has been observed to other invasive zoites (Håkansson et al., 1999; Siden-Kiamos et al., 2006). This phenomenon could potentially allow merozoites to reach above and adhere to erythrocytes flowing above them.

Gliding may also facilitate host cell invasion within extravascular environments, such as within the bone marrow or the liver. Recent evidence has shown that significant

proportions of schizonts from the closely related species, *P. vivax*, sequester to the bone marrow, liver, and lungs of infected Aotus monkeys (Obaldia et al., 2018). Additionally, significantly higher proportions of ring-stage *P. vivax* parasites have been identified in bone marrow aspirates vs. the peripheral blood of human patients (Baro et al., 2017) in line with evidence that suggests key target cells for *P. vivax* are very young, CD71+ reticulocytes, also found in bone marrow parenchyma (Malleret et al., 2014). One explanation for this phenomenon could be that infected cells are leaving the blood vessels and entering tissue compartments by extravasation (Malleret et al., 2014; Venugopal et al., 2020). However, another exciting possibility is that gliding motility may be providing merozoites with a mechanism to leave the bone marrow vasculature, cross through sinusoidal capillary linings, and enter the red bone marrow compartment. Additionally, once within the bone marrow, gliding could also enable merozoites (either those coming from the bloodstream or rupturing within tissue compartments) to sample the diverse cell types present within this tissue to identify cells susceptible to invasion. Recent evidence also suggests that both *P. falciparum* and *P. berghei* gametocytes can sequester to extra-vascular spaces within the bone marrow (De Niz et al., 2018; Joice et al., 2014). Again, while extravasation may be responsible for these findings, gliding may also play a role in granting sexually committed merozoites access to young reticulocytes (Venugopal et al., 2020). Thus, gliding may be a highly important but under-appreciated capability of merozoites of multiple *Plasmodium* species.

Importantly, our work has also shown that gliding and host cell deformation are inextricably linked, a finding that suggests that gliding is not just a mechanism merozoites use to move from cell to cell, but also an integral step of invasion. Excitingly, these findings have also been observed for *P. falciparum*, in a recent study performed in parallel to our work (Yahata and Hart et al., 2020). Disruption of *P. falciparum* motor complex components, including PfACT1 and PfGAP45, inhibited extra-cellular motility, as well as the ability of merozoites to deform host erythrocytes (Das et al., 2017; Perrin et al., 2018; Yahata and Hart et al., 2020). However, disrupting the merozoite's molecular motor does not prevent echinocytosis from occurring (Weiss et al., 2015; Das et al., 2017; Perrin et al., 2018) or the nascent moving junction from forming (Miller et al., 1979; Riglar et al., 2011). Thus, while the acto-myosin motor is clearly required for internalisation, pre-internalisation gliding

and deformation may not be absolutely essential steps. However, live microscopy of cytochalasin-D treated *P. falciparum* merozoites shows that they need to contact almost triple the number of erythrocytes before forming attachments leading to echinocytosis (Weiss et al., 2015). Therefore, both gliding and erythrocyte deformation likely increase the chances of a merozoite forming the interactions it needs to progress on to the next steps of invasion, and thus overall increase the efficiency of host cell selection.

After deformation subsides, *P. knowlesi* merozoites then re-orientate, so that the widest part of the zoite is vertically aligned with the erythrocyte, ready for entry to begin. Critically, the results from our work show that re-orientation is a distinct mechanical step to deformation, just as it also appears to be for *P. yoelii* (Yahata et al., 2012). Furthermore, we show that re-orientation is preceded firstly by a pause to gliding motility, and secondly by a calcium flux between merozoite and host cell. This is in contrast to the order of events described for *P. falciparum*, with both deformation and re-orientation predicted to occur simultaneously, and the calcium flux hypothesized to occur after re-orientation (Gilson and Crabb, 2009; Weiss et al., 2015; Volz et al., 2016; Introini et al., 2018). The possibility that these two species might be behaving in such a vastly different manner was intriguing. However, a closer examination of the *P. falciparum* videos published by Gilson and Crabb (2009) revealed that this might not be the case. The most obvious reason is the lower time resolution of that study, in which invasions were imaged at a rate of 1 frame every 2-5 seconds. Our *P. knowlesi* data, imaged at a rate of 1 frame/sec, showed that merozoites typically complete re-orientation within 3-4 seconds, suggesting that most *P. falciparum* re-orientation events may have been missed due to the slower frame rate. However, one video from Gilson and Crabb (2009), did manage to capture a re-orientation event, reminiscent of *P. knowlesi* invasions, with the merozoite pivoting after deformation had ceased (See attached Video 3.19 at 36-38 sec, taken from Gilson and Crabb, 2009). Importantly, this video also clearly shows the *P. falciparum* merozoite re-orientating on to its wider end, in good agreement with data from Yahata and Hart et al. (2020), which demonstrated that like *P. knowlesi*, *P. falciparum* merozoites also glide (and therefore invade) with their wide ends leading. Thus, although re-orientation appears to be a much more subtle event for *P. falciparum,* on the whole, it is likely that both species perform these steps in the same order.

Naturally, after considering all of this new information, questions arise regarding the molecular steps underpinning each morphological phase. For instance, if deformation and re-orientation are mechanically distinct steps, do separate molecular pathways underpin them? Or is deformation simply the by-product of the molecular interactions, which are necessary for re-orientation? For *P. falciparum*, members of the DBP and RBL families, aside from PfRh5, are hypothesized to perform overlapping roles, facilitating both deformation and re-orientation (Weiss et al., 2015; Tham et al., 2015). However, the complexity of the *P. falciparum* RBL and DBP families has meant that determining the individual roles for each family member has been difficult. In contrast, *P. knowlesi* relies on one DBP (PkDBPα) and one RBL (PkNBPXa) to invade human erythrocytes (Moon et al., 2016; Singh et al., 2005). Therefore, chapter 4 explores the roles of PkNBPXa and PkDBPα and attempts to address the question of which step, or steps, each ligand might facilitate.

Chapter 4: Exploring the roles of PkDBPα and PkNBPXa during invasion

4.1 Introduction

A cascade of molecular interactions governs the mechanical steps of invasion examined in chapter 3. For *P. falciparum*, some of these interactions have been well characterised, such as the binding of PfAMA-1 to its parasite-derived receptor, PfRON2, to form the moving junction (Lamarque et al., 2011; Srinivasan et al., 2011). However, the interpretation of molecular steps facilitating earlier events quickly becomes more complex. A particular subject of intense debate has been whether all of the *P. falciparum* RBL and DBP family members perform entirely synonymous roles (erythrocyte deformation and potentially apical re-orientation), or whether a subset of ligands performs unique functions (Gunalan et al., 2011, 2013, & 2020; Singh et al., 2010). The apparent redundancy between specific *P. falciparum* RBL and DBP family members, such as PfEBA-175 and PfRh4, has complicated phenotypic studies considerably (Duraisingh et al., 2003b; Stubbs et al., 2005; Gaur et al., 2006; Weiss et al., 2015). Immunofluorescence data has shown that the *P. falciparum* RBL and DBP members both localize to the apical surface of free merozoites pre internalisation (Taylor et al., 2002; Treeck et al., 2006; Triglia et al., 2009; Gunalan et al., 2011). Thus both families are suitably located to mediate apical attachment and re-orientation. However, the ectodomains of both families undergo multiple processing steps during invasion, which may lead to the release of different erythrocyte binding domains, which could, in theory, allow these ligands to perform secondary roles downstream of their initial functions (Triglia et al., 2009; Gunalan et al., 2011 & 2020).

Another source of debate, which has confused the issue further, is the question of whether the RBL ligands are secreted before the DBP ligands, or vice versa (Singh et al., 2010; Gao et al., 2013). *P. falciparum's* separation of invasion ligands between different organelles – primarily the rhoptries and micronemes - is presumed to play an important role in moderating the order of their release during invasion, and therefore, the sequence of molecular events leading to its completion (Harvey et al., 2012; Cowman et al., 2017). While the PfRBL ligands are localized to the rhoptry necks, the PfDBPs are localized to the micronemes (Lee Sim et al., 1992; Rayner et al., 2001;

Thompson et al., 2001; Triglia et al., 2001; Duraisingh et al., 2003b; Gilberger et al., 2003). Thus, if one family is secreted before the other, this could indicate that some DBP and RBL ligands perform sequential functions. However, the order of RBL/DBP secretion has never been systematically explored using fluorescently labelled lines and live microscopy techniques. Instead, protein localization has relied upon immunofluorescence data of fixed cells, which has lead to conflicting results regarding the order of their secretion. For instance, Singh et al. (2010) proposed that the PfEBA-175 secretion is triggered upon egress and that when it binds to its receptor, glycophorin A, the PfRBL ligands are released from the rhoptries. Conversely, Gao et al. (2013) came to the very opposite conclusion: that PfEBA-175 is secreted just before the formation of the moving junction, but after PfRh1 interacts with its host cell receptor. Therefore a conclusive answer to the question of whether one family is secreted before the other remains elusive. Furthermore, it is also not known whether all micronemal secretion precedes rhoptry secretion, or whether subsets of micronemes exist, which carry our distinct roles. Intriguingly, in contrast to *P. falciparum*, the *P. knowlesi* and *P. vivax* RBL and DBP families are both localized to the micronemes (Meyer et al., 2009; Han et al., 2016). Thus, there may be no hierarchy to RBL/DBP secretion for these species. Alternatively, if the *P. vivax* and *P. knowlesi* RBL and DBP families are secreted separately, this would support the hypothesis that micronemal subsets exist, and could provide a way for these species to release key invasion ligands temporally.

The relative simplicity of the *P. knowlesi* RBL and DBP families means that studying the order of their secretion and determining the roles of individual ligands is likely to be a much more straightforward process than studying their *P. falciparum* counterparts. Only one PkRBL and one PkDBP protein, PkNBPXa and PkDBPα, respectively, are critical for human erythrocyte invasion (Singh et al., 2005; Moon et al., 2016). Given the essential nature of each ligand, this suggests that PkDBPα and PkNBPXa may be facilitating separate steps of invasion. However, the precise role(s) of these two proteins remain largely unknown.

An early study investigating *P. knowlesi* merozoite interactions with Duffy negative erythrocytes reported that *P. knowlesi* merozoites were capable of deforming Duffy negative cells, even though they could not invade them (Miller et al., 1975). However, this study did not describe to what extent merozoites could deform Duffy negative

cells, or whether they could apically re-orientate. A later study examining PkDBPα KO parasites by EM depicted seemingly apically aligned merozoites attached to human erythrocytes but without evidence of a junction having formed between each parasite and host cell. Therefore, this study concluded that PkDBPα KO parasites are capable of performing all invasion steps up to, and including re-orientation, but that PkDBPα is instead required for junction formation (Singh et al., 2005). Arguably, though, it is possible that the apically aligned merozoites, as seen by EM could simply have been the result of random merozoite-RBC interactions, rather than the merozoite specifically pivoting on to its apical end after deformation. Therefore, further examination of these events by live microscopy will be necessary to understand whether PkDBPα is required for re-orientation, or not. Even less is known about the role of PkNBPXa, other than the fact that while PkNBPXa null parasites can stick to the outside of human erythrocytes, they cannot invade them (Moon et al., 2016).

I, therefore, adopted two distinct strategies to address the hypothesis that PkDBPα and PkNBPXa may be performing distinct roles during the early steps of invasion and to understand better how their storage, order of secretion, and localization before and during invasion relates to these roles. Firstly, I aimed to label both PkNBPXa and PkDBPα, as well as known moving junction markers PkAMA-1 and PkRON2, with fluorescent and epitope tags, using our newly developed CRISPR-Cas9 system (Mohring et al., 2019). This system relies on one plasmid that contains both the Cas9 and sgRNA cassettes, as well as two selectable markers: one for positive selection and one for negative selection. The positive selectable maker, the *hdhfr* gene, gives resistance to the drug pyrimethamine and selects for parasites that have taken up the Cas9 plasmid, immediately after transfection. The negative selectable marker, encoded by the *yfcu* gene, causes cell death upon addition of the drug, 5-fluorocytosine. Once integration of the donor DNA (provided as a separate construct, without any selectable marker) has occurred, parasites are treated with 5-fluorocytosine, killing all parasites still carrying the Cas9 plasmid, and resulting in marker-free cultures, ready for further modifications. An additional benefit of this system is that efficient homologous repair of Cas9 induced double-stranded DNA breaks can be achieved using donor DNA introduced as a PCR product, containing homology arms with ≥200 base pairs - thus eliminating the need for plasmid delivery and conventional cloning strategies. Importantly, the optimization of this strategy, which I contributed to throughout the

early stages of this project, paved the way for me to generate multi-tagged lines rapidly. These lines allowed me to investigate the dynamics of secretion and invasion directly, using live microscopy, on top of indirect, immunofluorescence methods to explore the localizations of each ligand relative to each other.

Our CRISPR-Cas9 system also enabled me to work towards strategy number two: the generation of PkNBPXa and PkDBPα conditional KO (cKO) lines, using the Dimerisable Cre-recombinase (DiCre) system (Andenmatten et al., 2013; Collins et al., 2013). This system relies upon parasites expressing the Cre-recombinase enzyme in two halves, each fused to a different rapamycin binding protein: either FKBP12 or FRB. Addition of rapamycin to culture media induces both binding partners to form a heterodimer, and in doing so brings each enzyme half together, resulting in an active form of the recombinase. Active Cre-recombinase can then recognize short 34bp sequences, called LoxP sites, and perform site-specific excision of DNA sequences within the parasite's genome, which are artificially flanked by LoxP sites, or 'floxed' (Andenmatten et al., 2013; Collins et al., 2013). In recent years, the DiCre system has been optimized particularly for *P. falciparum* to create inducible knockout lines, which have allowed robust analysis of multiple essential invasion genes, otherwise refractory to deletion (Yap et al., 2014; Volz et al., 2016; Das et al., 2017; Perrin et al., 2018). However, at the beginning of this study, no DiCre expressing background lines existed for *P. knowlesi*. Maintenance of previously generated PkNBPXa and PkDBPα KO lines relies upon a continuous supply of macaque RBCs (Singh et al., 2005; Moon et al., 2016). However, since macaque cells are a limited resource in the UK, relying on their availability was not a practical approach. Therefore, I worked to generate *P. knowlesi* DiCre background lines and iteratively modifying them to produce cKO lines, so that I could image these lines using live microscopy, to determine which steps of invasion are impeded when either PkNBPXa or PkDBPα is absent.

4.2 An overview of strategies used to generate transgenic P. knowlesi parasites

4.2.1 Using CRISPR-Cas9 to target P. knowlesi invasion ligands

The GC-rich (37.5%, as compared to *P. falciparum* - 19.4%) genome of *P. knowlesi* provides distinct advantages to genome editing, particularly for Cas9 mediated double-stranded breaks and their subsequent repair (Pain et al., 2008; Mohring et al., 2019). Cas9 activity requires recognition of a 20 bp guide sequence within the desired locus, that is immediately followed by an 'NGG' site. Disruption of either the target sequence or the NGG site prevents further DNA cleavage (Mojica et al., 2009; Jinek et al., 2012). Within the *P. knowlesi* genome, 'NGG' sites are relatively abundant, even within non-coding regions. Therefore, where possible, cut sites were chosen so that insertion of a new sequence, such as a tag, or LoxP sequence, would split the 20 bp guide sequence from its corresponding NGG site and ablate further Cas9 activity. This strategy worked particularly well for tagging *PkNBPXa*, *PkRON2*, and *PkAMA-1*, with c-terminal tags (see section 4.3), as all of these genes have NGG sites almost immediately following their stop codons (Figure 4.1A).

PkDBPα also contains NGG sites downstream of the stop codon; however as has previously been reported, all three PkDBPs share a high degree of sequence similarity (Adams et al., 1990, 1992) at both protein and DNA level (~94% similarity for *PkDBPα* vs. *PkDBPγ*), and in their 3'UTR regions. This feature means that designing constructs to target each PkDBP individually by CRISPR-Cas9 is challenging. Figure 4.1B shows the alignment of the c-terminal sequences of all three genes, with potential NGG target sites. No target sites unique to wild type *PkDBPα* are available within 40bp either side of the *PkDBPα* stop codon. Therefore, to overcome this problem, c-terminal modifications to *PkDBPα* were performed using a parasite line in which the entire DBPa ORF has been replaced with a recodonised *PkDBPα* (*RecDBPα*) sequence, which also lacks *PkDBPβ* (Mohring et al., 2019). The *PkDBPα* coding sequence of this line is unique enough to allow specific homology region and guide RNA design that allows *PkDBPα* to be modified, via a cut site just before the stop codon without off-target cutting of *PkDBPγ*. (Figure 4.1B). When targeting the C-terminus of *PkDBPα*, a silent mutation was introduced to the same site within repair

templates (TGG —> TTG) in order to prevent subsequent Cas9 cleavage at the modified locus.
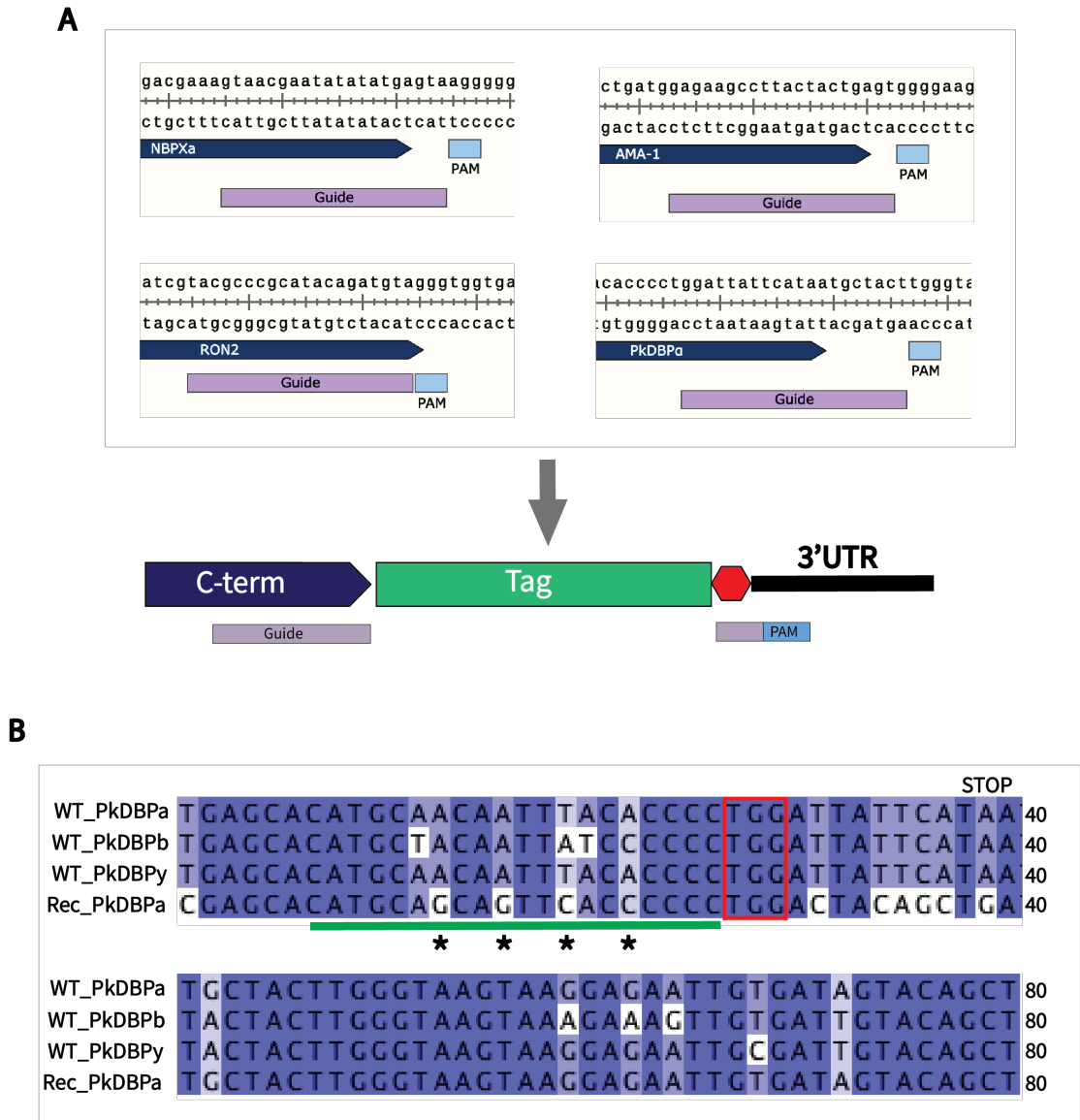
Figure 4.1. Choosing guide sequences to target *P. knowlesi* invasion genes. A) *PkNBPXa*, *PkDBPα*, *PkRON2*, and *PkAMA-1* all have 'NGG' Cas9 cut sites several base pairs after their respective stop codons. Addition of a tag immediately prior to the stop codon splits the guide sequence from the NGG site. **B)** Sequence alignment of the last 40bp of the coding sequence + the first 40 bp of the 3'UTR for all three WT PkDBP sequences and the *RecDBPα* sequence. The cut site used to target *RecDBPα* is indicated by a red rectangle, and the guide sequence is underlined in green. Asterisks indicate differences between *RecDBPα* and *PkDBPγ*, which enable specific targeting of *RecDBPα*.

4.2.2 A modified three Step PCR method enables quick and efficient Donor DNA generation

The cloning steps necessary to create donor DNA plasmid constructs can be time consuming and labour-intensive, and so we sought to develop methods to improve the efficiency of donor DNA construct synthesis (Mohring et al., 2019; Mohring et al., 2020). Mohring *et al.* demonstrated that efficient homologous repair of Cas9 induced double-stranded DNA breaks can be achieved using donor DNA introduced as a PCR product, containing homology arms with ≥200 base pairs, and thus eliminating the need for plasmid delivery and conventional cloning strategies. In order to quickly synthesize constructs containing a fluorescent tag, a previously established protocol (Ecker et al., 2006) was used as a starting point. This protocol consists of two amplification steps: the first to synthesize both homology regions (HR1 and HR2) from parasite gDNA, with overhangs to the tag of choice; and the second using both homology region PCR products and the plasmid template carrying tagging sequence, to amplify the full construct. As this approach varied in final product purity and yield, I attempted to improve reproducibility with a modified approach. By amplifying the tagging sequence (T3) separately, and using gel extracted PCR products as templates in a three-step nested PCR protocol (Figure 4.2A), it was possible to generate transfection-ready constructs within a day with both reliable final product purity and high yields (~100ng/μl for the PkNBPXa and PkDBPα constructs in Figure 4.2B). These high yields meant that 6-8 final (50 μl) reactions generated enough DNA for two transfections. Likewise, to generate constructs with a smaller insert, such as an epitope tag, a similar approach was applied. However, only two PCR steps were required: one to amplify both homology regions with overhangs to the tag and the second to fuse both homology regions and intervening tag together.
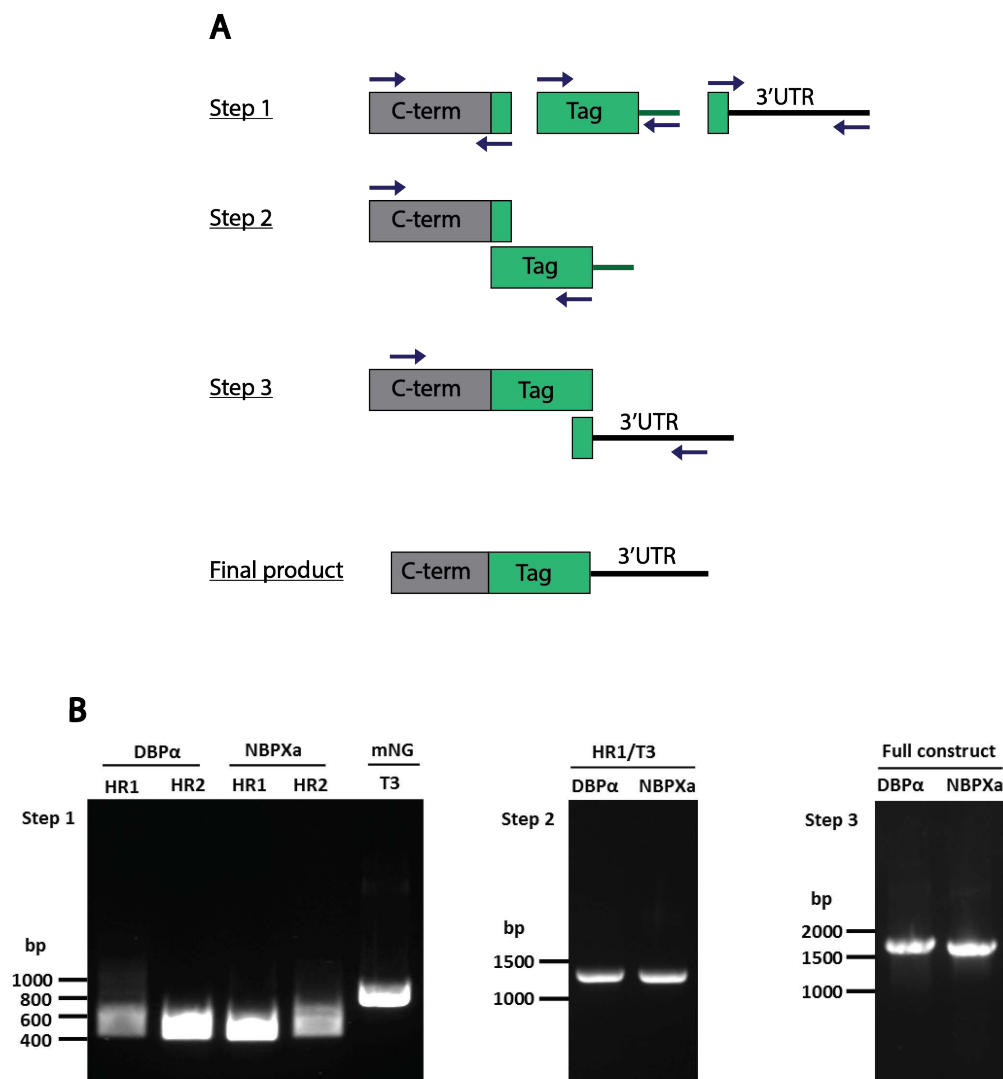
Figure 4.2. A Three-step PCR method for generating transfection constructs
(A) Schematic showing each PCR step. 1) Amplification of each homology region and tag separately: homology region 1 (HR1), the tag (T3), and homology region 2 (HR2). The tag (amplified from plasmid DNA) is amplified with an overhang to the plasmid it came from, which is removed in subsequent steps. Primers used to amplify HR1 and HR2 contain sequences to add on overhangs to T3. 2) Fusion of HR1 and T3 using a forward primer amplifying from the start of HR1, and a nested reverse primer inside of T3. 3) Fusion of the HR1/T3 template with HR2 to generate the full construct using nested primers placed inside of HR1 and HR2. **(B)** Example gel images of each of the three step PCR results for mNeonGreen (mNG) tagged PkNBPXa and PkDBPα constructs. Expected sizes: Homology regions left to right – 524 bp, 464 bp, 514 bp, 524 bp, 836 bp; HR1/3 – 1176bp, 1173 bp; Full constructs: 1617 bp, 1580 bp.

4.2.3 An overview of transgenic lines used and produced in this study

Being able to produce marker-less transgenic lines has opened up opportunities to make serial modifications to single parasite lines (Knuepfer et al., 2017; Zhang et al., 2017; Mohring et al., 2019). This has especially revolutionised *P. knowlesi* work, as prior to developing a marker-less Cas9 system, only one marker (*hDHFR*) had been reliably integrated into target loci to select for transgenic *P. knowlesi* parasites after transfection (Singh et al., 2005; Moon et al., 2013; Moon et al., 2016). Therefore, with these new developments, a key objective of this study has been not just to tag, or flox (flank with LoxP sites) single genes, but to begin to build libraries of multi-tagged and floxed lines, so that dynamic invasion processes can be dissected. For instance, a line produced by tagging PkDBPα with a fluorescent label, on top of an inducible *PkNBPXa* KO line, could be used to address the question of whether or not PkDBPα can be secreted in the absence of PkNBPXa.

Figure 4.3 shows a flowchart of the transgenic lines produced in this study, which are described in much greater detail in the following sections. At the beginning of this study, Dr Franziska Mohring (LSHTM) generated the PkRecDBPα line (line 2 from Figure 4.3, and described in Mohring *et al.,* 2019), which I used as a background for lines in which I targeted (or later intended to target) *PkDBPa* with a c-terminal tag. Additionally, it is also important to note that before beginning this study, no *P. knowlesi* DiCre expressing background line had been published, as had been for *P. falciparum* (Collins et al., 2013; Knuepfer et al., 2017). Thus early project work included the production of these lines. Dr Franziska Mohring and Dr Avnish Patel (LSHTM), synthesized the donor DNA and Cas9 plasmids for these transfections (described in section 4.5), and Dr Mohring transfected them into the WT PkA1-H.1 background, producing the WT DiCre line (line 3). I then transfected both plasmids into RecDBPa background lines (lines 2&5) to produce two additional DiCre lines (lines 7&11). One final note is that a second WT DiCre background line (line 4), kindly donated by Dr Ellen Knuepfer (Francis Crick Institute/RVC), was produced concurrently from a separate study, and was used to generate a *PkDBPα* cKO line (line 9) when we experienced difficulty producing this line from our WT A1-H.1 DiCre background (See section 4.7). Overall, 18 new transgenic lines were generated from this study. Due to time constraints, not all of them have been phenotyped (indicated by white boxes in the flow chart). However, they demonstrate the robustness of the

CRISPR-Cas9 system for use in *P. knowlesi* and will be a valuable resource for taking the findings of this study forwards.

4.3 Successful tagging of *P. knowlesi* invasion ligands

4.3.1 PkNBPXa, PkDBPα, PkAMA-1, and PkRON2 can all be modified to introduce C-terminal fluorescent protein tags

In order to investigate when the *P. knowlesi* RBL/DBP ligands are being secreted, and to determine their localizations throughout invasion, I attempted to tag the C-terminus of PkNBPXa and PkDBPα with mNeonGreen (mNG), an exceptionally bright fluorescent protein (Shaner et al., 2013). This would allow these ligands to be visualized using live microscopy, and enable dynamic processes such as secretion, and potential changes to localization, to be mapped to the distinct morphological steps of invasion. I also attempted to tag the micronemal protein PkAMA-1 (Healer et al., 2002) and the rhoptry neck protein, PkRON2 (Zuccala et al., 2012; Lyth et al., 2018) with mNG, so that the localization and secretion patterns of PkNBPXa and PkDBPα could be compared to these known moving junction markers (Lamarque et al., 2011; Srinivasan et al., 2011).
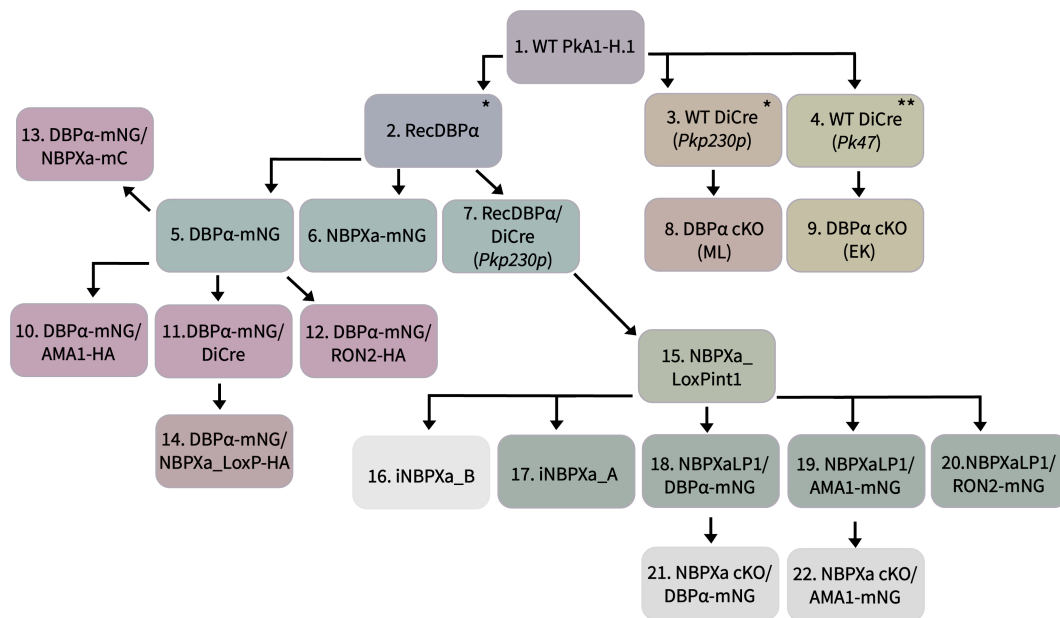
Figure 4.3. An overview of transgenic *P. knowlesi* lines produced in this study. Parasite lines marked with asterisks were generated outside of this study, but have subsequently been iteratively modified within this study. (*Mohring et al., 2019, and Moon lab, unpublished). (**Knuepfer et al., 2019).

PkAMA-1, *PkDBPα*, and *PkRON2* guide sequences were all cloned into plasmid pCas9/sg (described in Mohring et al., 2019). However, due to difficulty cloning the *PkNBPXa* guide sequence into pCas9/sg, this guide was instead inserted into an alternative Cas9 Plasmid, Pl_11 (Appendix figure 4B), which contains all of the components of pCas9/sg, but carries a smaller backbone and a high fidelity (HF) Cas9 sequence instead of the wild type version. Donor DNA constructs were synthesized to include the mNG tag inserted directly in front of the stop codon and flanked by 400 bp homology arms to the 3'end of the gene, as well as the 3'UTR (Figure 4.4A). *PkNBPXa*, *PkAMA-1,* and *PkRON2* donor constructs were all produced by overlapping PCR, and transfected as PCR products, along with their corresponding Cas9 guide plasmids. However, due to the similarity of the *PkDBPα* and *PkDBPγ* 3'UTR regions, the *PkDBPα-mNG* donor construct was synthesized by PCR, but cloned into a plasmid backbone to be sequenced prior to transfection.

PkDBPα-mNG and *PkNBPXa-mNG* constructs were transfected into the RecDBPα line (line 2, from Figure 4.3), before the development of DiCre expressing background lines, leading to the production of lines 5 and 6, respectively. Later, the PkDBPα-mNG construct was also transfected into a DiCre expressing background line (line 15, from Figure 4.3), as were the PkAMA-1-mNG and PkRON2-mNG constructs, generating lines 18, 19, and 20, respectively (Figure 4.3). Following transfection, cultures were screened by PCR for the presence of WT and transgenic parasites using primers listed in Table 2.5 and depicted in Figure 4.4B. Transgenic parasites in which the tags were correctly integrated into the genome were detected by PCR for all variants (Figure 4.4B).

All four fusion proteins could be visualised by live microscopy, localising to the apical ends of merozoites in schizonts, consistent with their proposed micronemal and rhoptry localisations (Figure 4.4C). Very interestingly, in some cases, PkAMA-1mNG staining was also evident on the merozoite surface, prior to rupture (Figure 4.4C), as has previously been noted for *P. falciparum* AMA-1 (Treeck et al., 2009; Riglar et al., 2011). However, no obvious early secretion of PkNBPXa or PkDBPα was observed, which could indicate that these ligands may be stored in different micronemal subsets to PkAMA-1, so that they can be secreted at a later point in time.
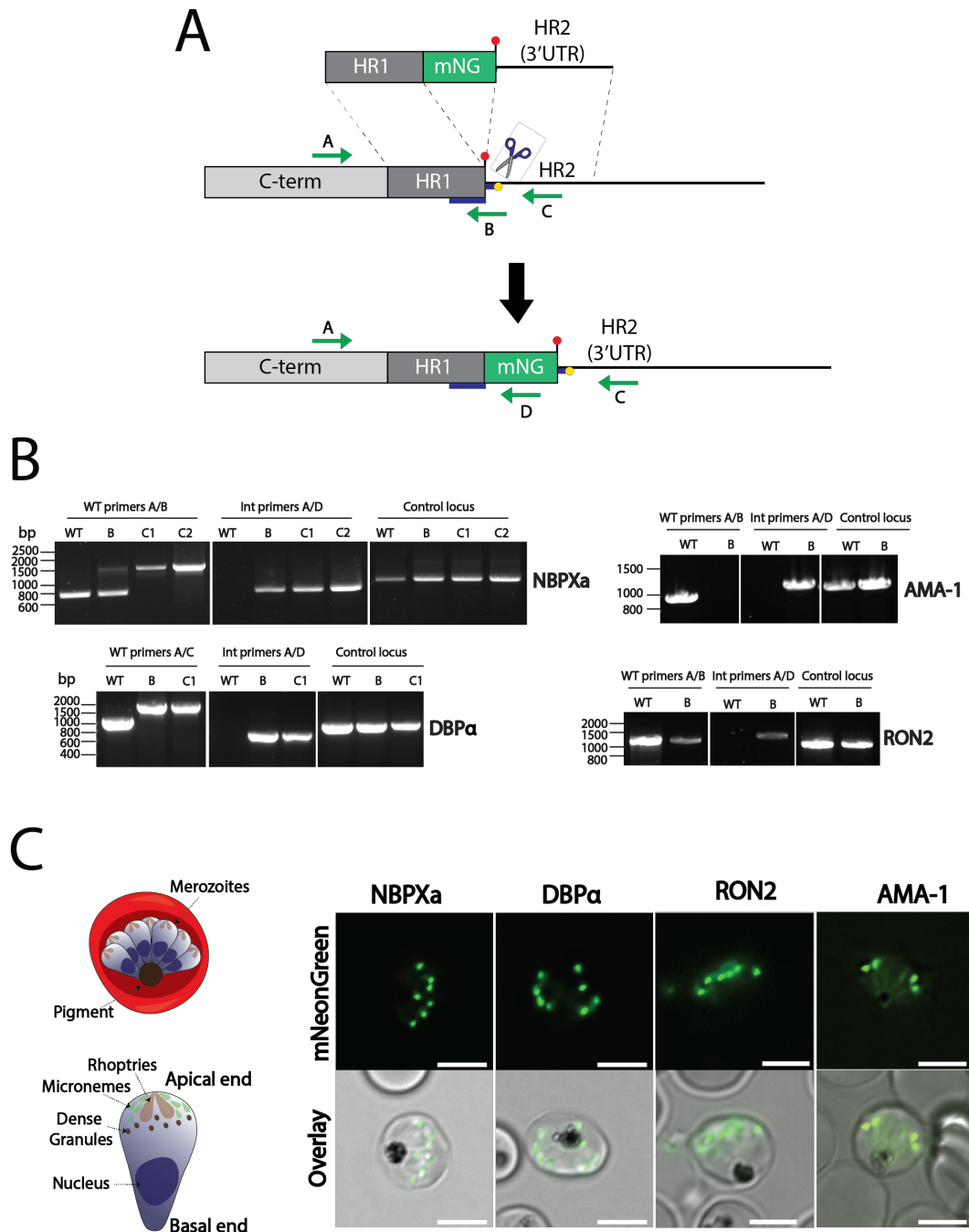
Figure 4.4. Generation of mNG tagged lines. (A) Schematic showing the insertion of an mNeonGreen (mNG) tag prior to the stop codon (red circle) of *P. knowlesi* invasion genes. Blue lines indicate the position of the Cas9 guide sequence used to target PkNBPXa, PkRON2, and PkAMA-1. Yellow dot indicates PAM sequence. Green arrows indicate positions of diagnostic primers used to detect WT and integrated parasites. **(B)** Diagnostic PCRs showing integration of the mNG tag to the *PkNBPXa*, *PkRON2*, and *PkAMA-1*, and *PkDBPα* loci. All primers are listed in Table 2.5 and positions outlined in above schematic. Expected PCR product sizes: PkDBPα WT (primer positions A/C): 1046 bp (or 1778 bp if tag present); PkDBPα integrated (primers A/D): 691bp; PkNBPXa WT (primers A/B): 863bp (or 1565 if tag present); PkNBPXa Integrated (primers A/D): 973bp; PkAMA-1 WT (primers A/B): 984bp; PkAMA-1 Integrated (Primers A/D): 1113 bp; PkRON2 WT (primers A/B): 1209bp; PkRON2 Integrated (primers A/D): 1338bp. **(C)** Cartoon (left) depicts how *P. knowlesi* merozoites are arranged in schizonts, with their wide, apical ends fanning around the haemozoin crystal. Live imaging of tagged parasites (panels, right) shows evidence of mNG fusion proteins, localized to the apical ends of merozoites. Scale bars = 5μm.

Almost all parasites in the PkAMA-1mNG line appeared to be transgenic, as seen by live microscopy, and PCR. However, the remaining lines exhibited a mixture of transgenic and WT parasites, and so the PkDBPα and PkNBPXa mNG lines were subsequently cloned by limiting dilution (Figure 4.4B). However, attempts to clone out the PkRON2-mNG line were unsuccessful, and WT parasites quickly outgrew transgenic parasites in the bulk culture, indicating that the mNG tag is likely detrimental to PkRON2 function, and thereby parasite growth. Therefore, further work using the PkRON2-mNG line was not pursued, and the AMA-1 mNG line was relied upon instead as a marker for the moving junction, for live microscopy work (See section 4.4).

4.3.2 Dual- tagging of apical markers demonstrates overlapping localisations of micronemal proteins

Having established that PkDBPα, PkNBPXa, and PkAMA-1 proteins can tolerate even a bulky fluorescent label, the next step was to produce multi-tagged lines for co-localisation studies. Firstly, further modifications were made to a clonal PkDBPα-mNG line (line 5, from Figure 4.3), targeting *PkAMA-1*, and *PkRON2* with a HA tag (Figure 4.5A), and PkNBPXa with a mCherry (mCh) tag. At the same time, a DiCre expression cassette was also introduced into the DBPα-mNG line (described in detail in 4.5.1). On top of this resulting line (line 11, from Figure 4.3), *PkNBPXa* was targeted with a construct to add both a HA tag before its stop codon and also a 34bp LoxP sequence directly after its stop codon (Figure 4.5A, box), so that this line could be modified again at a later point, to generate a floxed *PkNBPXa* cKO line (described in 4.5.2). All constructs were synthesized using the same overlapping PCR methods as described above and transfected with the same cas9 guide plasmids used to generate mNG tagged lines. Transgenic parasites (lines 10-14 from Figure 4.3) were successfully generated from all of the above constructs as confirmed by PCR (Figure 4.5B), IFA (Figure 4.5C), and live microscopy (Figure 4.5D).

Dual labelled IFAs showed that PkDBPα appears to mostly, but not entirely, co-localise with PkNBPXa and un-secreted PkAMA-1 within schizonts (Figure 4.5C; average Pearson R values = 0.94 and 0.96, calculated from 50 and 47 individual schizonts, respectively), as opposed to PkRON2, which clearly resides in separate organelles (average Pearson R value = 0.84, calculated from 50 schizonts). Likewise,

live images taken from parasites expressing both PkDBPα-mNG and PkNBPXa-mCherry show that these two fusion proteins exhibit very similar localisations (Figure 4.5D; average Pearson R value = 0.92, from 6 different schizonts). These slight differences observed between the micronemal proteins may be indicative of micronemal subsets. Ultimately, though, since the resolution of epi-fluorescence imaging is unlikely to be sufficient enough to distinguish between micronemal subsets anyway, at least super-resolution techniques will be needed to address this question at a later date. However, overall, these results are consistent with PkDBPα, PkNBPXa, and PkAMA-1 all residing, as predicted, in the micronemes (Healer et al., 2002; Meyer et al., 2009).

Unfortunately, in comparison to the PkNBPXa-mNG fusion protein, the PkNBPXa-mCh signal was very weak and bleached very quickly, when continuously imaged. Thus further live imaging was not carried out with this line. Instead, observations of secretion and invasion (Section 4.4) were carried out using the single tagged mNG lines.

A

HR1 HA HR2
(3'UTR)

NBPXa c-term LoxP   HR2
(3'UTR)
HR1 HA L

1
C-term HR1 HR2
2

1
C-term HR1 HA HR2
(3'UTR)
3

B

WT primers 1/2   Int primers 1/3   Control locus
bp WT B C1 C2   WT B C1 C2   WT B C1 C2
1500
1000
800   NBPXa
600   HA

WT control   Bulk culture
bp 1/2 1/3 Control   1/2 1/3 Control
1500
1000   AMA-1
800   HA
600

WT primers 1/2   Int primers 1/3   Control locus
WT B C1 C2 C3   WT B C1 C2 C3   WT B C1 C2 C3
2000
1500
1000   NBPXa
800   mC
600

WT control   Bulk culture
1/2 1/3 Control   1/2 1/3 Control
1500
1000   RON2
800   HA
600

C

	α-mNG	α-HA	Overlay	DIC
NBPXa				
AMA-1				
RON2				

D

	PkDBPa-mNG	PkNBPXa-mC	Overlay	Brightfield

Figure 4.5 legend on next page.

Figure 4.5. Generation of dual tagged lines. (A) Schematic showing the insertion of a HA tag after the stop codon of *PkRON2* and *PkAMA-1*. A very similar construct was also transfected for *PkNBPXa* (box), containing a HA tag, but also a 34bp LoxP sequence, directly after the stop codon. Positions of primers used to perform diagnostic PCRs depicted with green arrows. **(B)** Diagnostic PCRs demonstrating the production of transgenic HA tagged PkNBPXa, PkAMA-1, and PkRON2 lines as well as PkNBPXa mCherry parasites. All primers listed in table 2.5. Expected PCR sizes: PkNBPXa - WT: 1004bp; Integrated HA: 997bp; Integrated mC: 1053bp; PkAMA1 – WT: 984bp; Integrated HA: 996bp; PkRON2 – WT: 1209bp; Integrated HA: 1221bp. **(C)** Immunofluorescence assay showing HA tagged PkNBPXa, PkAMA-1, and PkRON2 (red panels), detected in transgenic segmented schizonts, using an anti-HA antibody (3F10, Sigma). PkDBPa-mNG detected in same parasites (green panels) with an anti-mNG antibody (32F6, Chromotek). Average Pearson R-values = 0.94, 0.96, and 0.84 calculated from 47, 50, and 50 individual schizonts, respectively **(D)** Late stage segmented schizont expressing PkDBPα-mNG and PkNBPXa-mCherry fusion proteins. Average Pearson R-value = 0.92 (n= 6 schizonts). All scale bars indicate 2μm.

4.4 From storage to invasion: investigating the fates of *P. knowlesi* micronemal ligands

4.4.1 PkNBPXa and PkDBPα are secreted simultaneously but show distinct distribution patterns from each other and PkAMA-1 once secreted.

If the *P. knowlesi* RBL and DBP ligands perform discrete functions, one expectation is that they may be released at different times. Previous research has suggested that secretion of the RBL ligands may be dependent on the DBP ligands binding to their respective host cell receptors, or vice versa (Singh et al., 2010; Gao et al., 2013). Nevertheless, for either scenario to be true, the *P. knowlesi* RBL and DBL ligands would need to be stored within different micronemal subsets. Therefore, in order to investigate when the *P. knowlesi* RBL and DBL homologs may be secreted, and whether the release of one family may trigger the release of the other, freshly egressed transgenic parasites, expressing fluorescently labelled PkNBPXa, PkDBPα, and PkAMA-1, for comparison, were examined by live microscopy to observe these events directly.

AMA-1 secretion has been visualized by live microscopy previously, for *P. falciparum* (Treeck et al., 2009). This study demonstrated that PfAMA-1 secretion begins before egress, but continues gradually, after egress, until PfAMA-1 is eventually evenly distributed along the merozoite's surface (Treeck et al., 2009). In contrast to these results, while some PkAMA-1 did appear to redistribute to the merozoite's periphery,

the majority remained at the apical end of the zoite throughout 3-4 minutes of filming (Figure 4.6; Video 4.1). Measuring the fluorescence intensity at three points around the periphery of the merozoite (Fig 4.6, cartoon) demonstrated that PkAMA-1 formed a gradient from its apical end to its basal end (Figure 4.6, graphs). Gradually, the ratio between the peak fluorescence intensity of the merozoite's apical: middle: basal parts did begin to equalize somewhat, over time (Figure 4.6), indicating that after egress, some PkAMA-1 re-distribution continued, albeit slowly. However, as Video 4.1 and Figure 4.6 shows, at 203 seconds post egress, a time point by which five other merozoites in this video had invaded host cells, the non-invasive merozoite's apical end still retained a visible concentration of PkAMA-1, almost double the fluorescence intensity of its basal end. Furthermore, invading merozoites also clearly exhibited strong apical concentrations of PkAMA-1-mNG (e.g. see invasion at 57 sec in Video 4.1). Thus an even distribution of PkAMA-1 along the merozoite surface is clearly not required for invasion.

It was unclear, though, whether apically concentrated PkAMA-1 had been secreted and simply remained at the apical tip of the merozoite, or whether this pattern represented un-secreted micronemal stores. Given AMA-1's role in junction formation, it does make sense that the majority of secreted protein would remain at the merozoite's apex, ready to interact with RON2 (Lamarque et al., 2011; Srinivasan et al., 2011). While the merozoites captured here were viable, with several within this video going on to invade erythrocytes, Treeck et al., (2009) did not demonstrate whether or not *P. falciparum* merozoites with evenly distributed PfAMA-1 were capable of invading erythrocytes. Therefore, these merozoites may have actually been rendered incapable of invading once micronemal stores were spent, and an apical concentration of AMA-1 may even be a requirement for invasion.
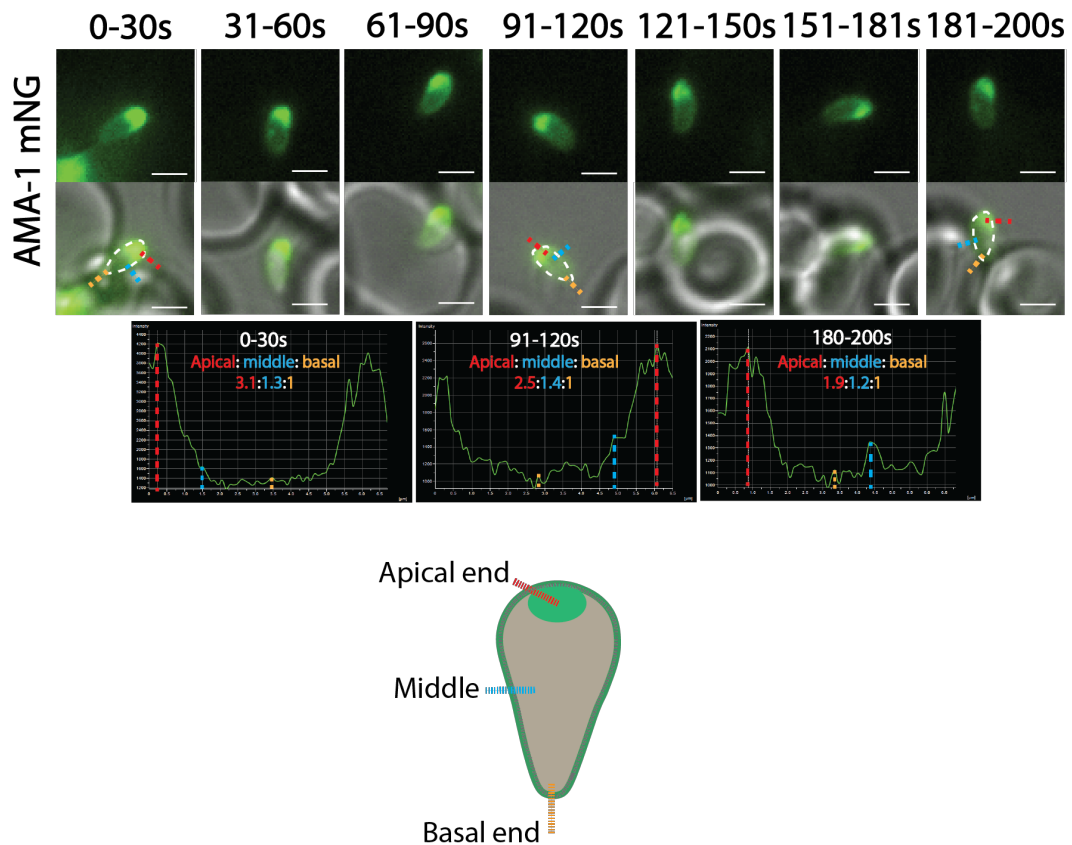
Figure 4.6. Secretion of PkAMA-1 post egress. Top panels follow the secretion of an example merozoite secreting PkAMA1-mNG from immediately after egress (time 0) to 200 sec post egress. Measuring the fluorescence intensity around the periphery of the merozoite (cartoon) shows that an apical gradient of PkAMA1-mNG remains throughout filming, rather than distributing evenly around the entire merozoite surface. Intensity values normalized to peak basal fluorescence intensity shown in red for apical end, blue for middle of the merozoite, and orange for the basal end. Scale bars = 2μm.

In contrast to PkAMA1, secretion of both PkNBPXa and PkDBPα began immediately after egress, even in the absence of merozoite-erythrocyte interactions (Videos 4.2 and 4.3). Critically, this provided strong evidence that receptor engagement of either RBL/DBP is not required for secretion of the other. Instead, both families appear to be secreted simultaneously, in contrast to what has been proposed for the *P. falciparum* RBL/DBP homologs (Singh et al., 2010; Gao et al., 2013). However, these results will need to be confirmed with fluorescently labelled ligands on top of KO backgrounds (e.g. PkDBPα-mNG + PkNBPXa cKO), as we cannot rule out the possibility yet that merozoites may be engaging with receptors on the erythrocyte membrane of the host cell they egressed from. What did become immediately apparent, though, was that once secreted, PkNBPXa and PkDBPα exhibited very distinct distribution patterns from each other, as well as PkAMA-1 (Figures 4.7 and 4.8).

As PkNBPXa is released from the micronemes, it spreads evenly down the length of the merozoite (Figure 4.7A, video 4.2), but does not appear to associate with the merozoite's periphery. One explanation for this could be that the ectodomain of PkNBPXa is being cleaved from the merozoite's surface after it is secreted to the apical surface and that its cytoplasmic tail domain (plus mNG tag) is simultaneously being released into the merozoite's cytosol. The *P. falciparum* RBL and DBL members are likely cleaved at sites within their transmembrane domains by the rhomboid like protease, PfROM4, at some point during invasion (Baker et al., 2006; O'Donnell et al., 2006). PkNBPXa also contains a putative ROM4 cleavage site within its TM domain (figure 4.7B). Thus ROM4 cleavage may be what is being observed in these videos. However, it will be necessary to perform western blot analysis of culture supernatants to investigate PkNBPXa shedding, as well as to label free merozoites with an antibody targeting the PkNBPXa ectodomain to see whether any of the ectodomain remains associated with the merozoite surface.

Notably, secretion appeared to be a continuous process from the point of egress onwards, both for merozoites that do eventually invade and for those that do not (Videos 4.2 and 4.4). Secretion could be monitored by determining the fluorescence ratio (FR) between the peak fluorescence intensity of the merozoite's apical end to the peak intensity of its body (Fig 4.7A, cartoon) every 10 seconds following egress. Where possible, two FR-values were calculated within a given 10-second window and averaged. Within the first 20 seconds after egress, FR-values were high, ranging from 7-41 times that of the body (n = 9 merozoites from 5 different schizonts). Over time, though, this ratio gradually decreased (Fig 4.7A and 4.7C), as the peak intensity of the merozoite's body increased relative to its peak apical intensity. Merozoites incubated with erythrocytes, which did not invade, eventually became uniformly green (FR=1), marking the end of secretion (Fig 4.7A, panel 6). It was difficult to pinpoint precisely when this occurred for every merozoite observed, as, after 2-3 minutes, most merozoites stopped gliding, detached from the coverslip surface, and moved out of focus. However, for those merozoites for which endpoints could be accurately determined (n = 8/12 merozoites, from 6 different schizonts), secretion was on average completed within 124 seconds, and up to 156 seconds post egress. Of the remaining four merozoites, for which an accurate endpoint time could not be determined, two had FR-values >1 at 156 seconds post egress. Thus, while the majority of merozoites

appear to fully secrete PkNBPXa within 2-3 minutes, a small proportion may take longer to secrete this ligand. Going forwards, this newly developed assay will allow us to analyse a much greater number of merozoites, in order to determine the full range of time it takes for merozoites to secrete micronemal contents.

Very interestingly, preliminary data also suggested that merozoites might be secreting their contents more quickly in the presence of erythrocytes, as opposed to without them. Analysis of 8 merozoites (from 7 different schizonts), which were not incubated with fresh erythrocytes, showed that only 3/8 merozoites had finished secreting their contents by the maximum end-point time (156 s) observed for the +RBCs group. Furthermore, at 156 sec post egress (+/- 15 s), the median FR value for the –RBCs group (median =1.75; n = 8 merozoites) was found to be significantly greater than the median value for the +RBCs group (median = 1; n=12 merozoites) (Fig 4.7D). Thus, while PkNBPXa secretion can occur without merozoites contacting fresh erythrocytes, secretion speed may be increased by merozoites interacting with host cells. However, again, much larger samples sizes will be needed to confirm these findings.

The distribution of PkDBPα post secretion (Video 4.3) was also intriguing. PfEBA-175 has been localised to the apical tips of free merozoites, with the aid of both a C-terminal epitope tag and antibodies targeting the N-terminus of this protein (Triglia et al., 2009). PkDBPα, however, accumulated primarily in three patches over the merozoite: the apical end, the widest portion of the merozoite, and at the tip of the basal end, resulting in three noticeable peaks when measuring the fluorescence intensity along the length of the merozoite (Fig 4.8A). Additionally, all three patches appeared to be connected by a fluorescent strip, running down the length of one side of the merozoite (See cartoon in Fig 4.8A). When PkDBPα-mNG tagged merozoites glide, this strip can be seen to rotate in and out of focus (Video 4.5).

Interestingly, this odd distribution pattern occurs regardless of whether merozoites interact with erythrocytes or not, and can be seen to form within ~30-60 seconds of egress (Videos 4.2 and 4.5, and Fig 4.8B) (n = 16 merozoites, from 6 different schizonts). However, the patchy PkDBPα pattern made monitoring the rate of secretion using the same methods applied to PkNBPXa secretion, difficult. Faster, 3D imaging techniques, such as spinning disk confocal microscopy, will be needed to determine

A

| | 0-30s | 31-60s | 61-90s | 91-120s | 121-150s | 181-200s |

NBPXa mNG

0-30s FR=18

91-120s FR=2.4

181-200s FR=1

Apical intensity (A)

Body intensity (B)

FR=A/B

B

```
PkNBPXa      -YAAGITVAFFIC-STAGYTVFTY
PfEBA-175    -YYAGAGVLFIILVILGA------
PkDBPa       VYFATGGAFLIILLLFASW-----
PvDBP        -YFAAAGALLILLLLIASRKMI--
PfRh1        MYFASGIVVSILFLSSLGFVI---
PfRh4        IFYAGGITAVLLLCSSTAFFFI--
```

C

apical: body fluorescence intensity (FR)

Time post egress (sec)

D

*

apical: body fluorescence intensity (R)

Plus RBCs   No RBCs

Figure 4.7. PkNBPXa is secreted gradually and continuously post egress. (A) Live microscopy stills show PkNBPXa secretion is completed within 2-3 minutes. Secretion can be measured by comparing the fluorescence intensity of the merozoite's apical end, to the peak intensity of its body (cartoon, and graphs). **(B)** Clustal alignment of predicted transmembrane domains of several RBL and DBP ligands. All contain a conserved alanine residue (red box), followed by potential helix destabilising motifs (underlined in green, and taken from Baker et al., 2006 & O'Donnell et al., 2006), making up putative ROM4 cleavage sites. The experimentally determined PfEBA-175 ROM4 recognition site is underlined in purple (O'Donnell et al., 2006). **(C)** Graph showing PkNBPXa secretion over time when merozoites are incubated with fresh erythrocytes. FR-values were calculated, where possible, every 10 seconds post egress for 15 merozoites, and plotted against time. Each data point represents an FR value from an individual merozoite at specified time point. Blue line shows a non-linear fit of FR values/time for all merozoites. Red dotted lines indicate 95% confidence interval **(D)** At 156 sec post egress, merozoites which have not been incubated with fresh erythrocytes exhibit a higher median FR-value (median=1.75) than those, which are incubated with fresh erythrocytes (median= 1). N = 12 merozoites for +RBCs group, and 8 merozoites for –RBCs group. Medians were found to be significantly different when compared by a Mann-Whitney U-test (p= 0.0305). Scale bars = 2μm.

how quickly PkDBPα is secreted after egress, and whether the speed of PkDBPα secretion is impacted by erythrocyte contact or not. Also, again, as for PkNBPXa, it is difficult to discern whether secreted PkDBPα is localized to the merozoite surface, or not, without probing free merozoites with an antibody targeting the N-terminus of this protein. Thus overall, what is clear from these initial results is that PkAMA-1 is secreted prior to both PkDBPα and PkNBPXa. Furthermore, despite PkDBPα and PkNBPXa exhibiting similar secretion dynamics, they appear to occupy distinct regions of the merozoite. Therefore, perhaps different localisations, and not secretion timings, may prepare them to perform their roles in discrete steps of invasion.
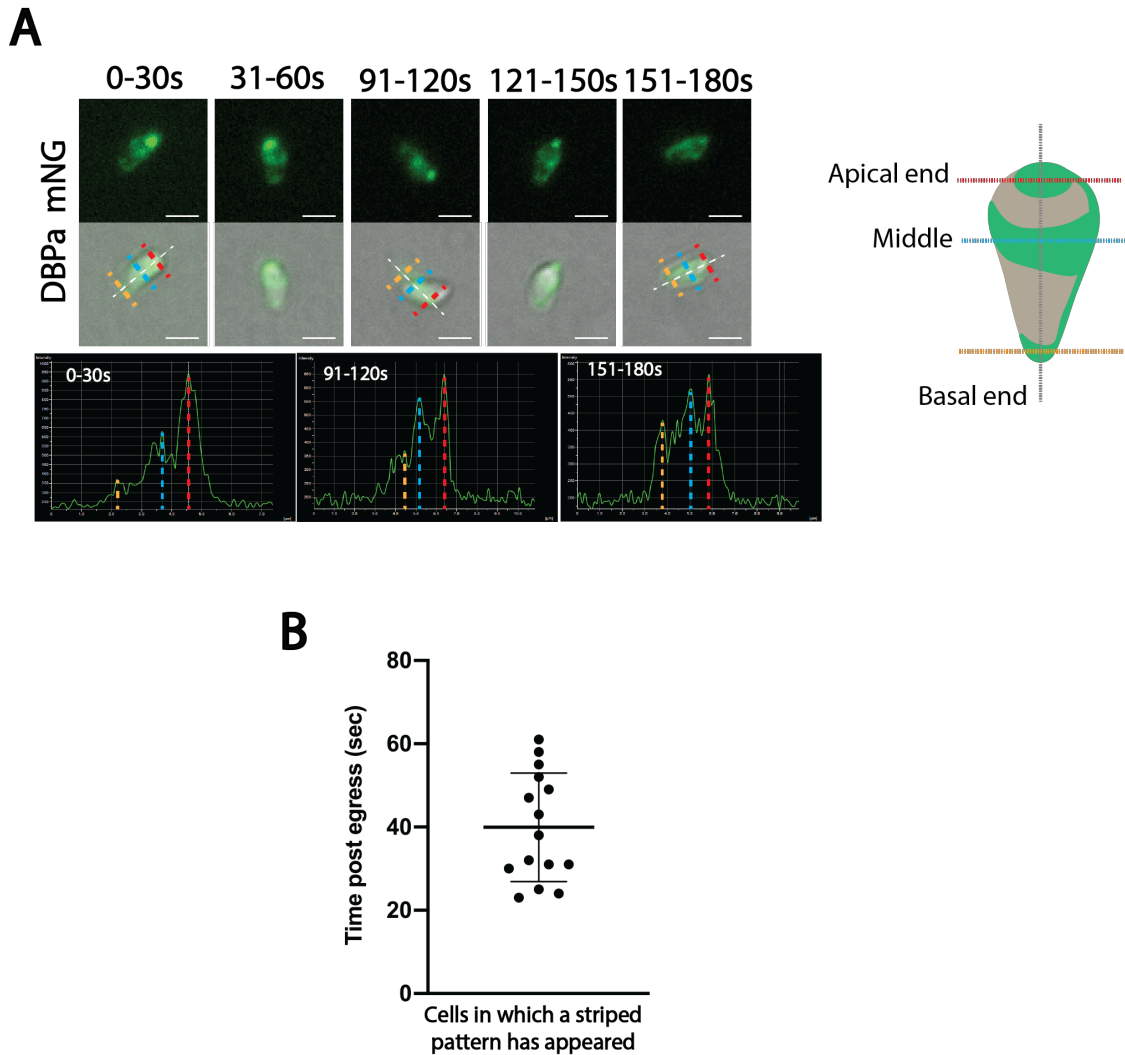
Figure 4.8. PkDBPα exhibits a striped distribution post secretion. (A) Stills from live microscopy (Video 4.3) showing PkDBPα secretion over time. PkDBPα-mNG concentrates around the widest portion of the merozoite, as well as the basal tip. Both of these concentrations are connected by a strip of PkDBPα running down one side of the merozoite (Cartoon, and particularly panels 3 and 5). **(B)** The striped PkDBPα pattern can be visualized within 60 seconds (and a mean of 40 seconds; n = 15 merozoites) after egress. Scale bars = 2μm.

4.4.2 Apical micronemal stores correlate with erythrocyte deformation and invasion

Next, since PkNBPXa-mNG parasites provided the clearest example of secretion, I used this line to investigate whether continuous micronemal secretion might be a requirement for early invasion events. Results from chapter 3 demonstrated that gliding and deformation are both linked, a finding in good agreement with Weiss and colleagues (2015), who showed that deformation is a motor dependent process. Since

gliding might also depend on continuous micronemal secretion (Gras et al., 2019), it follows that merozoites which have fully secreted their micronemal contents will not be able to deform their host cells, and thus will be far less likely to invade.

In order to explore the potential link between micronemal stores, host cell deformation, and invasion, the RBC interactions of 27 merozoites (from 12 different schizonts) expressing PkNBPXa-mNG were examined to see whether deformation occurs in the absence of apical stores. A breakdown of all deformation scores, according to merozoites with clear apical staining (FR > 1) vs. merozoites without prominent apical staining (FR =1), is shown in Figure 4.9A. Strikingly, almost all score 1-interactions (92%; n = 24 interactions) and all scale 2 and 3 interactions (n= 28) were performed by merozoites with prominent apical staining (FR>1). Furthermore, while the median FR-value for score 0 interactions was 2.5 (n=73 interactions), the median FR-value for scale 1-3 interactions was significantly higher (median FR-value = 4; n= 52 interactions), as determined by a Mann-Whitney u-test (Figure 4.9B; $p < 0.0001$). Importantly, all invasions observed (n=9) were initiated by merozoites with apical fluorescence intensities at least double (FR$\geq$2) and ranging up to 21 times that of the merozoite body. Therefore, merozoites do seem to exhibit a much greater chance of deforming host erythrocytes, and thus invading them prior to having fully secreted PkNBPXa. So, a merozoite's invasive half-life may be dependent on the rate at which it secretes micronemal proteins.
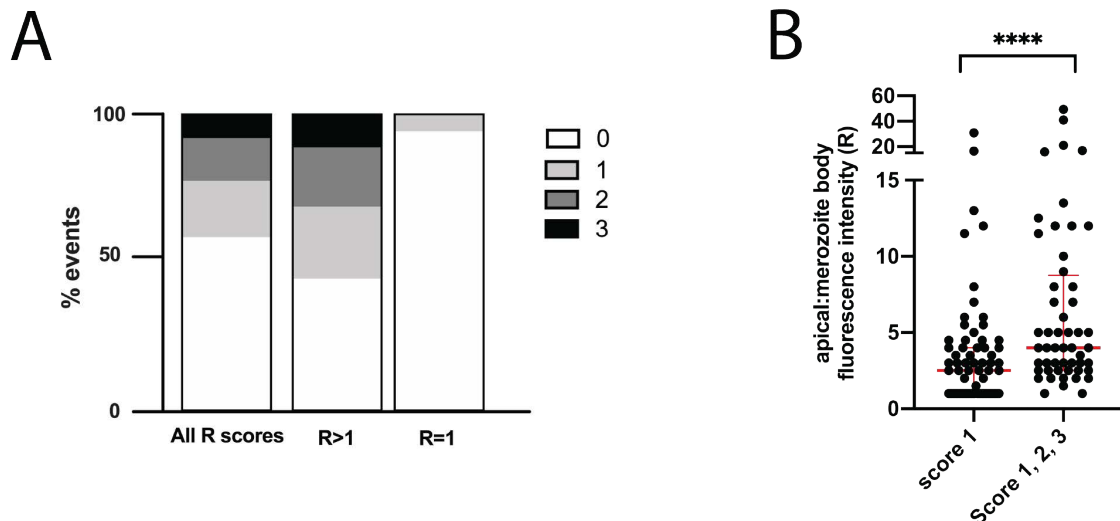
Figure 4.9. *P. knowlesi* merozoites cannot deform erythrocytes without apical PkNBPXa stores.
(A) The proportions of score 1-3 deformation events are significantly higher when merozoites possess apical stores of PkNBPXa (FR>1) as opposed to when secretion is complete (FR=1). (P<0.0001, determined by Chi squared test; n = 35 events where FR=1, and 90 events where FR>1). **(B)** The median FR-value (4) associated with score 1-3 deformation events is significantly greater than the median FR-value (2.5) associated with merozoite-RBC contacts which do not result in deformation (score 0 events). ****Indicates p<0.0001, when comparing the means by Mann-Whitney u-test; n = 52 score 1-3 events, and 73 score 0 events. Red bars indicate medians and interquartile ranges.

4.4.3 PkDBPα, but not PkNBPXa, associates with the moving junction during invasion

Several *P. falciparum* RBL and DBP members, including PfRh1, PfRh2a, and PfEBA-175 have been localised to or found to be in close proximity to the moving junction of merozoites captured mid invasion. These results have been obtained both with antibodies targeting tagged cytoplasmic domains, as well as with antibodies targeting the N-terminal ectodomains of these ligands (Triglia et al., 2009; Gunalan et al., 2011; Gao et al., 2013; Gunalan et al., 2020). Therefore, to investigate whether PkNBPXa and PkDBPα might also exhibit similar properties during invasion, mNG-tagged lines were examined using live microscopy, to visualise how the localisations of these ligands might change during host cell entry, in comparison to the moving junction marker, PkAMA-1.

Live imaging of PkAMA-1 mNG tagged parasites demonstrated junction formation and progression very clearly (Video 4.6, and corresponding Figure 4.10A, top panels). As parasites entered the host cell, some, likely un-secreted, PkAMA-1 remained at the tip of the merozoite (Fig 4.10A, top panels, 3 and 4). However, surface-bound

A

	Deformation	Re-orientation	Internalisation

PkAMA-1
113 sec · 133 sec · 148 sec · 161 sec

PkDBPa
17 sec · 17 sec · 42 sec · 81 sec

PkNBPXa
50 sec · 65 sec · 68 sec · 75 sec

B

α-mNG (PkDBPa)   α-HA (PkAMA-1)   Overlay

Fluorescence intensity

Distance (μm)
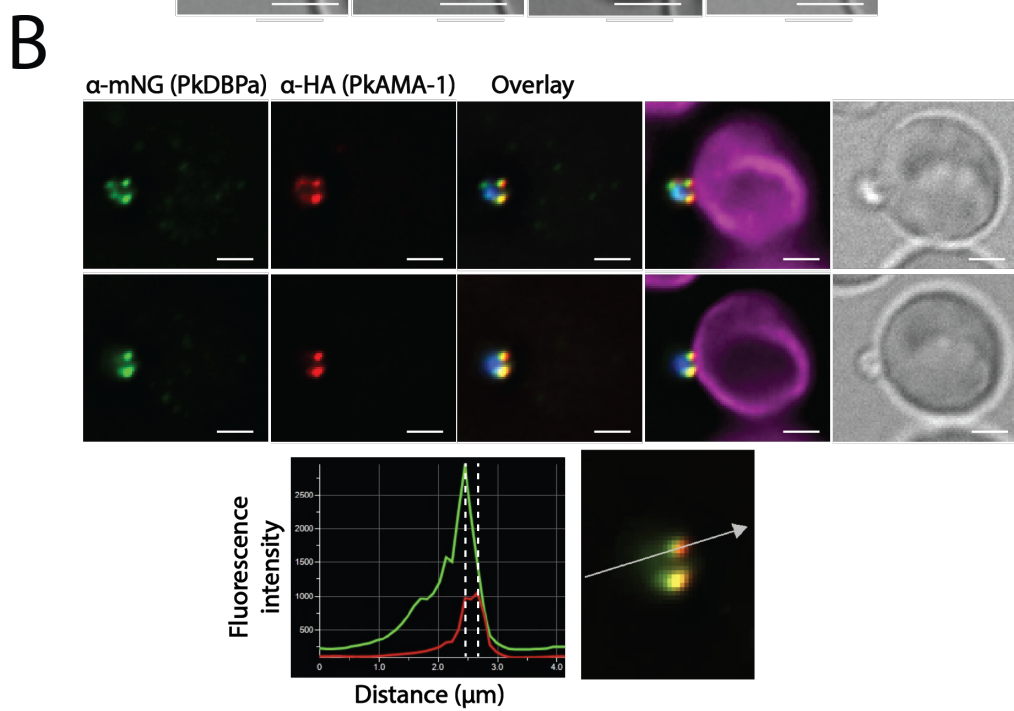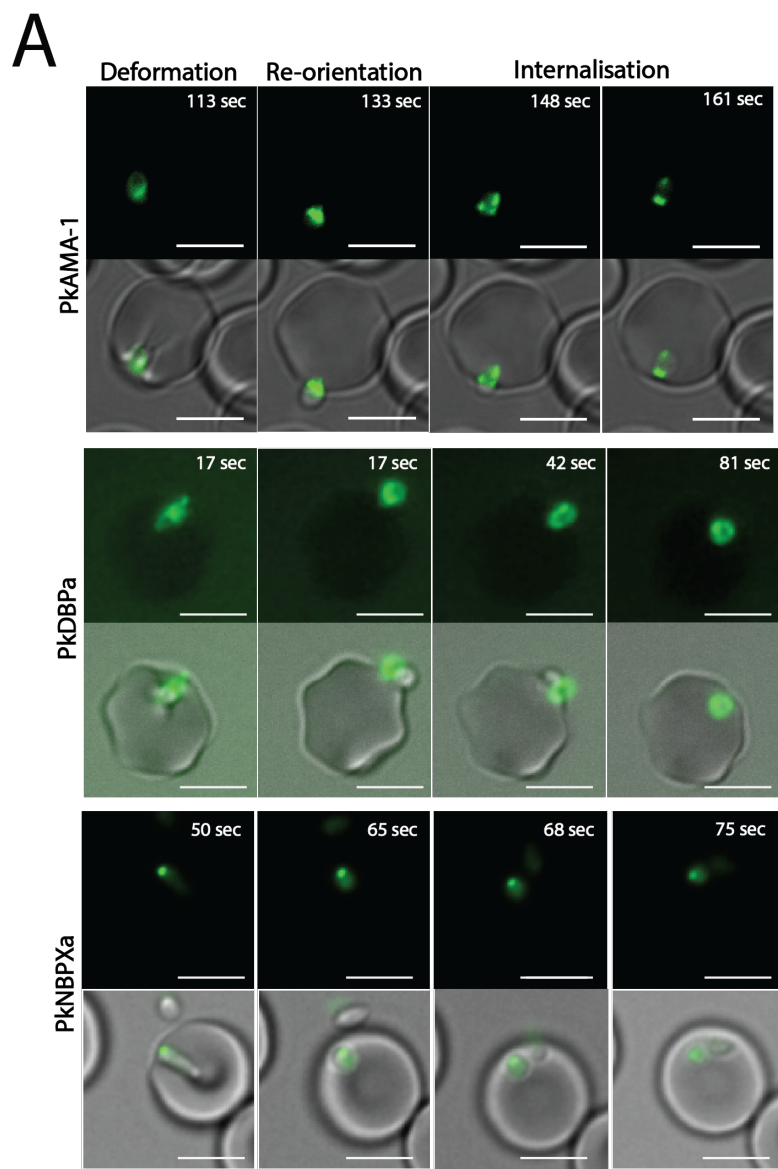
Figure 4.10. Legend on next page.

Figure 4.10. Capturing the localization of *P. knowlesi* invasion ligands during invasion (A)
Live stills of PkAMA1-mNG (top; taken from video 4.6), PkDBPα-mNG (middle; taken from Video 4.7) and PkNBPXa-mNG (bottom; taken from video 4.9) tagged parasites invading erythrocytes. S c a l e b a r s = 5 µ m . **(B)** Two slices from a z-stack, of an IFA of a *P. knowlesi* merozoite stalled mid-invasion with the addition of cytochalasin D. PkDBPα-mNG (green channel) and PkAMA1-HA (red channel) fusion proteins were detected using anti-mNG (32F6, Chromotek) and anti-HA (3F10, Sigma) antibodies, respectively. The graph below depicts the fluorescence intensity for each channel along a line drawn through one side of the moving junction. Scale bars = 2µm.

PkAMA1-mNG was translocated from the apical end of the merozoite to its basal end, appearing as two foci at the merozoite-RBC interface as internalisation progressed (Fig 4.10A, top panel 3). Strikingly, a close examination of the un-secreted apical stores showed that merozoites rotate in a corkscrew-like manner while entering host cells. Video 4.6, at 147-161 sec demonstrates this action, as apically stored PkAMA-1 comes in and out of focus, when the zoite glides into the erythrocyte, rotating its apical end in a clockwise manner. Additionally, at around 161 sec, after the junction closes, the merozoite continues to rotate, in a manner reminiscent of that described for *T. gondii* tachyzoites after host cell entry (Pavlou et al., 2018). This rotation continued for 20-30 seconds, possibly allowing the parasite to seal itself within the newly formed PVM and detach from the host cell membrane.

Next PkDBPα-mNG parasites were examined. Attempts were made to determine if prior to re-orientation, the merozoite is orientated so that the side of the merozoite containing a continuous line of PkDBPα (as in figure 4.8A, and Video 4.5) is attached to the erythrocyte surface. However, it was unclear, even after watching multiple videos, which side of the merozoite was pinned to the erythrocyte surface before entry. Faster, 3D imaging methods may reveal the answer to this question at a later date. Interestingly, whilst not as clear as for PkAMA-1, PkDBPα did appear to form a ring-like structure during entry (Videos 4.7&4. 8, and corresponding Fig 4.10A, middle panels 2-4). Double tagged PkDBPα-mNG/PkAMA-1-HA parasites were subsequently fixed mid-invasion and probed in solution with α-mNG and α-HA antibodies to directly compare the localization of PkDBPα with PkAMA-1 during host cell entry. Images taken from z-stacks of an invasion stalled by cytochalasin D show that PkDBPα appears to trail behind PkAMA-1 at the moving junction, partially co-localising with this structure (Fig 4.10B). These exciting findings suggest that PkDBPα might play a role during internalisation. Alternatively, though, it is also

possible that PkDBPα might be being shed from the merozoite surface as the junction moves back across the basal end of the zoite. Going forward, using super-resolution microscopy techniques may help to determine whether PkDBPα truly overlaps with the moving junction, or exists within a different structure facilitating host cell entry.

Finally, in contrast to both PkAMA-1, and PkDBPα, the localization of PkNBPXa did not change during invasion (Videos 4.4 and 4.9; Fig 4.10A, bottom panels). Like PkAMA-1, apically stored PkNBPXa was carried into the erythrocyte. However, PkNBPXa did not appear to be trans-located down the merozoite body, as entry progressed, and overall no evidence of a role for PkNBPXa during host cell entry was apparent. Since PkNBPXa secretion may correlate with cleavage from its C-terminal domain, though, going forward, it will be necessary to label invading parasites with antibodies targeting the PkNBPXa ectodomain, to determine whether or not processed PkNBPXa fragments contribute to host cell entry.

4.5 Exploring RBL/DBP function through a conditional KO approach

4.5.1 Establishment of *P. knowlesi* DiCre background lines

Since previously established PkDBPα and PkNBPXa KO lines can only be maintained in macaque erythrocytes, (Singh et al., 2005; Moon et al., 2016) it was necessary to establish conditional KO (cKO) lines for both of these ligands. The first step towards generating cKO lines was to generate stable, DiCre-expressing background lines, by integrating a DiCre cassette into the parasite's genome using CRISPR-Cas9, as has been successfully done for *P. falciparum* (Collins et al., 2013; Knuepfer et al., 2017). Following this, parasites could be iteratively modified using CRISPR-Cas9 to generate floxed *PkNBPXa* and *PkDBPα* lines.

Since the *Pkp230p* locus is redundant in the blood stages and has previously been used as a site for the integration of GFP expression cassettes (Moon et al., 2013; Mohring et al. 2019), a DiCre expression cassette was introduced into this locus by double homologous recombination (Figure 4.11A), using CRISPR-Cas9. Dr Franziska Mohring kindly provided both the Cas9 plasmid pCas9sg_p230p, targeting *Pkp230p* (Mohring et al., 2019), as well as the donor DNA plasmid, pDonor_DiCrePkp230p carrying the DiCre expression cassette, flanked by 500 bp homology arms to the *Pkp230p* target site (Figure 4.11A).

Both plasmids were transfected into the PkDBPα-mNG and PkRecDBPα backgrounds (lines 5 and 2, respectively, from Figure 4.3). Additionally, Dr Mohring (LSHTM) introduced the DiCre cassette into the wild type PkA1-H.1 line (line 1, from figure 4.3). Integration of the DiCre cassette into *Pkp230p* was shown to be successful by PCR for all background lines, and the RecDBPα and wild type DiCre lines (lines 7 and 3 from Figure 4.3) were subsequently cloned by limited dilution prior to further modifications (Figure 4.11B).
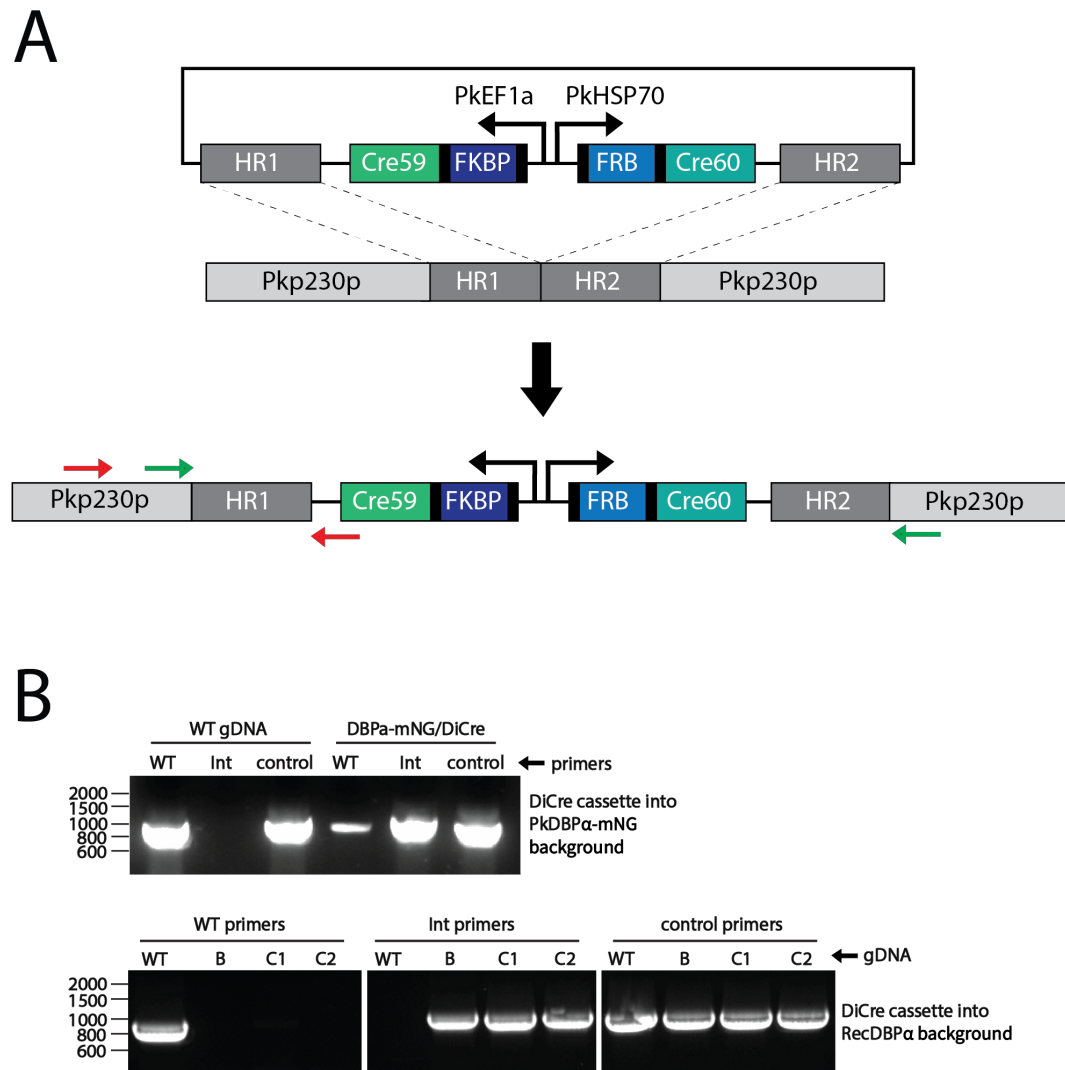
Figure 4.11. Generation and genotyping of *P. knowlesi* DiCre expressing background lines. (A) Schematic showing the integration of a DiCre expression cassette into the *Pkp230p* locus. Primers used to screen for WT parasites indicated with green arrows, and those used to screen for transgenic parasites indicated with red arrows). **(B)** Diagnostic PCRs showing the integration of the DiCre cassette into the RecDBPα and RecDBPα/DBPa-mNG backgrounds. All primers listed in Table 2.5. Expected PCR product sizes: Non-modified parasites: 969bp; Integrated parasites: 891bp. WT = wild type control parasites; B = bulk, uncloned parasites; C1 & C2 = clones 1&2.

4.5.2 Generation of *PkNBPXa* cKO lines

PkNBPXa is an 8.5 kbp gene located on chromosome 14. Due to its large size, LoxP sites were integrated into the gene in two separate steps (Figure 4.12A). As *PkNBPXa* contains a 186bp endogenous intron towards the 5' end of the gene, constructs were designed to take advantage of this feature and insert a LoxP site within this sequence. This new intron (PkLoxPint) would not only serve the purpose of this study but could also be introduced into other genes, for subsequent conditional knockout designs - a strategy that has been widely used for *P. falciparum* work (Jones et al., 2016; Knuepfer et al., 2017; Sherling et al., 2017; Boonyalai et al., 2018). The *P. falciparum* synthetic LoxP intron (PfLoxPint) was designed by placing a LoxP sequence into the *PfSERA2* intron after its predicted branch point, so to avoid disrupting this sequence and impede correct splicing of the gene (Jones et al., 2016). This branch point was predicted using a consensus sequence (YWH<u>W</u>W) derived from a previous study of *P. falciparum* intron structure (Zhang et al., 2011). The PkNBPXa intron was screened for possible branch point sites using this same consensus sequence. However, this search yielded many possible branch sites throughout the entire intron (Figure 4.12B). Therefore, two different insertion sites (LoxPint1 and LoxPint2) were chosen within the second half of the intron, to identify one that avoided branch point disruption. As introns cannot be 'recodonised', these positions were also chosen on the basis of available nearby Cas9 'NGG' cut sites so that insertion of the LoxP sequence would disrupt the Cas9 guide sequence from its corresponding NGG site, and therefore ablate subsequent Cas9 targeting.

Guide sequences targeting each potential insertion site, along with donor PCR products designed to replace the endogenous PkNBPXa intron with a LoxPint version, were transfected into the PkDBPα-mNG/PkNBPXaHA-LoxP background (line 14, from Figure 4.3). This line also contains a copy of *PkNBPXa* that is HA-tagged and flanked at its C-terminus by a LoxP sequence (section 4.3.2). Thus, if successful, this transfection would generate a floxed, and HA-tagged PkNBPXa line, also expressing a PkDBPα-mNG fusion protein. However, a rather frustrating finding was that the *PkDBPα-mNG/NBPXaHA-LoxP* line (line 14) was resistant to pyrimethamine treatment, even after being pre-treated with ancotil to remove the Cas9 plasmid from the previous transfection. Therefore, unfortunately, no further modifications could be made to this line. The reasons for this were puzzling, as no other transfection in this

study thus far had yielded irreversibly pyrimethamine resistant parasites. However, since the *PkNBPXa* guide sequence targeting the PkNBPXa C-terminus, was the only one to be cloned into the PL11HF Cas9 plasmid (Appendix Figure 4), instead of pCas9/sg (Mohring et al., 2019), we reasoned that this might be where the problem lay.

In the meantime, a second attempt was made to transfect the LoxPint constructs, this time into the RecDBPα/DiCre background, without any fluorescent tags (line 7, from Figure 4.3). Post transfection, parasites were screened for the presence of integrated or wild type parasites using primers depicted in Figure 4.12A and listed in Table 2.5. Diagnostic PCRs showed that the endogenous *PkNBPXa* intron was successfully substituted for PkLoxPint1, but not PkLoxPint2 (Figure 4.12C). Therefore, the PkNBPXa_LoxPint1 line (line 15) was cloned out by limiting dilution and used as the background line for iterative modifications. These included the addition of an mNG tag to PkAMA-1, PkRON2, and PkDBPα, generating lines NBPXaLP1/DBPα-mNG (line 18), NBPXaLP1/AMA-1mNG (line 19) and NBPXaLP1/RON2mNG (line 20), as already described in section 4.3.1 (also see figure 4.3). Finally, the PkDBPα-mNG, PkAMA1-mNG, and non-fluorescent PkLoxPint1 variants were modified to introduce both a HA tag and a LoxP site to the C-terminus of PkNBPXa (Fig 4.7A, step 2), using the same pL11_NBPXaCterm guide and accompanying donor DNA plasmids, as in section 4.3.2. This resulted in three PkNBPXa cKO variants: NBPXa_cKO/PkDBPα-mNG, NBPXa_cKO/AMA1-mNG, and NBPXa_cKO_A lines (lines 21, 22, and 17, respectively from Figure 4.3). Integrated parasites were detected by PCR (Figure 4.12C) using primers depicted in Figure 4.12A and listed in Table 2.5. Furthermore, HA-tagged PkNBPXa was also detected by western blot (Fig 4.12D), and IFA (Figure 4.12E) for the PkNBPXa_cKO_A line, which was subsequently cloned by limiting dilution. Notably, though, all three of these cKO lines were also permanently resistant to pyrimethamine treatment, just as line 14, strongly indicating a specific issue relating to the guide plasmid used.

Therefore, one last PkNBPXa cKO line was produced, by introducing the same donor DNA plasmid as above into the LoxPint1 background (line 13, Figure 4.3), but using the newly cloned pCas9/PkNBPXa_Cterm_sg plasmid, instead of the PL11HF Cas9 plasmid to target the PkNBPXa C-terminus. This time the resulting line, PkNBPXa cKO_B (line 16, Figure 4.3), responded to ancotil treatment after transfection, yielding a pyrimethamine sensitive line, which can be iteratively modified for future studies.

A

Step 1 ... Step 2

HR2 (3'UTR)

B

5′ gtacaatttcacaaaagagggtagaagtggattttcatgcacacatgaatagatgcgcaaatgtgcagttgtaatcggtgacaaatgggcaaattcatgaaccccaatta 3′
3′ catgttaaagtgtttctccatcttcacctaaaagtacgtgtgtacttatctacgcgtttacacgtcaacattagccactgtttaccccgtttaagtacttggggttaat 5′

NBPXa Intron

Guide 1 ... 110

gggctgatctatatggcattattatacatcctatgctaaacacccctttatgttaaaccttccacatttgttgtag 3′
ccgactagatatacgtaataatatgtaggatacgatttgtgtgggaaatacaatttggaaggtgtaaacaacatc 5′

NBPXa Intron

PAM 1 ... PAM2 ... Guide 2 ... 186

C

	WT primers (1/2)			Int primers (1/3)			Control locus			
bp	WT	B	C	WT	B	C	WT	B	C	

Step 1 PkLoxPint1, PkLoxPint2

	WT primers (4/5)			Int primers (4/6)			Control locus			
bp	WT	B	C	WT	B	C	WT	B	C	

Step 2 NBPXa_cKO A, NBPXa_cKO B, NBPXa_cKO/AMA1-mNG

D α-HA WT cKO A

E α-PkMSP1₁₉ | α-HA (PkNBPXa) | Overlay | DIC | NBPXa_cKO A

Figure 4.12. Legend on next page.

139

Figure 4.12. Generation and genotyping PkNBPXa cKO lines. (A) Schematic depicting the two-step modification process, to insert a LoxP site into 1) the endogenous *PkNBPXa* intron, towards the N-terminus of the gene, and 2) immediately after the stop codon. Positions of primers used to screen for WT and integrated parasites for step 1 indicated with red arrows, and for step 2 with green arrows. **(B)** Positions of guides (indicated in green) used to target cut sites (indicated in purple) within the *PkNBPXa* intron. Yellow highlighted sequences indicate potential branch points within the *PkNBPXa* intron, found when searching for the *P. falciparum* branch point consensus sequence (YWHWW), from Zhang et al., 2011. **(C)** (Top, step 1) Diagnostic PCRs showing integration of the PkLoxPint1, but not the PkLoxPint2 construct, into the *PkNBPXa* locus. (Bottom, step 2) Diagnostic PCRs showing integration of the c-terminal LoxP site + HA tag into the *PkNBPXa* locus, into various PkLoxPint1 backgrounds +/- fluorescently labelled parasites. All diagnostic primers can be found in Table 2.5. Expected band sizes = PkLoxPint1 WT: 1228bp, Int: 1250bp; PkLoxPint2 WT: 1261bp, Int: 1284bp; CtermLoxP WT: 1004bp, Int: 997bp. For all PCR sets, WT = wild type control gDNA; B = bulk, un-cloned transgenic gDNA; C = clonal line gDNA. **(D)** Western blot showing anti-HA tagged PkNBPXa in the NBPXa_cKO_A line, but not the WT control. HA tagged protein detected using an anti-HA antibody (3F10, Sigma). Expected size of full length PkNBPXa = 325 kDa. **(E)** Detection of HA tagged PkNBPXa and PkMSP1 in the NBPXa_cKO_A line, by probing late stage schizonts with anti-HA (3F10, Sigma) and anti-PkMSP1$_{19}$ (Ellen Knuepfer, Francis Crick Institute). Scale bars = 5μm.

4.5.3 Efficient conditional deletion of *PkNBPXa*

To investigate whether treating the PkNBPXa_cKO_A line with rapamycin results in efficient excision of the floxed gene, tightly synchronized ring-stage parasites (0-3 hours), were treated with 10nM rapamycin or its carrier, DMSO (0.005%) for 3 hours. Samples were taken at the end of the first cycle, when parasites were roughly 27-28 hours old, for PCR, western blot, and IFA analysis. Deletion of the 8.4kbp fragment between both LoxP sites should not only remove all of *PkNBPXa*, apart from its signal peptide, but also the C-terminal HA tag (Fig 4.13A).

PCR analysis, using primers depicted in Figure 4.13A, showed excision of the 8.4kbp *PkNBPXa* fragment for rapamycin-treated parasites (Fig 4.13B). Interestingly, a much fainter band of the same size (606bp) was also detected for the DMSO control. Therefore, some leaky excision appeared to occur even without rapamycin induction. As expected, no excision band was detected for the parental line control. Additionally, primers specific for the wild type sequence amplified a 404bp product specific to un-excised parasites (Fig 4.13B). Strong WT bands were detected for the parental line, and DMSO treated KO line, while a much fainter band was detected for the rap treated KO line.

A

exon 1 | NBPXa exon 2 | HA | HR2
(3'UTR)

1
2

↓ Plus rapamycin

3
exon 1 | HR2
(3'UTR)
4

B

WT | Floxed
- | +

500 —
400 —
300 —
200 —

WT (P1/P2)

800 —
600 —
500 —
400 —

excision (P3/P4)

1500 —
1000 —
800 —
600 —

control

C

KDa | WT | Floxed
- | +

460 —
268 —
238 —

α-HA (NBPXa)

71 —

55 —

41 —

α-DBPa

D

α-MSP1 | α-HA (NBPXa) | Overlay | DIC

DMSO

Rap

Figure 4.13. Legend on next page.

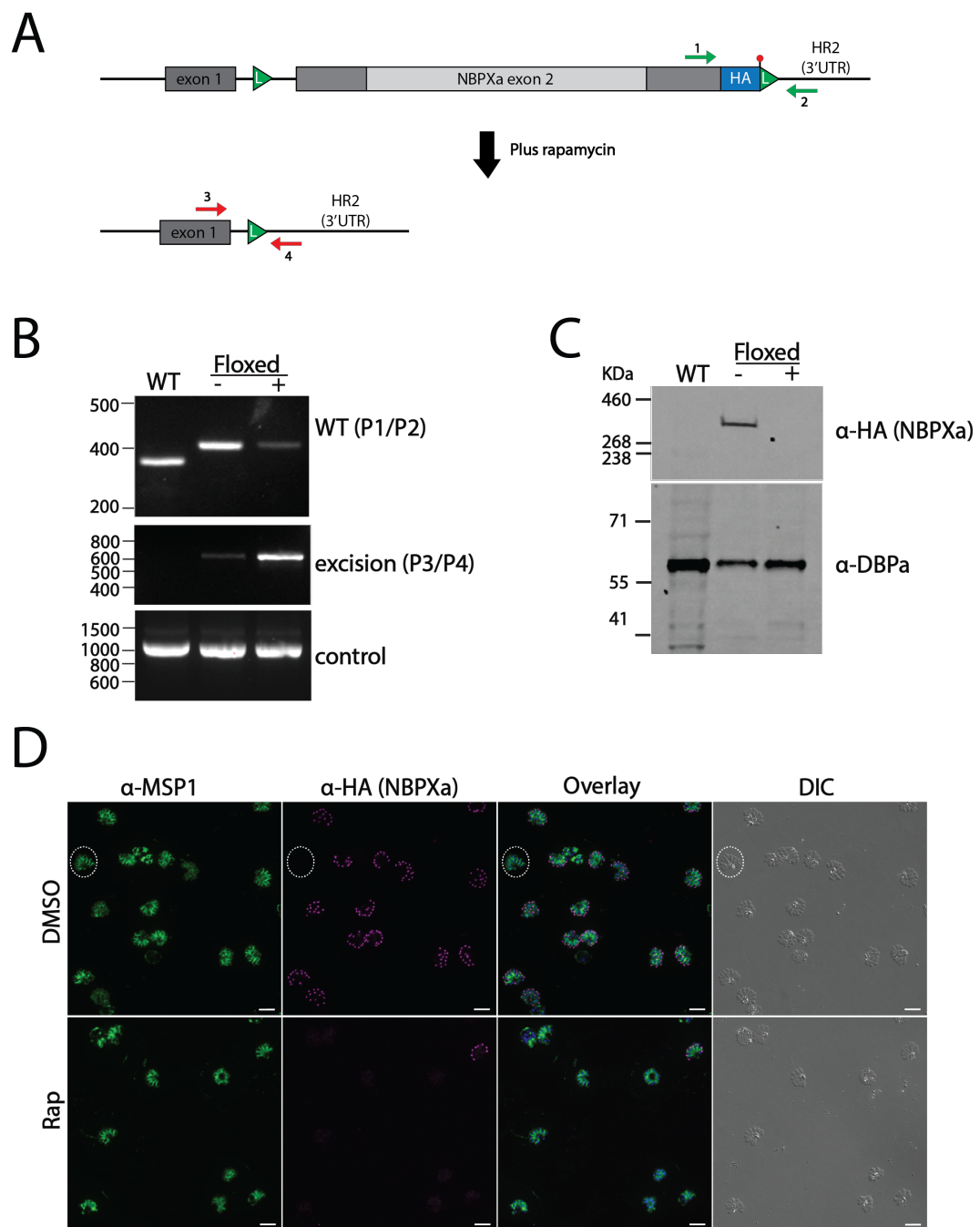**Figure 4.13. Efficient rapamycin induced excision of floxed PkNBPXa. (A)** A schematic depicting excision of an 8.5kbp fragment of *PkNBPXa* upon rapamycin treatment of the PkNBPXa cKO parasites. After treatment, only a short sequence, encoding a signal peptide remains. Positions of primers used to screen for wild type, un-excised parasites depicted with green arrows. Positions of primers used to screen for excised parasites depicted with red arrows. **(B)** Diagnostic PCRs showing excision of rap treated (Floxed +) PkNBPXa cKO parasites, using primers CH203/ CH206, positioned outside of LoxP sites (expected band size = 606bp). A faint excision band is also detected in the DMSO control (Floxed -). Primers MH1543, located 156bp upstream of the PkNBPXa stop codon, and CH206, within the PkNBPXa 3'UTR amplify an 340bp band in the WT control (lacking a HA tag and LoxP sequence), and a slightly larger 404bp band from un-excised, floxed parasites in both DMSO and rapamycin treated samples. **(C)** Western blot showing loss of ~325 kDa HA tagged PkNBPXa, from rapamycin treated (floxed +) PkNBPXa cKO parasites. HA-tagged PkNBPXa detected using rat anti-HA antibody (3F10, Sigma). Anti-PkDBPα antibody (Muh et al., 2018) used as a loading control (expected processed product size = ~60kDa) **(D)** IFAs showing that expression of HA-tagged PkNBPXa is ablated when the PkNBPXa cKO line is treated with rapamycin. A white circle indicates a PkNBPXa null parasite in the DMSO control, resulting from un-induced, leaky excision. Parasites labelled with a rat anti-HA antibody (3F10, Sigma) and rabbit anti-MSP1$_{19}$ antibody (Ellen knuepfer, Crick) to detect HA tagged PkNBPXa (un-excised) and mature, segmented schizonts. Scale bars = 5µm.

Furthermore, full-length HA-tagged PkNBPXa (around 325 kDa) could be detected by western blot for DMSO treated samples, but 3-hour incubation with 10nM rapamycin resulted in no detectable protein expression (Fig 4.13C), consistent with results for similar treatment regimes for *P. falciparum* (Knuepfer et al., 2017). Analysis of the same samples by IFA revealed that HA-tagged parasites were detectable for mock-treated parasites, but very infrequently for rap treated parasites (Fig 4.13D), allowing calculation of an overall excision rate of 93.4% (± 1% calculated from 4 individual experiments). One concern at the beginning of the study was that the horse serum *P. knowlesi* parasites are grown in could shift the working concentration of rapamycin, as has been the case for various other drugs (Lyth et al., 2018; van Schalkwyk et al., 2017). To address this potential problem, parasites were treated with increasing concentrations of rapamycin (up to 200 nM), and for an entire cycle, as opposed to 3 hours. However, neither increasing the concentration of rapamycin beyond 10nM nor leaving the drug in culture for the full cycle length, increased excision efficiency, indicating that the horse serum did not increase the concentration required.

Furthermore, in agreement with the above PCR results, around 5% of DMSO treated parasites showed no HA staining in mature, segmented schizonts (circled in Figure 4.13D). This is in contrast to non-floxed tagged lines, which show PkNBPXa staining for every segmented parasite. While this result does not present a problem to this

study, it is worth noting that leaky DiCre mediated excision may be a problem when attempting to interpret non-lethal conditional modifications. Deletion of *PkNBPXa* results in parasite death (Moon et al., 2016); however, deletion of a non-essential gene may eventually result in a mixed population of excised and non-excised parasites. Therefore a modified strategy would be needed when considering non-essential genes.

4.6 Investigating the role of PkNBPXa

4.6.1 PkNBPXa null parasites exhibit a severe growth defect in human but not macaque erythrocytes

Previous work has shown that disrupting *PkNBPXa* severely inhibits *P. knowlesi* replication in human erythrocytes, but does not impede growth in macaque erythrocytes (Moon et al., 2016). To investigate whether PkNBPXa cKO parasites exhibit this phenotype, DMSO and rapamycin-treated parasites were grown in both human and macaque erythrocytes, for a single cycle. This assay, performed with two biological replicates, clearly showed that rapamycin-treated PkNBPXa cKO parasites retain their ability to replicate in macaque erythrocytes, but exhibit very poor growth in human erythrocytes (Fig 4.14A).

It is worth noting, that for these experiments, the non-clonal PkNBPXa cKO/A line was used, as a clonal line had not yet been obtained prior to macaque erythrocytes becoming available (a very rare occurrence throughout this study!). Thus, it is probable that at least a small proportion of rapamycin-treated parasites, which successfully managed to invade human erythrocytes, did so because they were wild type parasites. Ideally, I will need to wait for more macaque erythrocytes to become available, and repeat this experiment in triplicate with the clonal line, for robust statistical analysis. Additionally, because PkNBPXa expression is not ablated for roughly 7% of floxed parasites, some residual invasions into human erythrocytes were to be expected. However, a third potential source of residual invasions was the possibility that some PkNBPXa null parasites really do manage to invade human erythrocytes, despite not expressing this ligand.

To investigate this third possibility, growth assays (three biological replicates) were performed over two cycles using the clonal PkNBPXa cKO/A line. While mock-treated parasites grew 3-4 fold over cycle 1 (Figure 4.14B), excised parasites did not
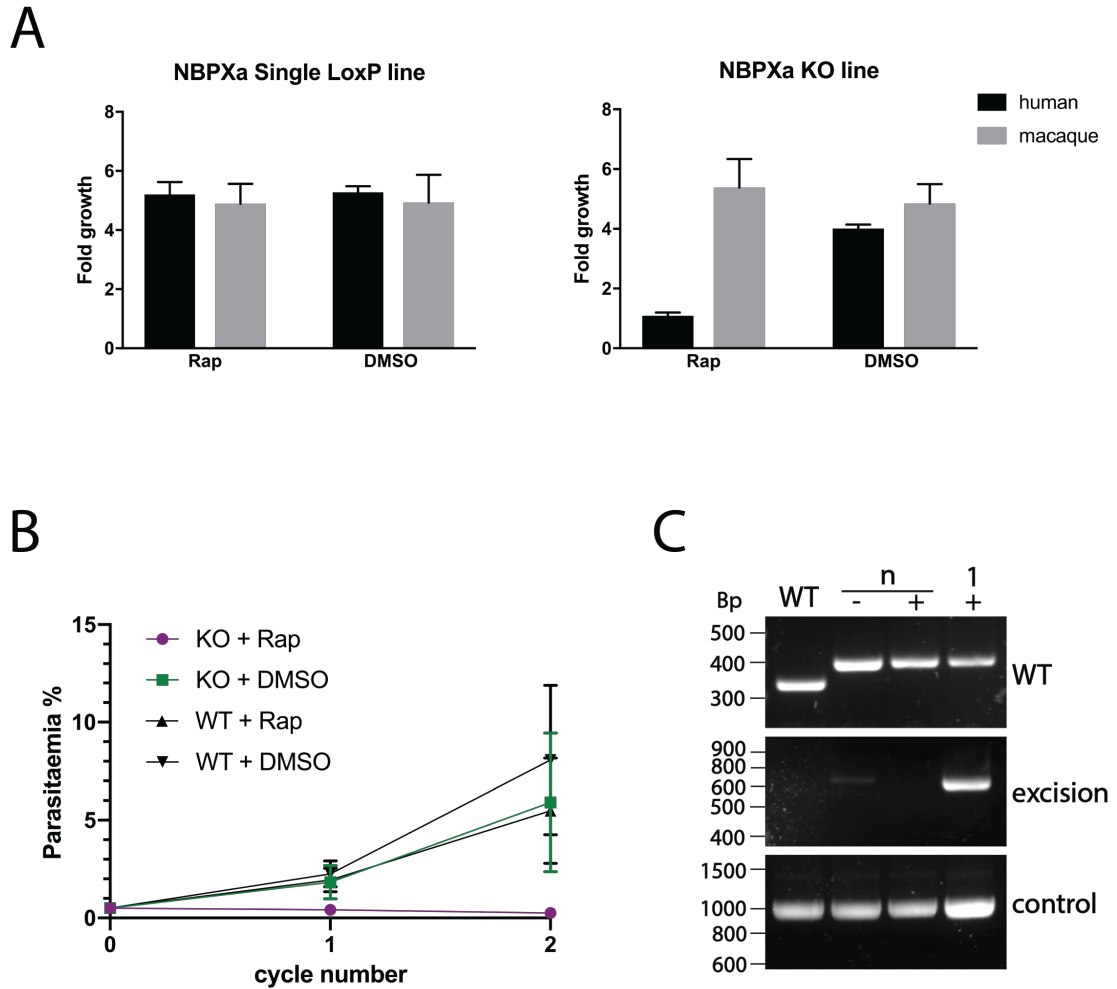
Figure 4.14. PkNBPXa is required for invasion of human, but not macaque erythrocytes. (A) Growth of the parental (PkLoxPint1) and non-clonal NBPXa_cKO/A lines measured 24 hours after treatment with either rapamycin or DMSO. Data shown are the mean of two independent experiments ± 1 SD. **(B)** Growth of the parental (PkLoxPint1) and clonal NBPXa_cKO/A lines measured at 24 and 48 hours after treatment with either rapamycin or DMSO. Data shown are the mean of three independent experiments ± 1 SD. **(C)** Diagnostic PCRs screening for excised and non-excised parasites using gDNA taken from NBPXa cKO/A parasites continuously treated with rapamcyin (n+) or DMSO (n-). Also included is a positive control for excision – gDNA taken from NBPXa_cKO/A parasites harvested 24hrs after treatment with rapamycin (1+), and a negative control for excision (WT, parental line). All primers listed in Section 2.3.7, and positions depicted in Fig 12A. Expected band sizes: Excised: 606bp; un-excised WT (parental): 340bp; un-excised floxed line: 404bp

exhibit multiplicative growth, and the parasitaemia decreased again over the following cycle. Still, a few rapamycin-treated parasites managed to re-invade over both cycles, forming rings discernable by Giemsa smear. These parasites were maintained in culture and grown continuously in the presence of rapamycin for 4-5 weeks, until they

eventually expanded, reaching a parasitaemia above 1%. Subsequent PCR analysis showed only the presence of wild type, un-excised parasites in the rapamycin-treated sample (Fig 4.14C). No band was detected using primers specific for excision, which is seen even for control floxed parasites maintained in DMSO (Fig 4.14C). These results confirmed that a small subset of parasites is resistant to rapamycin treatment and is eventually able to expand in culture if grown continuously. However, as no excised parasites were detected, this suggests that even if some PkNBPXa null parasites do manage to invade human erythrocytes, they suffer the same level of growth attrition in subsequent cycles, similar to that observed previously (Moon et al., 2016). Thus it is likely that PkNBPXa null parasites, which do manage to invade, do so by chance rather than because they possess any specific attributes, which would enable them to expand in culture.

4.6.2 Video microscopy shows that PkNBPXa null parasites are motile, but fail to deform host erythrocytes

A previous study using an immunofluorescence assay (IFA) to differentiate between newly formed rings and extracellular merozoites, showed that PkNBPXa KO parasites stick to the outer surface of human erythrocytes, rather than invading them (Moon et al., 2016). However, the precise reasons why PkNBPXa null parasites cannot invade human erythrocytes have never been explored. Therefore, a thorough analysis of how PkNBPXa KO parasites interact with human erythrocytes was undertaken using live microscopy.

An immediately noticeable feature of PkNBPXa KO merozoites is that they are still motile (Video 4.10). The median percentage of gliding merozoites/schizont was 85% for both mock-treated and rap treated parasites (Figure 4.15A; n = 17 schizonts for DMSO, and 15 schizonts for rapamycin-treated samples), demonstrating that PkNBPXa KO parasites are perfectly capable of attaching to erythrocytes and forming the initial parasite-host cell interactions required for motility (p= 0.5281, determined by performing a Mann-Whitney u-test).

However, while observing PkNBPXa KO parasites gliding across erythrocyte surfaces, it quickly became evident that they were unable to progress into, or beyond, the next step of erythrocyte invasion: host cell deformation. A hallmark of invasive merozoites, as discussed in chapter 3, is their ability to deform host erythrocytes strongly. Indeed,

high scoring score 2 and 3 interactions, characterized by pinching, or wrapping of the host cell membrane (Video 4.11) down the length of the merozoite, made up 17.6% of
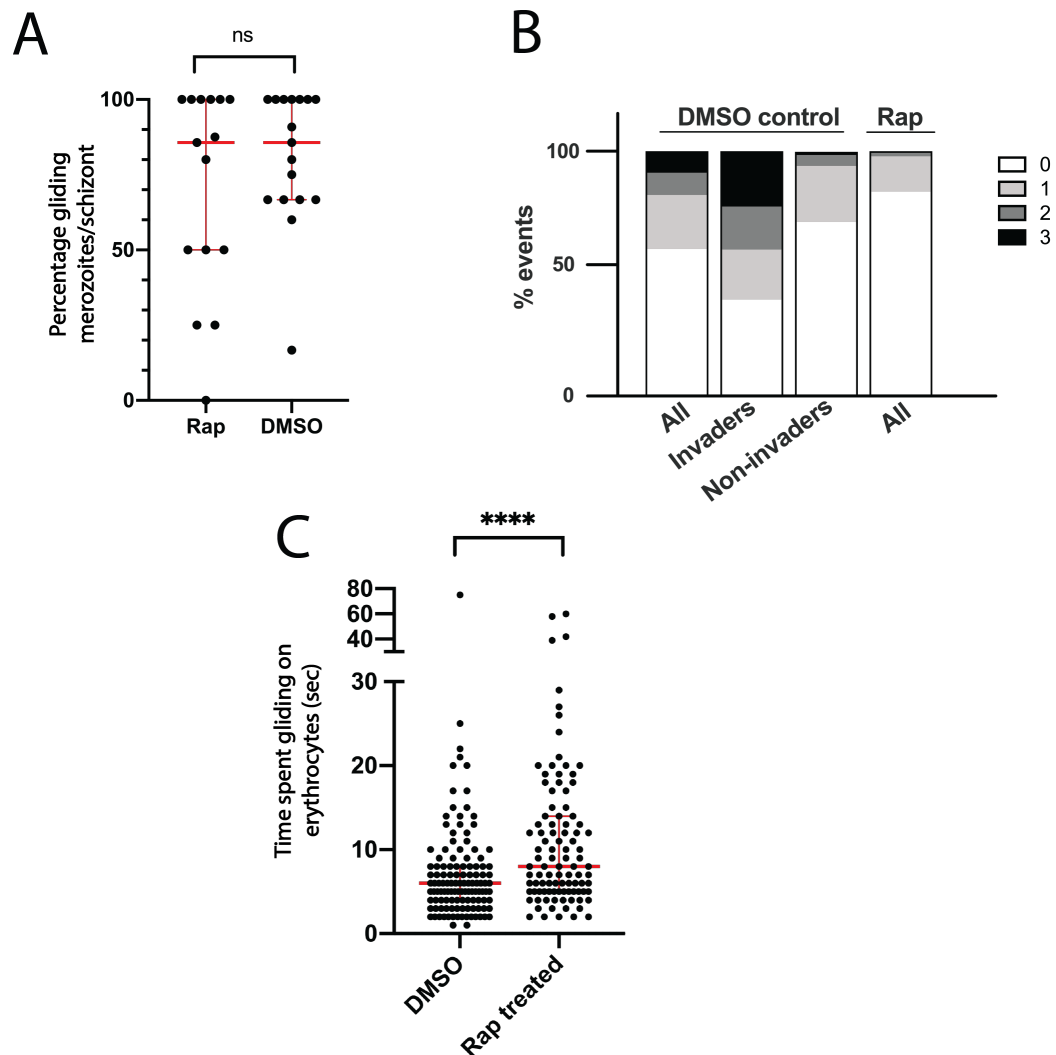
Figure 4.15. PkNBPXa null parasites are motile, but cannot deform host erythrocytes.
(A) There is no significant difference between the median percentage of gliding merozoites/ schizont of DMSO (85%) and rapamycin (85%) treated NBPXa_cKO/A parasites, as determined by a Mann-Whitney u-test (p=0.53; n = 17 DMSO treated schizonts, and 15 Rap treated). **(B)** The proportion of merozoite-RBC contacts leading to erythrocyte deformation (scores 1-3) is significantly less for rapamycin vs DMSO treated NBPXa_cKO/A parasites (measured by chi-squared test; p= 0.0005; n= 483 interactions for DMSO control, and 466 interactions for rap treated parasites). **(C)** The median length of time Rapamcyin treated NBPXa_cKO/A parasites spend gliding on erythrocytes is slightly, but significantly longer than the length of time DMSO control parasites spend gliding on erythrocyte surfaces (8 sec vs 6 sec), when compared using a Mann-Whitney u-test. (****p<0.0005; n = 122 gliding interactions for DMSO, and 99 interactions for rap treated parasites). For both graphs, thick red bars indicate the medians and thinner red bars indicate interquartile ranges.

all interactions between DMSO treated parasites and erythrocytes (n= 85/483 interactions). However, a breakdown of the interactions between rapamycin treated parasites and erythrocytes (n = 466 interactions), revealed that KO parasites initiated very few score 2 deformation events (<2% of all interactions) and no score 3 events at all (Fig 4.15B). Furthermore, the proportion of lower scoring, scale 1 interactions, which include very minor indentations, caused by collisions between merozoites and RBCs, was significantly, although not as drastically, reduced (14.6% vs 22.2% in comparison to the DMSO control; p= 0.0126, measured by a chi-squared test). Thus overall, PkNBPXa appears to be critical for strong host cell deformation, particularly score 2 and 3 interactions.

Importantly, the overall lack of deformation correlated with a considerably lower invasion efficiency for rapamycin treated parasites, in comparison to the DMSO control. While 58 DMSO treated merozoites invaded host erythrocytes (from 20 schizonts), only two clear invasions (from 2/20 schizonts) were observed for rapamycin treated parasites. Both of these invasions were preceded by score 2 deformations, and since the excision efficiency of the PkNBPXa cKO/A line ranges from 92-94%, it is reasonable to conclude that these two invasions (and scale 2 interactions) could be explained by non-excised parasites. However, a loss/gain of a fluorescent marker upon excision would be necessary to absolutely confirm this. Interestingly, no score 1 interactions lead to rap treated parasites invading erythrocytes. Under the imaging conditions used for this study, an invasion preceded by a score 1 interaction is a rare event and accounted for only 1/58 DMSO invasions. However, given that Rap treated parasites are still capable of performing scale 1 interactions, albeit fewer of them, an invasion or two, mediated by scale 1 interactions might have been expected to be observed, and could have offered an explanation towards why some PkNBPXa null parasites may still invade. One possibility is that strong deformation, mediated by PkNBPXa, is not essential for invasion, per se, but rather it just significantly increases the chances of an invasion occurring. Thus PkNBPXa null parasites might still be able to invade, albeit rarely, by chance, if PkNBPXa mediates only deformation and not an additional, essential role also. However, analysis of a much larger sample size, with fluorescently labelled parasites to confirm the KO status of individual merozoites, will clearly be required to address this outstanding question.

A final question was whether PkNBPXa KO parasites might spend a more extended period of time gliding on erythrocyte surfaces while attempting to establish the interactions required for deformation. Interestingly, overall KO parasites spent a median length of 8 seconds actively circling erythrocyte surfaces (n= 99 interactions), which is significantly longer than what was observed for DMSO treated parasites (median length of 6 seconds, n= 123 interactions; p=0.0001, determined by a Mann-Whitney u-test; Figure 4.15C). However, it is important to note that strong deformations tend to obscure the view of parasite motility, and the squeezing of the erythrocyte membrane around the merozoite may even immobilize it, holding it in place, in preparation for apical attachment and the calcium flux between zoite and host cell. Thus it may be that PkNBPXa null parasites simply glide on erythrocyte surfaces for a longer duration because forward motility is not impeded by strong deformations.

4.7 Investigating the role of PkDBPα

4.7.1 Towards generating a *PkDBPα* cKO line

PkDBPα is a considerably smaller (3.8kbp) gene than *PkNBPXa,* and therefore it is possible to replace the entire endogenous gene with a synthetic copy in a single transfection step, a strategy used to generate the RecDBPα line (Mohring et al., 2019). Therefore, in order to produce a floxed *PkDBPα* line, the donor DNA plasmid containing the entire *RecDBPα* sequence (pDonor_DBPα, from Mohring et al., 2019) was modified to introduce LoxP sites into the synthetic gene. This was achieved by inserting the PkLoxPint1 module after the *RecDBPα* signal peptide and inserting a HA/stop codon/LoxP sequence at the C-terminal end of the gene.

The final product, pDonor_floxedDBPα (Appendix Figure 3), was transfected into the WT DiCre line (line 3, from Figure 4.3), along with pCas9sg_DBPα, which targets a cut site in the middle of *PkDBPa*, specific to this gene (Figure 16A; Mohring et al., 2019). Modified parasites were subsequently detected by diagnostic PCR (Figure 4.16B), using primers shown in Figure 4.16A. Unfortunately, it appeared that a substantial proportion of wild type parasites remained after drug selection, based on the fact that limiting dilution produced only wild type clones. Dr Franziska Mohring (Moon lab, LSHTM) kindly performed a second transfection and cloned the resulting line as soon as parasites recovered from drug selection. At the same time, due to evidence that the RecDBPα DiCre line exhibits some leaky excision activity, even

without rapamycin induction (see section 4.5.3), this transfection was repeated, but into a second WT DiCre line, generated from a separate study (Knuepfer et al., 2019) and kindly provided by Dr Ellen Knuepfer (Francis Crick Institute). In this line, the DiCre cassette is under the control of a different promoter (PkHSP86) and has been integrated into an alternative locus (*Pk47*), and thus, in theory, might exhibit different properties. After transfection, transgenic parasites were detected via diagnostic PCR, and a single clone, EK_DBPα cKO, was isolated by limiting dilution (Fig 4.16C).
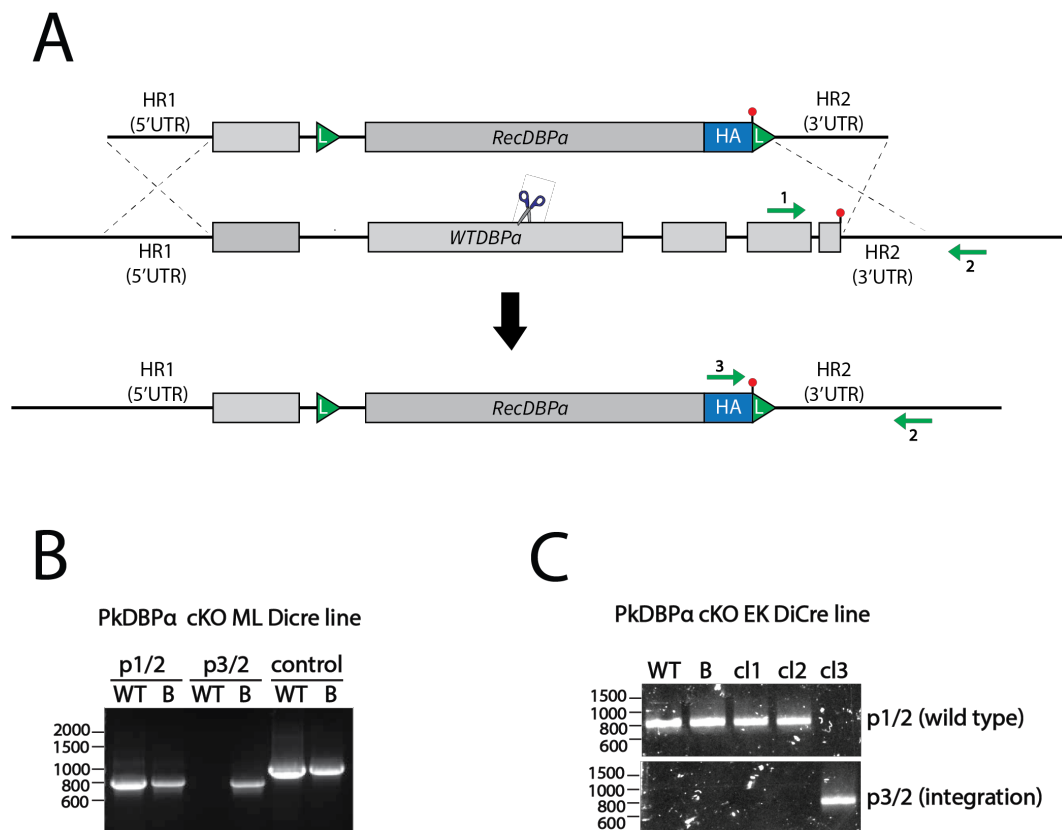
Figure 4.16. Generation and genotyping of an inducible PkDBPa KO line. (A) Schematic depicting the replacement of WT PkDBPa, with a recodonised, floxed copy. Green arrows depict primers used to screen lines for WT (positions 1 and 2) and transgenic (positions 3 and 2) parasites. **(B)** Diagnostic PCRs showing integration of the floxed RecDBPα construct into the WT PkDBPα locus, in the Moon lab (ML) DiCre background. Integration events detected with primers in positions 2 and 3 (Primers MH1041/CH193 from table 2.5) from schematic above. Expected band size = 824bp. Wild type parasites detected using primers in positions 1 and 2 from above schematic (Primers MH1041/MH562 from Table 2.5). Expected band size = 849bp. WT = wild type control parasites; B = bulk, uncloned transfection. **(C)** Diagnostic PCRs showing integration of the floxed RecDBPα construct into the WT PkDBPα locus, in Ellen Knuepfer's (EK) DiCre background. The same primers used in (B) detected wild type parasites in the wild type control (WT), bulk culture (B), and clones 1 and 2 (Cl1 & Cl2). Integrated parasites were detected for clone 3 (cl3) only.

4.7.2 Inefficient excision of *PkDBPα*

In contrast to the promising results seen with the PkNBPXa cKO line, treatment of the EK_DBPα cKO and ML_DBPα cKO clones did not yield high proportions of PkDBPα null parasites. Two independent experiments showed no loss of HA-tagged PkDBPα whatsoever for the ML_DBPa cKO line, upon rapamycin treatment. This line has since been sent off for sequencing, and we are awaiting results to see whether any mutations to either the integrated DiCre cassette or the floxed DBPα might be present, which
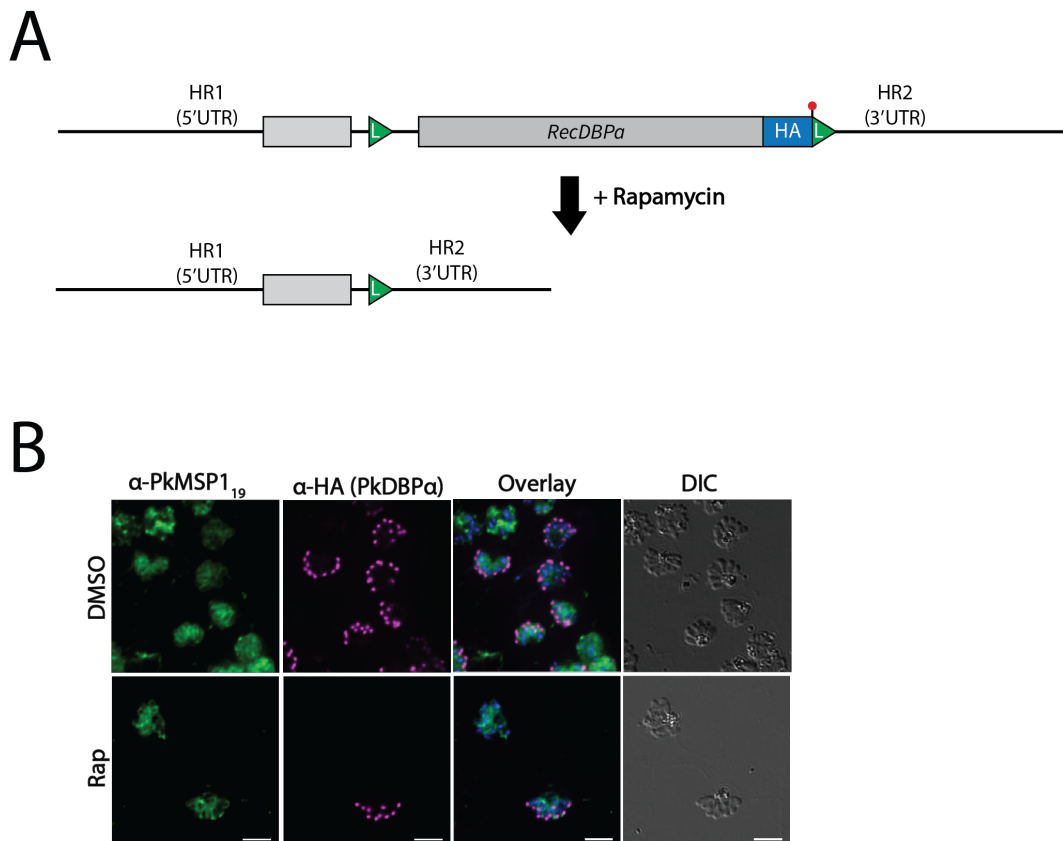
Figure 4.17. Inefficient excision of HA tagged PkDBPα. (A) A schematic depicting excision of an 8.5kbp fragment of *PkDBPα* upon rapamycin treatment of the EK_DBPα_cKO clonal line, also leading to a loss of the HA tag. **(B)** IFA showing ablation of PkDBPa-HA expression for only some (~30%), but not all rapamycin treated EK_DBPα_cKO parasites. Fixed parasites probed with anti-HA (3F10, Sigma), and anti-PkMSP1$_{19}$ (Ellen Knuepfer, Francis Crick Institute) antibodies. Scale bars = 2μm.

could be preventing excision from taking place. A better outcome was observed for the EK_DBPα cKO clone. However, two independent experiments showed that only ~30% of parasites lacked HA-tagged PkDBPα indicating low levels of excision (Fig 4.17A &B). Going forward, one way to obtain PkDBPα null parasites could be to clone the rapamycin-treated EK_DBPα cKO line by limiting dilution in macaque

erythrocytes. Although not ideal, this could at least allow us to isolate a PkDBPα null clone, which could then be transferred into human erythrocytes for phenotyping, as has been done for the conventional PkDBPα KO line (Singh et al., 2005).

4.7.3 *P. knowlesi* merozoites are capable of strongly deforming host cells without DBPα-DARC interactions.

As an alternative to using a cKO approach, I instead opted to target the PkDBPα erythrocyte receptor, DARC (Miller et al., 1975) using an antibody, which binds to its Fy6 epitope. Several studies have shown that targeting this epitope inhibits both PkDBPα and PvDBP from binding to DARC, and thus prevents merozoites from invading host erythrocytes (Smolarek et al., 2010; Russell et al., 2011; Muh et al., 2018; Rawlinson et al., 2019).

Live microscopy showed that treating parasites with 5μg/ml human anti-DARC (2C3 clone, Absolute Antibody) completely inhibited invasion (n= 0 invasions, from 20 egresses). In contrast, control parasites incubated with 5μg/ml anti-human IgG, exhibited normal levels of invasion, with an average of 2.8 invasions/egress observed (n= 56 invasions from 20 egresses; See video 4.12). Despite the block to invasion, it was immediately apparent that anti-DARC inhibited merozoites were entirely capable of gliding across and strongly deforming host cells (Video 4.13). This was not surprising, as *P. knowlesi* merozoites have been reported to be able to deform Duffy negative RBCs, despite not being able to invade them (Miller et al., 1975). Still, the extent to which they can deform Duffy negative host cells compared to Duffy positive cells has never been established. If PkDBPα does contribute to deformation, possible outcomes could be that blocking PkDBPα-DARC interactions causes the overall proportion of stronger deformations to decrease, or that merozoites might deform erythrocytes for shorter durations, even if deformation is not entirely ablated. Therefore, a thorough analysis of all merozoite-RBC interactions was undertaken in order to investigate if blocking PkDBPα-DARC interactions reduces the strength or the duration of erythrocyte deformation.

Figure 4.18A depicts the relative proportions of scored (0-3) deformation events for both anti-DARC treated (n = 396 interactions from 73 merozoites) and control parasites (n= 370 interactions from 89 merozoites) and shows that overall, there are no significant differences between the two groups (measured by a chi-squared test; p=

0.1882). Next, when considering the duration of deformation interactions, no significant difference was found between the lengths of score 2 interactions of anti-DARC (median = 6 s; n = 55 interactions) vs. control parasites (median = 9 s; n = 36 interactions). Furthermore, the duration of scale 3 deformations made by anti-DARC treated parasites was significantly longer (median = 18.5 s; n = 16 interactions) than those performed by control parasites (median = 12 s; n = 17 interactions) (Figure 4.18B). Thus, overall, deformation is not inhibited at all when the PkDBPα-DARC interaction pathway is blocked, and merozoites spend even longer performing the strongest interactions when downstream steps are inhibited. Therefore, PkDBPα does not appear to be required for deformation, in contrast to what is proposed for the *P. falciparum* DBP homologs (Weiss et al., 2015).

For control parasites, there was a very close association between score 3 deformation events and invasions, with 15/17 score 3 interactions leading directly to invasion. As a result, only one control merozoite performed more than a single score 3 deformation event. However, a surprising finding was that despite being unable to invade anti-DARC treated erythrocytes, merozoites did not perform many more score 3 interactions overall (0.25 vs. 0.20 score 3 events/merozoite, for anti-DARC vs. control), even though they performed almost double the number of score 2 interactions per merozoite compared to control parasites (0.78 vs. 0.46 score 2 interactions/merozoite for anti-DARC vs. control). Only 4/14 scale 3 events lead on to an additional score 3 interaction (for a total of 18 score 3 events) suggesting that parasites are limited in their ability to make multiple strong interaction events.

So, why was this the case? One possible reason could be that anti-DARC treated parasites spent a longer time performing score 3 (median = 18.5 sec; n = 16) vs. score 2 interactions (median = 6 sec; n = 55 interactions; Figure 4.18C). This was in contrast to control parasites, for which there was no significant difference between the lengths of score 2 and 3 interactions (Figure 4.18D). Whilst score 3 interactions quickly culminated in invasion of untreated erythrocytes, anti-DARC inhibited parasites continued deformation far longer, thus potentially expending greater resources associated with this intense activity - for example, secretion of PkNBPXa. Therefore, it could be that after longer score 3 interactions are completed; the merozoite has potentially run out of PkNBPXa. Thus, whilst score 3 interactions are not a commitment step per se, they may require more resource investment than lower
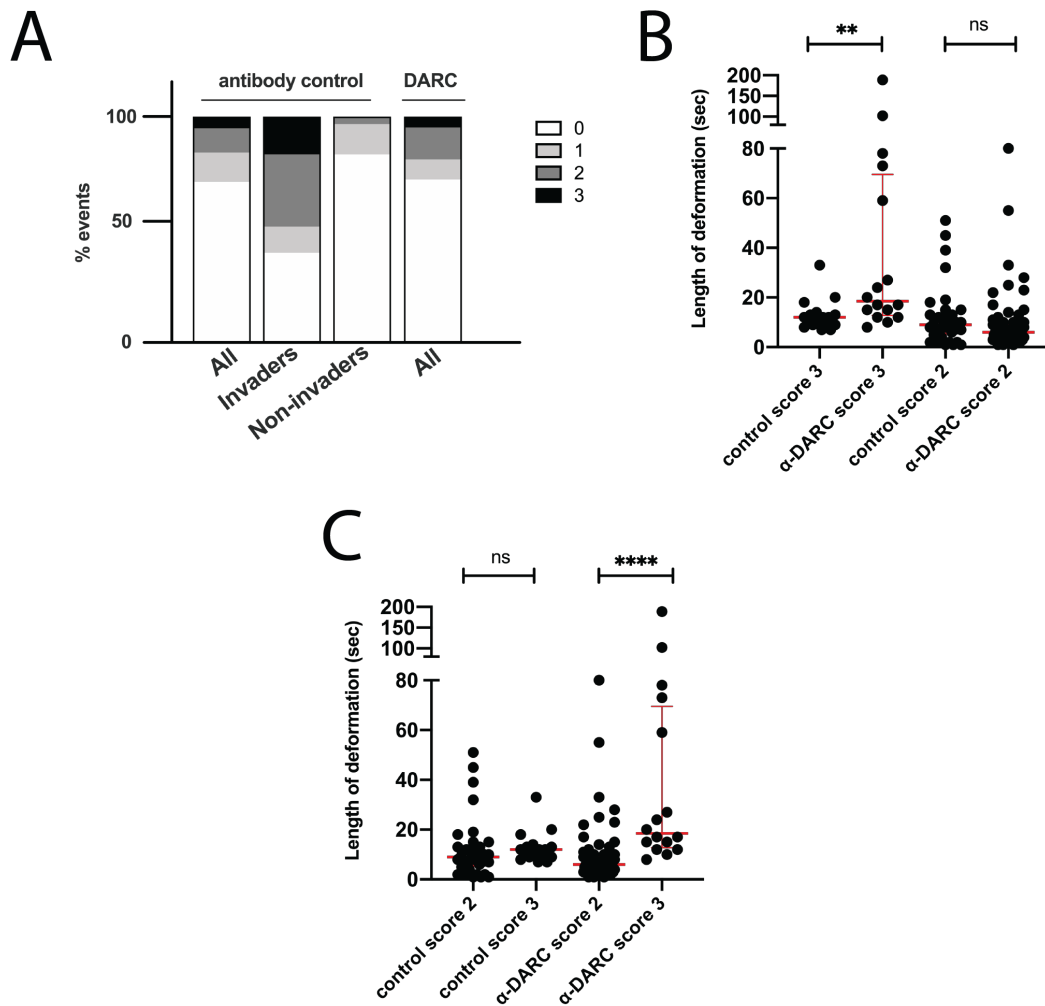
Figure 4.18. Anti-DARC blocked merozoites are capable of strongly deforming host erythrocytes. (A) There is no significant difference between the proportions of interactions leading to strong host cell deformation for control vs. anti-DARC treated parasites, measured by a Chi-squared test (p=0.19). For control parasites n = 264 score 0, 48 score 1, 40 score 2, and 18 score 3 interactions (from 89 merozoites, from 20 different schizonts); for anti-DARC treated parasites, n= 287 score 0, 35 score 1, 56 score 2, and 18 score 3 interactions (from 73 merozoites, from 20 different schizonts). **(B)** Score 3 deformation interactions persist for a longer duration for DARC treated (n= 16 interactions; median length = 18.5 sec) vs. control parasites (n = 17 interactions; median length = 12 sec). ** Indicates p = 0.003, as determined using a Mann-Whitney U-test. There is no significant difference (ns) between the median lengths of scale 2 interactions of control (median length = 9 sec; n = 36 interactions) vs. anti-DARC treated parasites (median length = 6 seconds; n= 55 interactions), as determined by a Mann-Whitney U-test (p= 0.12). **(C)** The median lengths of score 2 (6 sec) vs. score 3 (18.5 sec) merozoite-RBC interactions are significantly different for anti-DARC treated parasites, as determined by a Mann-Whitney u-test (****denotes p<0.0001; n= 55 score 2 interactions, and 18 score 3). However, there is no significant difference (ns) between the median lengths of score 2 (median = 9 sec; n = 36 interactions) vs. score 3 (median = 12 sec; n = 17 interactions) interactions for control parasites, as determined by a Mann-Whitney U-test (p = 0.09). For both graphs, thick red bars indicate medians and thinner red bars indicate interquartile ranges.

intensity deformations. Going forward, this theory could be tested by analysing interaction lengths of anti-DARC treated PkNBPXa-mNG parasites. Alternatively, another explanation could simply be that only a certain proportion of erythrocytes are amenable to the strongest deformation in the first instance. Thus, regardless of whether PkDBPα-DARC interactions are blocked or not, the number of scale 3 interactions overall would be relatively stable between control and anti-DARC treated groups.

4.7.4 *P. knowlesi* merozoites cannot re-orientate on the erythrocyte surface without PkDBPα-DARC interactions

Importantly, despite being able to deform host erythrocytes, not one anti-DARC blocked-merozoite (n= 73 merozoites and 396 merozoite-RBC interactions) initiated re-orientation (Figure 4.19). While control parasites clearly paused towards the end of deformation in preparation for re-orientation and invasion (n = 42 merozoites and 42/372 merozoite-RBC interactions), anti-DARC treated merozoites continued to glide throughout deformation (e.g. 45-65 s in video 13). Eventually, they either transitioned to gliding along another surface, or they ceased gliding altogether, switched to Brownian motion, and floated away from the erythrocyte. Thus it appears that PkDBPα plays a key role directly before re-orientation, likely during the period between the very end of deformation and the commencement of apical pivoting. However, further experiments are needed to narrow this window down even more and to determine, for instance, whether anti-DARC blocked merozoites can establish a calcium flux between parasite and host cell, or not.
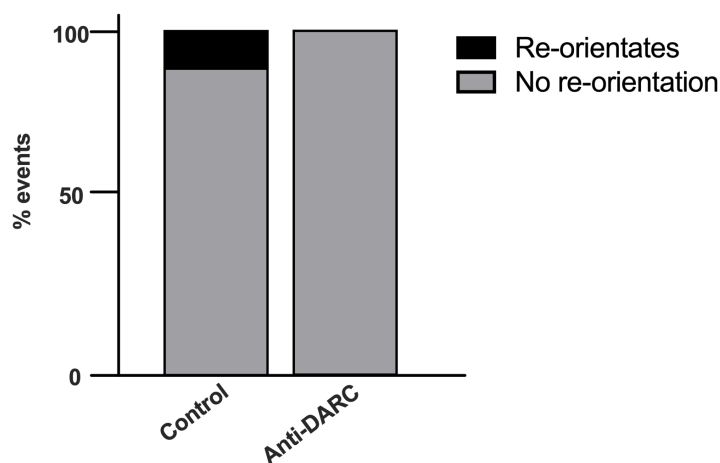
Figure 4.19. Blocking PkDBPα-DARC interactions prevents merozoites from re-orientating. Analysis of 372 (clear) merozoite-RBC interactions made by control parasites (n= 89 merozoites) shows that 11.3% (42/372 interactions) lead to re-orientation and invasion. In contrast, none of the 396 merozoite-RBC interactions performed by anti-DARC treated parasites (n= 73 merozoites) lead to re-orientation, or invasion. A Chi-squared test shows that these differences are significant ($p < 0.0001$).

4.8 Summary and discussion

The combination of *P. knowlesi'*s genetic amenability, the development of new genetic tools, and the large size of *P. knowlesi* merozoites have enabled us to use live microscopy to gain insight into molecular processes underlying invasion. We have demonstrated for the first time that although the *P. knowlesi* RBL and DBP ligands may be secreted simultaneously, once secreted, and during invasion itself, fluorescently labelled PkNBPXa and PkDBPα display different distribution patterns across the merozoite. While secreted PkNBPXa takes on a cytosolic appearance, PkDBPα forms an asymmetric surface pattern on free merozoites and a ring-like structure, trailing PkAMA-1 and the moving junction during host cell entry. We have also captured the formation and progression of the moving junction by live microscopy, for the first time using *Plasmodium* parasites, using parasites expressing fluorescently labelled PkAMA-1. Excitingly, these videos also demonstrated that the merozoite exhibits helical rotation to drive itself into the host cell, just as it does to transport itself across extracellular surfaces.

Additionally, we have now unequivocally shown that loss of PkNBPXa prevents merozoites from initiating strong deformation. However, blocking the interactions of PkDBPα with its host cell receptor DARC, does not hinder deformation but prevents merozoites from re-orientating on the surface of erythrocytes. Thus both the fluorescence and conditional KO data point to PkNBPXa and PkDBPα performing distinct roles, with PkDBPα functioning downstream of PkNBPXa. Still, many questions remain. How might PkNBPXa mediate deformation? What is the precise role of PkDBPα? Could PkNBPXa and PkDBPα perform any additional roles to those outlined in this study? Finally, might the remaining RBL/DBPs also contribute to the invasion of human erythrocytes? These questions highlight the need to carry this work forward so that the mechanisms by which these ligands act can be understood.

4.8.1 PkNBPXa mediates erythrocyte deformation – but how?

Video microscopy has shown that PkNBPXa is continuously secreted from the micronemes, for several minutes after egress. Intriguingly, once secreted, PkNBPXa does not appear to remain at the apical tip, unlike what has been previously reported for the *P. falciparum* RBLs (Taylor et al., 2002; Triglia et al., 2009) or localise to the periphery of the merozoite, as is seen to a certain extent for PkAMA-1. Instead, the

mNG signal appears to move from an apical to a cytosolic localisation. One possibility is that as PkNBPXa is being secreted from the micronemes, its ectodomain is being continuously cleaved from its transmembrane domain and that the mNG-tagged cytoplasmic tail is being released into the merozoite's cytosol.

The *P. falciparum* RBL and DBP ligands undergo several proteolytic steps both before and after egress. For instance, the PfRh1 ectodomain is cleaved by plasmepsin X (PMX) and at least one other protease likely just before egress (Favuzza et al., 2020; Gunalan et al., 2020). Additional proteolytically cleaved PfRh1 fragments can be found in free merozoites and culture supernatants, and the processing steps responsible for these fragments may take place during invasion itself. Processed regions of the PfRh1 ectodomain have been found to associate with the moving junction, and so some cleavage steps may be responsible for exposing new functional domains, and re-purposing this ligand for functions beyond its initial role in mediating pre-internalization steps (Triglia et al., 2009; Gunalan et al., 2020). One final processing step, though, is thought to occur as merozoite entry into the erythrocyte progresses: this is the action of the rhomboid-like protease, ROM4, which cleaves secreted RBL and DBP ligands at a site within their transmembrane domains, effectively shedding whatever is left of the membrane-bound ectodomain, into the supernatant (Baker et al., 2006; O'Donnell et al., 2006; Triglia et al., 2009; Favuzza et al., 2020). In the end, only short, cytoplasmic stubs are taken into the erythrocyte, and all ectodomain remnants are left behind.

While this final shedding step is theorized to take place during host cell entry, PfROM4 cleavage of RBL and DBP invasion ligands is seen regardless of whether merozoites are given the opportunity to re-invade, or not (Gunalan et al., 2020; Favuzza et al., 2020). We have identified a putative ROM4 cleavage site within the PkNBPXa transmembrane domain. Thus, it is entirely possible that PkNBPXa could be being cleaved after secretion, but prior to erythrocyte entry, in a PkROM4 dependent manner. Going forward, it will be important to investigate PkNBPXa processing, perhaps by mutagenesis of the putative ROM4 cleavage site, and to determine if any components of the PkNBPXa ectodomain remain associated with the merozoite surface, contributing to downstream invasion steps. Meyer et al. (2009) probed *P. knowlesi* supernatants with an anti-PkNBPXa antibody, targeting the middle of the PkNBPXa ectodomain. Two bands were observed, indicative of at least one

additional processing step, to the putative ROM4 cleavage event. Further experiments, using the tagged lines produced in this study, in combination with an antibody towards the N-terminus of PkNBPXa may reveal more processing events, which could be relevant for downstream invasion steps. Ideally, the best way to address this question would be to generate a dual fluorescently labelled PkNBPXa line, with one fluorescent protein tagging its C-terminus and another, its N-terminus. This would allow the fates of both the PkNBPXa N-terminus and C-terminus to be monitored concurrently with live microscopy, and allow us to see when processing occurs relative to each step of invasion. Our attempts to visualise PkNBPXa secretion using a mCherry tag were not successful, since this fluorescent protein (FP) is not particularly bright, and bleaches very quickly, relative to mNG. However, an array of brighter, more photostable red FPs has been engineered over the last several years (Cranfill et al., 2016). So one of these alternatives, such as mScarlet-I, which is reported to be 3-fold brighter than mCherry (Bindels et al., 2016), could potentially be used to tag the N-terminus of PkNBPXa at the same time its C-terminus is tagged with mNG.

Intriguingly, merozoites cannot deform host erythrocytes when PkNBPXa is not expressed, or when apical PkNBPXa stores are spent. Erythrocyte deformation, however, has also been shown to be a motor-dependent process (Weiss et al., 2015), and, as chapter 3 demonstrated, relies upon merozoites gliding across erythrocyte surfaces. Yet how are PkNBPXa secretion, gliding motility, and erythrocyte deformation all linked? PkNBPXa could be coupled to the merozoite's acto-myosin motor, as has been suggested, but not confirmed for the *P. falciparum* RBL/DBPs (Diaz et al., 2016; Pal-Bhowmick et al., 2012). However, another possible scenario is that when PkNBPXa is secreted to the merozoite's apical tip, it binds to its, as of yet, unknown host cell receptor, tightly connecting the merozoite's apex to the host cell. Receptor binding may induce structural changes to the host cell cytoskeleton, causing it to become more amenable to deformation, as has been observed when EBA-175 binds to its host cell receptor, glycophorin A (Koch et al., 2017; Sisquella et al., 2017). Then, as the merozoite glides forward on the erythrocyte surface, rotating as it does so, the tightly bound merozoite may pull the erythrocyte membrane around itself, resulting in the host cell "wrapping" around the merozoite. Finally, enzymatic cleavage of PkNBPXa, potentially by PkROM4 releasing the PkNBPXa ectodomain from the merozoite's apical tip, could sever merozoite-RBC contacts, allowing it to continue its

forward trajectory. Thus, PkNBPXa, and the RBLs in general, may not need to be directly connected to the merozoite's motor in order to mediate deformation, but could instead act to increase the "stickiness" or torque of the parasite surface to create torsion driven wrapping.

4.8.2 Towards determining a role for PkDBPα

Anti-DARC blocked merozoites are very clearly capable of deforming host erythrocytes. Although these results have not yet been validated with a conditional PkDBPα KO line, they do reflect the description of *P. knowlesi* merozoites attempting to invade Duffy negative erythrocytes (Miller et al., 1975). However, it is worth noting that these results only confirm that PkDBPα-DARC interactions are not responsible for deformation. Ideally, an investigation of how PkDBPα null parasites interact with human erythrocytes will need to be undertaken in order to rule out additional, DARC independent roles for PkDBPα during the early steps of invasion. However, analysis of the conditional *PkDBPα* KO line generated in this study showed very inefficient *PkDBPα* excision upon induction with rapamycin. Therefore, going forward, attempts will be made to clone out rapamycin-treated parasites using macaque erythrocytes, in order to isolate a clonal line of PkDBPα null parasites. Subsequently, these parasites could be purified, and added to human erythrocytes, in order to analyse the PkDBPα null phenotype and compare what is observed to the anti-DARC data.

Importantly, inhibiting PkDBPα engagement with DARC did show that without this crucial interaction, *P. knowlesi* merozoites are unable to pivot on their apical ends and align themselves into a position ready for host cell entry. This is in contrast to a previous study, which used electron microscopy to show a correctly aligned PkDBPα KO parasite in contact with a human erythrocyte (Singh et al., 2005). However, as no moving junction was observed between merozoite and host cell, likely, what was captured here was simply a merozoite randomly fixed in this orientation, rather than a merozoite which had undergone apical pivoting. Therefore, while valuable information was gleaned from this study, it does illustrate the importance of using video microscopy along-side EM techniques to capture both the dynamics of invasion, in addition to the high-resolution details (such as junction formation) provided by EM.

As chapter 3 illustrated, additional steps lie between the end of deformation and the moment the merozoite begins to pivot, including a calcium flux between the

merozoite's apical end and the host cell. Going forward, imaging anti-DARC blocked merozoites attempting to invade Fluo-4-AM loaded erythrocytes could demonstrate whether PkDBPα engagement with DARC precedes this step. Importantly, if no calcium flux is observed in the presence of anti-DARC, then this could indicate that PkDBPα may not mediate apical pivoting, but rather a step bridging deformation and re-orientation, such as rhoptry neck secretion. This would be in good agreement with work by Singh et al. (2010), showing that PfEBA-175 binding to soluble Glycophorin A results in free merozoites secreting rhoptry bulb contents. Evidence of rhoptry bulb secretion is also very clearly seen when *P. falciparum* merozoites are incubated with the R1 peptide, blocking PfAMA1-RON2 interactions, and when invasion is inhibited by cytochalasin D treatment (Riglar et al., 2011; Srinivasan et al., 2011). Thus it is plausible that once PfEBA-175, or an alternative appropriate DBP ligand, binds to its host cell receptor that rhoptry secretion is triggered, and maintained, regardless of whether junction formation is subsequently inhibited or not. An interesting experiment going forwards might be to generate a *P. knowlesi* line expressing a fluorescently labelled rhoptry bulb protein, such as PkRAP1, and incubating this line with soluble DARC. In theory, if PkDBPα-DARC interactions do activate a signalling cascade that leads to rhoptry secretion, then PkRAP1 secretion should not be observed when parasites are incubated with anti-DARC antibodies plus erythrocytes but should occur when parasites are incubated with the soluble receptor.

Another important consideration is that if blocking PkDBPα-DARC interactions does prevent the calcium flux/rhoptry secretion from occurring, then this phenotype would mimic that of disrupting the *PfRh5* complex. *P. falciparum* merozoites can deform host cells, but cannot initiate a calcium flux when PfRh5-Basigin interactions are inhibited with either anti-PfRh5 or anti-basigin antibodies (Weiss et al., 2015). Likewise, conditional deletion of PfCyRPA and PfRipr, two essential *P. falciparum* proteins that exist in a complex with PfRh5, also produces the same results (Chen et al., 2011; Reddy et al., 2015; Volz et al., 2015). However, like all non-laveranian malaria parasites, *P. knowlesi* does not have a PfRh5 ortholog. Nevertheless, *P. knowlesi* does possess orthologs to PfCyRPA and PfRipr (Knuepfer et al., 2019). Like their *P. falciparum* counterparts, both *PkRipr* and *PkCyRPA* are also essential for *P. knowlesi* proliferation (Knuepfer et al., 2019). In *P. knowlesi* these two proteins are not found in a complex together, but instead, PkRipr forms a complex with two alternative

proteins, PkCSS and PkPTRAMP, which are also essential for parasite growth. Therefore, the PkRipr complex may be performing a similar role to the PfRh5-CyRPA-RIPR complex, through PkTRAMP binding to an as of yet unknown receptor on the RBC surface (Knuepfer et al., 2019). If the PkRipr complex is functionally equivalent to the PfRh5 complex, then PkRipr may be inserted into, and form a pore within the erythrocyte membrane, as has been suggested for *P. falciparum* (Wong et al., 2019). If this is the case, it is possible that another outcome of PkDBPα-DARC interactions may be to hold the merozoite firmly in place or signal to the merozoite to temporarily stop gliding so that PkRipr can be deposited into the erythrocyte membrane, and pore formation can ensue. Therefore, going forwards, it will be important to explore the phenotype of PkRipr complex mutants using live microscopy techniques, to 1) determine whether this complex does act in a functionally equivalent manner to the PfRh5 complex, and 2) to ascertain when this complex acts with respect to PkDBPα.

4.8.3 A role for the remaining *P. knowlesi* RBL and DBP ligands?

A final consideration that needs to be addressed is whether the remaining *P. knowlesi* DBP and RBL ligands contribute to the invasion of human erythrocytes. Recent work has shown that the growth rate of *P. knowlesi* parasites actually increases, when either PkDBPβ, or PkDBPγ is deleted (Mohring et al., 2019). Therefore, it does not seem likely that either of these ligands contributes positively in the context of human erythrocyte invasion. Rather, they might even hinder invasion efforts, perhaps by competing with potential cytosolic PkDBPα interaction partners, especially since the cytoplasmic domains of these ligands are remarkably similar.

A similar effect might be seen for a PkNBPXb KO parasite line, as this ligand has been shown to bind to macaque erythrocytes, and ultimately cannot compensate for a lack of PkNBPXa when parasites are grown solely in human erythrocytes (Meyer et al., 2009; Semenya et al., 2012; Moon et al., 2016). However, it has never been definitively proven that PkNBPXb does not contribute in any way to the invasion of human erythrocytes. Furthermore, conventional PkNBPXb KO line has recently been generated but has proved difficult to clone out (Dr Mohring, personal communication), suggesting that PkNBPXb might play a minor role during human erythrocyte invasion.

Now that we have developed a PkNBPXa cKO line, it may be possible to test this theory, by knocking out PkNBPXb on top of this line. Comparing the growth rate of a double KO line with the single PkNBPXa KO line in human erythrocytes may shed some light on the issue of whether or not residual invasions are a result of PkNBPXb aiding and abetting PkNBPXa null parasites. Alternatively, if a slight redundancy between these two ligands does not account for the rare invasion events seen, then it may be the invasion step (deformation) rather than the proteins, which is partially redundant. Deformation may greatly aid invasion events, with wrapping perhaps increasing the speed at which downstream ligand-receptor interactions are formed, and even the likelihood of them occurring in the first instance (Weiss et al., 2015). However, if the only role of the RBL ligands is to act as enhancers for downstream steps, then it is feasible that a small proportion of merozoite-RBC interactions will lead to invasion, even in the absence of PkNBPXa and PkNBPXb interactions.

Chapter 5 – Discussion and future directions

5.1 Towards re-assessing the early molecular steps of invasion

This work has led to the discovery of gliding as a new pre-internalisation step and revealed that the order of events leading up to internalisation is gliding and deformation, followed by a pause to gliding, putative rhoptry secretion, and finally, re-orientation (Figure 5.1). With these findings comes the need to re-assess the molecular steps facilitating pre-internalisation events. Firstly, which merozoite ligands mediate extra-cellular gliding? *Plasmodium* ookinetes and sporozoites and *T. gondii* tachyzoites secrete members of the thrombospondin-related anonymous protein (TRAP) family from their micronemes, which connect the parasite's motor with the substrate it is gliding on (Sultan et al., 1997; Dessens et al., 1999; Frenal et al., 2017). Two TRAP family members are expressed during the *Plasmodium* blood stages, and are localized to the apical organelles of merozoites; these are merozoite TRAP (MTRAP) and *Plasmodium* thrombospondin-related apical merozoite protein, or PTRAMP (Thompson et al., 2004; Baum et al., 2006). Interestingly, PbMTRAP is dispensable for invasion, which suggests that it may not play a key role in gliding motility, or that if it is responsible for motility during this stage, that surface gliding itself is not an essential pre-internalisation step for *P. berghei* (Bargieri et al., 2016). PTRAMP, on the other hand, is essential for invasion (Zhang et al., 2018; Knuepfer et al., 2019) for both *P. falciparum* and *P. knowlesi*, and thus is potentially a promising candidate.

However, recent evidence has also shown that PkPTRAMP forms a complex with both PkCSS and PkRipr and that this complex might act in a way that is functionally equivalent to the PfRh5-CyRPA-Ripr complex (Knuepfer et al., 2019). The PfRh5 complex is predicted to act just prior to the calcium flux, and interaction of PfRh5 with its host cell receptor, Basigin, may result in PfRh5 and PfRipr being inserted into the erythrocyte membrane (Crosnier et al., 2011; Volz et al., 2016; Wong et al., 2019). Once embedded in the erythrocyte membrane, this ligand could potentially enable the formation of a pore between parasite and host cell, although a mechanism for this is yet to be elucidated (Weiss et al., 2015; Volz et al., 2016; Wong et al., 2019). Thus, the PkPTRAMP-CSS-Ripr complex may be acting to achieve a similar goal. Still, this hypothesis has never been investigated using live microscopy. Analysis of conditional

PkPTRAMP null parasites will be required to determine if 1) PkPTRAMP is required for gliding motility, and if this is not the case, then 2) which invasion steps are impeded when this ligand is absent.
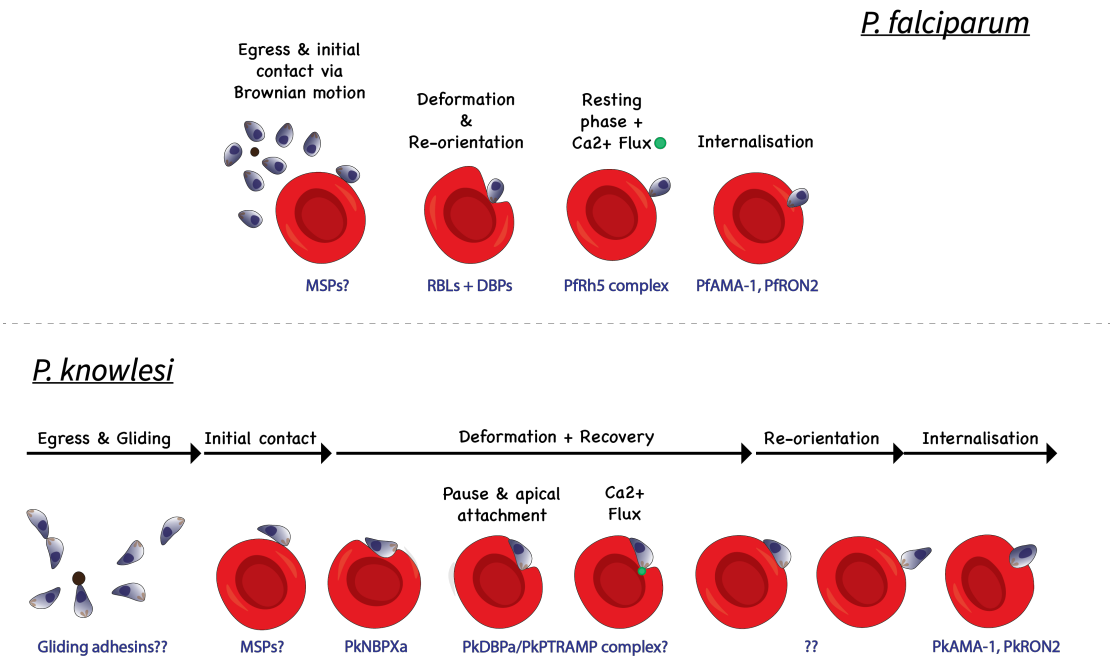
Figure 5.1. A comparison of the current *P. falciparum* model of invasion (top) vs. the new *P. knowlesi* model (bottom). For *P. falciparum*, deformation and re-orientation are thought to occur simultaneously, and be facilitated by both the RBL and DBL ligands. After re-orientation is completed, merozoites rest for several seconds, during with the calcium flux occurs. Internalisation follows. In contrast, our work shows (bottom) that gliding motility + NBPXa-receptor interactions facilitate deformation. PkDBPα acts downstream of this event, possibly mediating the pause between apical attachment and re-orientation. Re-orientation begins after the calcium flux and the host cell has recovered from deformation. No pause occurs between completion of re-orientation, and the beginning of internalisation.

Secondly, which ligand, or combination of ligands, is responsible for re-orientation? Furthermore, is re-orientation driven solely by a gradient of apical ligands, increasing in concentration towards the merozoite's apical tip, as proposed by Weiss et al. (2015)? We have definitively shown, in line with work carried out by Yahata et al., (2012), that deformation does not physically align the merozoite for host cell entry. On one level, these findings do support the results presented by Weiss and colleagues. Furthermore, although previous mathematical studies theorized that both deformation and apical gradients of invasion ligands are required for re-orientation, these models

were based on the assumption that the apical end of the merozoite is its thin, pointy end (Dasgupta et al., 2014; Hillringhaus et al., 2020, 2019). Thus, modifying these studies to take into account the merozoite's apical end being wider than its basal end may change the outcome of their findings to side with Weiss et al. (2015). In theory, aligning the merozoite's wider, rounder end with the erythrocyte surface should be an easier feat than pivoting it on to its thinner, pointy end.

However, an additional, important point worth making is that none of the above studies made their hypotheses taking into account the fact that merozoites can glide across erythrocyte surfaces. Yet, what if gliding mediates not just the steps leading up to, and directly after re-orientation, but also this crucial pivoting step itself? Our work has shown that directly before re-orientation, merozoites pause forward movement as the whole zoite, and in particular, its asymmetrically placed apical end becomes firmly attached to the erythrocyte surface. When host RBCs are loaded with the Ca^{2+} dye fluo-4, a calcium signal at the apical tip of the parasite can be seen to follow this pause – a sign assumed to be indicative of rhoptry secretion (Weiss et al., 2015). This, along with the fact that there is no subsequent pause between reorientation and internalization, would suggest that the moving junction forms before or even during re-orientation. Given the continuous nature of re-orientation and internalisation, then, is it possible that they are really one event?

We propose that this may be the case, and outline a potential "catapult model" in figure 5.2, which merozoites may use to spring themselves into apical alignment. How might this happen? Firstly, taking into account the fact that gliding events "sandwich" re-orientation, we hypothesize that the pause to extra-cellular motility observed towards the end of deformation may not really be a pause to motor-power, as such, but rather, that the merozoite is simply pinned in place on the erythrocyte surface by adhesive ligands. Thus the motor could still be generating force at this point in time, even though forward motion is curtailed. Nevertheless, this pause gives the merozoite time to fuse its apical end with the erythrocyte surface, and potentially establish the moving junction, both events which might ensure that the merozoite's apical end remains firmly attached to the erythrocyte surface. Next, after the calcium flux occurs, the merozoite begins to cleave molecular attachments to the host cell along the length of the merozoite, whilst maintaining the bonds at its apex (Figure 5.2, insets). As this process occurs, tension builds up at the merozoite's apical end, which is still firmly

attached to the host cell, possibly by the nascent tight junction. Eventually, cleavage of enough adhesive ligands along the merozoite's basal end releases it from the erythrocyte surface and allows the merozoite to spring forwards, pivoting on its anchored apical end – like cutting the rope of a catapult. Concurrently, the now unimpeded merozoite can return to performing corkscrew-like rotations. This then allows the merozoite to begin driving itself into the host cell, as soon as it has orientated itself to an optimal angle to do so. Thus, by this model, a combination of ligand binding and then cleavage steps, along with continuous motor activity, drives re-orientation and host cell entry.
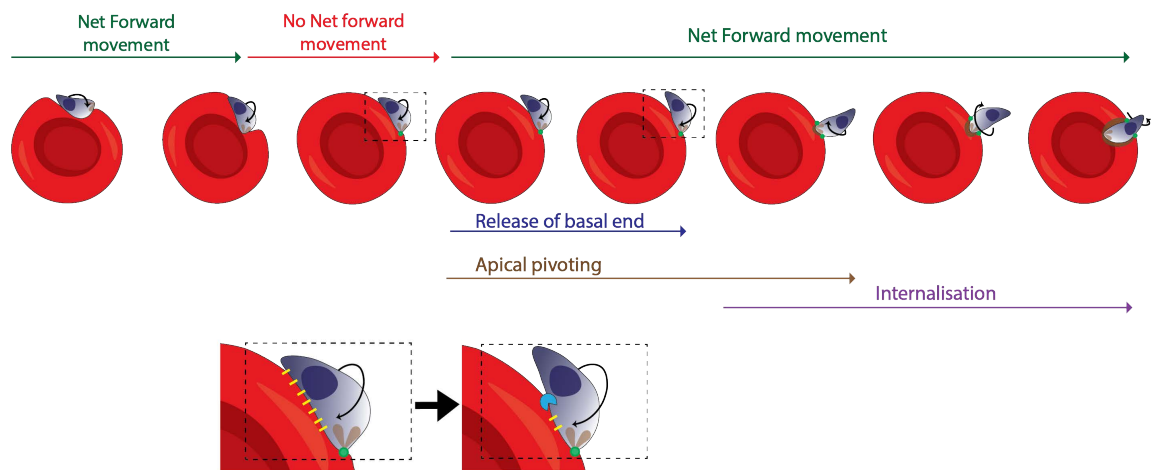
Figure 5.2. Continuous motor activity may drive re-orientation. Gliding is required for deformation (RBCs 1&2). However, forward motion pauses as the merozoite becomes pinned to the erythrocyte surface, by both its basal and apical ends, towards the end of deformation (RBC 2). While paused, the merozoite's molecular motor continues to run, building tension at the merozoite's apical end (RBC 3). Cleavage of adhesins between the merozoite's basal end (depicted in yellow, inset, and RBCs 4-5) by proteases, may release the merozoite's basal end from the erythrocyte surface, and allow the zoite to pivot on its apically anchored pivot point (green dots). Simultaneous helical rotation drives host cell entry (RBCs 5-8).

However, going forwards, the production and analysis of further *P. knowlesi* conditional KO lines will be required to investigate this theory and the molecular steps surrounding re-orientation more fully. To begin, the first logical step would be to attempt to generate a *P. knowlesi* line which could be conditionally induced to delete a core component of the parasite's acto-myosin motor, such as PkACT1 or PkGAP45, as has previously been achieved for *P. falciparum* (Das et al., 2017; Perrin et al., 2018). This would be preferable to relying on treating parasites with cytochalasin D, as this

drug is known to have off-target, invasion inhibitory effects (Das et al., 2017). PkGAP45 would likely be the best target for this, as deleting PfGAP45 does not appear to impact the morphology of merozoites, unlike deletion of PfACT1, which is reported to leave *P. falciparum* merozoites with a ruffled appearance, and prevent them from dispersing properly after egress (Das et al., 2017; Perrin et al., 2018). Conditional deletion of PfGAP45, like treating merozoites with cytochalasin D, prevents host cell deformation, but not echinocytosis or early junction formation (Weiss et al., 2015; Perrin et al., 2018; Yahata and Hart et al., 2020). However, if PkGAP45 null parasites cannot pivot on their apical ends, this would provide strong evidence for the merozoite's molecular motor being required for re-orientation, even if it is not required for precursory apical interactions, such as the calcium flux, or moving junction assembly.

Next, which ligand (or ligands) holds the merozoite in place on the erythrocyte surface before the release of the merozoite's basal end? Could this be a role for PkDBPα, which once secreted, is conveniently concentrated around the widest part of the merozoite as well as its basal end? One possibility is that forward motion is impeded when PkDBPα binds to DARC. This in turn could allow the merozoite's apical end time to firmly attach to the erythrocyte surface, possibly by the actions of the PkPTRAMP complex. As discussed above, The PkPTRAMP complex is potentially functionally equivalent to the PfRh5 complex (Knuepfer et al., 2019) and may facilitate a fusion event between the merozoite's apical tip and the erythrocyte surface (Weiss et al., 2015; Volz *et al.,* 2016; Knuepfer et al., 2019). If PkDBPα binding to DARC is responsible for pinning the merozoite to the host cell surface, this could explain why anti-DARC treated merozoites do not pause extra-cellular motility but continue to glide until they leave the erythrocyte surface. Conversely, if PkPTRAMP acts downstream of PkDBPα, then PkPTRAMP null parasites might exhibit periods of stasis on the erythrocyte surface, even if they are not capable of performing committed apical interactions. Thus a careful analysis of the recently published conditional PkPTRAMP KO line (Knuepfer et al., 2019) may shed some light on these matters.

Finally, which ligand-receptor combinations are responsible for committed apical attachments, and thus, creating a pivot point for the re-orientating merozoite? We, like others, hypothesize that junction formation occurs after the calcium flux (Weiss et al., 2015; Volz et al., 2016; Introini et al., 2018). However, is junction formation occurring

before or after re-orientation, and if it does normally occur before re-orientation, could the junction form the basis of the apical pivot point? Interestingly, Treeck et al., (2009) reported that blocking the interactions of PfAMA-1 and PfRON2 with the R1 peptide does not inhibit re-orientation. However, a closer examination of the video used to specifically demonstrate re-orientation, showed an R1 blocked merozoite interacting with a host cell via its pointed basal tip, which we now know is not indicative of re-orientation. Additional videos from the same study, though, did show R1 blocked parasites strongly deforming host cells, for extended periods of time, which lead firstly to echinocytosis, and finally to host cell lysis. Merozoites remained stuck to the surface of these lysed cells, indicating that even though re-orientation may not have occurred, committed apical attachment very likely did (Treeck et al., 2009). Likewise, Weiss and colleagues (2015) observed similar results. In theory, though, just as for cytochalasin treatment, all of these events could occur without apical pivoting, and if a pore were formed between merozoite and host cell, which was never sealed, this would explain lysis events. However, analysing conditional PkRON2 or PkAMA-1 null parasites should enable us to address this question more definitively, especially since re-orientation is a much more obvious event for *P. knowlesi* compared to *P. falciparum*. Alternatively, if PkAMA-1 or PkRON2 null parasites can pivot on their apical ends, this would indicate that junction formation is not required for re-orientation. Another option is that the actions of the PkPTRAMP complex may facilitate this role instead. Thus, the overall order of molecular events leading to internalisation could be PkNBPXa causing deformation, PkDBPα pinning the merozoite to the erythrocyte surface, and finally, PkTRAMP interactions/junction formation providing an apical anchor for re-orientation.

So overall, while these hypotheses are merely speculative at this point and need to be investigated with reverse genetics studies, the results from our work have opened up many intriguing possibilities as to how the early steps of invasion might be achieved. Going forwards, a thorough, systematic approach will be required to address these questions and to gain a more complete understanding of how merozoites commit to host cell entry.

5.2 A balancing act between the RBL and DBP ligands: when plan A doesn't work

Our work has shown that deformation is an important step for invading *P. knowlesi* merozoites. Varying degrees of deformation preceded every invasion observed in this study, and the strongest deformation interactions correlated with invasion success. We also demonstrated that PkNBPXa, but not PkDBPα, is responsible for facilitating this step. Yet, what is the precise purpose of deformation, and more specifically, the role of PkNBPXa? Before re-orientation, merozoites are immobilized on the erythrocyte surface. Therefore, one possibility is that PkNBPXa facilitated deformation forces the merozoite and RBC into closer contact and allows downstream molecular interactions, such as PkDBPα-DARC connections, to occur. These interactions may in turn pin the merozoite in place on the erythrocyte surface. PkNBPXa is a significantly larger ligand (~300kDa) than PkDBPα (~135kDa), and therefore likely projects much further from the merozoite surface than PkDBPα does (Singh et al., 2005; Meyer et al., 2009). Thus, a large ectodomain could make PkNBPXa the ideal facilitator of early merozoite-RBC interactions, and host cell wrapping may help embed the merozoite into the erythrocyte surface so that PkDBPα can reach DARC receptors.

Curiously, *P. knowlesi* merozoites exhibit higher invasion rates in macaque erythrocytes when expressing only one DBP ligand, as opposed to all three (Mohring et al., 2019). This suggests that it may be the RBL ligands rather than the DBPs, which enable *P. knowlesi* merozoites to invade macaque erythrocytes more efficiently than human erythrocytes. This phenomenon could be due to several reasons. Even though recombinant PkNBPXb does not bind to human erythrocytes, recombinant PkNBPXa and PkNBPXb fragments have both been shown to bind to macaque erythrocytes (Meyer et al., 2009; Semenya et al., 2012). Thus *P. knowlesi* merozoites may use both RBL ligands to initiate deformation whilst invading macaque erythrocytes. Practically speaking, this could mean that a greater proportion of merozoite-RBC interactions result in strong deformation, thus increasing the chances of effective DBP-receptor binding and invasion. However, another explanation could be that PkNBPXb binds to its host cell receptor more efficiently than PkNBPXa does, or that each macaque erythrocyte possesses more copies of the PkNBPXb receptor. Either of these two scenarios could also lead to greater levels of host cell wrapping and invasion. Future

studies comparing wild type, PkNBPXa KO, and PkNBPXb KO parasites attempting to invade macaque erythrocytes will help us to address these questions, and to understand whether or not a "better" RBL may speed up the pre-internalisation steps.

Interestingly, although strong deformation also correlates with invasion success for *P. falciparum*, a sizeable proportion of merozoites from some strains is capable of invading host cells with very little, if any deformation at all (Weiss et al., 2015). Could this be because certain *P. falciparum* DBPs bind to their respective host cell receptors more efficiently than the *P. knowlesi* DBPs do? In theory, this would mean that these strains are less reliant on their RBL ligands and deformation, overall. The *P. falciparum* RBL and DBP ligands are hypothesized to overlap functionally because W2mef parasites up-regulate PfRh4 expression when PfEBA-175 is genetically disrupted or when critical sialic acid residues are cleaved from its receptor, glycophorin A (GPA), by pre-treating host cells with neuraminidase (Dolan et al., 1990; Stubbs et al., 2005). Whilst PfRh4 may be functioning equivalently to PfEBA-175, another explanation could be that since the PfEBA-175-GPA pathway is hindered under these conditions, merozoites instead rely on less than optimal DBP-receptor interactions for subsequent steps. Thus, in response to this, merozoites up-regulate another RBL ligand to increase deformation, giving any remaining DBP-receptor interactions a chance to take hold. In support of this theory is evidence from Weiss and colleagues (2015) showing that PfEBA-175 null parasites engage with more erythrocytes overall before committing to invasion and that a greater proportion of these contacts lead to high scoring deformation events. Therefore, the *P. falciparum* DBPs and RBLs may not be functionally equivalent as previously proposed (Weiss et al., 2015). Instead, merozoites may attempt to compensate for weakened DBP interactions with increased deformation, by up-regulating additional RBL ligands.

5.3 Using *P. knowlesi* to investigate non-*falciparum* vaccine candidates

Excitingly, because *P. knowlesi* is a much closer relative to all of the other human infective species than *P. falciparum* is, the adaptation of *P. knowlesi* to growth in human erythrocytes has opened up opportunities to study its shared biology with these species (Pain et al., 2008; Moon et al., 2013). An example that is relevant to vaccine design is *P. knowlesi* and *P. vivax's* shared reliance on the DBP-DARC invasion

pathway (Miller et al., 1975; Miller et al., 1976; Haynes et al., 1988; Barnwell et al., 1989; Wertheimer and Barnwell et al., 1989). PvDBP is currently the lead vaccine candidate for *P. vivax* because antibodies towards this ligand confer protective immunity towards previously infected individuals, and Duffy negative individuals lacking the PvDBP receptor, DARC, are widely resistant to *P. vivax* infections in the first instance (Miller et al., 1976; King et al., 2008; Cole-Tobian et al., 2009; Nicolete et al., 2016).

However, studies assessing the inhibitory properties of anti-PvDBP antibodies purified from animals and human volunteers vaccinated with recombinant PvDBP, have largely relied upon *in vitro* receptor binding assays, without functional growth inhibitory assays (GIA) to validate results across different *P. vivax* strains (Moreno et al., 2008; Payne et al., 2017a; Singh et al., 2018). A follow on study from one of the human vaccination trials (Payne et al., 2017a), overcame this limitation by generating transgenic *P. knowlesi* parasites expressing different variants of PvDBP in place of PkDBPα, which were used as surrogates for corresponding *P. vivax* strains in GIA assays. In this study, Rawlinson *et al.,* (2019) generated a panel of recombinant monoclonal anti-PvDBP antibodies from vaccinated human volunteers (Payne *et al.,* 2017a) and assessed their ability to block recombinant PvDBP-DARC interactions, as well as to inhibit transgenic *P. knowlesi* growth in vitro. Excitingly, both assays identified a single monoclonal antibody (DB9) with strain-transcending inhibitory properties, which targets a conserved region of PvDBP, surprisingly away from its predicted DARC binding site. Additionally, the *P. knowlesi* GIA results also identified two further strain-specific inhibitory antibodies, which were not detected by the protein-protein assay. Importantly, these results were validated with *P. vivax ex-vivo* assays, demonstrating the overall reliability of transgenic *P. knowlesi* GIA assays as well as their increased sensitivity compared to relying on recombinant protein assays alone (Rawlinson et al., 2019).

Going forward, this technique could be used to screen much broader panels of variant *P. knowlesi* PvDBP parasites to further validate DB9's strain transcending potential and to identify other conserved epitopes, which also induce potent inhibitory immune responses (Rawlinson et al., 2019). Additionally, testing these same anti-PvDBP antibody panels across transgenic *P. knowlesi* lines expressing different *PkDBPα* alleles may reveal key target epitopes shared by both PkDBPα and PvDBP variants.

170

Therefore, by doing so it may eventually be possible to target PkDBPα and PvDBP and thus, both *P. knowlesi* and *P. vivax* with a single vaccine.

Furthermore, the results from our work have demonstrated for the very first time, that key *P. knowlesi* RBL and DBL ligands perform highly important, and sequential roles during invasion. Thus targeting both PkDBPα and PkNBPXa together within a single vaccine might be even more effective for preventing *P. knowlesi* infections, than targeting PkDBPα/PvDBP alone, as not just one, but two critical invasion steps would be inhibited. Thus a vaccine including components of PkDBPα/PvDBP, and PkNBPXa might effectively confer protection against two *Plasmodium* species.

It is important to note, however, that the amino acid sequence of PkNBPXa is highly divergent to the *P. vivax* RBL ligands. Furthermore, both of the *P. vivax* orthologs to *PkNBPXa* and *PkNBPXb* (*PvRBP3* and *PvRBP2e*, respectively) are in fact pseudogenes (Meyer et al., 2009; Chan et al., 2019). Therefore, it is less likely that a vaccine targeting PkNBPXa would also inhibit the function of the *P. vivax* RBLs. However, now that we have a conditional PkNBPXa KO background line, it may be possible to use this line to express the PvRBLs in the place of PkNBPXa. By doing so, we could firstly, determine whether any of the PvRBLs can complement the loss of PkNBPXa, and allow PkNBPXa null parasites to grow in either normocytes or reticulocytes. This in itself would be valuable information and could enable us to determine which PvRBPs restrict *P. vivax* growth to reticulocytes, a question, which remains outstanding for all PvRBLs, apart from PvRBP2b, which has recently been shown to bind to transferrin receptor 1 on reticulocytes (Gruszczyk et al., 2018; Chan et al., 2019). Secondly, though, a similar approach to the one applied by Rawlinson et al., (2019) could be used, once a suitable complementary PvRBP has been identified. Thus we could begin to identify PvRBP epitopes, which when presented to the immune system within a vaccine, might stimulate the production of highly potent, invasion-inhibitory antibodies.

Finally, Knuepfer *et al.,* (2019) recently demonstrated that although the non-*falciparum* species do not express a homolog to the leading *P. falciparum* vaccine candidate, PfRh5, all do still likely rely on a divergent PkRIPR-CSS-PTRAMP complex to invade host erythrocytes. Antibodies targeting PkRIPR, in particular, potently inhibit the growth of PkA1-H.1 parasites *in vitro* (Knuepfer et al., 2019).

Therefore, in the future, *P. knowlesi* could potentially be used as a surrogate to express not just *P. vivax* RIPR variants, but also variants from the remaining neglected species, for further study. Additionally, now that we can generate marker-less transgenic lines using CRISPR Cas9 (Mohring et al., 2019), we could potentially express multiple target ligands at once from each species. This would enable us to examine whether antibodies against two or more targets act synergistically, and help us to decide which antigens could be used in multi-subunit vaccines.

5.4 Conclusions

In conclusion, our work has elucidated a clear order to the early, morphological steps of invasion leading up to parasite entry into the host erythrocyte. In particular, we have shown that deformation, facilitated by PkNBPXa, is a distinct step to re-orientation. We also highlight the importance of the parasite's acto-myosin motor, showing that extra-cellular motility, although perhaps previously under-appreciated, potentially underpins almost every morphological step of invasion. While further work is required to identify the precise role of PkDBPα, we now know that this ligand likely functions downstream of PkNBPXa, confirming our hypothesis that the PkRBL and PkDBP ligands perform separate roles during invasion. This finding has important implications, especially when considering vaccine designs. In recent years, the *P. falciparum* RBL and DBP ligands (aside from PfRh5) have been largely abandoned as vaccine candidates, since these families show frustrating levels of redundancy between family members. Targeting one *P. falciparum* RBL/DBL invasion pathway simply gives rise to another (Beeson et al., 2016; Duffy and Patrick Gorres, 2020). However, our findings demonstrate that this is definitely not the case for *P. knowlesi* and that excitingly, these results may be representative of other *Plasmodium* species too. For instance, given that none of the 5 PvRBL ligands can compensate for inhibition of PvDBP (Miller et al., 1976; Chan et al., 2020), this suggests that like PkNBPXa, the PvRBLs may also be facilitating a separate step to PvDBP. Thus, as for *P. knowlesi*, targeting a critical PvRBL ligand along with PvDBP may be the key to developing an efficacious *P. vivax* vaccine.

Additionally, the parasite lines generated from this study, including the DiCre background lines, tagged lines, and most importantly, the conditional PkNBPXa KO line will be invaluable for future work. We now have the tools to complement the

inducible PkNBPXa KO line with RBL constructs from different species. Future work will also focus on phenotyping the PkNBPXa KO lines that express additional fluorescently labelled invasion ligands, to investigate the fates of these proteins when PkNBPXa is absent. Ultimately, as this study has shown, the combined use of our marker-less, CRISPR cas9 system (Mohring et al., 2019), with the DiCre system (Andenmatten et al., 2013; Collins et al., 2013; Knuepfer et al., 2019) means that we have the potential to rapidly build parasite libraries, which enable us to examine dynamic processes in great detail using live microscopy. In our hands, the DiCre system is certainly not perfect, so far, and further efforts will be required to investigate why, for instance, we only achieved very low excision levels for the conditional PkDBPα KO line. However, we now have no shortage of potential target genes, which could be used to investigate whether these issues are commonplace, or not; and of course, if targeting these genes is successful, the resulting lines could also be used to address a whole range of biological questions. Excitingly, the results from this study demonstrated that phenotyping *P. knowlesi* lines using live microscopy can give very clear answers to questions that are otherwise challenging to address using *P. falciparum*. Overall, then, using *P. knowlesi* to continue to systematically explore the roles of additional invasion ligands has the potential to greatly expand our understanding of invasion biology, and aid our continued search for vaccine targets.

Bibliography

Adams, J.H., Hudson, D.E., Torii, M., Ward, G.E., Wellems, T.E., Aikawa, M., Miller, L.H., 1990. The Duffy receptor family of *Plasmodium knowlesi* is located within the micronemes of invasive malaria merozoites. Cell 63, 141–153.

Adams, J.H., Kim, B., Simt, L., Dolan, S.A., Fang, X., Kaslow, D.C., Miller, L.H., 1992. A family of erythrocyte binding proteins of malaria parasites. Microbiology 89, 7085–7089.

Adams, J.H., Mueller, I., 2017. The biology of *Plasmodium vivax*. Cold Spring Harb. Perspect. Med. 7, 1–12.

Aikawa, M., 1967. Ultrastructure of the pellicular complex of *Plasmodium fallax*. J. Cell Biol. 35, 103–113.

Aikawa, M., 1966. The fine structure of the erythrocytic stages of three avian malarial parasites, *Plasmodium fallax*, *P. lophurae*, and *P. cathemerium*. Am. J. Trop. Med. Hyg. 15, 449–471.

Aikawa, M., Miller, L.H., Johnson, J., Rabbege, J., 1978. Erythrocyte entry by malarial parasites. A moving junction between erythrocyte and parasite. J. Cell Biol. 77, 72–82.

Alanine, D.G.W., Quinkert, D., Kumarasingha, R., Mehmood, S., Donnellan, F.R., Minkah, N.K., Dadonaite, B., Diouf, A., Galaway, F., Silk, S.E., Jamwal, A., Marshall, J.M., Miura, K., Foquet, L., Elias, S.C., Labbé, G.M., Douglas, A.D., Jin, J., Payne, R.O., Illingworth, J.J., Pattinson, D.J., Pulido, D., Williams, B.G., de Jongh, W.A., Wright, G.J., Kappe, S.H.I., Robinson, C. V., Long, C.A., Crabb, B.S., Gilson, P.R., Higgins, M.K., Draper, S.J., 2019. Human Antibodies that Slow Erythrocyte Invasion Potentiate Malaria-Neutralizing Antibodies. Cell 178, 216-228.e21.

Alexander, D.L., Arastu-Kapur, S., Dubremetz, J.F., Boothroyd, J.C., 2006. Plasmodium falciparum AMA1 binds a rhoptry neck protein homologous to TgRON4, a component of the moving junction in *Toxoplasma gondii*. Eukaryot. Cell 5, 1169–1173.

Amino, R., Thiberge, S., Martin, B., Celli, S., Shorte, S., Frischknecht, F., Ménard, R., 2006. Quantitative imaging of *Plasmodium* transmission from mosquito to mammal. Nat. Med. 12, 220–224.

Andenmatten, N., Egarter, S., Jackson, A.J., Jullien, N., Herman, J.P., Meissner, M., 2013. Conditional genome engineering in *Toxoplasma gondii* uncovers alternative invasion mechanisms. Nat. Methods 10, 125–127.

Angrisano, F., Riglar, D.T., Sturm, A., Volz, J.C., Delves, M.J., Zuccala, E.S., Turnbull, L., Dekiwadia, C., Olshina, M.A., Marapana, D.S., Wong, W., Mollard, V., Bradin, C.H., Tonkin, C.J., Gunning, P.W., Ralph, S.A., Whitchurch, C.B., Sinden, R.E., Cowman, A.F., McFadden, G.I., Baum, J., 2012. Spatial localisation of actin filaments across developmental stages of the malaria parasite. PLoS One 7(2):e32188

Arredondo, S.A., Swearingen, K.E., Martinson, T., Steel, R., Dankwa, D.A., Harupa, A., Camargo, N., Betz, W., Vigdorovich, V., Oliver, B.G., Kangwanrangsan, N., Ishino, T., Sather, N., Mikolajczak, S., Vaughan, A.M., Torii, M., Moritz, R.L., Kappe, S.H.I., 2018. The Micronemal Plasmodium Proteins P36 and P52 Act in Concert to Establish the Replication-Permissive Compartment Within Infected Hepatocytes. Front. Cell. Infect. Microbiol. 8, 413.

Asada, M., Goto, Y., Yahata, K., Yokoyama, N., Kawai, S., Inoue, N., Kaneko, O., Kawazu, S. ichiro, 2012. Gliding motility of babesia bovis merozoites visualized by time-lapse video microscopy. PLoS One 7(4):e35227.

Ashley, E.A., Dhorda, M., Fairhurst, R.M., Amaratunga, C., Lim, P., Suon, S., Sreng, S., Anderson, J.M., Mao, S., Sam, B., Sopha, C., Chuor, C.M., Nguon, C., Sovannaroth, S., Pukrittayakamee, S., Jittamala, P., Chotivanich, K., Chutasmit, K., Suchatsoonthorn, C., Runcharoen, R., Hien, T.T., Thuy-Nhien, N.T., Thanh, N. V., Phu, N.H., Htut, Y., Han, K.T., Aye, K.H., Mokuolu, O.A., Olaosebikan, R.R., Folaranmi, O.O., Mayxay, M., Khanthavong, M., Hongvanthong, B., Newton, P.N., Onyamboko, M.A., Fanello, C.I., Tshefu, A.K., Mishra, N., Valecha, N., Phyo, A.P., Nosten, F., Yi, P., Tripura, R., Borrmann, S., Bashraheil, M., Peshu, J., Faiz, M.A., Ghose, A., Hossain, M.A., Samad, R., Rahman, M.R., Hasan, M.M., Islam, A., Miotto, O., Amato, R., MacInnis, B., Stalker, J.,

Kwiatkowski, D.P., Bozdech, Z., Jeeyapant, A., Cheah, P.Y., Sakulthaew, T., Chalk, J., Intharabut, B., Silamut, K., Lee, S.J., Vihokhern, B., Kunasol, C., Imwong, M., Tarning, J., Taylor, W.J., Yeung, S., Woodrow, C.J., Flegg, J.A., Das, D., Smith, J., Venkatesan, M., Plowe, C. V., Stepniewska, K., Guerin, P.J., Dondorp, A.M., Day, N.P., White, N.J., 2014. Spread of artemisinin resistance in Plasmodium falciparum malaria. N. Engl. J. Med. 371, 411–423.

Baer, K., Klotz, C., Kappe, S.H.I., Schnieder, T., Frevert, U., 2007. Release of hepatic Plasmodium yoelii merozoites into the pulmonary microvasculature. PLoS Pathog. 3, 1651–1668.

Baker, R.P., Wijetilaka, R., Urban, S., 2006. Two *Plasmodium* rhomboid proteases preferentially cleave different adhesins implicated in all invasive stages of malaria. PLoS Pathog. 2, 0922–0932.

Baldwin, M.R., Li, X., Hanada, T., Liu, S.C., Chishti, A.H., 2015. Merozoite surface protein 1 recognition of host glycophorin a mediates malaria parasite invasion of red blood cells. Blood 125, 2704–2711.

Bannister, L. H., Butcher, G.A., Dennis, E.D., Mitchell, G.H., 1975. Structure and invasive behaviour of *Plasmodium knowlesi* merozoites *in vitro*. Parasitology 71, 483–491.

Bannister, L H, Butcher, G.A., Dennis, E.D., Mitchell, G.H., 1975. Structure and invasive behaviour of Plasmodium knowlesi merozoites in vitro. Parasitology 71, 483–491.

Bannister, L.H., Hopkins, J.M., Dluzewski, A.R., Margos, G., Williams, I.T., Blackman, M.J., Kocken, C.H., Thomas, A.W., Mitchell, G.H., 2003. Plasmodium falciparum apical membrane antigen 1 (PfAMA-1) is translocated within micronemes along subpellicular microtubules during merozoite development. J. Cell Sci. 116, 3825–3834.

Bannister, L.H., Hopkins, J.M., Fowler, R.E., Krishna, S., Mitchell, G.H., 2000. A brief illustrated guide to the ultrastructure of *Plasmodium falciparum* asexual blood stages. Parasitol. Today 16, 427–433.

Bannister, L.H., Mitchell, G.H., 1995. The role of the cytoskeleton in *Plasmodium*

falciparum merozoite biology: an electron-microscopic view. Ann. Trop. Med. Parasitol. 89, 105–111.

Bannister, L.H., Mitchell, G.H., Butcher, G.A., Dennis, E.D., Cohen, S., 1986. Structure and development of the surface coat of erythrocytic merozoites of *Plasmodium knowlesi*. Cell Tissue Res. 245, 281–290.

Barber, B.E., William, T., Dhararaj, P., Anderios, F., Grigg, M.J., Yeo, T.W., Anstey, N.M., 2012. Epidemiology of *Plasmodium knowlesi* malaria in north-east Sabah, Malaysia: Family clusters and wide age distribution. Malar. J. 11, 1.

Bargieri, D.Y., Thiberge, S., Tay, C.L., Carey, A.F., Rantz, A., Hischen, F., Lorthiois, A., Straschil, U., Singh, P., Singh, S., Triglia, T., Tsuboi, T., Cowman, A., Chitnis, C., Alano, P., Baum, J., Pradel, G., Lavazec, C., Ménard, R., 2016. *Plasmodium Merozoite* TRAP Family Protein Is Essential for Vacuole Membrane Disruption and Gamete Egress from Erythrocytes. Cell Host Microbe 20, 618–630.

Baro, B., Deroost, K., Raiol, T., Brito, M., Almeida, A.C.G., de Menezes-Neto, A., Figueiredo, E.F.G., Alencar, A., Leitão, R., Val, F., Monteiro, W., Oliveira, A., Armengol, M. del P., Fernández-Becerra, C., Lacerda, M. V., del Portillo, H.A., 2017. *Plasmodium vivax* gametocytes in the bone marrow of an acute malaria patient and changes in the erythroid miRNA profile. PLoS Negl. Trop. Dis. 11, 6–13.

Baum, J., Chen, L., Healer, J., Lopaticki, S., Boyle, M., Triglia, T., Ehlgen, F., Ralph, S.A., Beeson, J.G., Cowman, A.F., 2009. Reticulocyte-binding protein homologue 5 - An essential adhesin involved in invasion of human erythrocytes by *Plasmodium falciparum*. Int. J. Parasitol. 39, 371–380.

Baum, J., Richard, D., Healer, J., Rug, M., Krnajski, Z., Gilberger, T.W., Green, J.L., Holder, A.A., Cowman, A.F., 2006. A conserved molecular motor drives cell invasion and gliding motility across malaria life cycle stages and other apicomplexan parasites. J. Biol. Chem. 281, 5197–5208.

Beeson, J.G., Drew, D.R., Boyle, M.J., Feng, G., Fowkes, F.J.I., Richards, J.S., 2016. Merozoite surface proteins in red blood cell invasion, immunity and vaccines

against malaria. FEMS Microbiol. Rev. 40, 343–372.

Beeson, J.G., Kurtovic, L., Dobaño, C., Opi, D.H., Chan, J.A., Feng, G., Good, M.F., Reiling, L., Boyle, M.J., 2019. Challenges and strategies for developing efficacious and long-lasting malaria vaccines. Sci. Transl. Med. 11.

Bennink, S., Kiesow, M.J., Pradel, G., 2016. The development of malaria parasites in the mosquito midgut. Cell. Microbiol. 18, 905–918.

Bichet, M., Joly, C., Hadj Henni, A., Guilbert, T., Xémard, M., Tafani, V., Lagal, V., Charras, G., Tardieux, I., 2014. The *toxoplasma*-host cell junction is anchored to the cell cortex to sustain parasite invasive force. BMC Biol. 12.

Bichet, M., Touquet, B., Gonzalez, V., Florent, I., Meissner, M., Tardieux, I., 2016. Genetic impairment of parasite myosin motors uncovers the contribution of host cell membrane dynamics to *Toxoplasma* invasion forces. BMC Biol. 14.

Billker, O., Shaw, M.K., Margos, G., Sinden, R.E., 1997. The roles of temperature, pH and mosquito factors as triggers of male and female gametogenesis of *Plasmodium berghei* in vitro. Parasitology 115, 1–7.

Boonyalai, N., Collins, C.R., Hackett, F., Withers-Martinez, C., Blackman, M.J., 2018. Essentiality of *Plasmodium falciparum* plasmepsin V. PLoS One 13, 1–15.

Boyle, M.J., Richards, J.S., Gilson, P.R., Chai, W., Beeson, J.G., 2010a. Interactions with heparin-like molecules during erythrocyte invasion by *Plasmodium falciparum* merozoites. Blood 115, 4559–4568.

Boyle, M.J., Wilson, D.W., Richards, J.S., Riglar, D.T., Tetteh, K.K.A., Conway, D.J., Ralph, S.A., Baum, J., Beeson, J.G., 2010b. Isolation of viable *Plasmodium falciparum* merozoites to define erythrocyte invasion events and advance vaccine and drug development. Proc. Natl. Acad. Sci. 107, 14378–14383.

Brant, H.L., Ewers, R.M., Vythilingam, I., Drakeley, C., Benedick, S., Mumford, J.D., 2016. Vertical stratification of adult mosquitoes (Diptera: Culicidae) within a tropical rainforest in Sabah, Malaysia. Malar. J. 15, 1–9.

Brock, P.M., Fornace, K.M., Grigg, M.J., Anstey, N.M., William, T., Cox, J., Drakeley, C.J., Ferguson, H.M., Kao, R.R., 2019. Predictive analysis across

spatial scales links zoonotic malaria to deforestation. Proc. R. Soc. B Biol. Sci. 286.

Burns, A.L., Dans, M.G., Balbin, J.M., De Koning-Ward, T.F., Gilson, P.R., Beeson, J.G., Boyle, M.J., Wilson, D.W., 2019. Targeting malaria parasite invasion of red blood cells as an antimalarial strategy. FEMS Microbiol. Rev. 43, 223–238.

Butcher, G.A., 1979. Factors affecting the in vitro culture of *Plasmodium falciparum* and *Plasmodium knowlesi*. Bull. World Health Organ. 57, 17–26.

Camus, D., Hadley, T.J., 1985. A Plasmodium falciparum antigen that binds to host erythrocytes and merozoites. Science (80). 230, 553–556.

Canning, E.U., Sinden, R.E., 1973. The organization of the ookinete and observations on nuclear division in oocysts of *Plasmodium berghei*. Parasitology 67, 29–40.

Cao, J., Kaneko, O., Thongkukiatkul, A., Tachibana, M., Otsuki, H., Gao, Q., Tsuboi, T., Torii, M., 2009. Rhoptry neck protein RON2 forms a complex with microneme protein AMA1 in *Plasmodium falciparum* merozoites. Parasitol. Int. 58, 29–35.

Carlton, J.M., Adams, J.H., Silva, J.C., Bidwell, S.L., Lorenzi, H., Caler, E., Crabtree, J., Angiuoli, S. V., Merino, E.F., Amedeo, P., Cheng, Q., Coulson, R.M.R., Crabb, B.S., Del Portillo, H.A., Essien, K., Feldblyum, T. V., Fernandez-Becerra, C., Gilson, P.R., Gueye, A.H., Guo, X., Kang'A, S., Kooij, T.W.A., Korsinczky, M., Meyer, E.V.S., Nene, V., Paulsen, I., White, O., Ralph, S.A., Ren, Q., Sargeant, T.J., Salzberg, S.L., Stoeckert, C.J., Sullivan, S.A., Yamamoto, M.M., Hoffman, S.L., Wortman, J.R., Gardner, M.J., Galinski, M.R., Barnwell, J.W., Fraser-Liggett, C.M., 2008. Comparative genomics of the neglected human malaria parasite *Plasmodium vivax*. Nature 455, 757–763.

Cavasini, C.E., De Mattos, L.C., Couto, Á.A.R.D.A., Couto, V.S.C.D.A., Gollino, Y., Moretti, L.J., Bonini-Domingos, C.R., Rossit, A.R.B., Castilho, L., Machado, R.L.D., 2007. Duffy blood group gene polymorphisms among malaria *vivax* patients in four areas of the Brazilian Amazon region. Malar. J. 6, 1–8.

CDC, 2020. *CDC - Malaria - Malaria Worldwide - Impact Of Malaria*. [online] Available at: https://www.cdc.gov/malaria/malaria_worldwide/impact.html

[Accessed 16 October 2020].

Chan, L.J., Dietrich, M.H., Nguitragool, W., Tham, W.H., 2020. *Plasmodium vivax* Reticulocyte Binding Proteins for invasion into reticulocytes. Cell. Microbiol. 22, 1–11.

Chan, L.J., Dietrich, M.H., Nguitragool, W., Tham, W.H., 2019. *Plasmodium vivax* Reticulocyte Binding Proteins for invasion into reticulocytes. Cell. Microbiol. 22, 1–11.

Chen, L., Lopaticki, S., Riglar, D.T., Dekiwadia, C., Uboldi, A.D., Tham, W.H., O'Neill, M.T., Richard, D., Baum, J., Ralph, S.A., Cowman, A.F., 2011. An egf-like protein forms a complex with pfrh5 and is required for invasion of human erythrocytes by *Plasmodium falciparum*. PLoS Pathog. 7.

Cohen, S., McGregor, I.A., Carington, S., 1961. Gamma-Globulin and Acquired Immunity to Human Malaria. Nature 192, 733–737.

Cole-Tobian, J.L., Michon, P., Biasor, M., Richards, J.S., Beeson, J.G., Mueller, I., King, C.L., 2009. Strain-specific Duffy binding protein antibodies correlate with protection against infection with homologous compared to heterologous *Plasmodium vivax* strains in Papua New Guinean children. Infect. Immun. 77, 4009–4017.

Collins, C.R., Das, S., Wong, E.H., Andenmatten, N., Stallmach, R., Hackett, F., Herman, J.P., Müller, S., Meissner, M., Blackman, M.J., 2013. Robust inducible Cre recombinase activity in the human malaria parasite *Plasmodium falciparum* enables efficient gene deletion within a single asexual erythrocytic growth cycle. Mol. Microbiol. 88, 687–701.

Collins, C.R., Hackett, F., Howell, S.A., Snijders, A.P.L., Russell, M.R.G., Collinson, L.M., Blackman, M.J., 2020. The malaria parasite sheddase SUB2 governs host red blood cell membrane sealing at invasion 3. bioRxiv 1–47.

Cooper, D.J., Rajahram, G.S., William, T., Jelip, J., Mohammad, R., Benedict, J., Alaza, D.A., Malacova, E., Yeo, T.W., Grigg, M.J., Anstey, N.M., Barber, B.E., 2020. Plasmodium knowlesi Malaria in Sabah, Malaysia, 2015-2017: Ongoing Increase in Incidence Despite Near-elimination of the Human-only *Plasmodium*

Species. Clin. Infect. Dis. 70, 361–367.

Cowman, A.F., Berry, D., Baum, J., 2012. The cellular and molecular basis for malaria parasite invasion of the human red blood cell. J. Cell Biol. 198, 961–971.

Cowman, A.F., Crabb, B.S., 2006. Invasion of red blood cells by malaria parasites. Cell 124, 755–766.

Cowman, A.F., Tonkin, C.J., Tham, W.H., Duraisingh, M.T., 2017. The Molecular Basis of Erythrocyte Invasion by Malaria Parasites. Cell Host Microbe 22, 232–245.

Cox Singh, J., Davis, T.M.E., Lee, K.S., Shamsul, S.S.G., Matusop, A., Ratnam, S., Rahman, H.A., Conway, D.J., Singh, B., 2008. Plasmodium knowlesiMalaria in Humans Is Widely Distributed and Potentially Life Threatening. Clin. Infect. Dis. 46, 165–171.

Crosnier, C., Bustamante, L.Y., Bartholdson, S.J., Bei, A.K., Theron, M., Uchikawa, M., Mboup, S., Ndir, O., Kwiatkowski, D.P., Duraisingh, M.T., Rayner, J.C., Wright, G.J., 2011. Basigin is a receptor essential for erythrocyte invasion by Plasmodium falciparum. Nature 480, 534–537.

Dankwa, S., Lim, C., Bei, A.K., Jiang, R.H.Y., Abshire, J.R., Patel, S.D., Goldberg, J.M., Moreno, Y., Kono, M., Niles, J.C., Duraisingh, M.T., 2016. Ancient human sialic acid variant restricts an emerging zoonotic malaria parasite. Nat. Commun. 7, 11187.

Das, S., Hertrich, N., Perrin, A.J., Withers-Martinez, C., Collins, C.R., Jones, M.L., Watermeyer, J.M., Fobes, E.T., Martin, S.R., Saibil, H.R., Wright, G.J., Treeck, M., Epp, C., Blackman, M.J., 2015. Processing of *Plasmodium falciparum* Merozoite Surface Protein MSP1 Activates a Spectrin-Binding Function Enabling Parasite Egress from RBCs. Cell Host Microbe 18, 433–444.

Das, S., Lemgruber, L., Tay, C.L., Baum, J., Meissner, M., 2017. Multiple essential functions of Plasmodium falciparum actin-1 during malaria blood-stage development. BMC Biol. 15, 1–16.

Dasgupta, S., Auth, T., Gov, N.S., Satchwell, T.J., Hanssen, E., Zuccala, E.S., Riglar,

D.T., Toye, A.M., Betz, T., Baum, J., Gompper, G., 2014. Membrane-wrapping contributions to malaria parasite invasion of the human erythrocyte. Biophys. J. 107, 43–54.

De Niz, M., Meibalan, E., Mejia, P., Ma, S., Brancucci, N.M.B., Agop-Nersesian, C., Mandt, R., Ngotho, P., Hughes, K.R., Waters, A.P., Huttenhower, C., Mitchell, J.R., Martinelli, R., Frischknecht, F., Seydel, K.B., Taylor, T., Milner, D., Heussler, V.T., Marti, M., 2018. *Plasmodium* gametocytes display homing and vascular transmigration in the host bone marrow. Sci. Adv. 4, 1–16.

Dechavanne, C., Dechavanne, S., Metral, S., Roeper, B., Krishnan, S., Fong, R., Bennett, S., Carias, L., Chen, E., Salinas, N.D., Ghosh, A., Tolia, N.H., Woost, P.G., Jacobberger, J.W., Colin, Y., Gamain, B., King, C.L., Zimmerman, P.A., 2018. Duffy Antigen Expression in Erythroid Bone Marrow Precursor Cells of Genotypically Duffy Negative Individuals. bioRxiv 508481.

Dembélé, L., Franetich, J.F., Lorthiois, A., Gego, A., Zeeman, A.M., Kocken, C.H.M., Le Grand, R., Dereuddre-Bosquet, N., Van Gemert, G.J., Sauerwein, R., Vaillant, J.C., Hannoun, L., Fuchter, M.J., Diagana, T.T., Malmquist, N.A., Scherf, A., Snounou, G., Mazier, D., 2014. Persistence and activation of malaria hypnozoites in long-term primary hepatocyte cultures. Nat. Med. 20, 307–

Dennis, E.D., Mitchell, G.H., Butcher, G.A., Cohen, S., 1975. In vitro isolation of Plasmodium knowlesi merozoites using polyearbonate sieves. Parasitology 71, 475–481.

DeSimone, T.M., Jennings, C. V, Bei, A.K., Comeaux, C., Coleman, B.I., Refour, P., Triglia, T., Stubbs, J., Cowman, A.F., Duraisingh, M.T., 2009. Cooperativity between *Plasmodium falciparum* adhesive proteins for invasion into erythrocytes. Mol. Microbiol. 72, 578–589.

Dessens, J.T., Beetsma, A.L., Dimopoulos, G., Wengelnik, K., Crisanti, A., Kafatos, F.C., Sinden, R.E., 1999. CTRP is essential for mosquito infection by malaria ookinetes. EMBO J. 18, 6221–6227.

Diaz, S.A., Martin, S.R., Howell, S.A., Grainger, M., Moon, R.W., Green, J.L., Holder, A.A., 2016. The binding of *plasmodium falciparum* adhesins and

erythrocyte invasion proteins to aldolase is enhanced by phosphorylation. PLoS One 11, 1–20.

Dobrowolski, J.M., Carruthers, V.B., Sibley, L.D., 1997. Participation of myosin in gliding motility and host cell invasion by *Toxoplasma gondii.* Mol. Microbiol. 26, 163–173.

Dolan, S.A., Miller, L.H., Wellems, T.E., 1990. Evidence for a switching mechanism in the invasion of erythrocytes by *Plasmodium falciparum*. J. Clin. Invest. 86, 618–624.

Douglas, A.D., Williams, A.R., Illingworth, J.J., Kamuyu, G., Biswas, S., Goodman, A.L., Wyllie, D.H., Crosnier, C., Miura, K., Wright, G.J., Long, C.A., Osier, F.H., Marsh, K., Turner, A. V., Hill, A.V.S., Draper, S.J., 2011. The blood-stage malaria antigen PfRH5 is susceptible to vaccine-inducible cross-strain neutralizing antibody. Nat. Commun. 2.

Draper, S.J., Sack, B.K., King, C.R., Nielsen, C.M., Rayner, J.C., Higgins, M.K., Long, C.A., Seder, R.A., 2018. Malaria Vaccines: Recent Advances and New Horizons. Cell Host Microbe 24, 43–56.

Duffy, P.E., Patrick Gorres, J., 2020. Malaria vaccines since 2000: progress, priorities, products. npj Vaccines 5, 1–9.

Duraisingh, Manoj T, Maier, A.G., Triglia, T., Cowman, A.F., 2003. Erythrocyte-binding antigen 175 mediates invasion in *Plasmodium falciparum* utilizing sialic acid-dependent and -independent pathways. Proc. Natl. Acad. Sci. U. S. A. 100, 4796–801.

Duraisingh, Manoj T., Triglia, T., Ralph, S.A., Rayner, J.C., Barnwell, J.W., McFadden, G.I., Cowman, A.F., 2003a. Phenotypic variation of *Plasmodium falciparum* merozoite proteins directs receptor targeting for invasion of human erythrocytes. EMBO J. 22, 1047–1057.

Duraisingh, Manoj T., Triglia, T., Ralph, S.A., Rayner, J.C., Barnwell, J.W., McFadden, G.I., Cowman, A.F., 2003b. Phenotypic variation of *Plasmodium falciparum* merozoite proteins directs receptor targeting for invasion of human erythrocytes. EMBO J. 22, 1047–1057.

Dvorak, J.A., Miller, L.H., Whitehouse, W.C., Shiroishi, T., 1975. Invasion of erythrocytes by malaria merozoites. Science (80). 187, 748–750.

Ecker, A., Moon, R., Sinden, R.E., Billker, O., 2006. Generation of gene targeting constructs for *Plasmodium berghei* by a PCR-based method amenable to high throughput applications. Mol. Biochem. Parasitol. 145, 265–268.

Egarter, S., Andenmatten, N., Jackson, A.J., Whitelaw, J.A., Pall, G., Black, J.A., Ferguson, D.J.P., Tardieux, I., Mogilner, A., Meissner, M., 2014. The *toxoplasma* acto-myoA motor complex is important but not essential for gliding motility and host cell invasion. PLoS One 9(3): e91819.

Fang, X., Kaslow, D.C., Adams, J.H., Miller, L.H., 1991. Cloning of the *Plasmodium vivax* Duffy receptor. Mol. Biochem. Parasitol. 44, 125–132.

Favuzza, P., de Lera Ruiz, M., Thompson, J.K., Mccauley, J.A., Olsen, D.B., Cowman, A.F., Triglia, T., Ngo, A., Steel, R.W.J., Vavrek, M., Christensen, J., Healer, J., Boyce, C., Guo, Z., Hu, M., Khan, T., Murgolo, N., Zhao, L., Penington, J.S., Reaksudsan, K., Jarman, K., Dietrich, M.H., Richardson, L., Guo, K.-Y., Lopaticki, S., Tham, W.-H., Rottmann, M., Papenfuss, T., Robbins, J.A., Boddey, J.A., Sleebs, B.E., Lè Ne, H., Sabroux, J., 2020. Dual Plasmepsin-Targeting Antimalarial Agents Disrupt Multiple Stages of the Malaria Parasite Life Cycle. Cell Host Microbe 27, 642–658.

Fornace, K., Abidin, T.R., Alexander, N., Brock, P., Grigg, M., Murphy, A., William, T., Menon, J., Drakeley, C., Cox, J., 2016. Association between Landscape Factors and Spatial Patterns of *Plasmodium knowlesi* Infections in Sabah, Malaysia. Emerg. Infect. Dis. J. 22, 201.

Frénal, K., Dubremetz, J.F., Lebrun, M., Soldati-Favre, D., 2017. Gliding motility powers invasion and egress in Apicomplexa. Nat. Rev. Microbiol. 15, 645–660.

Galatas, B., Bassat, Q., Mayor, A., 2016. Malaria Parasites in the Asymptomatic: Looking for the Hay in the Haystack. Trends Parasitol. 32, 296–308.

Galinski, M.R., Medina, C.C., Ingravallo, P., Barnwell, J.W., 1992. A reticulocyte-binding protein complex of *plasmodium vivax* merozoites. Cell 69, 1213–1226.

Garcia, G.E., Wirtz, R.A., Barr, J.R., Woolfitt, A., Rosenbergt, R., 1998. Xanthurenic acid induces gametogenesis in *Plasmodium*, the malaria parasite. J. Biol. Chem. 273, 12003–12005.

Gaur, D., Furuya, T., Mu, J., Jiang, L. Bin, Su, X.Z., Miller, L.H., 2006. Upregulation of expression of the reticulocyte homology gene 4 in the *Plasmodium falciparum* clone Dd2 is associated with a switch in the erythrocyte invasion pathway. Mol. Biochem. Parasitol. 145, 205–215.

Ghosh, S., Kennedy, K., Sanders, P., Matthews, K., Ralph, S.A., Counihan, N.A., de Koning-Ward, T.F., 2017. The *Plasmodium* rhoptry associated protein complex is important for parasitophorous vacuole membrane structure and intraerythrocytic parasite growth. Cell. Microbiol. 19, 1–16.

Gilberger, T., Thompson, J.K., Triglia, T., Good, R.T., Duraisingh, M.T., Cowman, A.F., 2003. A Novel Erythrocyte Binding Antigen-175 Paralogue from *Plasmodium falciparum* Defines a New Trypsin-resistant Receptor on Human Erythrocytes. J. Biol. Chem. 278, 14480–14486.

Gilson, P.R., Crabb, B.S., 2009. Morphology and kinetics of the three distinct phases of red blood cell invasion by *Plasmodium falciparum* merozoites. Int. J. Parasitol. 39, 91–96.

Glushakova, S., Yin, D., Li, T., Zimmerberg, J., 2005. Membrane transformation during malaria parasite release from human red blood cells. Curr. Biol. 15, 1645–1650.

Goel, V.K., Li, X., Chen, H., Liu, S.C., Chisti, A.H., Oh, S.S., 2003. Band 3 is a host receptor binding merozoite surface protein 1 during the *Plasmodium falciparum* invasion of erythrocytes. Proc. Natl. Acad. Sci. U. S. A. 100, 5164–5169.

Gras, S., Jimenez-Ruiz, E., Klinger, C.M., Schneider, K., Klingl, A., Lemgruber, L., Meissner, M., 2019. An endocytic-secretory cycle participates in *Toxoplasma gondii* in motility. PLoS Biol.17(6):e3000060.

Green, J.L., Hinds, L., Grainger, M., Knuepfer, E., Holder, A.A., 2006. *Plasmodium* thrombospondin related apical merozoite protein (PTRAMP) is shed from the surface of merozoites by PfSUB2 upon invasion of erythrocytes. Mol. Biochem.

Parasitol. 150, 114–117.

Grigg, M.J., Cox, J., William, T., Jelip, J., Fornace, K.M., Brock, P.M., von Seidlein, L., Barber, B.E., Anstey, N.M., Yeo, T.W., Drakeley, C.J., 2017. Individual-level factors associated with the risk of acquiring human *Plasmodium knowlesi* malaria in Malaysia: a case-control study. Lancet Planet. Heal. 1, e97–e104.

Grüring, C., Moon, R.W., Lim, C., Holder, A.A., Blackman, M.J., Duraisingh, M.T., 2014. Human red blood cell-adapted *Plasmodium knowlesi* parasites: a new model system for malaria research. Cell. Microbiol. 16, 612–620.

Gruszczyk, J., Kanjee, U., Chan, L.J., Menant, S., Malleret, B., Lim, N.T.Y., Schmidt, C.Q., Mok, Y.F., Lin, K.M., Pearson, R.D., Rangel, G., Smith, B.J., Call, M.J., Weekes, M.P., Griffin, M.D.W., Murphy, J.M., Abraham, J., Sriprawat, K., Menezes, M.J., Ferreira, M.U., Russell, B., Renia, L., Duraisingh, M.T., Tham, W.H., 2018. Transferrin receptor 1 is a reticulocyte-specific receptor for *Plasmodium vivax*. Science (80-). 359, 48–55.

Gunalan, K., Gao, X., Liew, K.J.L., Preiser, P.R., 2011. Differences in erythrocyte receptor specificity of different parts of the *Plasmodium falciparum* reticulocyte binding protein homologue. Infect. Immun. 79, 3421–3430.

Gunalan, K., Gao, X., Yap, S.S.L., Huang, X., Preiser, P.R., 2013. The role of the reticulocyte-binding-like protein homologues of *Plasmodium* in erythrocyte sensing and invasion. Cell. Microbiol. 15, 35–44.

Gunalan, K., Gao, X., Yap, S.S.L., Lai, S.K., Ravasio, A., Ganesan, S., Li, H.Y., Preiser, P.R., 2020. A processing product of the *Plasmodium falciparum* reticulocyte binding protein RH1 shows a close association with AMA1 during junction formation. Cell. Microbiol. 22.

Håkansson, S., Morisaki, H., Heuser, J., Sibley, L.D., 1999. Time-lapse video microscopy of gliding motility in *Toxoplasma gondii* reveals a novel, biphasic mechanism of cell locomotion. Mol. Biol. Cell 10, 3539–3547.

Hale, V.L., Watermeyer, J.M., Hackett, F., Vizcay-Barrena, G., van Ooij, C., Thomas, J.A., Spink, M.C., Harkiolaki, M., Duke, E., Fleck, R.A., Blackman, M.J., Saibil, H.R., 2017. Parasitophorous vacuole poration precedes its rupture and rapid host

erythrocyte cytoskeleton collapse in *Plasmodium falciparum* egress. Proc. Natl. Acad. Sci. 114, 3439–3444.

Han, J.H., Lee, S.K., Wang, B., Muh, F., Nyunt, M.H., Na, S., Ha, K.S., Hong, S.H., Park, W.S., Sattabongkot, J., Tsuboi, T., Han, E.T., 2016. Identification of a reticulocyte-specific binding domain of *Plasmodium vivax* reticulocyte-binding protein 1 that is homologous to the PfRh4 erythrocyte-binding domain. Sci. Rep. 6, 1–12.

Hans, N., Singh, S., Pandey, A.K., Reddy, K.S., Gaur, D., Chauhan, V.S., 2013. Identification and Characterization of a Novel *Plasmodium falciparum* Adhesin Involved in Erythrocyte Invasion. PLoS One 8, 1–16.

Hanssen, E., Dekiwadia, C., Riglar, D.T., Rug, M., Lemgruber, L., Cowman, A.F., Cyrklaff, M., Kudryashev, M., Frischknecht, F., Baum, J., Ralph, S.A., 2013. Electron tomography of *Plasmodium falciparum* merozoites reveals core cellular events that underpin erythrocyte invasion. Cell. Microbiol. 15, 1457–1472.

Harris, P.K., Yeoh, S., Dluzewski, A.R., O'Donnell, R.A., Withers-Martinez, C., Hackett, F., Bannister, L.H., Mitchell, G.H., Blackman, M.J., 2005. Molecular identification of a malaria merozoite surface sheddase. PLoS Pathog. 1, 0241–0251.

Harvey, K.L., Gilson, P.R., Crabb, B.S., 2012. A model for the progression of receptor-ligand interactions during erythrocyte invasion by *Plasmodium falciparum*. Int. J. Parasitol. 42, 567–573.

Hawking, F., Wilson, M., Kenneth, G., 1971. Evidence for cyclic development and short lived maturity in the gametocytes of *Plasmodium falciparum*. Trans R Soc Trop Med Hyg. 65, 549–559.

Hawking, F., Worms, M.J., Gammage, K., 1968. Host temperature and control of 24-hour and 48-hour cycles in malaria parasites. Lancet. 7541, 506–509.

Haynes, J.D., Dalton, J.P., Klotz, F.W., McGinniss, M.H., Hadley, T.J., Hudson, D.E., Miller, L.H., 1988. Receptor-like specificity of a *Plasmodium knowlesi* malarial protein that binds to Duffy antigen ligands on erythrocytes. J. Exp. Med. 167, 1873–1881.

Haynes, J.D., DIggs, C.L., Hines, F.A., Desjardins, R.E., 1976. Culture of human malaria parasites *Plasmodium falciparum*. Nature 263, 767–769.

Hayton, K., Gaur, D., Liu, A., Takahashi, J., Henschen, B., Singh, S., Lambert, L., Furuya, T., Bouttenot, R., Doll, M., Nawaz, F., Mu, J., Jiang, L., Miller, L.H., Wellems, T.E., 2008. Erythrocyte Binding Protein PfRH5 Polymorphisms Determine Species-Specific Pathways of *Plasmodium falciparum* Invasion. Cell Host Microbe 4, 40–51.

Healer, J., Chiu, C.Y., Hansen, Di.S., 2018. Mechanisms of naturally acquired immunity to *P. falciparum* and approaches to identify merozoite antigen targets. Parasitology 145, 839–847.

Healer, J., Crawford, S., Ralph, S., McFadden, G., Cowman, A.F., 2002a. Independent translocation of two micronemal proteins in developing *Plasmodium falciparum* merozoites. Infect. Immun. 70, 5751–8.

Hepler, P.K., Huff, C.G., Sprinz, H., 1966. The fine structure of the exoerythrocytic stages of *Plasmodium fallax*. J. Cell Biol. 30, 333–358.

Herdiana, H., Cotter, C., Coutrier, F.N., Zarlinda, I., Zelman, B.W., Tirta, Y.K., Greenhouse, B., Gosling, R.D., Baker, P., Whittaker, M., Hsiang, M.S., 2016. Malaria risk factor assessment using active and passive surveillance data from Aceh Besar, Indonesia, a low endemic, malaria elimination setting with *Plasmodium knowlesi*, *Plasmodium vivax*, and *Plasmodium falciparum*. Malar. J. 15, 468.

Hillringhaus, S., Dasanna, A.K., Gompper, G., Fedosov, D.A., 2020. Stochastic bond dynamics facilitates alignment of malaria parasite at erythrocyte membrane upon invasion. Elife 9:e56500

Hillringhaus, S., Dasanna, A.K., Gompper, G., Fedosov, D.A., 2019. Importance of Erythrocyte Deformability for the Alignment of Malaria Parasite upon Invasion. Biophys. J. 117, 1202–1214.

Holder, A.A., Freeman, R.R., 1984. The three major antigens on the surface of *Plasmodium falciparum* merozoites are derived from a single high molecular weight precursor. J. Exp. Med. 160, 624–629.

Holder, A.A., Freeman, R.R., 1982. Biosynthesis and processing of a *plasmodium falciparum* schizont antigen recognized by immune serum and a monoclonal antibody. J. Exp. Med. 156, 1528–1538.

Howes, R.E., Battle, K.E., Mendis, K.N., Smith, D.L., Cibulskis, R.E., Baird, J.K., Hay, S.I., 2016. Global epidemiology of *Plasmodium vivax*. Am. J. Trop. Med. Hyg. 95, 15–34.

Howes, R.E., Patil, A.P., Piel, F.B., Nyangiri, O.A., Kabaria, C.W., Gething, P.W., Zimmerman, P.A., Barnadas, C., Beall, C.M., Gebremedhin, A., Ménard, D., Williams, T.N., Weatherall, D.J., Hay, S.I., 2011. The global distribution of the Duffy blood group. Nat. Commun. 2.

Introini, V., Crick, A., Tiffert, T., Kotar, J., Lin, Y.C., Cicuta, P., Lew, V.L., 2018a. Evidence against a Role of Elevated Intracellular Ca2+ during Plasmodium falciparum Preinvasion. Biophys. J. 114, 1695–1706.

Introini, V., Crick, A., Tiffert, T., Kotar, J., Lin, Y.C., Cicuta, P., Lew, V.L., 2018b. Evidence against a Role of Elevated Intracellular Ca2+ during *Plasmodium falciparum* Preinvasion. Biophys. J. 114, 1695–1706.

Ishino, T., Yano, K., Chinzei, Y., Yuda, M., 2004. Cell-passage activity is required for the malarial parasite to cross the liver sinusoidal cell layer. PLoS Biol. 2, 77–84.

Jacot, D., Tosetti, N., Pires, I., Stock, J., Graindorge, A., Hung, Y.F., Han, H., Tewari, R., Kursula, I., Soldati-Favre, D., 2016. An Apicomplexan Actin-Binding Protein Serves as a Connector and Lipid Sensor to Coordinate Motility and Invasion. Cell Host Microbe 20, 731–743.

Janse, C.J., Ponnudurai, T., Lensen, A.H.W., Meuwissen, J.H.E.T., Ramesar, J., Van Der Ploeg, M., Overdulve1, J.P., 1988. DNA synthesis in gametocytes of *Plasmodium falciparum*. Parasitology 96, 1–7.

Janse, C.J., Van Der Klooster, P.F., Van Der Kaay, H.J., Van Der Ploeg, M., Overdulve, J.P., 1986. Rapid repeated dna replication during microgametogenesis and dna synthesis in young zygotes of *Plasmodium berghei*. Trans. R. Soc. Trop. Med. Hyg. 80, 154–157.

Janse, C.J., Waters, A.P., 2007. The Exoneme Helps Malaria Parasites to Break out of Blood Cells. Cell 131, 1036–1038.

Jewett, T.J., Sibley, L.D., 2003. Aldolase forms a bridge between cell surface adhesins and the actin cytoskeleton in apicomplexan parasites. Mol. Cell 11, 885–894.

Jinek, M., Chylinski, K., Fonfara, I., Hauer, M., Doudna, J.A., Charpentier, E., 2012. A Programmable Dual-RNA – Guided DNA Endonuclease in Adaptive Bacterial Immunity. Science (80). 337, 816–822.

Joice, R., Nilsson, S.K., Montgomery, J., Dankwa, S., Egan, E., Morahan, B., Seydel, K.B., Bertuccini, L., Alano, P., Williamson, K.C., Duraisingh, M.T., Taylor, T.E., Milner, D.A., Marti, M., 2014. *Plasmodium falciparum* transmission stages accumulate in the human bone marrow. Sci. Transl. Med. 6, 1–9.

Jones, M.L., Das, S., Belda, H., Collins, C.R., Blackman, M.J., Treeck, M., 2016. A versatile strategy for rapid conditional genome engineering using loxP sites in a small synthetic intron in *Plasmodium falciparum*. Sci. Rep. 6, 1–9.

Kaneko, O., Mu, J., Tsuboi, T., Su, X., Torii, M., 2002. Gene structure and expression of a *Plasmodium falciparum* 220-kDa protein homologous to the Plasmodium vivax reticulocyte binding proteins. Mol. Biochem. Parasitol. 121, 275–278.

Kegawa, Y., Asada, M., Ishizaki, T., Yahata, K., Kaneko, O., 2018. Critical role of Erythrocyte Binding-Like protein of the rodent malaria parasite *Plasmodium yoelii* to establish an irreversible connection with the erythrocyte during invasion. Parasitol. Int. 67, 706–714.

King, C.L., Michon, P., Shakri, A.R., Marcotty, A., Stanisic, D., Zimmerman, P.A., Cole-Tobian, J.L., Mueller, I., Chitnis, C.E., 2008. Naturally acquired Duffy-binding protein-specific binding inhibitory antibodies confer protection from blood-stage *Plasmodium vivax* infection. Proc. Natl. Acad. Sci. U. S. A. 105, 8363–8368.

Kisalu, N.K., Idris, A.H., Weidle, C., Flores-Garcia, Y., Flynn, B.J., Sack, B.K., Murphy, S., Schön, A., Freire, E., Francica, J.R., Miller, A.B., Gregory, J., March, S., Liao, H.X., Haynes, B.F., Wiehe, K., Trama, A.M., Saunders, K.O., Gladden, M.A., Monroe, A., Bonsignori, M., Kanekiyo, M., Wheatley, A.K.,

McDermott, A.B., Farney, S.K., Chuang, G.Y., Zhang, B., Kc, N., Chakravarty, S., Kwong, P.D., Sinnis, P., Bhatia, S.N., Kappe, S.H.I., Sim, B.K.L., Hoffman, S.L., Zavala, F., Pancera, M., Seder, R.A., 2018. A human monoclonal antibody prevents malaria infection by targeting a new site of vulnerability on the parasite. Nat. Med. 24, 408–416.

Knuepfer, E., Napiorkowska, M., Van Ooij, C., Holder, A.A., 2017. Generating conditional gene knockouts in Plasmodium - A toolkit to produce stable DiCre recombinase-expressing parasite lines using CRISPR/Cas9. Sci. Rep. 7, 1–12.

Knuepfer, E., Suleyman, O., Dluzewski, A.R., Straschil, U., O'Keeffe, A.H., Ogun, S.A., Green, J.L., Grainger, M., Tewari, R., Holder, A.A., 2014. RON12, a novel *Plasmodium*-specific rhoptry neck protein important for parasite proliferation. Cell. Microbiol. 16, 657–672.

Knuepfer, E., Wright, K.E., Prajapati, S.K., Rawlinson, T.A., Mohring, F., Koch, M., Lyth, O.R., Howell, S.A., Villasis, E., Snijders, A.P., Moon, R.W., Draper, S.J., Rosanas-Urgell, A., Higgins, M.K., Baum, J., Holder, A.A., 2019. Divergent roles for the RH5 complex components, CyRPA and RIPR in human-infective malaria parasites. PLoS Pathog. 15, e1007809.

Koch, M., Wright, K.E., Otto, O., Herbig, M., Salinas, N.D., Tolia, N.H., Satchwell, T.J., Guck, J., Brooks, N.J., Baum, J., 2017. *Plasmodium falciparum* erythrocyte-binding antigen 175 triggers a biophysical change in the red blood cell that facilitates invasion. Proc. Natl. Acad. Sci. U. S. A. 114, 4225–4230.

Kocken, C.H.M., Ozwara, H., Van der Wel, A., Beetsma, A.L., Mwenda, J.M., Thomas, A.W., 2002. *Plasmodium knowlesi* provides a rapid in vitro and in vivo transfection system that enables double-crossover gene knockout studies. Infect. Immun. 70, 655–660.

Kremer, K., Kamin, D., Rittweger, E., Wilkes, J., Flammer, H., Mahler, S., Heng, J., Tonkin, C.J., Langsley, G., Hell, S.W., Carruthers, V.B., Ferguson, D.J.P., Meissner, M., 2013. An Overexpression Screen of *Toxoplasma gondii* Rab-GTPases Reveals Distinct Transport Routes to the Micronemes. PLoS Pathog. 9.

Krotoski, W.A., Collins, W.E., Bray, R.S., Garnham, P.C., Cogswell, F.B., Gwadz,

R.W., Killick-Kendrick, R., Wolf, R., Sinden, R., Koontz, L.C., Stanfill, P.S., 1982. Demonstration of hypnozoites in sporozoite-transmitted *Plasmodium vivax* infection. Am. J. Trop. Med. Hyg. 31, 1291–1293.

Kudryashev, M., Münter, S., Lemgruber, L., Montagna, G., Stahlberg, H., Matuschewski, K., Meissner, M., Cyrklaff, M., Frischknecht, F., 2012. Structural basis for chirality and directional motility of *Plasmodium* sporozoites. Cell. Microbiol. 14, 1757–1768.

Kwong, P.D., 2017. What are the most powerful immunogen design vaccine strategies?: A structural biologist's perspective. Cold Spring Harb. Perspect. Biol. 9.

Ladda, R., Aikawa, M., Sprinz, H., 1969. Penetration of erythrocytes by merozoites of mammalian and avian malarial parasites. J. Parasitol. 55, 663–664.

Lamarque, M., Besteiro, S., Papoin, J., Roques, M., Vulliez-Le Normand, B., Morlon-Guyot, J., Dubremetz, J.F., Fauquenoy, S., Tomavo, S., Faber, B.W., Kocken, C.H., Thomas, A.W., Boulanger, M.J., Bentley, G.A., Lebrun, M., 2011. The RON2-AMA1 interaction is a critical step in moving junction-dependent invasion by apicomplexan parasites. PLoS Pathog. 7(2):e1001276.

Lee, K.-S., Cox-Singh, J., Singh, B., 2009. Morphological features and differential counts of *Plasmodium knowlesi* parasites in naturally acquired human infections. Malar. J. 8, 1–10.

Lee, M.C.S., Lindner, S.E., Lopez-Rubio, J.J., Llinás, M., 2019. Cutting back malaria: CRISPR/Cas9 genome editing of *Plasmodium*. Brief. Funct. Genomics 18, 281–289.

Lee Sim, B.K., Toyoshima, T., David Haynes, J., Aikawa, M., 1992. Localization of the 175-kilodalton erythrocyte binding antigen in micronemes of *Plasmodium falciparum* merozoites. Mol. Biochem. Parasitol. 51, 157–159.

Lim, C., Pereira, L., Saliba, K.S., Mascarenhas, A., Maki, J.N., Chery, L., Gomes, E., Rathod, P.K., Duraisingh, M.T., 2016. Reticulocyte Preference and Stage Development of *Plasmodium vivax* Isolates. J. Infect. Dis. 214, 1081–1084.

Lin, C.S., Uboldi, A.D., Marapana, D., Czabotar, P.E., Epp, C., Bujard, H., Taylor, N.L., Perugini, M.A., Hodder, A.N., Cowman, A.F., 2014. The merozoite surface protein 1 complex is a platform for binding to human erythrocytes by *Plasmodium falciparum*. J. Biol. Chem. 289, 25655–25669.

Lo, E., Hostetler, J.B., Yewhalaw, D., Pearson, R.D., Hamid, M.M.A., Gunalan, K., Kepple, D., Ford, A., Janies, D.A., Rayner, J.C., Miller, L.H., Yan, G., 2019. Frequent expansion of *Plasmodium vivax* Duffy Binding Protein in Ethiopia and its epidemiological significance. PLoS Negl. Trop. Dis. 13, 1–18.

Lobo, C.A., Rodriguez, M., Reid, M., Lustigman, S., 2003. Glycophorin C is the receptor for the *Plasmodium falciparum* erythrocyte binding ligand PfEBP-2 (baebl). Blood 101, 4628–4631.

Lubis, I.N.D., Wijaya, H., Lubis, M., Lubis, C.P., Divis, P.C.S., Beshir, K.B., Sutherland, C.J., 2017. Contribution of *Plasmodium knowlesi* to multispecies human Malaria infections in North Sumatera, Indonesia. J. Infect. Dis. 215, 1148–1155.

Lyth, O., Vizcay-Barrena, G., Wright, K.E., Haase, S., Mohring, F., Najer, A., Henshall, I.G., Ashdown, G.W., Bannister, L.H., Drew, D.R., Beeson, J.G., Fleck, R.A., Moon, R.W., Wilson, D.W., Baum, J., 2018. Cellular dissection of malaria parasite invasion of human erythrocytes using viable *Plasmodium knowlesi* merozoites. Sci. Rep. 8, 1–11.

MacPherson, C.R., Scherf, A., 2015. Flexible guide-RNA design for CRISPR applications using protospacer workbench. Nat. Biotechnol. 33, 1–2.

Maier, A.G., Duraisingh, M.T., Reeder, J.C., Patel, S.S., Kazura, J.W., Zimmerman, P.A., Cowman, A.F., 2003. *Plasmodium falciparum* erythrocyte invasion through glycophorin C and selection for Gerbich negativity in human populations. Nat. Med. 9, 87–92.

Mair, G.R., Braks, J.A.M., Garver, L.S., Wiegant, J.C.A.G., Hall, N., Dirks, R.W., Khan, S.M., Dimopoulos, G., Janse, C.J., Waters, A.P., 2006. Regulation of Sexual Development of *Plasmodium* by Translational Repression. Science (80). 313, 667 LP – 669.

Mairet-Khedim, M., Leang, R., Marmai, C., Khim, N., Kim, S., Ke, S., Kauy, C., Kloeung, N., Eam, R., Chy, S., Izac, B., Bouth, D.M., Bustos, M.D., Ringwald, P., Ariey, F., Witkowski, B., 2020. Clinical and in vitro resistance of *Plasmodium falciparum* to artesunate-amodiaquine in Cambodia. Clin. Infect. Dis.

Malleret, B., Li, A., Zhang, R., Tan, K.S.W., Suwanarusk, R., Claser, C., Cho, J.S., Koh, E.G.L., Chu, C.S., Pukrittayakamee, S., Ng, M.L., Ginhoux, F., Ng, L.G., Lim, C.T., Nosten, F., Snounou, G., Rénia, L., Russell, B., 2014. *Plasmodium vivax*: Restricted tropism and rapid remodeling of CD71-positive reticulocytes. Blood 125, 1314–1324.

Manin, B.O., Ferguson, H.M., Vythilingam, I., Fornace, K., William, T., Torr, S.J., Drakeley, C., Chua, T.H., 2016. Investigating the Contribution of Peri-domestic Transmission to Risk of Zoonotic Malaria Infection in Humans. PLoS Negl. Trop. Dis. 10, 1–14.

Mann, T., Beckers, C., 2001. Characterization of the subpellicular network, a filamentous membrane skeletal component in the parasite *Toxoplasma gondi*i. Mol. Biochem. Parasitol. 115, 257–268.

Maskus, D.J., Królik, M., Bethke, S., Spiegel, H., Kapelski, S., Seidel, M., Addai-Mensah, O., Reimann, A., Klockenbring, T., Barth, S., Fischer, R., Fendel, R., 2016. Characterization of a novel inhibitory human monoclonal antibody directed against *Plasmodium falciparum* Apical Membrane Antigen 1. Sci. Rep. 6, 1–14.

Matuschewski, K., Mota, M.M., Pinder, J.C., Nussenzweig, V., Kappe, S.H.I., 2001. Identification of the class XIV myosins Pb-MyoA and Py-MyoA and expression in *Plasmodium* sporozoites. Mol. Biochem. Parasitol. 112, 157–161.

Mayer, D.C., Kaneko, O., Hudson-Taylor, D.E., Reid, M.E., Miller, L.H., 2001. Characterization of a *Plasmodium falciparum* erythrocyte-binding protein paralogous to EBA-175. Proc. Natl. Acad. Sci. U. S. A. 98, 5222–5227.

Mayer, D.C.G., Cofie, J., Jiang, L., Hartl, D.L., Tracy, E., Kabat, J., Mendoza, L.H., Miller, L.H., 2009. Glycophorin B is the erythrocyte receptor of *Plasmodium falciparum* erythrocyte-binding ligand, EBL-1. Proc. Natl. Acad. Sci. U. S. A. 106, 5348–52.

McKay, G.N., Mohan, N., Durr, N.J., 2020. Imaging human blood cells in vivo with oblique back-illumination capillaroscopy. Biomed. Opt. Express 11, 2373.

Ménard, D., Barnadas, C., Bouchier, C., Henry-Halldin, C., Gray, L.R., Ratsimbasoa, A., Thonier, V., Carod, J.F., Domarle, O., Colin, Y., Bertrand, O., Picot, J., King, C.L., Grimberg, B.T., Mercereau-Puijalon, O., Zimmerman, P.A., 2010. *Plasmodium vivax* clinical malaria is commonly observed in Duffy-negative Malagasy people. Proc. Natl. Acad. Sci. U. S. A. 107, 5967–5971.

Meyer, E.V.S., Semenya, A.A., Okenu, D.M.N., Anton, R., Bannister, L.H., Barnwell, J.W., Galinski, M.R., 2009. The reticulocyte binding-like proteins of *P. knowlesi* locate to the micronemes of merozoites and define two new members of this invasion ligand family. Mol. Biochem. Parasitol. 165, 111–121.

Millar, S.B., Cox-Singh, J., 2015. Human infections with *Plasmodium knowlesi*-zoonotic malaria. Clin. Microbiol. Infect. 21, 640–648.

Miller, L.H., Aikawa, M., Johnson, J.G., Shiroishi, T., 1979. Interaction between cytochalasin B-treated malarial parasites and erythrocytes. Attachment and junction formation. J. Exp. Med. 149, 172–84.

Miller, L.H., Carter, R., 1976. Innate resistance in malaria. Exp. Parasitol. 40, 132–146.

Miller, L H, Mason, S.J., Dvorak, J. a, McGinniss, M.H., Rothman, I.K., 1975. Erythrocyte receptors for (*Plasmodium knowlesi*) malaria: Duffy blood group determinants. Science (80). 189, 561–563.

Miller, Louis H., Mason, S.J., Dvorak, J.A., Mcginniss, M.H., Rothman, I.K., 1975. Erythrocyte receptors for (*Plasmodium knowlesi*) malaria: Duffy blood group determinants. Science (80). 189, 561–563.

Mohring, F., Hart, M.N., Rawlinson, T.A., Henrici, R., Charleston, J.A., Diez Benavente, E., Patel, A., Hall, J., Almond, N., Campino, S., Clark, T.G., Sutherland, C.J., Baker, D.A., Draper, S.J., Moon, R.W., 2019. Rapid and iterative genome editing in the malaria parasite Plasmodium knowlesi provides new tools for P. vivax research. Elife 8:e45829

Mojica, F.J.M., Díez-Villaseñor, C., García-Martínez, J., Almendros, C., 2009. Short motif sequences determine the targets of the prokaryotic CRISPR defence system. Microbiology 155, 733–740.

Moon, R.W., Hall, J., Rangkuti, F., Shwen, Y., Almond, N., Mitchell, G.H., 2013. Adaptation of the genetically tractable malaria pathogen *Plasmodium knowles*i to continuous culture in human erythrocytes. PNAS 110, 531–536.

Moon, R.W., Sharaf, H., Hastings, C.H., Ho, Y.S., Nair, M.B., Rchiad, Z., Knuepfer, E., Ramaprasad, A., Mohring, F., Amir, A., Yusuf, N.A., Hall, J., Almond, N., Lau, Y.L., Pain, A., Blackman, M.J., Holder, A.A., 2016. Normocyte-binding protein required for human erythrocyte invasion by the zoonotic malaria parasite *Plasmodium knowlesi.* Proc. Natl. Acad. Sci. U. S. A. 113, 7231–7236.

Moreno, A., Caro-Aguilar, I., Yazdani, S.S., Shakri, A.R., Lapp, S., Strobert, E., McClure, H., Chitnis, C.E., Galinski, M.R., 2008. Preclinical assessment of the receptor-binding domain of *Plasmodium vivax* Duffy-binding protein as a vaccine candidate in rhesus macaques. Vaccine 26, 4338–4344.

Morita, M., Nagaoka, H., Ntege, E.H., Kanoi, B.N., Ito, D., Nakata, T., Lee, J.W., Tokunaga, K., Iimura, T., Torii, M., Tsuboi, T., Takashima, E., 2018. PV1, a novel *Plasmodium falciparum* merozoite dense granule protein, interacts with exported protein in infected erythrocytes. Sci. Rep. 8, 1–11.

Mota, M.M., Pradel, G., Vanderberg, J.P., Hafalla, J.C.R., Frevert, U., Nussenzweig, R.S., Nussenzweig, V., Rodríguez, A., 2001. Migration of *Plasmodium* Sporozoites Through Cells Before Infection. Science (80). 291, 141 LP – 144.

Mueller, C., Klages, N., Jacot, D., Santos, J.M., Cabrera, A., Gilberger, T.W., Dubremetz, J.F., Soldati-Favre, D., 2013. The *toxoplasma* protein ARO mediates the apical positioning of rhoptry organelles, a prerequisite for host cell invasion. Cell Host Microbe 13, 289–301.

Muh, F., Kim, N., Nyunt, M.H., Firdaus, E.R., Han, J.H., Hoque, M.R., Lee, S.K., Park, J.H., Moon, R.W., Lau, Y.L., Kaneko, O., Hanid, E.T., 2020. Cross-species reactivity of antibodies against *Plasmodium vivax* blood-stage antigens to *Plasmodium knowlesi*. PLoS Negl. Trop. Dis. 14, 1–21.

Muh, F., Lee, S.K., Hoque, M.R., Han, J.H., Park, J.H., Firdaus, E.R., Moon, R.W., Lau, Y.L., Han, E.T., 2018. In vitro invasion inhibition assay using antibodies against *Plasmodium knowlesi* Duffy binding protein alpha and apical membrane antigen protein 1 in human erythrocyte-adapted *P. knowlesi* A1-H.1 strain. Malar. J. 17.

Ndegwa, D.N., Hostetler, J.B., Marin-Menendez, A., Sanderson, T., Mwikali, K., Verzier, L.H., Coyle, R., Adjalley, S., Rayner, J.C., 2020. Using *Plasmodium knowlesi* as a model for screening *Plasmodium vivax* blood-stage malaria vaccine targets reveals new candidates. bioRxiv.

Nicolete, V.C., Frischmann, S., Barbosa, S., King, C.L., Ferreira, M.U., 2016. Naturally acquired binding-inhibitory antibodies to *Plasmodium vivax* Duffy binding protein and clinical immunity to malaria in rural Amazonians. J. Infect. Dis. 214, 1539–1546.

Noedl, H., Se, Y., Schaecher, K., Smith, B.L., Socheat, D., Fukuda, M.M., 2008. Evidence of artemisinin-resistant malaria in Western Cambodia. N. Engl. J. Med. 359, 2619–2620.

O'Donnell, R.A., Hackett, F., Howell, S.A., Treeck, M., Struck, N., Krnajski, Z., Withers-Martinez, C., Gilberger, T.W., Blackman, M.J., 2006. Intramembrane proteolysis mediates shedding of a key adhesin during erythrocyte invasion by the malaria parasite. J. Cell Biol. 174, 1023–1033.

Obaldia, N., Meibalan, E., Sa, J.M., Ma, S., Clark, M.A., Mejia, P., Moraes Barros, R.R., Otero, W., Ferreira, M.U., Mitchell, J.R., Milner, D.A., Huttenhower, C., Wirth, D.F., Duraisingh, M.T., Wellems, T.E., Marti, M., 2018. Bone marrow is a major parasite reservoir in *Plasmodium vivax* infection. MBio 9, 1–16.

Ogutu, B.R., Apollo, O.J., McKinney, D., Okoth, W., Siangla, J., Dubovsky, F., Tucker, K., Waitumbi, J.N., Diggs, C., Wittes, J., Malkin, E., Leach, A., Soisson, L.A., Milman, J.B., Otieno, L., Holland, C.A., Polhemus, M., Remich, S.A., Ockenhouse, C.F., Cohen, J., Ballou, W.R., Martin, S.K., Angov, E., Stewart, V.A., Lyon, J.A., Heppner, D.G., Withers, M.R., 2009. Blood stage malaria vaccine eliciting high antigen-specific antibody concentrations confers no protection to young children in Western Kenya. PLoS One 4.

Opitz, C., Soldati, D., 2002. "The glideosome": A dynamic complex powering gliding motion and host cell invasion by *Toxoplasma gondii*. Mol. Microbiol. 45, 597–604.

Pain, A., Bohme, U., Berry, A., Mungall, K., Finn, R., Jacksin, A., Mourier, T., Mistry, J., Pasini, E.M., Aslett, M.A., Balasubrammaniam, S., Borgwardt, K., Brooks, K., Carret, C., Carver, T.J., Cherevach, I., Chillingworth, T., Clark, T.G., Galinski, M., Hall, N., Harper, D., Harris, D., Hauser, H., Ivens, A., Janssen, C.S., Keane, T., Larke, N., Lapp, S., Marti, M., Moule, S., Meyer, I.M., Ormond, D., Peters, N., Sanders, M., Sanders, S., Sargeant, T.J., Simmonds, M., Smith, F., Squares, R., Thurston, S., Tivey, A.R., Walker, D., White, B., Zuiderwijk, E., Churcher, C., Quail, M.A., Cowman, A.F., Turner, C.M.R., Rajandream, M.A., Kocken, C.H.M., Thomas, A.W., Newbold, I., Barrell, B., Berriman, M., 2008. The genome of the simian and human malaria parasite *P. knowlesi*. Nature 455, 799–803.

Pal-Bhowmick, I., Andersen, J., Srinivasan, P., Narum, D.L., Bosch, J., Miller, L.H., 2012. Binding of Aldolase and Glyceraldehyde-3-Phosphate Dehydrogenase to the Cytoplasmic Tails of *Plasmodium falciparum* Merozoite Duffy Binding-Like and Reticulocyte Homology Ligands. MBio 3, 1–8.

Partey, F.D., Castberg, F.C., Sarbah, E.W., Silk, S.E., Awandare, G.A., Draper, S.J., Opoku, N., Kweku, M., Ofori, M.F., Hviid, L., Barfod, L., 2018. Kinetics of antibody responses to pfrh5-complex antigens in ghanaian children with *plasmodium falciparum* malaria. PLoS One 13, 1–14.

Partnership, R.S.C.T., 2015. Efficacy and safety of RTS,S/AS01 malaria vaccine with or without a booster dose in infants and children in Africa: Final results of a phase 3, individually randomised, controlled trial. Lancet 386, 31–45.

Pavlou, G., Biesaga, M., Touquet, B., Lagal, V., Balland, M., Dufour, A., Hakimi, M. ali, Tardieux, I., 2018. *Toxoplasma* Parasite Twisting Motion Mechanically Induces Host Cell Membrane Fission to Complete Invasion within a Protective Vacuole. Cell Host Microbe 24, 81-96.e5.

Payne, R.O., Silk, S.E., Elias, S.C., Milne, K.H., Rawlinson, T.A., Llewellyn, D., Shakri, A.R., Jin, J., Labbé, G.M., Edwards, N.J., Poulton, I.D., Roberts, R.,

Farid, R., Jørgensen, T., Alanine, D.G., de Cassan, S.C., Higgins, M.K., Otto, T.D., McCarthy, J.S., de Jongh, W.A., Nicosia, A., Moyle, S., Hill, A.V., Berrie, E., Chitnis, C.E., Lawrie, A.M., Draper, S.J., 2017a. Human vaccination against *Plasmodium vivax* Duffy-binding protein induces strain-transcending antibodies. JCI insight 2, 1–17.

Payne, R.O., Silk, S.E., Elias, S.C., Miura, K., Diouf, A., Galaway, F., De Graaf, H., Brendish, N.J., Poulton, I.D., Griffiths, O.J., Edwards, N.J., Jin, J., Labbé, G.M., Alanine, D.G.W., Siani, L., Marco, S. Di, Roberts, R., Green, N., Berrie, E., Ishizuka, A.S., Nielsen, C.M., Bardelli, M., Partey, F.D., Ofori, M.F., Barfod, L., Wambua, J., Murungi, L.M., Osier, F.H., Biswas, S., McCarthy, J.S., Minassian, A.M., Ashfield, R., Viebig, N.K., Nugent, F.L., Douglas, A.D., Vekemans, J., Wright, G.J., Faust, S.N., Hill, A.V.S., Long, C.A., Lawrie, A.M., Draper, S.J., 2017b. Human vaccination against RH5 induces neutralizing antimalarial antibodies that inhibit RH5 invasion complex interactions. JCI Insight 2, 1–19.

Pearson, R., Amato, R., Kwiatkowski, D., 2019. An open dataset of *Plasmodium falciparum* genome variation in 7,000 worldwide samples. bioRxiv.

Perrin, A.J., Collins, C.R., Russell, M.R.G., Collinson, L.M., Baker, D.A., Blackman, M.J., 2018. The actinomyosin motor drives malaria parasite red blood cell invasion but not egress. MBio 9, 1–13.

Peterson, D.S., Wellems, T.E., 2000. EBL-1, a putative erythrocyte binding protein of *Plasmodium falciparum*, maps within a favored linkage group in two genetic crosses. Mol. Biochem. Parasitol. 105, 105–113.

Phillips, M.A., Burrows, J.N., Manyando, C., Van Huijsduijnen, R.H., Van Voorhis, W.C., Wells, T.N.C., 2017. Malaria. Nat. Rev. Dis. Prim. 3, 1–24.

PIMENTA, P.F., TOURAY, M., MILLER, L., 1994. The Journey of Malaria Sporozoites in the Mosquito Salivary Gland. J. Eukaryot. Microbiol. 41, 608–624.

Pinder, J.C., Fowler, R.E., Bannister, L.H., Dluzewski, A.R., Mitchell, G.H., 2000. Motile systems in malaria merozoites: How is the red blood cell invaded? Parasitol. Today 16, 240–245.

Popovici, J., Roesch, C., Rougeron, V., 2020. The enigmatic mechanisms by which

Plasmodium vivax infects Duffy-negative individuals. PLoS Pathog. 16, 1–14.

Pradel, G., Frevert, U., 2001. Malaria sporozoites actively enter and pass through rat Kupffer cells prior to hepatocyte invasion. Hepatology 33, 1154–1165.

Prasad, C.D., Singh, A.P., Chitnis, C.E., Sharma, A., 2003. A *Plasmodium yoelii yoelii* erythrocyte binding protein that uses Duffy binding-like domain for invasion: A rodent model for studying erythrocyte invasion. Mol. Biochem. Parasitol. 128, 101–105.

Preiser, P.R., Jarra, W., Capiod, T., Snounou, G., 1999. A rhoptry-protein-associated mechanism of clonal phenotypic variation in rodent malaria. Nature 398, 618–622.

Quadt, K.A., Streichfuss, M., Moreau, C.A., Spatz, J.P., Frischknecht, F., 2016. Coupling of Retrograde Flow to Force Production during Malaria Parasite Migration. ACS Nano 10, 2091–2102.

Ragotte, R.J., Higgins, M.K., Draper, S.J., 2020. The RH5-CyRPA-Ripr Complex as a Malaria Vaccine Target. Trends Parasitol. 36, 545–559.

Rawlinson, T.A., Barber, N.M., Mohring, F., Cho, J.S., Kosaisavee, V., Gérard, S.F., Alanine, D.G.W., Labbé, G.M., Elias, S.C., Silk, S.E., Quinkert, D., Jin, J., Marshall, J.M., Payne, R.O., Minassian, A.M., Russell, B., Rénia, L., Nosten, F.H., Moon, R.W., Higgins, M.K., Draper, S.J., 2019. Structural basis for inhibition of *Plasmodium vivax* invasion by a broadly neutralizing vaccine-induced human antibody. Nat. Microbiol. 4, 1497–1507.

Rayner, J.C., Vargas-Serrato, E., Huber, C.S., Galinski, M.R., Barnwell, J.W., 2001. A *Plasmodium falciparum* homologue of *Plasmodium vivax* reticulocyte binding protein (PvRBP1) defines a trypsin-resistant erythrocyte invasion pathway. J. Exp. Med. 194, 1571–81.

Reddy, K.S., Amlabu, E., Pandey, A.K., Mitra, P., Chauhan, V.S., Gaur, D., 2015a. Multiprotein complex between the GPI-anchored CyRPA with PfRH5 and PfRipr is crucial for *Plasmodium falciparum* erythrocyte invasion. Proc. Natl. Acad. Sci. U. S. A. 112, 1179–1184.

Reddy, K.S., Amlabu, E., Pandey, A.K., Mitra, P., Chauhan, V.S., Gaur, D., 2015b. Multiprotein complex between the GPI-anchored CyRPA with PfRH5 and PfRipr is crucial for *Plasmodium falciparum* erythrocyte invasion. Proc. Natl. Acad. Sci. U. S. A. 112, 1179–1184.

Richard, D., MacRaild, C.A., Riglar, D.T., Chan, J.A., Foley, M., Baum, J., Ralph, S.A., Norton, R.S., Cowman, A.F., 2010a. Interaction between *Plasmodium falciparum* apical membrane antigen 1 and the rhoptry neck protein complex defines a key step in the erythrocyte invasion process of malaria parasites. J. Biol. Chem. 285, 14815–14822.

Richard, D., MacRaild, C.A., Riglar, D.T., Chan, J.A., Foley, M., Baum, J., Ralph, S.A., Norton, R.S., Cowman, A.F., 2010b. Interaction between Plasmodium falciparum apical membrane antigen 1 and the rhoptry neck protein complex defines a key step in the erythrocyte invasion process of malaria parasites. J. Biol. Chem. 285, 14815–14822.

Richards, J.S., Arumugam, T.U., Reiling, L., Healer, J., Hodder, A.N., Fowkes, F.J.I., Cross, N., Langer, C., Takeo, S., Uboldi, A.D., Thompson, J.K., Gilson, P.R., Coppel, R.L., Siba, P.M., King, C.L., Torii, M., Chitnis, C.E., Narum, D.L., Mueller, I., Crabb, B.S., Cowman, A.F., Tsuboi, T., Beeson, J.G., 2013. Identification and Prioritization of Merozoite Antigens as Targets of Protective Human Immunity to *Plasmodium falciparum* Malaria for Vaccine and Biomarker Development . J. Immunol. 191, 795–809.

Richter, J., Franken, G., Mehlhorn, H., Labisch, A., Häussinger, D., 2010. What is the evidence for the existence of *Plasmodium ovale* hypnozoites? Parasitol. Res. 107, 1285–1290.

Riglar, D.T., Richard, D., Wilson, D.W., Boyle, M.J., Dekiwadia, C., Turnbull, L., Angrisano, F., Marapana, D.S., Rogers, K.L., Whitchurch, C.B., Beeson, J.G., Cowman, A.F., Ralph, S.A., Baum, J., 2011. Super-resolution dissection of coordinated events during malaria parasite invasion of the human erythrocyte. Cell Host Microbe 9, 9–20.

Robert-Paganin, J., Robblee, J.P., Auguin, D., Blake, T.C.A., Bookwalter, C.S., Krementsova, E.B., Moussaoui, D., Previs, M.J., Jousset, G., Baum, J., Trybus,

K.M., Houdusse, A., 2019. Plasmodium myosin A drives parasite invasion by an atypical force generating mechanism. Nat. Commun. 10.

Robinson, L.J., Wampfler, R., Betuela, I., Karl, S., White, M.T., Li Wai Suen, C.S.N., Hofmann, N.E., Kinboro, B., Waltmann, A., Brewster, J., Lorry, L., Tarongka, N., Samol, L., Silkey, M., Bassat, Q., Siba, P.M., Schofield, L., Felger, I., Mueller, I., 2015. Strategies for Understanding and Reducing the *Plasmodium vivax* and *Plasmodium ovale* Hypnozoite Reservoir in Papua New Guinean Children: A Randomised Placebo-Controlled Trial and Mathematical Model. PLoS Med. 12, 1–26.

Rodriguez, M., Lustigman, S., Montero, E., Oksov, Y., Lobo, C.A., 2008. PfRH5: A novel reticulocyte-binding family homolog of *Plasmodium falciparum* that binds to the erythrocyte, and an investigation of its receptor. PLoS One 3, 1–8.

RTS, S Clinical Trials Partnership, 2011. First Results of Phase 3 Trial of RTS,S/AS01 Malaria Vaccine in African Children. N. Engl. J. Med. 365, 1863–1875.

RTS, S Clinical Trials Partnership (2015). Efficacy and safety of RTS,S/AS01 malaria vaccine with or without a booster dose in infants and children in Africa: Final results of a phase 3, individually randomised, controlled trial. Lancet 386(9988), 31–45.

Russell, B., Suwanarusk, R., Borlon, C., Costa, F.T.M., Chu, C.S., Rijken, M.J., Sriprawat, K., Warter, L., Koh, E.G.L., Malleret, B., Colin, Y., Bertrand, O., Adams, J.H., D'Alessandro, U., Snounou, G., Nosten, F., Rénia, L., 2011. A reliable ex vivo invasion assay of human reticulocytes by *Plasmodium vivax*. Blood 118, 74–81.

Rutledge, G.G., Böhme, U., Sanders, M., Reid, A.J., Cotton, J.A., Maiga-Ascofare, O., Djimdé, A.A., Apinjoh, T.O., Amenga-Etego, L., Manske, M., Barnwell, J.W., Renaud, F., Ollomo, B., Prugnolle, F., Anstey, N.M., Auburn, S., Price, R.N., McCarthy, J.S., Kwiatkowski, D.P., Newbold, C.I., Berriman, M., Otto, T.D., 2017. *Plasmodium malariae* and *P. ovale* genomes provide insights into malaria parasite evolution. Nature 542, 101–104.

Ryning, F.W., Remington, J.S., 1978. Effect of cytochalasin D on *Toxoplasma gondii*

cell entry. Infect. Immun. 20, 739–743.

Salinas, N.D., Tolia, N.H., 2016. Red cell receptors as access points for malaria infection Nichole. Curr. Opin. Hematol. 23, 139–148.

Semenya, A.A., Tran, T.M., Meyer, E.V., Barnwell, J.W., Galinski, M.R., 2012. Two functional reticulocyte binding-like (RBL) invasion ligands of zoonotic *Plasmodium knowlesi* exhibit differential adhesion to monkey and human erythrocytes. Malar. J. 11, 1.

Shaner, N.C., Lambert, G.G., Chammas, A., Ni, Y., Paula, J., Baird, M.A., Sell, B.R., Allen, J.R., Day, R.N., Davidson, M.W., Wang, J., 2013. A bright monomeric green fluorescent protein derived from Branchiostoma lanceolatum. Nat. Methods 10, 407–409.

Sheehy, S.H., Duncan, C.J., Elias, S.C., Choudhary, P., Biswas, S., Halstead, F.D., Collins, K.A., Edwards, N.J., Douglas, A.D., Anagnostou, N.A., Ewer, K.J., Havelock, T., Mahungu, T., Bliss, C.M., Miura, K., Poulton, I.D., Lillie, P.J., Antrobus, R.D., Berrie, E., Moyle, S., Gantlett, K., Colloca, S., Cortese, R., Long, C.A., Sinden, R.E., Gilbert, S.C., Lawrie, A.M., Doherty, T., Faust, S.N., Nicosia, A., Hill, A.V., Draper, S.J., 2012. ChAd63-MVA-vectored blood-stage Malaria vaccines targeting MSP1 and AMA1: Assessment of efficacy against mosquito bite challenge in humans. Mol. Ther. 20, 2355–2368.

Sheiner, L., Santos, J.M., Klages, N., Parussini, F., Jemmely, N., Friedrich, N., Ward, G.E., Soldati-Favre, D., 2010. *Toxoplasma gondii* transmembrane microneme proteins and their modular design. Mol. Microbiol. 77, 912–929.

Shen, B., Sibley, L.D., 2014. *Toxoplasma* aldolase is required for metabolism but dispensable for host-cell invasion. Proc. Natl. Acad. Sci. U. S. A. 111, 3567–3572.

Sherling, E.S., Knuepfer, E., Brzostowski, J.A., Miller, L.H., Blackman, M.J., Van Ooij, C., 2017. The *Plasmodium falciparum* rhoptry protein RhopH3 plays essential roles in host cell invasion and nutrient uptake. Elife 6, 1–23.

Siden-Kiamos, I., Ecker, A., Nybäck, S., Louis, C., Sinden, R.E., Billker, O., 2006. *Plasmodium berghei* calcium-dependent protein kinase 3 is required for ookinete

gliding motility and mosquito midgut invasion. Mol. Microbiol. 60, 1355–1363.

Sim, B.K.L., Chitnis, C.E., Wasniowska, K., Hadley, T.J., Miller, L.H., 1994. Receptor and ligand domains for invasion of erythrocytes by *Plasmodium falciparum*. Science (80). 264, 1941–1944.

Sinden, R.E., 1982. Gametocytogenesis of Plasmodium falciparum in vitro: An electron microscopic study. Parasitology 84, 1–11.

Singh, A.P., Ozwara, H., Kocken, C.H.M., Puri, S.K., Thomas, A.W., Chitnis, C.E., 2005. Targeted deletion of *Plasmodium knowlesi* Duffy binding protein confirms its role in junction formation during invasion. Mol. Microbiol. 55, 1925–1934.

Singh, B., Daneshvar, C., 2013. Human infections and detection of *Plasmodium knowlesi*. Clin. Microbiol. Rev. 26, 165–184.

Singh, K., Mukherjee, P., Shakri, A.R., Singh, Ankita, Pandey, G., Bakshi, M., Uppal, G., Jena, R., Rawat, A., Kumar, P., Bhardwaj, R., Yazdani, S.S., Hans, D., Mehta, S., Srinivasan, A., Anil, K., Madhusudhan, R.L., Patel, J., Singh, Amit, Rao, R., Gangireddy, S., Patil, R., Kaviraj, S., Singh, S., Carter, D., Reed, S., Kaslow, D.C., Birkett, A., Chauhan, V.S., Chitnis, C.E., 2018. Malaria vaccine candidate based on Duffy-binding protein elicits strain transcending functional antibodies in a Phase I trial. npj Vaccines 3.

Singh, S., Alam, M.M., Pal-Bhowmick, I., Brzostowski, J.A., Chitnis, C.E., 2010. Distinct external signals trigger sequential release of apical organelles during erythrocyte invasion by malaria parasites. PLoS Pathog. 6(2):e1000746.

Sisquella, X., Nebl, T., Thompson, J.K., Whitehead, L., Malpede, B.M., Salinas, N.D., Rogers, K., Tolia, N.H., Fleig, A., O'Neill, J., Tham, W.-H., David Horgen, F., Cowman, A.F., 2017. *Plasmodium falciparum* ligand binding to erythrocytes induce alterations in deformability essential for invasion. Elife 6, 1–20.

Smalley, M.E., Sinden, R.E., 1977. *Plasmodium falciparum* gametocytes: their longevity and infectivity. Parasitology 74, 1–8.

Smolarek, D., Hattab, C., Hassanzadeh-Ghassabeh, G., Cochet, S., Gutiérrez, C., de Brevern, A.G., Udomsangpetch, R., Picot, J., Grodecka, M., Wasniowska, K.,

Muyldermans, S., Colin, Y., Le Van Kim, C., Czerwinski, M., Bertrand, O., 2010. A recombinant dromedary antibody fragment (VHH or nanobody) directed against human Duffy antigen receptor for chemokines. Cell. Mol. Life Sci. 67, 3371–3387.

Srinivasan, P., Beatty, W.L., Diouf, A., Herrera, R., Ambroggio, X., Moch, J.K., Tyler, J.S., Narum, D.L., Pierce, S.K., Boothroyd, J.C., Haynes, J.D., Miller, L.H., 2011. Binding of *Plasmodium* merozoite proteins RON2 and AMA1 triggers commitment to invasion. Proc. Natl. Acad. Sci. U. S. A. 108, 13275–80.

Stark, D.J., Fornace, K.M., Brock, P.M., Abidin, T.R., Gilhooly, L., Jalius, C., Goossens, B., Drakeley, C.J., Salgado-Lynn, M., 2019. Long-Tailed Macaque Response to Deforestation in a *Plasmodium knowlesi*-Endemic Area. Ecohealth 16, 638–646.

Stewart, M.J., Nawrot, R.J., Schulman, S., Vanderberg, J.P., 1986. *Plasmodium berghei* sporozoite invasion is blocked in vitro by sporozoite-immobilizing antibodies. Infect. Immun. 51, 859–864.

Stewart, M.J., Vanderberg, J.P., 1988. Malaria Sporozoites Leave Behind Trails of Circurnsporozoite Protein During Gliding Motility. J. Protozool. 51, 859–864.

Straub, K.W., Peng, E.D., Hajagos, B.E., Tyler, J.S., Bradley, P.J., 2011. The moving junction protein RON8 facilitates firm attachment and host cell invasion in Toxoplasma gondii. PLoS Pathog. 7.

Stubbs, J., Simpson, K.M., Triglia, T., Plouffe, D., Tonkin, C.J., Duraisingh, M.T., Maier, A.C., Winzeler, E.A., Cowman, A.F., 2005. Microbiology: Molecular mechanism for switching of *P. falciparum* invasion pathways into human erythrocytes. Science (80-.). 309, 1384–1387.

Sturm, A., Amino, R., Van De Sand, C., Regen, T., Retzlaff, S., Rennenberg, A., Krueger, A., Pollok, J.M., Menard, R., Heussler, V.T., 2006. Manipulation of host hepatocytes by the malaria parasite for delivery into liver sinusoids. Science (80). 313, 1287–1290.

Sultan, A.A., Thathy, V., Frevert, U., Robson, K.J.H., Crisanti, A., Nussenzweig, V., Nussenzweig, R.S., Ménard, R., 1997. TRAP is necessary for gliding motility and

infectivity of *Plasmodium* sporozoites. Cell 90, 511–522.

Takemae, H., Sugi, T., Kobayashi, K., Gong, H., Ishiwa, A., Recuenco, F.C., Murakoshi, F., Iwanaga, T., Inomata, A., Horimoto, T., Akashi, H., Kato, K., 2013. Characterization of the interaction between *Toxoplasma gondii* rhoptry neck protein 4 and host cellular β-tubulin. Sci. Rep. 3, 1–9.

Tan, J., Sack, B.K., Oyen, D., Zenklusen, I., Piccoli, L., Barbieri, S., Foglierini, M., Fregni, C.S., Marcandalli, J., Jongo, S., Abdulla, S., Perez, L., Corradin, G., Varani, L., Sallusto, F., Sim, B.K.L., Hoffman, S.L., Kappe, S.H.I., Daubenberger, C., Wilson, I.A., Lanzavecchia, A., 2018. A public antibody lineage that potently inhibits malaria infection through dual binding to the circumsporozoite protein. Nat. Med. 24, 401–407.

Tardieux, I., Baum, J., 2016. Reassessing the mechanics of parasite motility and host-cell invasion. J. Cell Biol. 214, 507–515.

Tavares, J., Formaglio, P., Thiberge, S., Mordelet, E., Van Rooijen, N., Medvinsky, A., Ménard, R., Amino, R., 2013. Role of host cell traversal by the malaria sporozoite during liver infection. J. Exp. Med. 210, 905–915.

Taylor, H.M., Grainger, M., Holder, A.A., 2002. Variation in the expression of a *Plasmodium falciparum* protein family implicated in erythrocyte invasion. Infect. Immun. 70, 5779–89.

Tham, W.H., Healer, J., Cowman, A.F., 2012. Erythrocyte and reticulocyte binding-like proteins of *Plasmodium falciparum*. Trends Parasitol. 28, 23–30.

Tham, W.H., Lim, N.T.Y., Weiss, G.E., Lopaticki, S., Ansell, B.R.E., Bird, M., Lucet, I., Dorin-Semblat, D., Doerig, C., Gilson, P.R., Crabb, B.S., Cowman, A.F., 2015. *Plasmodium falciparum* Adhesins Play an Essential Role in Signalling and Activation of Invasion into Human Erythrocytes. PLoS Pathog. 11, 1–22.

Tham, W.H., Schmidt, C.Q., Hauhart, R.E., Guariento, M., Tetteh-Quarcoo, P.B., Lopaticki, S., Atkinson, J.P., Barlow, P.N., Cowman, A.F., 2011. *Plasmodium falciparum* uses a key functional site in complement receptor type-1 for invasion of human erythrocytes. Blood 118, 1923–1933.

Tham, W.H., Wilson, D.W., Lopaticki, S., Schmidt, C.Q., Tetteh-Quarcoo, P.B., Barlow, P.N., Richard, D., Corbin, J.E., Beeson, J.G., Cowman, A.F., 2010. Complement receptor 1 is the host erythrocyte receptor for *Plasmodium falciparum* PfRh4 invasion ligand. Proc. Natl. Acad. Sci. U. S. A. 107, 17327–17332.

Thera, M.A., Doumbo, O.K., Coulibaly, D., Laurens, M.B., Ouattara, A., Kone, A.K., Guindo, A.B., Traore, K., Traore, I., Kouriba, B., Diallo, D.A., Diarra, I., Daou, M., Dolo, A., Tolo, Y., Sissoko, M.S., Niangaly, A., Sissoko, M., Takala-Harrison, S., Lyke, K.E., Wu, Y., Blackwelder, W.C., Godeaux, O., Vekemans, J., Dubois, M.-C., Ballou, W.R., Cohen, J., Thompson, D., Dube, T., Soisson, L., Diggs, C.L., House, B., Lanar, D.E., Dutta, S., Heppner, D.G., Plowe, C. V, 2011. A Field Trial to Assess a Blood-Stage Malaria Vaccine. N. Engl. J. Med. 365, 1004–1013.

Thompson, J., Cooke, R.E., Moore, S., Anderson, L.F., Janse, C.J., Waters, A.P., 2004. PTRAMP; a conserved *Plasmodium* thrombospondin-related apical merozoite protein. Mol. Biochem. Parasitol. 134, 225–232.

Thompson, J.K., Triglia, T., Reed, M.B., Cowman, A.F., 2001. A novel ligand from *Plasmodium falciparum* that binds to a sialic acid-containing receptor on the surface of human erythrocytes. Mol. Microbiol. 41, 47–58.

Tolia, N.H., Enemark, E.J., Sim, B.K.L., Joshua-Tor, L., 2005. Structural basis for the EBA-175 erythrocyte invasion pathway of the malaria parasite *Plasmodium falciparum*. Cell 122, 183–193.

Torii, M., Adams, J.H., Miller, L.H., Aikawa, M., 1989. Release of merozoite dense granules during erythrocyte invasion by *Plasmodium knowlesi*. Infect. Immun. 57, 3230–3233.

Tournamille, C., Colin, Y., Cartron, J.P., Kim, C.L. Van, Cabanel, A., Paris, I., 1995. Duffy gene promoter abolishes Duffy-negative individuals 10, 224–228.

Trager, W., Jensen, J.B., 1976. Human malaria parasites in continuous culture. Science (80). 193, 673 LP – 675.

Tran, T.M., Ongoiba, A., Coursen, J., Crosnier, C., Diouf, A., Huang, C.Y., Li, S.,

Doumbo, S., Doumtabe, D., Kone, Y., Bathily, A., Dia, S., Niangaly, M., Dara, C., Sangala, J., Miller, L.H., Doumbo, O.K., Kayentao, K., Long, C.A., Miura, K., Wright, G.J., Traore, B., Crompton, P.D., 2014. Naturally acquired antibodies specific for *Plasmodium falciparum* reticulocyte-binding protein homologue 5 inhibit parasite growth and predict protection from malaria. J. Infect. Dis. 209, 789–798.

Treeck, M., Struck, N.S., Haase, S., Langer, C., Herrmann, S., Healer, J., Cowman, A.F., Gilberger, T.W., 2006. A conserved region in the EBL proteins is implicated in microneme targeting of the malaria parasite *Plasmodium falciparum*. J. Biol. Chem. 281, 31995–32003.

Treeck, M., Zacherl, S., Herrmann, S., Cabrera, A., Kono, M., Struck, N.S., Engelberg, K., Haase, S., Frischknecht, F., Miura, K., Spielmann, T., Gilberger, T.W., 2009. Functional analysis of the leading malaria vaccine candidate AMA-1 reveals an essential role for the cytoplasmic domain in the invasion process. PLoS Pathog. 5, 1–13.

Tremp, A.Z., Al-Khattaf, F.S., Dessens, J.T., 2014. Distinct temporal recruitment of *Plasmodium* alveolins to the subpellicular network. Parasitol. Res. 113, 4177–4188.

Triglia, T., Duraisingh, M.T., Good, R.T., Cowman, A.F., 2005. Reticulocyte-binding protein homologue 1 is required for sialic acid-dependent invasion into human erythrocytes by *Plasmodium falciparum*. Mol. Microbiol. 55, 162–174.

Triglia, T., Tham, W.H., Hodder, A., Cowman, A.F., 2009. Reticulocyte binding protein homologues are key adhesins during erythrocyte invasion by *Plasmodium falciparum*. Cell. Microbiol. 11, 1671–1687.

Triglia, T., Thompson, J., Caruana, S.R., Delorenzi, M., Speed, T., Cowman, A.F., 2001. Identification of Proteins from *Plasmodium falciparum* That Are Homologous to Reticulocyte Binding Proteins in *Plasmodium vivax*. Infect. Immun. 69, 1084–1092.

van Schalkwyk, D.A., Moon, R.W., Blasco, B., Sutherland, C.J., 2017. Comparison of the susceptibility of *Plasmodium knowles*i and *Plasmodium falciparum* to

antimalarial agents. J. Antimicrob. Chemother. 72, 3051–3058.

Vanderberg, J.P., 1974. Studies on the Motility of *Plasmodium* Sporozoites. J. Protozool. 21, 527–537.

Vaughan, A.M., Mikolajczak, S.A., Wilson, E.M., Grompe, M., Kaushansky, A., Camargo, N., Bial, J., Ploss, A., Kappe, S.H.I., 2012. Complete *Plasmodium falciparum* liver stage development in liver-chimeric mice. J. Clin. Invest. 122, 3618–3628.

Venugopal, K., Hentzschel, F., Valkiūnas, G., Marti, M., 2020. *Plasmodium* asexual growth and sexual development in the haematopoietic niche of the host. Nat. Rev. Microbiol. 18, 177–189.

Vlachou, D., Zimmermann, T., Cantera, R., Janse, C.J., Waters, A.P., Kafatos, F.C., 2004. Real-time, in vivo analysis of malaria ookinete locomotion and mosquito midgut invasion. Cell. Microbiol. 6, 671–685.

Volz, J.C., Yap, A., Sisquella, X., Thompson, J.K., Lim, N.T.Y., Whitehead, L.W., Chen, L., Lampe, M., Tham, W.H., Wilson, D., Nebl, T., Marapana, D., Triglia, T., Wong, W., Rogers, K.L., Cowman, A.F., 2016. Essential Role of the PfRh5/PfRipr/CyRPA Complex during *Plasmodium falciparum* Invasion of Erythrocytes. Cell Host Microbe 20, 60–71.

Volz, J.C., Yap, A., Sisquella, X., Thompson, J.K., Lim, N.T.Y., Whitehead, L.W., Chen, L., Lampe, M., Tham, W.H., Wilson, D., Nebl, T., Marapana, D., Triglia, T., Wong, W., Rogers, K.L., Cowman, A.F., 2015. Essential Role of the PfRh5/PfRipr/CyRPA Complex during *Plasmodium falciparum* Invasion of Erythrocytes. Cell Host Microbe 20, 60–71.

Weiss, G.E., Gilson, P.R., Taechalertpaisarn, T., Tham, W.H., de Jong, N.W.M., Harvey, K.L., Fowkes, F.J.I., Barlow, P.N., Rayner, J.C., Wright, G.J., Cowman, A.F., Crabb, B.S., 2015. Revealing the Sequence and Resulting Cellular Morphology of Receptor-Ligand Interactions during *Plasmodium falciparum* Invasion of Erythrocytes. PLoS Pathog. 11, 1–25.

Wertheimer, S.P., Barnwell, A.W., 1989. *Plasmodium vivax* interaction with the Human Duffy Blood Group Glycoprotein : Identification of a Parasite Receptor-

like Protein. 69(3). 340–350.

Whitelaw, J.A., Latorre-Barragan, F., Gras, S., Pall, G.S., Leung, J.M., Heaslip, A., Egarter, S., Andenmatten, N., Nelson, S.R., Warshaw, D.M., Ward, G.E.,

WHO, 2016. Eliminating Malaria. [online] Available at: https://www.who.int/malaria/publications/atoz/eliminating-malaria/en/[Accessed 16 October 2020].

WHO, 2019. Malaria factsheet. [online] Available at: https://www.who.int/en/news-room/fact-sheets/detail/malaria [Accessed 16 October 2020].

World Health Organization Strategic Advisory Group on Malaria, 2020. Malaria eradication : benefits , future scenarios and feasiblity: A report of the Strategic Advisory Group on Malaria Eradication. [online] Available at: https://www.who.int/publications/i/item/malaria-eradication-benefits-future-scenarios-feasibility [Accessed 16 October 2020].

WHO, 2019. World malaria report 2019. [online] Available at: https://www.who.int/publications/i/item/9789241565721 [Accessed 16 October 2020].

Meissner, M., 2017. Surface attachment, promoted by the actomyosin system of *Toxoplasma gondii* is important for efficient gliding motility and invasion. BMC Biol. 15, 1–23.

Wickham, M.E., Culvenor, J.G., Cowman, A.F., 2003. Selective inhibition of a two-step egress of malaria parasites from the host erythrocyte. J. Biol. Chem. 278, 37658–37663.

William, T., Jelip, J., Menon, J., Anderios, F., Mohammad, R., Awang Mohammad, T.A., Grigg, M.J., Yeo, T.W., Anstey, N.M., Barber, B.E., 2014. Changing epidemiology of malaria in Sabah, Malaysia: Increasing incidence of *Plasmodium knowlesi*. Malar. J. 13, 1–11.

William, T., Rahman, H.A., Jelip, J., Ibrahim, M.Y., Menon, J., Grigg, M.J., Yeo, T.W., Anstey, N.M., Barber, B.E., 2013. Increasing Incidence of *Plasmodium knowlesi* Malaria following Control of *P. falciparum* and *P. vivax* Malaria in Sabah, Malaysia. PLoS Negl. Trop. Dis. 7.

Woldearegai, T.G., Kremsner, P.G., Kun, J. rgen F.J., Mordmü ller, B., 2013.
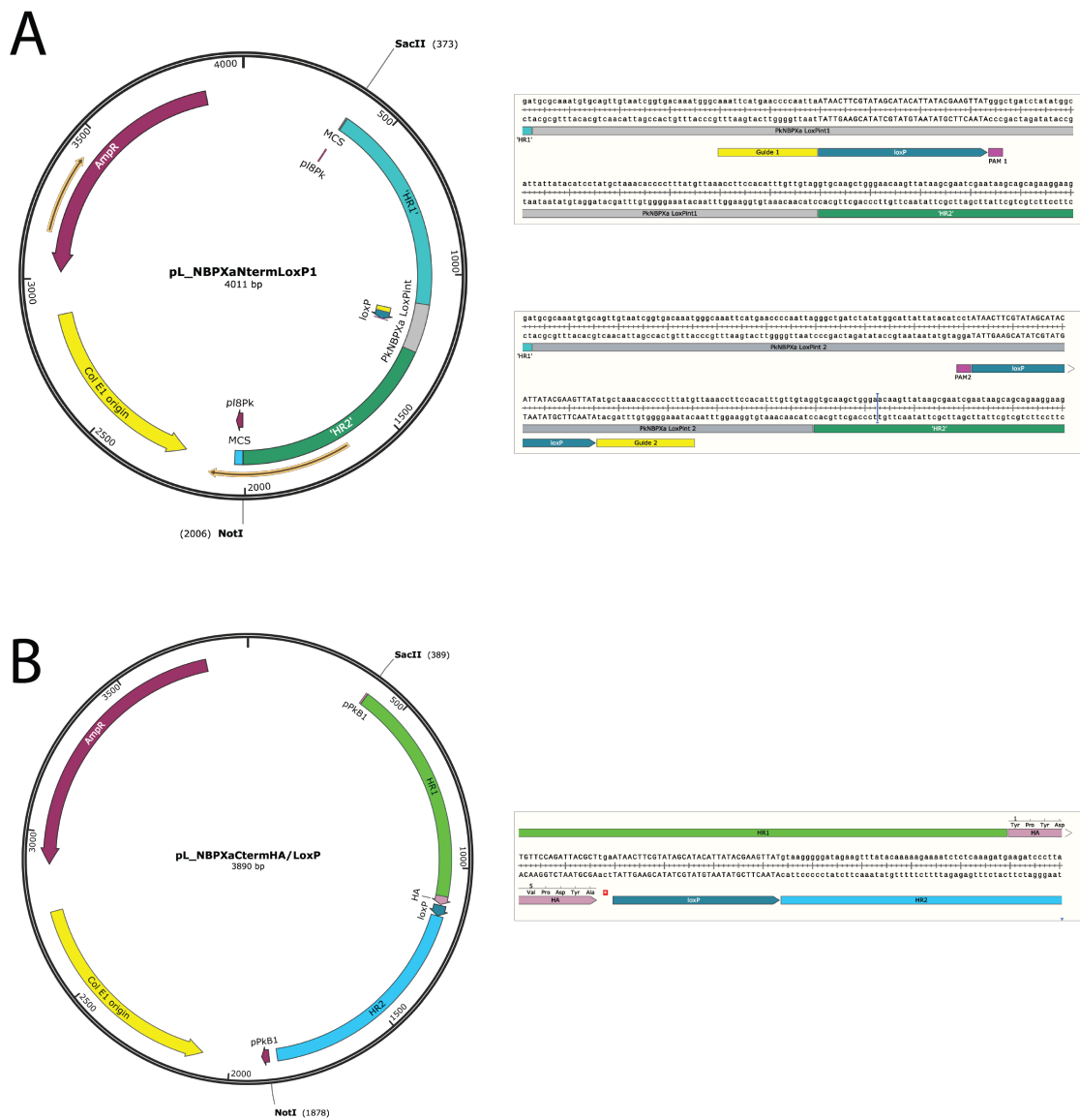
Plasmodium vivax malaria in Duffy-negative individuals from Ethiopia. Trans. R. Soc. Trop. Med. Hyg. 107, 328–331.

Wong, W., Huang, R., Menant, S., Hong, C., Sandow, J.J., Birkinshaw, R.W., Healer, J., Hodder, A.N., Kanjee, U., Tonkin, C.J., Heckmann, D., Soroka, V., Søgaard, T.M.M., Jørgensen, T., Duraisingh, M.T., Czabotar, P.E., de Jongh, W.A., Tham, W.H., Webb, A.I., Yu, Z., Cowman, A.F., 2019. Structure of *Plasmodium falciparum* Rh5–CyRPA–Ripr invasion complex. Nature 565, 118–121.

Wright, G.J., Rayner, J.C., 2014. *Plasmodium falciparum* Erythrocyte Invasion: Combining Function with Immune Evasion. PLoS Pathog. 10, 1–7.

Yahata, K., Hart, M.N., Davies, H., Asada, M., Templeton, T.J., Treeck, M., Moon, R.W., Kaneko, O., 2020. Gliding motility of *Plasmodium* merozoites. bioRxiv 2020.05.01.072637.

Yahata, K., Treeck, M., Culleton, R., Gilberger, T.W., Kaneko, O., 2012. Time-Lapse Imaging of Red Blood Cell Invasion by the Rodent Malaria Parasite *Plasmodium yoelii*. PLoS One 7, 1–7.

Yap, A., Azevedo, M.F., Gilson, P.R., Weiss, G.E., O'Neill, M.T., Wilson, D.W., Crabb, B.S., Cowman, A.F., 2014. Conditional expression of apical membrane antigen 1 in *Plasmodium falciparum* shows it is required for erythrocyte invasion by merozoites. Cell. Microbiol. 16, 642–656.

Yeoh, S., O'Donnell, R.A., Koussis, K., Dluzewski, A.R., Ansell, K.H., Osborne, S.A., Hackett, F., Withers-Martinez, C., Mitchell, G.H., Bannister, L.H., Bryans, J.S., Kettleborough, C.A., Blackman, M.J., 2007. Subcellular Discharge of a Serine Protease Mediates Release of Invasive Malaria Parasites from Host Erythrocytes. Cell 131, 1072–1083.

Yusof, R., Lau, Y.L., Mahmud, R., Fong, M.Y., Jelip, J., Ngian, H.U., Mustakim, S., Hussin, H.M., Marzuki, N., Mohd Ali, M., 2014. High proportion of *knowlesi malaria* in recent malaria cases in Malaysia. Malar. J. 13, 168.

Zhang, C., Gao, H., Zhenke, Y., Jiang, Y., Li, Z., Xiao, B., Su, X., Cui, H., Yuan, J., 2017. CRISPR/Cas9 mediated sequential editing of genes critical for ookinete motility in *Plasmodium yoelii*. Mol. Biochem. Parasitol. 212, 1–8..
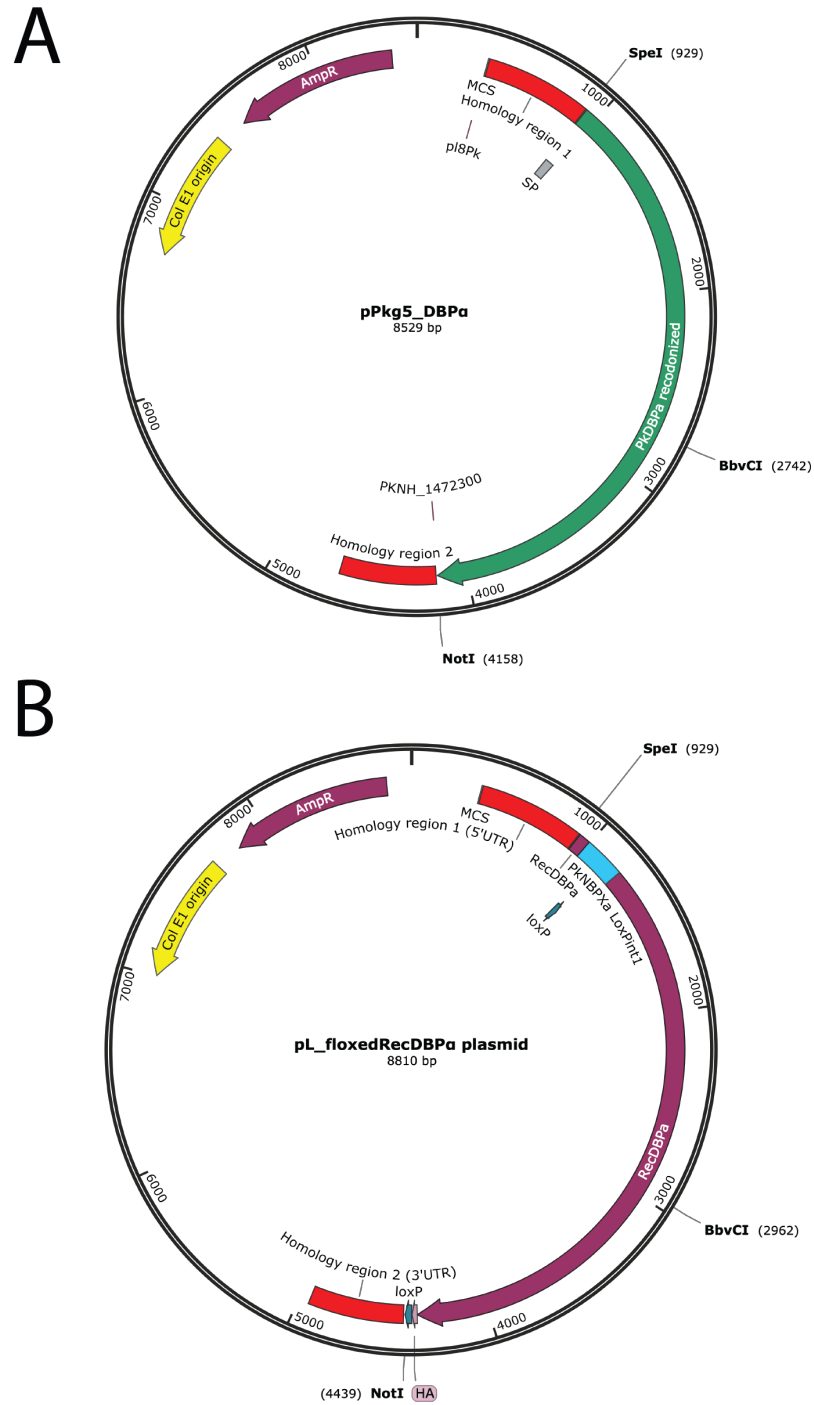
Zhang, M., Wang, C., Otto, T.D., Oberstaller, J., Liao, X., Adapa, S.R., Udenze, K., Bronner, I.F., Casandra, D., Mayho, M., Brown, J., Li, S., Swanson, J., Rayner, J.C., Jiang, R.H.Y., Adams, J.H., 2018. Uncovering the essential genes of the human malaria parasite *Plasmodium falciparum* by saturation mutagenesis. Science. 360(6388):eaap7847.

Zhang, X., Tolzmann, C.A., Melcher, M., Haas, B.J., Gardner, M.J., Smith, J.D., Feagin, J.E., 2011. Branch point identification and sequence requirements for intron splicing in *Plasmodium falciparum*. Eukaryot. Cell 10, 1422–1428.

Zuccala, E.S., Gout, A.M., Dekiwadia, C., Marapana, D.S., Angrisano, F., Turnbull, L., Riglar, D.T., Rogers, K.L., Whitchurch, C.B., Ralph, S.A., Speed, T.P., Baum, J., 2012. Subcompartmentalisation of Proteins in the Rhoptries Correlates with Ordered Events of Erythrocyte Invasion by the Blood Stage Malaria Parasite. PLoS One 7(9): e46160.
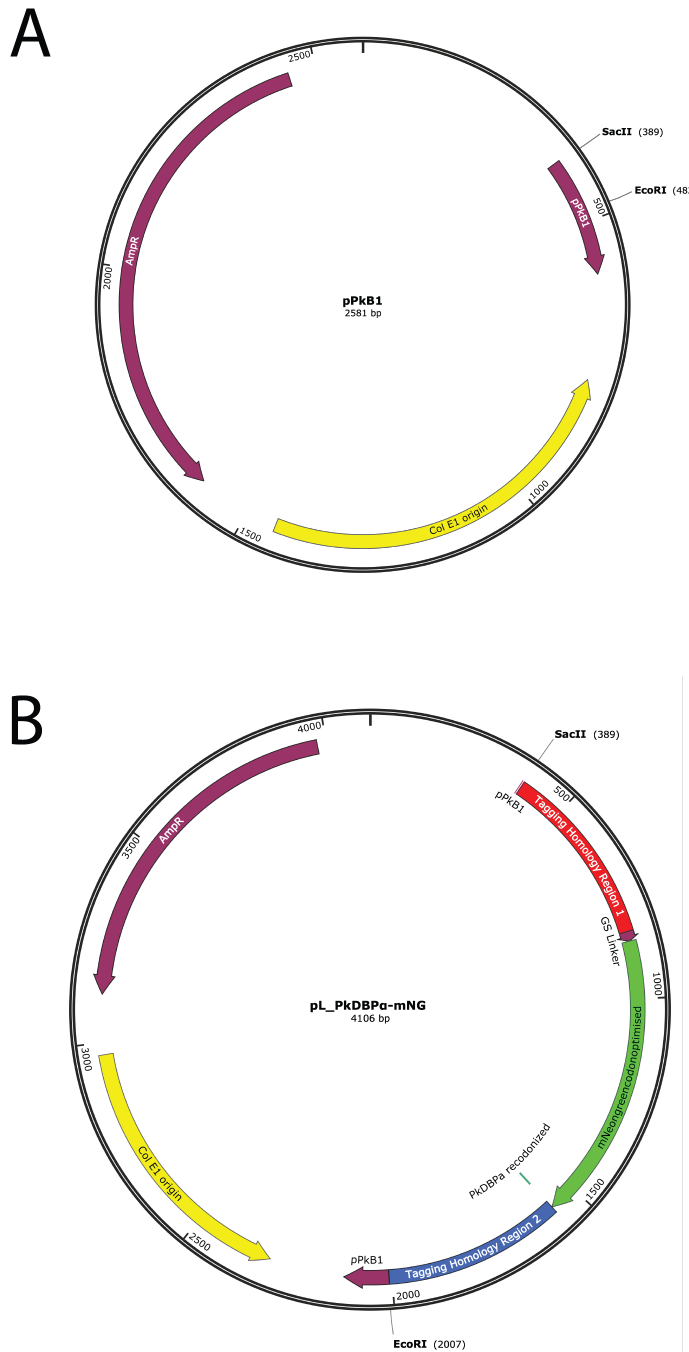
Appendix Figure 1. Generation of the PkDBPα-mNG Donor DNA plasmid.
(A) The pPkB1 backbone contains SacII/EcoRI sites, which were used to insert
the PkDBPα-mNG PCR product, generating **(B)** pL_PkDBPα-mNG, used to
target the C-terminus of PkDBPα with an mNeonGreen (mNG) fluorescent tag. A
Glycine-Serine linker (GS) separates the mNG tag from the PkDBPα C-terminus.

Appendix Figure 2. Generation of PkNBPXa cKO Donor DNA plasmids. (A)
PkNBPXaLoxPint1 and PkNBPXaLoxPint2 PCR products were inserted into vector
pPkB1 (Appendix Figure 1A) via SacII/NotI sites. Sequences to the right show LoxPint1
and LoxPint2 variants. **(B)** The PkNBPXaCtermHA/LoxP PCR product was inserted into
pPkB1 also using SacII/NotI sites, generating vector pLNBPXaCtermHA/LoxP, targeting
the PkNBPXa C-terminus with a HA/Stop/LoxP sequence, to the right.

Appendix Figure 3. Generation of pL_floxedRecDBPα donor DNA plasmid (A) The recodonised PkDBPα (RecDBPα) sequence in vector pPkg5_DBPα (Mohring et al., 2019) was modified to introduce the PkLoxPint1 module immediately after the PkDBPα signal peptide (SP) and a HA tag/STOP/LoxP sequence at the C-terminal end of the gene. The PkLoxPint sequence was introduced via SpeI/BbvCI sites, and the C-terminal LoxP sequence was added via BbvCI/NotI sites. The final product **(B)** replaces the entire endogenous WT PkDBPα sequence with the recodonised floxed version.
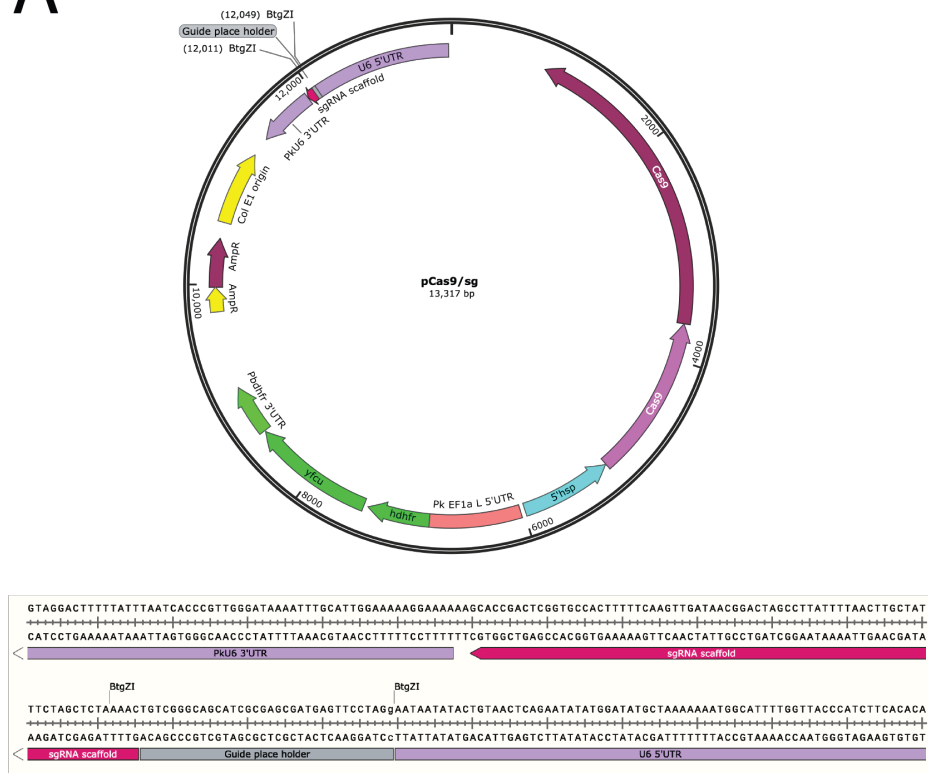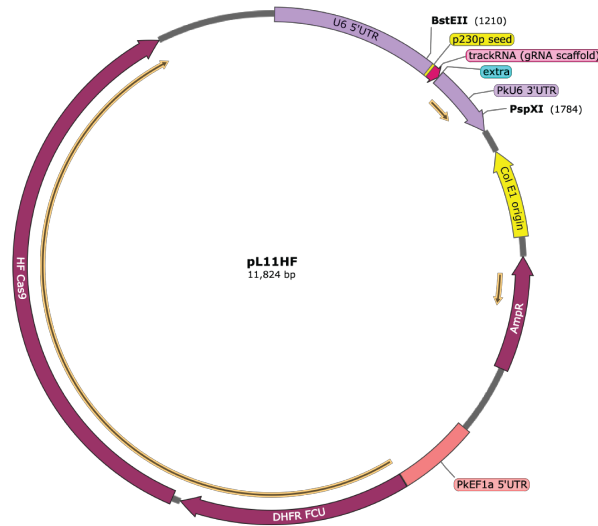
Appendix Figure 4. The Cas9 plasmids used in this study. (A) All but one guide sequence was cloned into pCas9/sg (Mohring et al., 2019), via BtgZI. This vector contains the Cas9 sequence, guide RNA cassette, and positive (hDHFR) and negative (FCU) selection markers. **(B)** The PkNBPXa C-terminal guide sequence was also cloned into pL11HF, which contains all of the above, with the exception of a high fidelity (HF) Cas9 enzyme sequence and smaller plasmid backbone. To insert the PkNBPXa guide, the entire sgRNA cassette was amplified by overlapping PCR, with primers containing the PkNBPXa guide sequence. This PCR product was ligated into pL11HF via BstEII/PspXI sites.

Appendix Table 1. Primers used to synthesise donor DNA constructs

Primer name	Sequence
MH297	GGATCCGGTGGAGGCAGCGG
MH295	CGACAGGTTTCCCGACTGGAAAG
MH227	GAAAATAAATCTATTAGAGGAAGAGGAAGTTAAGC
MH306	ACAGATGTTATGGGAATGGATGAATTGTATAAATAATGAGTAAGGGGGATAGAAGTTTATACAAAAAG
MH298	CAGTTACTAGCAATTTGAATGAGCAGT
MH229	ACCTCCGCTGCCTCCACCGGATCCTATATATTCGTTACTTTCGTCAAAGGTAACTTCA
MH231	TTCGTTTTTCAAAATATGTCTTTTAGGCACC
MH296	TTATTTATACAATTCATCCATTCCCATAACATCTGT
MH299	AGTTTCTCTGATTATCTAATTAATTGATATAAATTCCCATC
MH221	ACAACCGGAAACTGAACCGG
MH224	GGAATGGATGAATTGTATAAATAATGATGCTACTTGGGTAAGTAAGGAGA
MH222	TTTATCCGCGGAGAAGATCATCCTGATGAGCGAAG
MH223	ACCTCCGCTGCCTCCACCGGATCCGCTGTAGTCAAGGGGGGTGAACTG
MH225	CGGGGCTAATTTGTCCGTGTA
MH226	TTTATGAATTCGACAAATTAATGGCACATTTTTCTCTTTTGG
MH847	TTCAGTGTAGCTAGAAACCCGGG
MH1062	GGGAATGGATGAATTGTATAAATAATAGGGTGGTGACTTGTCCATCTC
MH848	GCTGATCATTGTTCTGCCTTGTG
MH337	ACCTCCGCTGCCTCCACCGGATCCCATCTGTATGCGGGCGTACGATAT
MH851	TGCAAAATCCTCTTGTTTTCCCC
MH852	GGTTCAAAATAGGATAAGTCAAAACGGC
MH841	CAACCGAATCGTTTTCGAAGCTAG
MH1063	GGGAATGGATGAATTGTATAAATAATGAGTGGGGAAGCAACGTATTATTCG
MH842	TGATTAAAAGTGCCTTTCTTCCAGTGG
MH331	ACCTCCGCTGCCTCCACCGGATCCGTAGTAAGGCTTCTCCATCAGAACAG
MH845	TATGGATTATATTAAAGTAAGCGTATACGCCATG
MH846	TAGAGTGCTCATATAAGGCACGCAC
MH850	TACCCATACGATGTTCCAGATTACGCTTAGGGTGGTGACTTGTCCATCTC
MH849	AGCGTAATCTGGAACATCGTATGGGTACATCTGTATGCGGGCGTACGA
MH844	TACCCATACGATGTTCCAGATTACGCTTGAGTGGGGAAGCAACGTATTATTCG
MH843	AGCGTAATCTGGAACATCGTATGGGTAGTAGTAAGGCTTCTCCATCAGAACAG
MH953	CTTGTGGTGCTCTTTTAGGTAAAATTACC
MH962	ATAGCATACATTATACGAAGTTATGGGCTGATCTATATGGCATTATTATACATCC
MH954	TTATCCGCGGGAAGCTGTTTGAGGTAATCGTGTG
MH963	ATAACTTCGTATAATGTATGCTATACGAAGTTATTAATTGGGGTTCATGAATTTGCCCA
MH957	CAGCCGAATTGCACTCCTTAG
MH958	TTATGCGGCCGCCCTGTTCGTTACCTTCTGTCTGTG

MH966	CTTCGTATAGCATACATTATACGAAGTTATATGCTAAACACCCCTTTATGTTAAACC
MH967	TCGTATAATGTATGCTATACGAAGTTATAGGATGTATAATAATGCCATATAGATCAGCC
MH835	GGCAAGATAGAAGCATATATCGAAAACATTTC
MH838	ATAGCATACATTATACGAAGTTATGTAAGGGGGATAGAAGTTTATACAAAAAGAAAATC
MH975	TTATCCGCGGGAATCCTATAATGAAGAGGCAAGGAAAAAATTAC
MH238	AGCGTAATCTGGAACATCGTATGGGTATATATATTCGTTACTTTCGTCAAAGGTAACTTCA
MH837	ATAACTTCGTATAATGTATGCTATACGAAGTTATTCAAGCGTAATCTGGAACATCGTATG
MH839	CGTATTTCCCCATAAAGATGAATGCG
MH1023	TTATGCGGCCGCGAAAATTATGAAAACGCCATGTTTAAATTTGC
FM62	CCGCGGGAAATTTTGGATTGTTGGAAACGCAAAAAAATATTG
MH1350	GCCAACAACGTGCTGTTCGAG
MH1348	GTGCTGCTGCTGAGCCACAAGGTACAATTTCACAAAAGAGGGTAG
MH1347	TACCTTGTGGCTCAGCAGCAGCAC
MH1367	TTTGTTCTCTTCGGTCACGGTG
CH204	CATAGTATGATTCTAAGGAAAAGACTAACTCC
MH1349	CATTCTCTCGAACAGCACGTTGTTGGCCTACAACAAATGTGGAAGGTTTAACATAAAG
MH1341	TGAACAAAGGGGAGGGCAAGTC
MH1342	TGCTTCCAGAAGCGTGGACG
MH1343	GAAGTTATTCAAGCGTAATCTGGAACATCGTATGGGTAGCTGTAGTCCAGGGGGGTGAAC
MH1344	TAGCAGCGGCCGCATAACTTCGTATAATGTATGCTATACGAAGTTATTCAAGCGTAATCTGG
MH1058	GGCGGCATGGACGAGCTGTACAAGTGAGTAAGGGGGATAGAAGTTTATACAAAAAG
MH1059	CTTGTACAGCTCGTCCATGCCGCC
MH1057	GGATCCGGTGGAGGCAGCGGAGGTGTGAGCAAGGGCGAGGAGGATAAC

Appendix Table 2. Primers used to insert gRNA sequences into pCas9/sg Guide sequences indicated in red text

Primer name	Sequence
MH235	TTACAGTATATTATTGTAACGAATATATATGAGTAGTTTTAGAGCTAGAA
MH236	TTCTAGCTCTAAAACTACTCATATATATTCGTTACAATAATATACTGTAA
MH964	TTACAGTATATTATTAAATTCATGAACCCCAATTAGTTTTAGAGCTAGAA
MH965	TTCTAGCTCTAAAACTAATTGGGGTTCATGAATTTAATAATATACTGTAA
MH968	TTACAGTATATTATTCATAAAGGGGTGTTTAGCATGTTTTAGAGCTAGAA
MH969	TTCTAGCTCTAAAACATGCTAAACACCCCTTTATGAATAATATACTGTAA
FM512	TTACAGTATATTATTTACGCCCGCATACAGATGTAGTTTTAGAGCTAGAA
FM513	TTCTAGCTCTAAAACTACATCTGTATGCGGGCGTAAATAATATACTGTAA
FM510	TTACAGTATATTATTGAGAAGCCTTACTACTGAGTGTTTTAGAGCTAGAA
FM511	TTCTAGCTCTAAAACACTCAGTAGTAAGGCTTCTCAATAATATACTGTAA

Appendix Table 3. Diagnostic PCR primers used in this study

Primer name	Primer sequence	Description
MH890	TGCTAGAAAAAGTGGCAGAGTTACATAAG	RON2 Fwd
MH909	AGTCACCACCCTACATCTGTATGC	RON2 WT rev
MH291	TTGGATTTCCTGTTCCTTGTCCAACC	mNeonGreen reverse
MH563	CGTAATCTGGAACATCGTATGGG	HA tag reverse
MH892	GTAATGATTGGGAAAACAAGTGCCC	AMA-1 Fwd
MH904	GCTTCCCCACTCAGTAGTAAGG	AMA-1 WT rev
MH835	GGCAAGATAGAAGCATATATCGAAAACATTTC	NBPXaC-term Fwd (1)
MH1128	CTTTTTGTATAAACTTCTATCCCCCTTACTCATATATATTC	NBPXa C-term WT rev
MH959	CCCCTTTCCCAGGAACAAATTG	NBPXa N term Fwd
MH1353	ATGCCATATAGATCAGCCCTAATTG	NBPXa LoxP1 WT rev
MH1171	TCAGCCCATAACTTCGTATAATGTATGC	NBPXa LoxP1 Integration rev
MH1143	CATAAAGGGGTGTTTAGCATAGGATG	NBPXa LoxP2 WT rev
MH1172	GTTTAGCATATAACTTCGTATAATGTATGCTATACGAAG	NBPXa LoxP2 Integration rev
MH1129	GAAGGCATATACGAAATATGGAAAAGAGC	NBPXa Cterm Fwd (2)
FM421	TTCATGCGGAACAGCAACAG	RecPkDBPa Fwd
MH225	CGGGGCTAATTTGTCCGTGTA	RecPkDBPa WT rev
CH193	ATGAAGAAATATTACACCATTCTGCATTATTCC	WT PkDBPa Fwd
MH562	CCATACGATGTTCCAGATTACGC	HA tag Fwd
MH1041	GTAGGGAACATTTCTTTCTGCGG	PkDBPa C-term rev
RM75	CCCGGGGCGTTTTCGCGTATCTGCGCTTTTTC	Control Fwd
RM76	CCTAGGGGACAATATATCCTCACAGAACAACTTG	Control Rev
MH1160	CTTGAAGCGCATGAACTCCTTG	mCherry Rev
FM49	GAAGATTCCGCAAAGCTTTGTCGGTTA	p230p WT Fwd
FM50	ACGCTATGGAAGCAGTTGTCTGGAT	p230p WT Rev
FM32	CCTAATCATGTAAATCTTAAATTTTTCTTTTTAAACATATG	p230p Integration Rev
FM90	TGGGAAATACAGGAAATAACGGTGTTATGT	p230p Integration Fwd